AD_____

Award Number: W81XWH-05-1-0004

TITLE: Identification and Characterization of Genomic Amplifications in Ovarian Serous Carcinoma

PRINCIPAL INVESTIGATOR: Tian-Li Wang, Ph.D.

CONTRACTING ORGANIZATION: Johns Hopkins University School of Medicine
Baltimore, MD 21205

REPORT DATE: January 2009

TYPE OF REPORT: Annual

PREPARED FOR: U.S. Army Medical Research and Materiel Command
Fort Detrick, Maryland 21702-5012

REPORT DOCUMENTATION PAGE

Form Approved
OMB No. 0704-0188

1. REPORT DATE	2. REPORT TYPE	3. DATES COVERED
1 Jan 2009	Annual	1 Jan 2008 – 31 Dec 2008

4. TITLE AND SUBTITLE

Identification and Characterization of Genomic Amplifications in Ovarian Serous Carcinoma

5a. CONTRACT NUMBER

5b. GRANT NUMBER
W81XWH-05-1-0004

5c. PROGRAM ELEMENT NUMBER

6. AUTHOR(S)

Tian-Li Wang, Ph.D.

E-Mail: tlw@jhmi.edu

5d. PROJECT NUMBER

5e. TASK NUMBER

5f. WORK UNIT NUMBER

7. PERFORMING ORGANIZATION NAME(S) AND ADDRESS(ES)

Johns Hopkins University School of Medicine
Baltimore, MD 21205

8. PERFORMING ORGANIZATION REPORT NUMBER

9. SPONSORING / MONITORING AGENCY NAME(S) AND ADDRESS(ES)
U.S. Army Medical Research and Materiel Command
Fort Detrick, Maryland 21702-5012

10. SPONSOR/MONITOR'S ACRONYM(S)

11. SPONSOR/MONITOR'S REPORT NUMBER(S)

12. DISTRIBUTION / AVAILABILITY STATEMENT
Approved for Public Release; Distribution Unlimited

13. SUPPLEMENTARY NOTES

14. ABSTRACT
The purpose of this proposed study is to apply genome-wide technologies to analyze ovarian cancer genome and transcriptome. We have accomplished all the proposed tasks as stated in the original grant. They include generating digital karyotyping libraries from ovarian carcinomas and perform transcirptome analysis in each amplicon. This effort leads us to identify at least two novel candidate oncogenes, Rsf1 and Notch3, which were up-regulated in both genomic DNA and transcript levels in ovarian cancer. In a large-scale FISH analysis, Rsf1 gene amplification was found to be correlated with a worse disease outcome. Furthermore, Rsf1 overexpression was found to lead to taxol resistance, which may explain why patient with Rsf1 amplification has a shorter overall survival. Because of recent advances in technology refinement, we have found that high density SNP array can provide a similar performance as digital karyotyping. Due to its lower cost, we are able to perform SNP array on more than 40 affinity purified ovarian serous tumors, initially with 10K platform and later on with 250K array platform. Our results demonstrated that CCNE1, Notch3, Rsf1, AKT2 and PIK3CA were among the most frequently amplified loci in high-grade ovarian serous carcinomas. In addition, we have further characterized the biological functions of the two commonly amplified genes, Notch3 and Rsf1. Our study is the first comprehensive analysis of the detailed copy number profiles in ovarian cancerors. The results from this study shall provide a new insight into how amplified or deleted genes contribute to survival and growth advantages in ovarian cancer cells.

15. SUBJECT TERMS
amplification, genetics, digital karyotyping, SNP array, oncogene, pathogenesis

16. SECURITY CLASSIFICATION OF:			17. LIMITATION OF ABSTRACT	18. NUMBER OF PAGES	19a. NAME OF RESPONSIBLE PERSON
a. REPORT	b. ABSTRACT	c. THIS PAGE			USAMRMC
U	U	U	UU	148	19b. TELEPHONE NUMBER *(include area code)*

Table of Contents

Introduction

Identification of new oncogenes and tumor suppressors that participate in the development of ovarian carcinoma holds great promise to develop new strategies for diagnosing and treating this devastating disease. Several elegant studies have employed gene expression profiling as the discovery tool (such as DNA-based microarray) and have identified multiple candidate genes associated with ovarian carcinomas. Several of these over-expressed genes have proven to be novel biomarkers of cancer (Hough et al., 2000). However, it is challenging to use such approach alone to distinguish the truly important genes that directly drive tumor progression from a larger number of the “passenger” genes that are co-overexpressed but lack the biological roles in tumor development. This is because gene expression is dynamic, depending on both genetic program and tumor microenvironment. In contrast, molecular genetic changes such as gene amplification and point mutation are inheritable traits as a result of clonal selection and they likely confer a growth advantage to tumor cells and propel tumorigenesis.

We hypothesize that a comprehensive analysis of ovarian cancer genome by combining genomic analysis and gene expression analysis would significantly facilitate the identification of oncogenes or tumor suppressors that directly contribute to the development of ovarian tumors. The main objective in this study is to identify critical genetic alterations that participate in the development of ovarian serous carcinoma, the most common and malignant type of ovarian cancer. This goal is achieved through a parallel analysis of cancer genome and transcriptome. This approach would identify genes demonstrating increases in copy numbers of both genomic DNA and mRNA and those genes will be characterized through mutational analysis. Digital karyotyping, a technology developed in our research team, and high resolution SNP arrays permit a detailed analysis of cancer genome (Wang et al., 2002), and both techniques were employed to scan ovarian cancer genome. SAGE (serial analysis of gene expression) (Velculescu et al., 1995) and high throughput quantitative real-time PCR were performed to reveal the transcriptome in each amplified region. Using the above approaches, we have identified several candidate oncogenes with concurrent gene amplification and transcript up-regulation. We have also performed functional studies on candidate oncogenes to determine their roles in ovarian cancer pathogenesis.

Body

We have accomplished all the proposed tasks using digital karyotyping technology. In addition, because of technique advancement in recent years, we have performed high density SNP array analysis on additional 80 ovarian tumor samples to extend our study. The accomplishments associated with each task outlined in the approved statement of work are detailed, point by point, in the followings. Further details can be found in the published and in-press papers in Reportable Outcomes.

Task 1. To identify genome-wide amplifications in ovarian serous carcinomas using Digital Karyotyping.

By the end of the funding period, we have finished generating digital karyotyping libraries for serous carcinomas as originally proposed. In the mean time, we also used SNP arrays for the same purpose. This is because the technology and analysis software of high density SNP arrays have become cost effective. We have performed side-by-side comparison of digital karyotyping and high density SNP array and found the results were comparable between these two methods. Discrete amplicon and homozygous deletion can be identified by both techniques. Due to much lower cost for SNP array analysis, we were able to analyze a larger number of clinical samples that yield much information than what has been proposed. As a result, we have analyzed a total of 43 additional affinity-purified ovarian tumors using 10K SNP array and 37 additional samples using 250K SNP array. Because of the higher sensitivity associated with 250K SNP array platform, we were able to analyze deletion with high confidence. We have created a web-link in Johns Hopkins to permit access to 10K SNP array database by the public (https://jshare.johnshopkins.edu/twang16/10K%20SNP%20array%20Data). We plan to post the 250K SNP array database once our two new manuscripts using this platform are published.

Based on the SNP array and originally proposed digital karyotyping analyses, we have focused on two of the most frequently amplified regions, 11q13.2 (the Rsf1 locus) and 19p13 (the Notch3 locus), for detailed mapping and functional characterization (Appendix #1, #4 & #10). For the study of Rsf1 gene, we were able to demonstrate that its expression was associated with chemoresistance to taxol (Appendix #17) and its interaction with another chromatin remodeling protein, hSNF2H, was essential for tumor promotion (Appendix #14). Furthermore, gene amplification is associated with worse disease outcome, suggesting that Rsf1 could be potentially used as a prognostic marker in the future (Appendix #1). For the study of Notch3 gene, we identified the ligands present in the tumor microenviroment that could trigger Notch signaling and be involved in tumor dissemination onto mesothelial cells of the peritoneal wall (Appendix #15). We also identified target genes of Notch3 signaling using the Affymetry expression microarrays. Our results indicated that Pbx1 was a critical gene involved in Notch3 signaling (Appendix #16).

It needs to be mentioned that while analyzing digital karyotyping libraries during the early phase of this study, we have identified a gene named NAC1 which was highly amplified and over-expressed in a recurrent carcinoma. Although the follow-up study in a larger-scale sample size did not demonstrate clear amplification in NAC1 region, we did confirm that NAC1 protein was over-expressed in the recurrent ovarian carcinomas and was functionally important in cancer cell survival (Appendix #3 & #12).

In addition to gene amplifications, our genome scan using digital karyotyping and 250K SNP array also identified genomic deletions. We had characterized a region with homozygous deletion at 17p12. This region harbors a candidate tumor suppressor: MKK4. Function study by others as well as by us suggested that MKK4 could suppress the metastasis potential of cancer cells (Appendix #7). Additional homozygous deletions have been more recently identified by high-density 250K SNP array analysis and currently we are pinpointing the culprit tumor suppressors within the regions harboring homozygous deletion. The results are currently in revision in *Cancer Research*.

With this study kindly supported by DoD, we were able to obtain additional research funding from NCI and American Cancer Society.

Task 2. To analyze genome-wide mRNA expression in the same tumors studied in AIM 1.
It is expected that each amplicon identified in Aim 1 harbored only one or few oncogenes(s) among hundreds of co-amplified "passenger" genes that were not involved in tumorigenesis. In order to distinguish the "driver" genes from the "passenger" genes and thus narrow down the candidate oncogenes list, we proposed to correlate the gene amplification and expression in the same tumors. The rationale is that oncogenes that are amplified are always over-expressed at mRNA and protein levels. In contrast, the co-amplified "passenger" genes that are unrelated to tumor development are less likely to be over-expressed (Kinzler and Vogelstein, 2002). We performed bioinformatics to search for all annotated genes in each amplicon, used the Primer 3 program to design PCR primers, and performed quantitative real-time PCR for all the genes within each amplicon for the tumors with specific amplification. The result is further analyzed in Task 3. The outcome of this task was published and please see Appendix #1 & #4 for details.

Task 3. To generate transcriptome map and compare to genomic map to identify the genes with both amplification and over-expression in the same tumor samples.
The data derived from Task 2 was used to generate a heat map and transcriptome results from amplified tumors were compared with non-amplified tumors. Wilcoson test was performed to compute the difference between these two groups. Genes with most statistical difference was prioritized for further studies. Using this approach, we successfully analyzed the chr11q13.2 and ch19p13 amplicons and identified potential driver gene, Rsf1 and Notch3, in each amplicon, respectively. The outcome of this task was published in Appendix #1 & #4.

Task 4. To identify somatic mutations in candidate genes with both amplification and over-expression.
We have performed mutational analysis for the candidate genes with the chr11q13.2 and chr19p13 amplicons including *Notch3*, *Rsf1*, *PAK4* and *Gab2* in a panel of 24 purified ovarian carcinomas. However, no somatic mutation was identified indicating that sequence mutation is a rare event as compared to gene amplification.

In addition, we have performed mutation analysis in the TP53 and kinase gene families using a high throughput platform in a series of ovarian serous tumors. We specifically focus on the kinase genes in which the mutations have been identified in human cancer and the inhibitors are available in clinical trials for other types of cancer. Once somatic mutation is identified, we then tested whether the compounds that inhibited a specific kinase pathway can abolish tumor growth in tumors that harbored the specific mutations. We reported rare somatic mutation in *PIK3CA* and *AKT2*, while gene amplification at the loci of both genes was common in ovarian serous tumors (Appendix #8). In addition, taking advantage of purified tumor cells, we re-evaluated mutation frequency of TP53 in high-grade ovarian carcinoma and found the frequency was approaching 80%, placing TP53 as the most significant tumor suppressor gene in high-grade ovarian carcinomas (Appendix #13).

More recently, we have analyzed mutational status of *KRAS, BRAF, PIK3CA, TP53, PTEN* and *CTNNB1* in a panel of ovarian clear cell carcinomas (CCC) and identified a mutation frequency of *PIK3CA* of 46% when purified tumor samples and cell lines were analyzed. This finding indicated that the importance of PIK3CA in CCC and targeting this pathway may be a more effective therapy than current chemotherapeutic agents for patients with ovarian clear cell carcinoma. The outcome of this task is in press in *American Journal of Pathology* (Appendix #18).

Key Research Accomplishments

- Perform digital karyotyping and high density SNP array analysis on more than 80 purified ovarian carcinomas and identify novel discrete genomic alterations. Part of the SNP array database has been deposited in a public accessible web-link.

- Perform large scale FISH analysis on seven of the most frequently amplified chromosomal loci including *CCNE1, AKT2, Notch3, Rsf-1, PIK3CA*, and *chr12p13*. Demonstrate Rsf1 gene amplification correlated with worse disease outcome. Establish the database of chromosomal amplification in ovarian carcinoma.

- Transcription and functional analysis of Rsf-1 as the cancer associated genes, identify its interaction with another chromatin remodeling protein, hSNF2H, is critical for its tumor promoting property and is related to resistance to taxol.

- Transcription and functional analysis of Notch3, its receptor ligand, and its downstream target genes in ovarian cancer.

- Mutational analysis of kinase gene family including *PIK3CA* and *AKT2*. So far, somatic mutation was identified in *KRAS, BRAF, PIK3CA*, and *ERBB*2. Identify frequent PIK3CA mutations in ovarian clear cell carcinoma.

Reportable Outcomes

Articles published during the entire funding period (January, 2007-current)

- I-M Shih, J J-C Sheu, A Santillan, K Nakayama, M J Yen, R E. Bristow, R Vang, G Parmigiani, RJ Kurman, CG Trope, B Davidson and **T-L Wang** (2005) Amplification of a Chromatin Remodeling Gene, Rsf-1/HBXAP, in Ovarian Carcinoma. ***Proc Natl Acad Sci USA*** 99: 3076-3080.
- IM Shih and **T-L Wang** (2005) Exploring cancer genome using innovative technologies. ***Curr Opin Oncol***, 17:33-38. (review)
- K Nakayama, N Nakayama, B Davidson, JJ Sheu, N Jinawath, A Santillan, R Salani, RE Bristow, PJ Morin, RJ Kurman, **T-L Wang**, IM Shih (2006) A BTB/POZ protein, NAC-1, is related to tumor recurrence and is essential for tumor growth and survival. ***Proc Natl Acad Sci U S A***. 103:18739-44
- JT Park, M Li, K Nakayama, T-L Mao, B Davidson, Z Zhang, RJ Kurman, CG Eberhart, IM Shih, **T-L Wang** (2006) Notch3 gene amplification in ovarian cancer. ***Cancer Research*** 12:6312-8.
- TL Mao, CY Hsu, MJ Yen, B Gilks, JJ Sheu, E Gabrielson, R Vang, L Cope, RJ Kurman, **T-L Wang**, IeM Shih (2006) Expression of Rsf-1, a chromatin-remodeling gene, in ovarian and breast carcinoma. ***Hum Pathol.*** 37:1169-75.
- R Salani, CL Chang, L Cope, **T-L Wang** (2006) Digital karyotyping: an update of its applications in cancer. ***Mol Diagn Ther.*** 10(4):231-7. (review)

- K Nakayama, N Nakayama, B Davidson, H Katabuchi, RJ Kurman, VE Velculescu, IM Shih, **T-L Wang** (2006) Homozygous Deletion of MKK4 in Ovarian Serous Carcinoma. ***Cancer Biol Ther*** 5:630-4
- K Nakayama, N Nakayama, RJ Kurman, L Cope, G Pohl, Y Samuels, VE Velculescu, **T-L Wang***, IM Shih (2006) Sequence mutations and amplification of PIK3CA and AKT2 genes in purified ovarian serous neoplasms. ***Cancer Biol Ther*** 5: 779-785

  *Corresponding author
- R Salani, B Davidson, M Fiegl, C Marth, E Müller-Holzner, G Gastl, HY Huang, JC Hsiao, HS Lin, **T-L Wang**, BL Lin, IeM Shih (2007) Measurement of cyclin E genomic copy number and strand length in cell-free DNA distinguish malignant versus benign effusions. ***Clin Cancer Res***. 13:5805-9.
- Leary RJ, Cummins J, **Wang TL**, Velculescu VE (2007) *Digital karyotyping*. ***Nature Protocol.*** 2:1973-86.
- K Nakayama, N Nakayama, N Jinawath, R Salani, RJ Kurman, IeM Shih, **T-L Wang** (2007) Amplicon profiles in ovarian serous carcinomas**.** ***Int J Cancer*** 120(12):2613-7
- IeM Shih and **T-L Wang** (2007) Notch signaling, gamma secretase inhibitors and cancer therapy. ***Cancer Res***. 67(5):1879-82. (review)
- Nakayama K, Nakayama N**, Wang TL**, Shih IeM (2007) NAC-1 controls cell growth and survival by repressing transcription of Gadd45GIP1, a candidate tumor suppressor. ***Cancer Res*** 67(17):8058-64
- R Salani, RJ Kurman, R 2nd Giuntoli, G Gardner, R Bristow, **T-L Wang**, IeM Shih (2008) Assessment of TP53 mutation using purified tissue samples of ovarian serous carcinomas reveals a higher mutation rate than previously reported and does not correlate with drug resistance. ***Int J Gynecol Cancer***. 8(3):487-91
- J J-C Sheu, J H Choi, I Yýldýz, F-J Tsai, Y Shaul, **T-L Wang**, and IeM Shih (2008) Modulating the tumor-promoting functions of Rsf-1 by dimmer formation with hSNF2H. ***Cancer Research*** 68:4050-7
- J-H Choi, J T Park, B Davidson, P J Morin, IeM Shih, and **T-L Wang** (2008) Jagged-1 and Notch3 juxtacrine loop regulates ovarian tumor growth and adhesion. ***Cancer Research*** 68:5716-23
- J T Park, IeM Shih, **T-L Wang** (2008) Identification of Pbx1, a potential oncogene, as a Notch3 target gene in ovarian cancer. ***Cancer Research*** 68:8852-60
- B Davidson, IeM Shih, and **T-L Wang** (2008) Different clinical roles for p21-activated kinase-1 in primary and recurrent ovarian carcinoma. ***Human Pathology*** 39 (11): 1630-1636
- J-H Choi, J J-C Sheu, B Guan, N Jinawath, P Markowski, **Tian-Li Wang**, IeM Shih (2009) Functional analysis of 11q13.5 amplicon identifies Rsf-1 (HBXAP) as a gene involved in paclitaxel resistance in ovarian cancer. ***Cancer Research (in press)***
- K-T Kuo, T-L Mao, S Jones, E Veras, A Ayhan, **T-L Wang**, Ruth Glas, Dennis Slamon, VE Velculescu, RJ Kurman, IeM Shih (2009) Frequent activating mutations of PIK3CA in ovarian clear cell carcinoma. ***Am J Pathol (in press)***

Grant received based on the results from this project

1 R01 CA129080-01A1 (Shih) 04/01/08 - 03/31/13
NCI/NIH
The Roles of HBXAP Gene in Ovarian Cancer

GMC-113937 (Wang) 07/01/2008 - 06/30/2012
American Cancer Society
Notch3 Signaling Pathway in the Ovarian Carcinoma

Individual Investigator Award 1/1/2008 to 12/31/2009
Ovarian Cancer Research Fund

Provost Research Award
Johns Hopkins University
Graduate student Rebecca Busch

Research resource

A centralized web deposit of digital karyotyping data is initiated by the Cancer Genome Anatomy Project, NCI (http://cgap-stage.nci.nih.gov/SAGE/DKViewHome). All the sequence tags from each digital karyotyping libraries can be retrieved from this website and the browser provides bioinformatics tools to analyze the DNA copy number alterations using varying parameters, including window scales, and size and fold of alterations. Currently there are libraries deposited and in the future all the data generated from this project will be publicly available at this web link.

For SNP array database, we have deposited 10K array data onto URL web link at Johns Hopkins University. The link is:
https://jshare.johnshopkins.edu/twang16/10K%20SNP%20array%20Data
These data are publicly accessible to general audiences.

Conclusions

Ovarian epithelial tumor is the most common and most lethal type of gynecologic malignancy. The main purpose of this project is to delineate the genomic alterations in ovarian serous tumors and identity the genes that contribute to tumor progression. We have accomplished all of the tasks proposed in the timetable. Because of the low cost associated with high-density SNP array analysis, we are able to perform analysis on 43 additional purified ovarian tumors using 10K SNP array platform and 37 purified tumor samples using 250K SNP array platform. As a result, an array of novel genomic alterations was identified.

We had performed detailed transcriptome analysis of 11q13 and 19p13 amplicons and identified *Rsf-1* and *Notch3* as the genes with most consistent gene amplification and transcript/protein up-regulation. Furthermore, survival data showed that the patients with *Rsf-1* amplification fared worse than patients without the ramped-up genes. The function of Rsf-1 and Notch3 in proliferation was also established by RNAi knock-down assays. Currently we are studying the mechanism of these two oncogenic pathways in ovarian carcinoma.

Our genome scan also identified deleted regions in ovarian cancer genome. We had characterized a region with frequent homozygous deletion at 17p12. This region harbors a candidate tumor suppressor: MKK4. Function study by others as well as by us suggested that MKK4 could suppress the metastasis potential of cancer cells. Additional homozygous deletions have been more

recently identified by high-density 250K SNP array analysis and we are currently pinpointing the culprit tumor suppressors within the regions with homozygous deletion.

Implications and significance of the accomplished research findings: This proposal represents a relatively comprehensive analysis of molecular genetic changes in ovarian carcinomas. Our data implies that genome-wide analyses and tools are useful in identifying novel amplified and deleted genes in ovarian cancer. The reported unique molecular genetic landscape in ovarian neoplasm can serve as a roadmap for future studies aiming at elucidating molecular pathogenesis, as well as in developing new diagnostic test and target-based therapy.

References

- Hough, C.D., Sherman-Baust, C.A., Pizer, E.S., Montz, F.J., Im, D.D., Rosenshein, N.B., Cho, K.R., Riggins, G.J., and Morin, P.J. (2000). Large-scale serial analysis of gene expression reveals genes differentially expressed in ovarian cancer. Cancer Res 60, 6281-6287.
- Wang, T.L., Maierhofer, C., Speicher, M.R., Lengauer, C., Vogelstein, B., Kinzler, K.W., and Velculescu, V.E. (2002). Digital karyotyping. Proc Natl Acad Sci U S A 99, 16156-16161.
- Velculescu, V.E., Zhang, L., Vogelstein, B., and Kinzler, K.W. (1995). Serial analysis of gene expression. Science 270, 484-487.
- Kinzler, K.W., and Vogelstein, B. (2002). The Genetic Basis of Human Cancer, 2nd Edition (Toronto: McGraw-Hill).

Appendices (published manuscripts using USAMRMC grant money)

1. I-M Shih, J J-C Sheu, A Santillan, K Nakayama, M J Yen, R E. Bristow, R Vang, G Parmigiani, RJ Kurman, CG Trope, B Davidson and **T-L Wang** (2005) Amplification of a Chromatin Remodeling Gene, Rsf-1/HBXAP, in Ovarian Carcinoma. ***Proc Natl Acad Sci USA*** 99: 3076-3080.
2. IM Shih and **T-L Wang** (2005) Exploring cancer genome using innovative technologies. ***Curr Opin Oncol***, 17:33-38. (review)
3. K Nakayama, N Nakayama, B Davidson, JJ Sheu, N Jinawath, A Santillan, R Salani, RE Bristow, PJ Morin, RJ Kurman, T-L Wang, IM Shih (2006) A BTB/POZ protein, NAC-1, is related to tumor recurrence and is essential for tumor growth and survival. ***Proc Natl Acad Sci U S A***. 103:18739-44
4. JT Park, M Li, K Nakayama, T-L Mao, B Davidson, Z Zhang, RJ Kurman, CG Eberhart, IM Shih, **T-L Wang** (2006) Notch3 gene amplification in ovarian cancer. ***Cancer Research*** 12:6312-8.
5. TL Mao, CY Hsu, MJ Yen, B Gilks, JJ Sheu, E Gabrielson, R Vang, L Cope, RJ Kurman, **T-L Wang**, IeM Shih (2006) Expression of Rsf-1, a chromatin-remodeling gene, in ovarian and breast carcinoma. ***Hum Pathol.*** 37:1169-75.
6. R Salani, CL Chang, L Cope, **T-L Wang** (2006) Digital karyotyping: an update of its applications in cancer. ***Mol Diagn Ther.*** 10(4):231-7. (review)
7. K Nakayama, N Nakayama, B Davidson, H Katabuchi, RJ Kurman, VE Velculescu, IM Shih, **T-L Wang** (2006) Homozygous Deletion of MKK4 in Ovarian Serous Carcinoma. ***Cancer Biol Ther*** 5:630-4
8. K Nakayama, N Nakayama, RJ Kurman, L Cope, G Pohl, Y Samuels, VE Velculescu, **T-L Wang***, IM Shih (2006) Sequence mutations and amplification of PIK3CA and AKT2 genes in purified ovarian serous neoplasms. ***Cancer Biol Ther*** 5: 779-785
9. R Salani, B Davidson, M Fiegl, C Marth, E Müller-Holzner, G Gastl, HY Huang, JC Hsiao, HS Lin, **T-L Wang**, BL Lin, IeM Shih (2007) Measurement of cyclin E genomic copy number and strand length in cell-free DNA distinguish malignant versus benign effusions. ***Clin Cancer Res***. 13:5805-9.
10. K Nakayama, N Nakayama, N Jinawath, R Salani, RJ Kurman, IeM Shih, **T-L Wang** (2007) Amplicon profiles in ovarian serous carcinomas**.** ***Int J Cancer*** 120(12):2613-7
11. IeM Shih and **T-L Wang** (2007) Notch signaling, gamma secretase inhibitors and cancer therapy. ***Cancer Res***. 67(5):1879-82. (review)
12. Nakayama K, Nakayama N, Wang TL, Shih IeM (2007) NAC-1 controls cell growth and survival by repressing transcription of Gadd45GIP1, a candidate tumor suppressor. ***Cancer Res*** 67(17):8058-64
13. R Salani, RJ Kurman, R 2nd Giuntoli, G Gardner, R Bristow, **T-L Wang**, IeM Shih (2008) Assessment of TP53 mutation using purified tissue samples of ovarian serous carcinomas reveals a higher mutation rate than previously reported and does not correlate with drug resistance. ***Int J Gynecol Cancer***. 8(3):487-91
14. J J-C Sheu, J H Choi, I Yýldýz, F-J Tsai, Y Shaul, **T-L Wang**, and IeM Shih (2008) Modulating the tumor-promoting functions of Rsf-1 by dimmer formation with hSNF2H. ***Cancer Research*** 68:4050-7

15. J-H Choi, J T Park, B Davidson, P J Morin, IeM Shih, and **T-L Wang** (2008) Jagged-1 and Notch3 juxtacrine loop regulates ovarian tumor growth and adhesion. ***Cancer Research*** 68:5716-23

16. J T Park, IeM Shih, **T-L Wang** (2008) Identification of Pbx1, a potential oncogene, as a Notch3 target gene in ovarian cancer. ***Cancer Research*** 68:8852-60

17. J-H Choi, J J-C Sheu, B Guan, N Jinawath, P Markowski, **Tian-Li Wang**, IeM Shih (2009) Functional analysis of 11q13.5 amplicon identifies Rsf-1 (HBXAP) as a gene involved in paclitaxel resistance in ovarian cancer. ***Cancer Research (in press)***

18. K-T Kuo, T-L Mao, S Jones, E Veras, A Ayhan, **T-L Wang**, Ruth Glas, Dennis Slamon, VE Velculescu, RJ Kurman, IeM Shih (2009) Frequent activating mutations of PIK3CA in ovarian clear cell carcinoma. ***Am J Pathol (in press)***

Amplification of a chromatin remodeling gene, Rsf-1/HBXAP, in ovarian carcinoma

Ie-Ming Shih*†, Jim Jinn-Chyuan Sheu*, Antonio Santillan*, Kentaro Nakayama*, M. Jim Yen*, Robert E. Bristow*, Russell Vang*, Giovanni Parmigiani*‡, Robert J. Kurman*, Claes G. Trope§, Ben Davidson§, and Tian-Li Wang*†

*Departments of Pathology, Gynecology, and Oncology, ‡Department of Biostatistics, The Johns Hopkins University School of Medicine, Baltimore, MD 21231; and §Departments of Pathology and Gynecologic Oncology, Norwegian Radium Hospital, University of Oslo, Montebello, N-0310 Oslo, Norway

Edited by Bert Vogelstein, The Sidney Kimmel Comprehensive Cancer Center at Johns Hopkins, Baltimore, MD, and approved August 15, 2005 (received for review May 20, 2005)

A genomewide technology, digital karyotyping, was used to identify subchromosomal alterations in ovarian cancer. Amplification at 11q13.5 was found in three of seven ovarian carcinomas, and amplicon mapping delineated a 1.8-Mb core of amplification that contained 13 genes. FISH analysis demonstrated amplification of this region in 13.2% of high-grade ovarian carcinomas but not in any of low-grade carcinomas or benign ovarian tumors. Combined genetic and transcriptome analyses showed that Rsf-1 (HBXAPalpha) was the only gene that demonstrated consistent overexpression in all of the tumors harboring the 11q13.5 amplification. Patients with Rsf-1 amplification or overexpression had a significantly shorter overall survival than those without. Overexpression of Rsf-1 gene stimulated cell proliferation and transform nonneoplastic cells by conferring serum-independent and anchorage-independent growth. Furthermore, Rsf-1 gene knockdown inhibited cell growth in OVCAR3 cells, which harbor Rsf-1 amplification. Taken together, these findings indicate an important role of Rsf-1 amplification in ovarian cancer.

digital karyotyping | gene amplification | oncogene

Gene amplification is a common mechanism underlying oncogenic activation in human cancer (1). Amplifications of cyclin E, HER2/neu, AKT2, and L-Myc have been reported in ovarian cancer, and it is expected that many unknown oncogenic amplifications remain to be identified. Recent advances in molecular genetic techniques and the success of the human genome assembly have provided investigators new opportunities to explore cancer genome in great details and to identify novel cancer-associated genes. Digital karyotyping has recently been developed to provide a genomewide analysis of DNA copy number alterations at high resolution (2) and has been applied in cancer genetic studies (3–6). The principle of digital karyotyping is based on extracting and counting the 21-bp sequence tags that represent different loci in human genome. Populations of tags can be directly matched to the unique loci in genome assembly, and digital enumeration of tags provides quantitative measure of DNA copy number along chromosomes. The major advantage of digital karyotyping is that it directly counts the sequence tags, thus providing an unbiased and precise digital readout of DNA copy numbers. The current study has applied this new technology to search for DNA copy number alterations in high-grade ovarian serous carcinoma, the most common and lethal type of ovarian cancer.

Materials and Methods

Tissue Samples. Tissue samples were obtained from the Department of Pathology at The Johns Hopkins Hospital between 1990 and 2004. Effusion (peritoneal and pleural) samples were obtained from the Norwegian Radium Hospital in Norway. All ovarian carcinomas were of serous type from sporadic cases. Acquisition of tissue specimens and clinical information was approved by an institutional review board (The Johns Hopkins University) or by the Regional Ethics Committee (Norway).

Digital Karyotyping. Carcinoma cells were affinity purified by using magnetic beads conjugated with the Epi-CAM antibody (Dynal, Oslo). The purity of tumor cells was confirmed by immunostaining with an anti-cytokeratin antibody, CAM 5.2 (Becton Dickinson, San Jose, CA) and samples with greater than 95% epithelial cells were used in this study. Digital karyotyping library construction and data analysis were performed by following the protocol in refs. 2 and 3. Approximately 120,000 genomic tags were obtained for each digital karyotyping library. After removing the nucleotide repeats in the human genome, the average of filtered tags was 66,000 for each library. We set up a window size of 300 for the analysis in this study. Based on Monte Carlo simulation, the parameters used in this study can reliably detect >0.5-Mb amplicon with >5-fold amplification with >99% sensitivity and 100% positive predictive value.

FISH and Immunohistochemistry. Formalin-fixed, paraffin-embedded tissues were arranged onto tissue microarrays to facilitate FISH analysis. Three representative cores (1.5-mm diameter) from each tumor were placed on the tissue microarrays. Bacterial artificial chromosome clones containing the genomic sequences of the 11q13.5 amplicon at 77.05–77.23 Mb (RP11–1107J12) and EMSY at 75.88–76.09 Mb (CTD-2501F13) were purchased from Bacpac Resources (Children's Hospital Oakland, CA) and Invitrogen (Carlsbad, CA), respectively. The RP11–846G12 bacterial artificial chromosome clone, located at 11q11 (55.88–56.05 Mb), was used as the control probe. The method for FISH has been detailed in ref. 3. Two individuals who were not aware of the tumor grade and clinical information evaluated FISH signals. Approximately 100 tumor cells were examined for each specimen. Amplification of the Rsf-1 and EMSY genes was defined as a ratio of the gene probe signal to the control probe signal exceeding 2.

A mouse monoclonal anti-Rsf-1 antibody (gift from Danny Reinberg, University of Medicine and Dentistry of New Jersey, Piscataway, NJ) was used in the immunohistochemistry study. Immunohistochemistry was performed by standard protocol with an EnVision+System peroxidase kit (DAKO, Carpinteria, CA).

Quantitative Real-Time PCR. Real-time PCR for genomic DNA copy numbers and gene expression levels was performed by using methods described in ref. 7, and PCR primers were listed in the Tables 1 and 2, which are published as supporting information on the PNAS web site. PCR reactions were performed by using an iCycler (Bio-Rad, Hercules, CA). For quantitative PCR performed with genomic DNA, we used a cutoff ratio of 2.2 to define genomic amplification. This cutoff value was determined as the mean + 2 standard deviations based on quantitative PCR analyses of normal

This paper was submitted directly (Track II) to the PNAS office.

Abbreviations: OSE, ovarian surface epithelial; shRNA, short hairpin RNA; siRNA, short interfering RNA.

†To whom correspondence may be addressed. E-mail: tlw@jhmi.edu and shihie@yahoo.com.

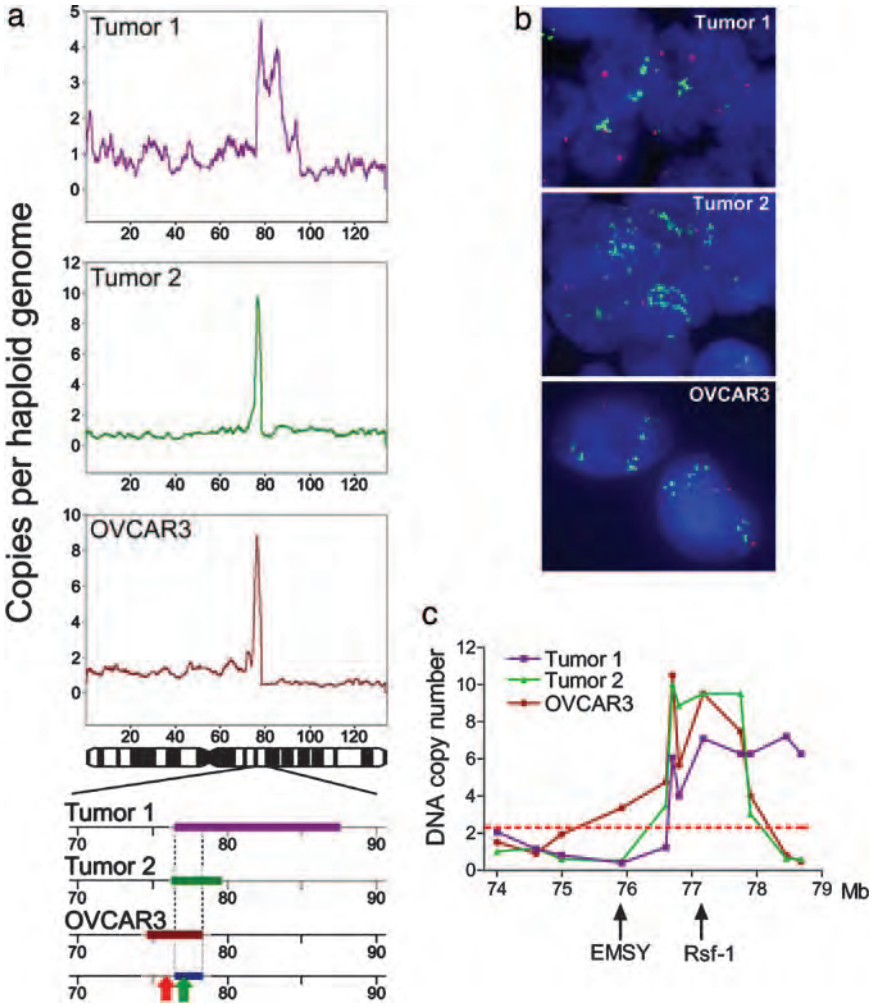

Fig. 1. Identification of the 11q13.5 amplicon in ovarian cancers. (*a*) Digital karyotyping identified three ovarian carcinomas that contained discrete amplifications at 11q13.5 region. Alignment of the amplicons revealed a common region of amplification (blue line in *Bottom*) spanning from 76.6 Mb to 78.4 Mb at chromosome 11q. Red and green arrows indicate the physical locations of EMSY and Rsf-1, respectively. (*b*) Validation of 11q13.5 amplification was performed by FISH analysis in the same three tumors by using a probe (green) located within the minimal amplicon of 11q13.5 and a control probe (red) located at 11q11 (21 Mb centromeric to the minimal amplicon). (*c*) 11q13.5 amplification was further validated in the three tumors by using quantitative real-time PCR on genomic DNA. For each tumor, an increase in the DNA copy number (*y* axis) is present at a specific subchromosomal region that corresponds to the amplification identified by digital karyotyping. The dashed line indicates a cutoff of 2.2 that represents the threshold for amplification with a confidence level of 97.5%.

diploid cells by using all of the primer sets. This cutoff value gave a confidence level of 97.5%.

Cell Proliferation Assay. Cells were seeded in 96-well plates at a density of 4,000 cells per well. The cell number was determined indirectly by the fluorescence intensity of SYBR Green I nucleic acid gel stain (Molecular Probes, Eugene, OR) by using a microplate reader (Fluostar, BMG, Durham, NC). Data were expressed as the mean ± 1 standard deviation from five replicates in each experimental group. Anchorage-independent growth assay was performed as described in ref. 8. Data were expressed as the mean ± 1 standard deviation from triplicates.

Short Interfering RNA (siRNA)-Mediated Knockdown of Rsf-1 Expression. Three siRNAs that targeted Rsf-1 were designed and their sense sequences were as follows: GGAAAGACAUCUCUACUAUUU, UAAAUGAUCUGGACAGUGAUU, and GGACUUACCUUCAACCAAUUU. Control siRNA (off-target control, catalog no. D-001210-02-05) was purchased from Dharmacon (Lafayette, CO). Cells were seeded in 96 wells and transfected with siRNAs by using oligofectamine (Invitrogen). BrdUrd uptake and staining were performed by using a cell proliferation kit (Amersham Pharmacia, Buckinghamshire, U.K.). Apoptotic cells were detected by using an annexin V staining kit (BioVision, Mountain View, CA). The percentage of BrdUrd-positive and annexin V positive cells was determined by counting ≈300 cells from each well in 96-well plates. The data were expressed as mean ± 1 standard deviation from triplicates.

Statistical Method for Clinical Correlation. Overall survival was calculated from the date of the primary surgery for ovarian tumors to the date of death or last followup. Patients with Rsf-1 amplification and without amplification had similar age distributions and received optimal tumor debulking surgery, followed by carboplatin and taxol-based chemotherapy. The data were plotted as Kaplan–Meier curves, and the statistical significance was determined by the Log-rank test. Data were censored when patients were lost to followup. In a Cox proportional hazard model, the *P* values were assessed by using a likelihood ratio test as implemented by the "survival" package in the statistical programming language R (www.r-project.org). Student *t* test was used to examine the statistical significance in the difference of growth assay data.

Results

Digital Karyotyping of Ovarian Carcinomas. Digital karyotyping was used to evaluate the genomic alterations in seven ovarian cancer samples, including six high-grade ovarian serous carcinomas and one ovarian cancer cell line, OVCAR3. Analysis of the genomic tag densities along chromosomes revealed a discrete amplification at chromosome 11q13.5 in three libraries, including two high-grade ovarian carcinomas and the OVCAR3 cell line. No evidence of other amplification cores was detected in chromosome 11 in any of the ovarian cancer libraries (Fig. 6, which is published as supporting information on the PNAS web site). Alignment of these three amplicons delineated an overlapping region of amplification, spanning from 76.6 to 78.4 Mb on the chromosome 11q (Fig. 1*a*). Examination of the RefSeq database in the human genome assem-

bly (July 2003 freeze, University of California, Santa Cruz) revealed that 13 genes were completely located within the minimal amplicon (Fig. 7, which is published as supporting information on the PNAS web site). EMSY gene, which has recently been reported as a candidate oncogene in breast and ovarian carcinomas, was located at 76 Mb (9), close to but outside the minimal region of the amplification (Fig. 1*a*). Two methods were used to validate the digital karyotyping results. First, dual-color FISH was performed to validate the 11q13.5 amplification in these three tumors by using a bacterial artificial chromosomes probe located at the 11q13.5 minimal amplicon (Fig. 7) and a control probe located at 11q11 (21 Mb centromeric to the minimal amplicon). As shown in Fig. 1*b*, we found that all three amplified tumors defined by digital karyotyping showed distinct 11q13.5 amplification. Second, quantitative real-time PCR was performed to measure the DNA copy numbers at 12 loci flanking and within the amplicon, including the EMSY gene in these three tumors (Fig. 1*c*). We found that increases in the DNA copy number were present at subchromosomal regions similar to the amplifications delineated by digital karyotyping. Furthermore, the fold of DNA copy number increase detected by quantitative PCR is at similar levels to that of digital karyotyping. A cutoff ratio of 2.2 was used to search for amplifications with >97.5% confidence, and the delineated common region of amplification (from Loc220032 locus to FLJ23441 locus) was consistent with that derived from digital karyotyping.

To determine the frequency of the 11q13.5 minimal amplicon, we performed dual-color FISH on 211 paraffin-embedded ovarian tissue specimens by using the FISH probe located at the minimal amplicon and the control FISH probe that is the same as described above (located on 11q11). The advantage of selecting the control FISH probe on the same chromosomal arm as the minimal amplicon is that it could facilitate distinguishing chromosome duplication from gene amplification, the latter involving smaller subchromosomal region (10). Using this method, we found 11q13.5 amplification in 16 of 121 (13.2%) high-grade serous carcinomas. In contrast, 11q13.5 gene amplification was not detected in any of 40 low-grade serous carcinomas, 14 serous borderline tumors, 19 benign cystadenomas, and 17 normal ovaries. Thus, 11q13.5 amplification was detected exclusively in high-grade serous carcinomas. Among the 16 tumors with 11q13.5 amplification, 5 cases showed a homogeneous staining region pattern, 3 cases showed a high level gain (>4.5-fold), and the remaining 8 tumors exhibited a moderate gain (between 2.5- and 4-fold). It should be noted that in addition to the 16 tumors with discrete amplification, we observed 11q polysomy in another 14 tumors based on an equal number of signals for both 11q13.5 and control probes. These tumors were not considered to have amplification specific to the 11q13.5 region in this study.

To further elucidate the physical relationship between EMSY and the minimal amplicon, we performed dual-color FISH in the same set of tumor samples by using EMSY probe and same control probe. We found that EMSY was amplified in 12 of 117 (10.3%) high-grade serous carcinomas that were available for analysis. All 12 EMSY amplified carcinomas also demonstrated amplification at 11q13.5 minimal amplicon. Conversely, 4 of the 16 carcinomas that contained 11q13.5 minimal region amplification did not harbor EMSY amplification (Fig. 8, which is published as supporting information on the PNAS web site). This result indicated that 11q13.5 minimal amplicon is more frequently amplified than its neighborhood region that contained EMSY gene in high-grade serous carcinomas.

Transcript Analysis of the 11q13.5 Minimal Amplicon. To identify the potential amplified oncogene within the 11q13.5 amplicon, we applied an approach based on the rationale that a tumor-driving gene, when amplified, almost always overexpresses to activate the tumorigenic pathway, whereas coamplified "passenger" genes that are unrelated to tumor development may or may not do so (10).

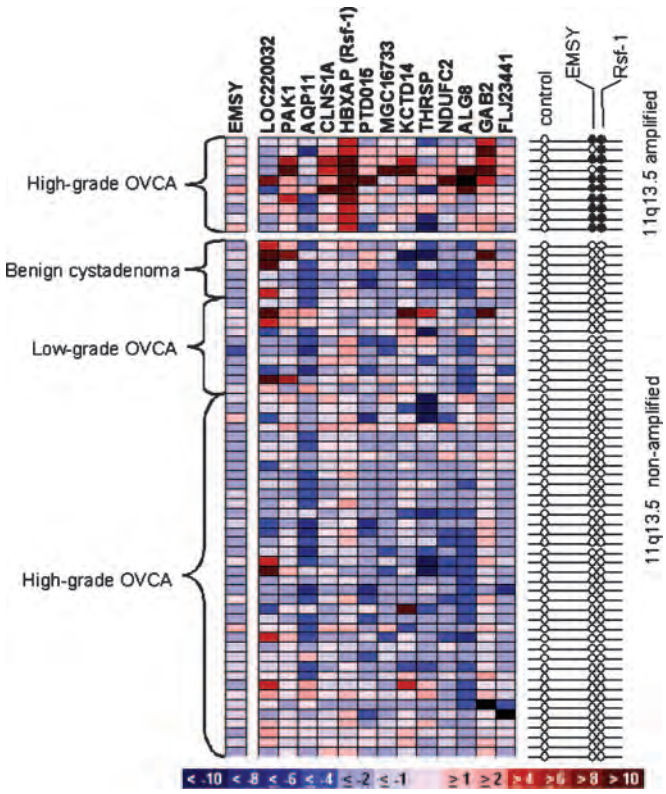

Fig. 2. Gene expression analysis of the 11q13.5 amplicon in ovarian tumors. Quantitative real-time PCR was performed for all 13 genes located within the minimal amplicon in benign cystadenomas, low-grade ovarian carcinomas and high-grade ovarian carcinomas with or without 11q13.5 amplification. The expression level of each gene (left to right: centromeric to telomeric) in individual specimen is shown as a pseudocolor gradient based on the relative expression level of a given specimen to the normal ovarian surface epithelium. (*Right*) The amplification status of Rsf-1, EMSY, and the 11q11 (control locus for FISH) for each specimen was determined by FISH analysis. Filled circles indicate amplification, and open circles indicate no amplification.

Therefore, we searched for genes with both DNA amplification and transcript up-regulation in the same tumor samples. Ten high-grade ovarian carcinomas that contained 11q13.5 amplification and had their frozen tissues available were analyzed by quantitative real-time PCR to assess mRNA levels in all of the genes within the minimal amplicon. The same assay was also performed in six benign cystadenomas, 10 serous borderline tumors, and 36 high-grade carcinomas that did not contain 11q13.5 amplification. Freshly brushed ovarian surface epithelium (kind gift from M. J. Birrer, National Cancer Institute, Rockville, MD), which has been considered as an appropriate normal control, was used for normalization of gene expression (11). We used the Wilcoxon test to compute and compare the difference in gene expression levels between 11q13.5 amplified versus nonamplified high-grade carcinomas. We found that among the genes within the minimal amplicon, Rsf-1 (HBXAP) had the most significant difference ($P = 8.5 \times 10^{-6}$) in expression levels between 11q13.5 amplified and nonamplified specimens. Furthermore, Rsf-1 was the only gene demonstrating consistent overexpression among the amplified tumors. Accordingly, Rsf-1 was prioritized for further characterization in this study. EMSY mRNA levels were also measured in parallel. We observed that although the EMSY gene was coamplified in eight of the tested samples, its RNA level was not consistently up-regulated as five of the tumors that harbored EMSY amplification down-regulated EMSY mRNA expression (Fig. 2).

Correlation of Rsf-1 Protein Overexpression and Gene Amplification. To demonstrate a more comprehensive correlation between Rsf-1 gene amplification and protein expression, we performed immu-

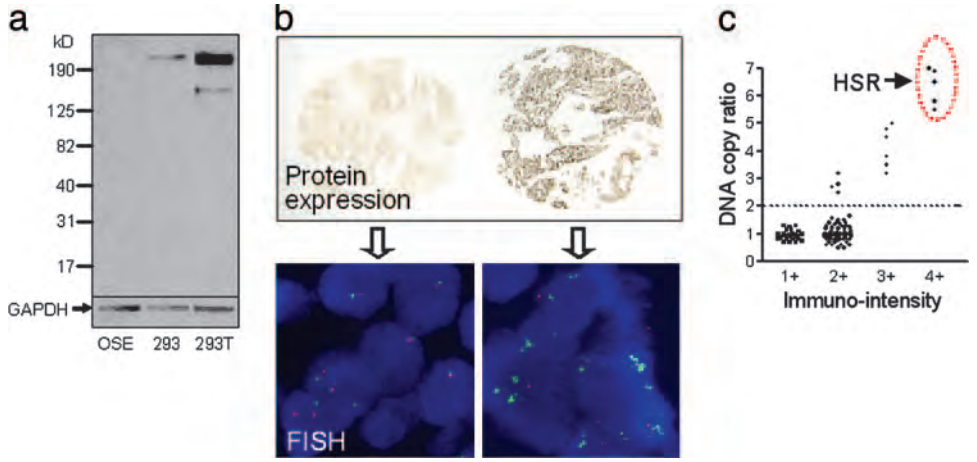

Fig. 3. Correlation of Rsf-1 DNA copy numbers and Rsf-1 protein expression in high-grade ovarian carcinomas. (*a*) The specificity of the anti-Rsf-1 antibody is demonstrated by Western blot analysis. 293, human embryonic kidney (HEK) 293 cells; 293T, HEK293 cells transfected with a full-length Rsf-1 gene. A predominant band of Rsf-1 protein at 215 kDa that represents the full-length Rsf-1 gene is detected in 293T cells. The faint lower band represents the degradation product of Rsf-1 protein. Endogenous Rsf-1 expression is also observed in 293 cells but not in OSE cells. (*Lower*) The GAPDH expression as the loading control. (*b Left*) A high-grade carcinoma shows weak Rsf-1 immunoreactivity (1+) and does not display Rsf-1 gene amplification. (*Right*) A high-grade tumor demonstrates an intense Rsf-1 immunoreactivity (4+) and displays Rsf-1 gene amplification. (*c*) Rsf-1 protein expression correlates with the Rsf-1 gene copy number in high-grade ovarian carcinomas. Tumors with the highest copy number of Rsf-1 DNA [manifested as homogenous staining regions (HSR)] express the highest level of Rsf-1 protein (4+). Tumors that lack Rsf-1 amplification demonstrate weak to moderate Rsf-1 immunoreactivity (1+ and 2+). Each dot represents an individual specimen. Among 16 amplified tumors, there are 15 available for immunohistochemistry.

nohistochemistry with an anti-Rsf-1 monoclonal antibody on the same panel of tissues used in FISH analysis. The specificity of the Rsf-1 monoclonal antibody has been demonstrated in ref. 12 and was independently confirmed in this study (Fig. 3*a*). Overall, there was a statistically significant correlation between Rsf-1 gene amplification and Rsf-1 immunoreactivity ($P < 0.001$, Spearman correlation). We found that 11q13.5 nonamplified tumors demonstrated either weak (1+, 21% of tumors) or moderate (2+, 74% of tumors) Rsf-1 immunoreactivity (Fig. 3 *b* and *c*). In contrast, all of the tumors with Rsf-1 amplification demonstrated an immunointensity of 2+-4+, with the most intense immunoreactivity (4+) found in those with a homogeneous staining region pattern ($n = 5$) and a strong immunoreactivity (3+, $n = 6$) found in those with high-fold DNA gain (3- to 5-fold) (Fig. 3 *b* and *c*). Four tumors with mild gain (2- to 3.5-fold) in the Rsf-1 DNA copy number demonstrated moderate immunointensity (2+), and, thus, they were similar to the majority of the high-grade tumors without Rsf-1 amplification. This finding is likely attributed to the semiquantitative nature inherent to immunohistochemistry in scoring mild to moderate immunointensity because such limitation in scoring Her2/neu immunointensity has been reported in ref. 13.

Clinical Significance of 11q13.5 Amplification and Rsf-1 Overexpression. Amplification of the Rsf-1 locus and Rsf-1 overexpression were correlated with clinical outcome in patients with high-grade ovarian serous carcinoma. Because the FISH probe used to assess 11q13.5 amplification contained the whole Rsf-1 coding region (Fig. 7), it allowed us to use the same FISH data and analyze the clinical significance of Rsf-1 amplification. A total of 107 of 121 patients were available for survival analysis. The other 14 tumors harboring chromosome11q polysomy were excluded in the analysis because polysomy was considered as duplication of chromosomal arms or large genomic segments and could not simply be grouped to either Rsf-1 amplified or nonamplified cases.

We found that all 107 patients had advanced stage high-grade serous carcinomas (the majority at FIGO stage III). Among them, 16 patients who had Rsf-1 amplification in their tumors had a shorter overall survival compared with those without amplification ($P = 0.015$; Log rank test) (Fig. 4*a*). The median overall survival was 29 months [95% confidence index (CI): 18.8–39.1 months] for the amplified group and 36 months (95% CI: 24.3–47.7 months) for the nonamplified group. Quantitative real-time PCR was also used to measure Rsf-1 mRNA in tumor cell pellets from 53 effusion samples that were not feasible for FISH analysis. An arbitrary cutoff of the expression level (>2.4 fold compared with normal ovarian surface epithelium) was used to assign specimens to either high expression ($n = 11$) or low expression ($n = 42$) groups. The results indicated that high levels of Rsf-1 mRNA expression (>2.4 fold) were correlated with poor outcome ($P = 0.037$; Log rank test) (Fig. 4*b*) with median overall survival of 19 months (95% CI: 14.5–23.6) in patients with Rsf-1 mRNA overexpression and 38 months (95% CI: 28.3–47.8) in patients without Rsf-1 mRNA overexpression. Rsf-1 amplification and overexpression appeared as independent prognostic factors based on a multivariate analysis adjusted for patient age, clinical stage, and differentiation status of tumor histology.

To further test whether the clinical significance of Rsf-1 amplification and overexpression depended on the arbitrary cutoffs, we performed a survival analysis by using continuous variables in a Cox proportional hazard model. The *P* values assessed by a likelihood

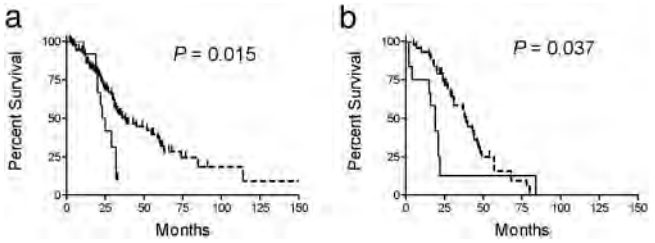

Fig. 4. Rsf-1 amplification and overexpression correlate with shorter overall survival in patients. (*a*) Kaplan–Meier survival analysis shows that Rsf-1 amplification (solid line, $n = 16$) is associated with a shorter overall survival compared with tumors without Rsf-1 amplification (dashed line, $n = 91$) ($P = 0.015$, Log-rank test). (*b*) Quantitative real-time PCR in effusion samples of ovarian high-grade serous carcinomas demonstrates that Rsf-1 overexpression (> 2.4 fold of normal ovarian surface epithelium; solid line; $n = 11$) correlates significantly with shorter overall survival than those with a low expression level (< 2.4 fold; dash line; $n = 42$) ($P = 0.037$, Log-rank test).

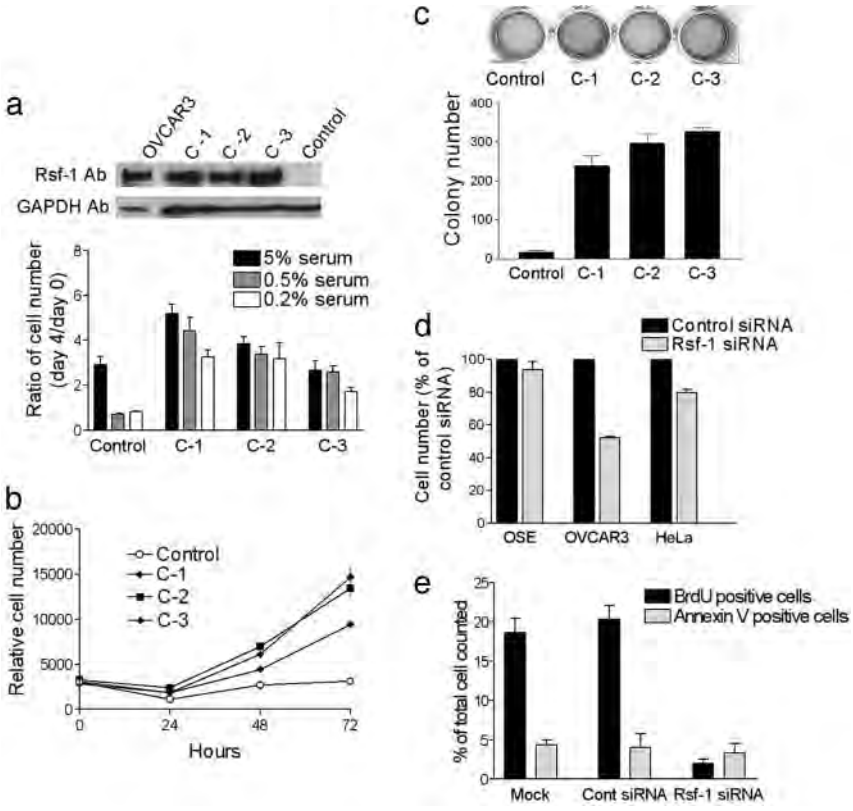

Fig. 5. Functional analyses of Rsf-1 expression. (*a*) Western blot analysis shows that Rsf-1-transfected RK3E clones (C-1, -2, and -3) express Rsf-1 protein with a predominant molecular mass of 215 kDa that is similar to the endogenous Rsf-1 protein expressed in OVCAR3 cells. Control RK3E cells, which are transfected with an empty vector, do not express Rsf-1 protein. As compared with the control RK3E cells, Rsf-1 clones continue proliferating at low serum concentrations (0.5% and 0.2%). (*b*) The Rsf-1 clones demonstrate a higher proliferative activity than the vector only control, as evidenced by a time-dependent increase in cell number at low (0.5%) serum-containing medium. (*c*) Anchorage-independent assay demonstrates that colonies observed in the Rsf-1 clones are more than those in the vector only control. (*d*) Effects of Rsf-1 gene knockdown. Knockdown of Rsf-1 significantly reduces cell number in OVCAR3 cells that harbor Rsf-1 amplification and in HeLa cells that express Rsf-1. In contrast, Rsf-1 siRNA has only a minimal effect on cell growth in OSE cells that do not express detectable Rsf-1. (*e*) Rsf-1 targeting siRNA reduces cell proliferation as measured by the percentage of BrdUrd-positive cells but not in control siRNA or in nontreated (mock control) OVCAR3 cells. The percentage of apoptotic cells as measured by annexin V staining is similar among Rsf-1 siRNA, control siRNA, and nontreated OVCAR3 cells.

ratio test were 0.025 for FISH assay and 0.0013 for real-time PCR. These results further indicated that Rsf-1 amplification and overexpression were significantly correlated with poor survival, independent of the cutoffs.

In this study, we further compared the statistical significance in correlating gene amplification and overexpression with overall survival of Rsf-1 gene to those of EMSY gene. For gene amplification, Rsf-1 had a more significant P value than that of EMSY (0.015 vs. 0.08). Similarly, for gene expression, Rsf-1 expression also had a more significant P value than EMSY expression by using a low stringent cutoff value of >1-fold (0.037 vs. 0.153).

Functional Analyses of Rsf-1 Expression. We therefore stably expressed the Rsf-1 gene in the nonneoplastic epithelial cells, RK3E, to assess whether Rsf-1 expression induced transformation (*Supporting Methods*, which is published as supporting information on the PNAS web site). RK3E cells have been used to evaluate the oncogenic potential of GL1, c-Myc, and mutant β-catenin and were considered as an appropriate *in vitro* model for oncogenic transformation (14–16). Using quantitative real-time PCR, we found that ovarian serous carcinomas predominantly expressed the full-length form of the Rsf-1 gene (or HBXAPa), therefore RK3E cells were transfected with a vector expressing the full-length Rsf-1, and three independent clones were randomly selected for functional analyses. Western blot analysis confirmed the Rsf-1 expression in these clones (Fig. 5*a*). All of the Rsf-1-expressing clones proliferated better at very low (0.2% and 0.5%) serum concentrations and showed a higher proliferative activity than control RK3E cells (transfected with vector alone) based on increased cell numbers (Fig. 5 *a* and *b*) and BrdUrd incorporation (data not shown). Rsf-1-expressing clones grew anchorage independently as more colonies were observed in Rsf-1-expressing cells than in control cells (Fig. 5*c*). All of the above differences were of statistical significance ($P < 0.001$, t test).

To further determine whether Rsf-1 expression was essential for cell survival in cell lines that overexpress Rsf-1, we used RNA interference to knock down Rsf-1 expression in three cell lines, including OVCAR3 cells (with Rsf-1 amplification and overexpression), HeLa cells (without amplification but with Rsf-1 expression), and ovarian surface epithelial (OSE; without Rsf-1 amplification or expression) cells. The effect of Rsf-1 siRNA in suppressing Rsf-1 expression was confirmed by quantitative real-time PCR (Fig. 9, which is published as supporting information on the PNAS web site). Reduction of Rsf-1 expression significantly inhibited cell growth in Rsf-1-expressing cells, including OVCAR3 and HeLa cells (Fig. 5*d*, $P < 0.001$, t test), with a more prominent inhibitory effect in Rsf-1 amplified OVCAR3 cells. In contrast, the same treatment did not affect cell growth in OSE cells, which had minimal Rsf-1 expression ($P = 0.26$, t test). The inhibition of cell growth after repressing Rsf-1 expression in OVCAR3 was likely a result of growth suppression as the percentage of BrdUrd-labeled cells was significantly decreased in Rsf-1 siRNA-treated cells as compared with control siRNA-treated OVCAR3 cells (Fig. 5*e*, $P < 0.001$). In contrast, the percentage of apoptotic cells as measured by annexin V staining was similar between the Rsf-1 siRNA and control groups. To extend the findings of Rsf-1 gene knockdown *in vitro*, we transfected OVCAR3 cells with Rsf-1 short hairpin RNA (shRNA) before injecting the cells into nude mice (*Supporting Methods*). Western blot analysis demonstrated that Rsf-1 expression was substantially reduced in Rsf-1 shRNA-transfected OVCAR3 cells as compared with the control shRNA-transfected cells (Fig. 10, which is published as supporting information on the PNAS web site). All mice injected with Rsf-1 shRNA-treated OVCAR3 cells develop much smaller intraabdominal xenograft tumors than the mice carrying control (scramble) shRNA-transfected cells (Fig. 10, $P < 0.001$, $n = 5$).

Discussion

This study provides cogent evidence that amplification of Rsf-1 within the 11q13.5 minimal amplicon is involved in ovarian

tumorigenesis based on a comprehensive study including molecular genetics, transcriptome analysis, clinical correlation, and functional characterization. Chromosome 11q13.5 amplification is one of the most frequently amplified regions in human tumors including ovarian, breast, head, and neck carcinomas. The frequency of 11q13.5 amplification in ovarian carcinoma detected in this study (13.2%) is similar to but slightly lower than that previously reported (17%) (9). This result is likely due to more stringent criteria used for FISH analysis in the current study. For example, we have used a reference probe on chromosome 11q arm instead of on chromosome 11 centromere to exclude cases that belong to polysomy or large segment duplication. It should be noted that EMSY was located near the minimal amplicon delineated in the current study. EMSY functions as a BRAC2-interacting gene and was previously thought of as a candidate oncogene for ovarian cancers (9). However, the oncogenic property of EMSY in ovarian tumor was not demonstrated in that study. Furthermore, our findings with a larger scale of ovarian tumor samples did not demonstrate a significant correlation of EMSY gene amplification and mRNA overexpression, a finding arguing against EMSY as the "driver" gene within the amplicon.

Based on our combined genetic and expression analyses, we have found that Rsf-1 is consistently overexpressed in all of the amplified tumors examined. In addition to Rsf-1, several other genes close to Rsf-1, including CLNS1A, ALG8, and GAB2, were coup-regulated in a subset of tumors with 11q13.5 amplification. It would be interesting in the future to determine whether cooverexpression of these genes would further provide growth advantages in the development of ovarian cancer. The association of Rsf-1 amplification/overexpression with worse survival in ovarian cancer patient is similar to oncogenes, including HER2/neu in breast cancer (17, 18) and N-myc in neuroblastoma (19), in which overexpression of both oncogenes stimulates cell proliferation and confers a shorter survival. The mechanism of how Rsf-1 amplification contributes to shorter survival is not known; however, because the mortality of ovarian cancer patients is directly related to the recurrent disease after chemotherapy, it is conceivable that Rsf-1 amplification may confer drug resistance and/or enhance cell proliferation in the chemoresistant recurrent tumors.

Our study with gene overexpression and RNA interference knockdown has established an important functional role of Rsf-1 in ovarian cancer. How can Rsf-1 contribute to tumor progression at the molecular level? Recent *in vitro* studies have indicated that Rsf-1 plays a role in chromatin remodeling (12) and transcriptional regulation (20, 21) that may contribute to tumorigenesis. Rsf-1 has been shown to function as a histone chaperone, whereas its binding partner, hSNF2H, possesses nucleosome-dependent ATPase activity. The Rsf-1/hSNF2H complex (or RSF complex) participates in chromatin remodeling by mobilizing nucleosomes in response to a variety of growth modifying signals and environmental cues. Such nucleosome remodeling is essential for transcriptional activation or repression (22), DNA replication (23), and cell cycle progression (24). Recently, a growing body of evidences has accumulated to support a novel role of chromatin remodeling in cancer (25, 26). For example, mutations and deletions of a hSNF2H homolog, Brg1, were found in different tumor types (27), and furthermore, heterozygous deletion of Brg1 in mice resulted in a cancer-prone phenotype (28, 29). It is plausible that Rsf-1 gene amplification and overexpression in tumor cells could disrupt the homeostatic kinetics in the chromatin remodeling machinery and fine tune gene regulation that facilitates tumorigenesis. Because the current study identifies and characterizes the previously undescribed Rsf-1 gene amplification in ovarian cancer, further studies are required to elucidate the etiological roles of Rsf-1 amplification and overexpression in chromatin remodeling and cancer development.

We thank Dr. M. J. Birrer for the brushed normal ovarian epithelium; Dr. D. Reinberg for the full-length Rsf-1 clone and the anti-Rsf-1 antibody; Drs. M. Shamay and Y. Shaul for the help at the initial stage of this study; Dr. Z. Wang and other members in the Molecular Genetic Laboratory for critical reading of the manuscript; and M. Skrede and Dr. Y.-W. Kim for technical assistance. This work was supported by U.S. Department of Defense Grants OC0400600 and OC010017, National Institutes of Health Grant R01 CA103937, and grants from The Alexander and Margaret Stewart Trust fund and The Richard TeLinde Endowed Fund.

1. Meltzer, P. S., Kallioniemi, A. & Trent, J. M. (2002) in *The Genetic Basis of Human Cancer*, eds. Vogelstein, B. & Kinzler, K. W. (McGraw–Hill, New York), pp. 93–113.
2. Wang, T.-L., Maierhofer, C., Speicher, M. R., Lengauer, C., Vogelstein, B., Kinzler, K. W. & Velculescu, V. E. (2002) *Proc. Natl. Acad. Sci. USA* **99,** 16156–16161.
3. Wang, T.-L., Diaz, L. A., Jr., Romans, K., Bardelli, A., Saha, S., Galizia, G., Choti, M., Donehower, R., Parmigiani, G., Shih, I.-M., *et al.* (2004) *Proc. Natl. Acad. Sci. USA* **101,** 3089–3094.
4. Di, C., Liao, S., Adamson, D. C., Parrett, T. J., Broderick, D. K., Shi, Q., Lengauer, C., Cummins, J. M., Velculescu, V. E., Fults, D. W., *et al.* (2005) *Cancer Res.* **65,** 919–924.
5. Hu, M., Yao, J., Cai, L., Bachman, K. E., van den Brule, F., Velculescu, V. & Polyak, K. (2005) *Nat. Genet.* **37,** 899–905.
6. Boon, K., Eberhart, C. G. & Riggins, G. J. (2005) *Cancer Res.* **65,** 703–707.
7. Buckhaults, P., Zhang, Z., Chen, Y. C., Wang, T.-L., St. Croix, B., Saha, S., Bardelli, A., Morin, P. J., Polyak, K., Hruban, R. H., *et al.* (2003) *Cancer Res.* **63,** 4144–4149.
8. Shih, I.-M., Yu, J., He, T. C., Vogelstein, B. & Kinzler, K. W. (2000) *Cancer Res.* **60,** 1671–1676.
9. Hughes-Davies, L., Huntsman, D., Ruas, M., Fuks, F., Bye, J., Chin, S. F., Milner, J., Brown, L. A., Hsu, F., Gilks, B., *et al.* (2003) *Cell* **115,** 523–535.
10. Hogarty, M. D. & Brodeur, G. M. (2002) in *The Genetic Basis of Human Cancer*, eds. Vogelstein, B. & Kinzler, K. W. (McGraw–Hill, New York), pp. 115–128.
11. Zorn, K. K., Jazaeri, A. A., Awtrey, C. S., Gardner, G. J., Mok, S. C., Boyd, J. & Birrer, M. J. (2003) *Clin. Cancer Res.* **9,** 4811–4818.
12. Loyola, A., Huang, J.-Y., LeRoy, G., Hu, S., Wang, Y.-H., Donnelly, R. J., Lane, W. S., Lee, S.-C. & Reinberg, D. (2003) *Mol. Cell. Biol.* **23,** 6759–6768.
13. Hicks, D. G. & Tubbs, R. R. (2005) *Hum. Pathol.* **36,** 250–261.
14. Ruppert, J. M., Vogelstein, B. & Kinzler, K. W. (1991) *Mol. Cell. Biol.* **11,** 1724–1728.
15. Foster, K. W., Ren, S., Louro, I. D., Lobo-Ruppert, S. M., McKie-Bell, P., Grizzle, W., Hayes, M. R., Broker, T. R., Chow, L. T. & Ruppert, J. M. (1999) *Cell Growth Differ.* **10,** 423–434.
16. Kolligs, F. T., Hu, G., Dang, C. V. & Fearon, E. R. (1999) *Mol. Cell. Biol.* **19,** 5696–5706.
17. Borg, A., Tandon, A. K., Sigurdsson, H., Clark, G. M., Ferno, M., Fuqua, S. A., Killander, D. & McGuire, W. L. (1990) *Cancer Res.* **50,** 4332–4337.
18. Tsuda, H., Hirohashi, S., Shimosato, Y., Hirota, T., Tsugane, S., Yamamoto, H., Miyajima, N., Toyoshima, K., Yamamoto, T., Yokota, J., *et al.* (1989) *Cancer Res.* **49,** 3104–3108.
19. Rubie, H., Hartmann, O., Michon, J., Frappaz, D., Coze, C., Chastagner, P., Baranzelli, M. C., Plantaz, D., Avet-Loiseau, H., Benard, J., *et al.* (1997) *J. Clin. Oncol.* **15,** 1171–1182.
20. Shamay, M., Barak, O., Doitsh, G., Ben-Dor, I. & Shaul, Y. (2002) *J. Biol. Chem.* **277,** 9982–9988.
21. Shamay, M., Barak, O. & Shaul, Y. (2002) *Genomics* **79,** 523–529.
22. Vignali, M., Hassan, A.H., Neely, K. E. & Workman, J. L. (2000) *Mol. Cell. Biol.* **20,** 1899–1910.
23. Flanagan, J. F. & Peterson, C. L. (1999) *Nucleic Acids Res.* **27,** 2022–2028.
24. Cosma, M. P., Tanaka, T. & Nasmyth, K. (1999) *Cell* **97,** 299–311.
25. Wolffe, A. P. (2001) *Oncogene* **20,** 2988–2990.
26. Klochendler-Yeivin, A., Muchardt, C. & Yaniv, M. (2002) *Curr. Opin. Genet. Dev.* **12,** 73–79.
27. Wong, A. K., Shanahan, F., Chen, Y., Lian, L., Ha, P., Hendricks, K., Ghaffari, S., Iliev, D., Penn, B., Woodland, A. M., *et al.* (2000) *Cancer Res.* **60,** 6171–6177.
28. Klochendler-Yeivin, A., Fiette, L., Barra, J., Muchardt, C., Babinet, C. & Yaniv, M. (2000) *EMBO Rep.* **1,** 500–506.
29. Guidi, C. J., Sands, A. T., Zambrowicz, B. P., Turner, T. K., Demers, D. A., Webster, W., Smith, T. W., Imbalzano, A. N. & Jones, S. N. (2001) *Mol. Cell. Biol.* **21,** 3598–3603.

Apply innovative technologies to explore cancer genome

Ie-Ming Shih and Tian-Li Wang

Purpose of review
Molecular genetic alterations characterize the development of human cancer. Recent advances in molecular genetic technology and the success of the human genome project have empowered investigators with new tools in dissecting the cancer genome for discovery of new cancer-associated genes. The purpose of this review is to highlight the emerging molecular genetic methodologies and summarize their principles, applications, and potential technical challenges. The critical issue in sample preparation and a strategy that combines different molecular techniques to facilitate the identification of novel cancer-associated genes will be discussed.

Recent findings
Digital karyotyping and array-based techniques including array comparative genomic hybridization and representational oligonucleotide microarray analysis have been recently developed to study the genomic landscape in human cancer. These innovations provide tools to quantitatively measure DNA copy number changes in cancer and to map those changes directly onto the human genome. Digital karyotyping is based on counting the sequence tags that are distributed in the human genome and thus, it provides a digital readout to precisely outline the amplified and deleted chromosomal regions. Array-based technologies, on the other hand, compare the content of cancer and reference genomes followed by localizing the amplified or deleted signals in chromosomal regions using an array hybridization technique. In addition, a high-throughput mutational analysis platform has been available for a large-scale mutational analysis by using an automated capillary sequencing device and sophisticated bioinformatic tools. A number of examples have demonstrated the promise of these new molecular genetic approaches in identifying several potential new oncogenes and tumor suppressors.

Summary
As compared with conventional cytogenetics methods, digital karyotyping, array comparative genomic hybridization, and representational oligonucleotide microarray analysis provide an unprecedented mapping resolution that allows a precise localization of the amplified and deleted chromosomal regions. These technologies can be combined with gene expression profiling and high-throughput mutational analysis to facilitate the search for new cancer-associated genes. It is expected that applying these new technologies will lead to discovery of a host of novel oncogenes and tumor suppressors, which will have a significant impact in our understanding of tumorigenesis and in the clinical management of cancer patients.

Keywords
cancer genome, amplification, deletion, mutation, digital karyotyping, array comparative genomic hybridization, representational oligonucleotide microarray analysis

Curr Opin Oncol 17:33–38. © 2004 Lippincott Williams & Wilkins.

Gynecological Cancer Genomic Laboratory, Departments of Pathology, Oncology, Gynecology and Obstetrics, Johns Hopkins Medical Institutions, Baltimore, Maryland, USA

Correspondence to Tian-Li Wang, Johns Hopkins Medical Institutions, 1503 E. Jefferson Street, B-317, Baltimore, MD 21231, USA
Tel: 410 502 7774; fax: 410 502 7943; e-mail: tlw@jhmi.edu

This work is supported by a DoD grant (OC040060).

Current Opinion in Oncology 2005, 17:33–38

Abbreviations

CGH	comparative genomic hybridization
ROMA	representational oligonucleotide microarray analysis

1040-8746

Introduction

It is well known that tumors develop as a result of accumulated molecular genetic or genomic alterations including amplification, deletion, point mutation, and translocation [1]. Analysis of molecular genetic changes has historically led to identification of oncogenes and tumor suppressors. For example, characterization of amplified regions of the breast cancer genome has revealed several important oncogenes including Her-2/neu and c-Myc. Studies of these alterations are critical to understanding the molecular basis of cancer and providing potential diagnostic/outcome markers and therapeutic targets for cancer patients [1,2]. For example, amplification of cyclin E and Her2/neu is frequently associated with advanced stages of disease and a poor clinical outcome in ovarian cancer patients [3–5]. Antagonizing the oncogenic function using the anti-Her2/neu antibody therapy (trastuzumab; Herceptin, Genentech, CA, USA) prolongs the disease-free interval in patients

with Her2/neu gene amplification [6]. Although several oncogenes and tumor suppressors have been studied in past decades, many oncogenes and tumor suppressors remain to be identified.

The rate-limiting step in discovering new oncogenes and tumor suppressors has been the lack of effective approaches for their discovery. Several elegant studies have used gene expression profiling as the discovery tool and have identified myriad candidate markers associated with different types of cancer [7,8]. However, the challenge is how to use such an expression-based approach alone to distinguish the cancer-driving genes that directly propel tumor progression from a larger number of passenger genes that are concurrently overexpressed but lack biologic relevance in tumor development. This is because gene expression is dynamic, depending on both genetic and epigenetic programs in tumor cells. In contrast, molecular genetic changes, such as alterations in DNA copy number (for example, amplifications and deletions), and point mutations are inheritable traits and are the result of Darwinian selection in tumors because of growth advantage conferred by these alterations [1]. Conventional methods used to reveal DNA copy number changes include comparative genomic hybridization (CGH), representational difference analysis, spectral karyotyping/metaphase fluorescence *in situ* hybridization, and conventional cytogenetics. These methods have aided in the identification of genetic aberrations in human cancer, but they generally have a limited mapping resolution (5 to 20 Mb) and, therefore, are not suitable to detect smaller chromosomal alterations. The success of the human genome database has accelerated cancer genome study because it provides precise and detailed maps to facilitate chromosomal mapping and localization of potential oncogenes and tumor suppressors. However, the question remains regarding the availability of suitable technical platforms that would allow a comprehensive survey of the cancer genome. It cannot be overemphasized that a high-resolution readout of the techniques is essential because precise genomic locations of amplification and deletion are required for further identification of novel oncogenes and tumor suppressors.

Recent developments of technologies including digital karyotyping, array-based CGH, and representational oligonucleotide microarray analysis (ROMA) provide molecular solutions, for the first time, to detect DNA copy number changes at a genome-wide scale with an excellent resolution. In addition, an automated capillary sequencing platform has become available for a large-scale mutational analysis. In this article, we will focus on reviewing these new technical advances and will briefly discuss a critical issue in sample preparation. Finally, we will review a rational strategy by combining genomic analysis, gene expression profiling, and large-scale mutational analysis to expedite the identification of oncogenes and tumor suppressors.

Digital karyotyping

Digital karyotyping has recently been developed for a genome-wide analysis of DNA copy number alterations at high resolution [9]. The principle of this approach is similar to the serial analysis of gene expression method [8,10], which is based on the isolation and enumeration of short sequence tags. However, the sequence tags in digital karyotyping are obtained from genomic DNA rather than from mRNA, and they are isolated by different methods. These tags (21 bp each) contain sufficient information that allows assigning the tag sequences to their corresponding genomic loci from which they are derived. After isolation, the tags are ligated to each other and are cloned into bacteria. Therefore, every bacterial clone represents homogeneous plasmid that contains a certain number of different tags (approximately 32 tags). Generally, approximately 5000 clones are sequenced from each tumor sample to establish a digital karyotyping library that collects a total of 160,000 tags (32 × 5000). Populations of tags can then be uniquely matched to the assembled genomic sequence in a public domain, allowing observed tags to be sequentially ordered along each chromosome. The number of each unique tag along each chromosome can be used to quantitatively evaluate DNA content in tumor samples. To prove the above concept, digital karyotyping libraries have been generated from a colorectal cancer cell line (DiFi) and an ovarian cell line (SKOV3) in which the preexisting CGH data are available for comparison. Digital karyotyping identified all the known chromosomal alterations including whole chromosome changes, gains or losses of chromosomal arms, and interstitial amplifications or deletions in both cell lines. More importantly, digital karyotyping revealed several distinct genetic alterations including amplifications of relatively small amplicons (less than 1 Mb) and homozygous deletions that have never been previously described using other methods. For example, the SKOV3 cell line was known to contain Her2/neu gene amplification [11]. Digital karyotyping of SKOV3 cells is able to demonstrate a distinct amplification in the Her2/neu locus (17q12) (Fig. 1B), which was not evident by CGH or SKY analysis [12,13]. These analyses suggest that a potentially large number of undiscovered copy number alterations exist in cancer genomes and many of these could be detected through digital karyotyping. Examples of amplification and deletion revealed by digital karyotyping are shown in Figure 1. Digital karyotyping has been recently applied in identifying specific gene amplification that is associated with resistance to chemotherapy [14••]. In that study, a significant fraction of colorectal cancer patients undergoing 5-fluorouracil treatment were found to have amplification of the thy-

Figure 1. Detection of amplified and deleted chromosomal regions by digital karyotyping

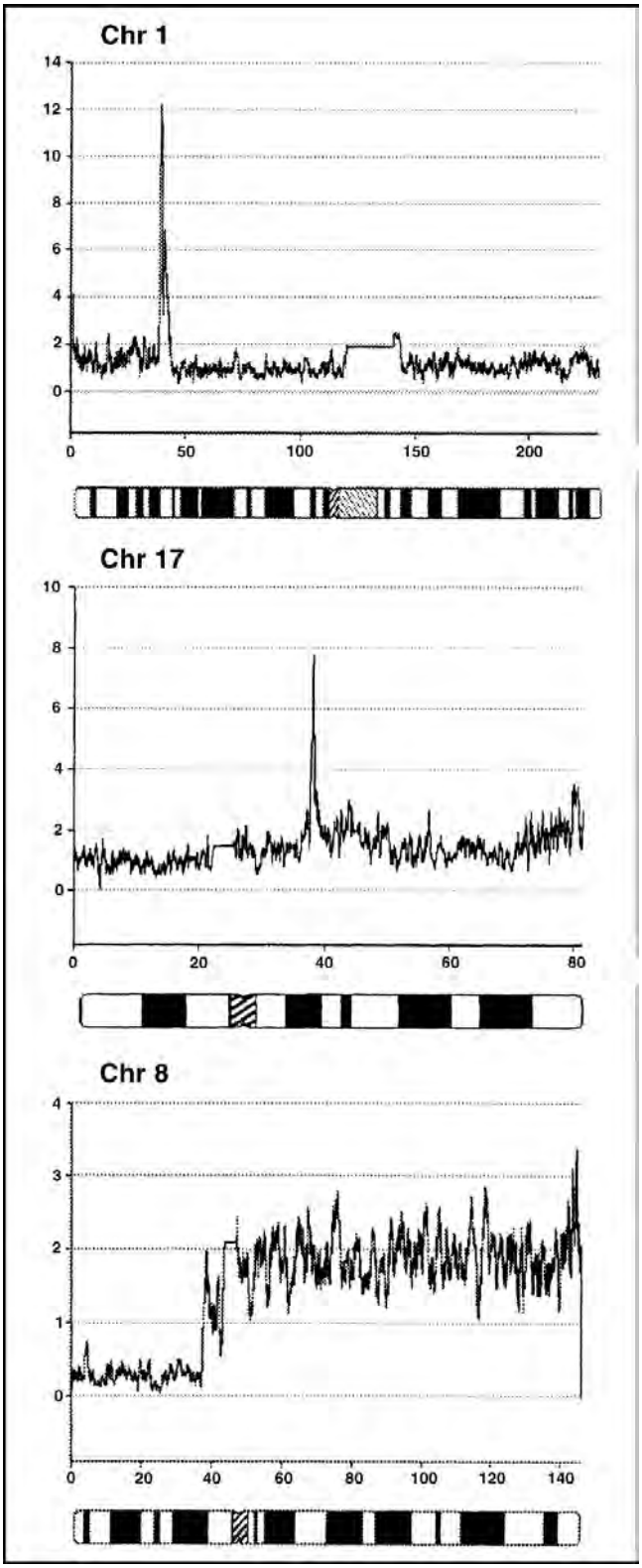

Digital karyotyping libraries were generated using isolated tumor cells from ovarian serous carcinoma tissues. Analysis of the libraries reveals two distinct amplifications in chromosomes 1p34.2 and 17q12, which are know to contain L-myc and Her2/neu oncogenes, respectively (top and center). A deletion in chromosome 8p is also evident (bottom). The chromosome ideograms are aligned with the results of digital karyotyping for reference.

midylate synthase (TYMS) locus. Patients with TYMS gene amplification have been shown to have a shorter survival than those do not. This finding could have significant implications for the clinical management of cancer patients with colorectal cancer.

The major advantage of digital karyotyping in exploring the cancer genome is its higher resolution than the conventional methods. This is because the technique involves using SacI as the mapping enzyme in which the enzyme sites are abundant in human genome (spanning an interval of approximately 4 kb). Therefore, a high resolution can be theoretically achieved if a sufficient number of tags can be obtained (sequenced). Furthermore, digital karyotyping provides unbiased gene dosage readout because digital karyotyping directly counts the tags in contrast to the analog signal generated by hybridization that is associated with an array format. However, it is possible that a small portion of the genome has a lower density of mapping enzyme SacI sites and could be incompletely evaluated by digital karyotyping. This potential problem could be overcome through the application of different mapping and fragmenting enzymes.

Array-based technologies to detect DNA copy number changes: array comparative genomic hybridization and representational oligonucleotide microarray analysis

In contrast to a tag counting strategy used in digital karyotyping, two related technologies, array CGH and ROMA, have been developed by using the format of DNA microarrays to map the loci of amplification and deletion. Array-based CGH is a technique that combines conventional CGH and DNA microarray for detection of DNA copy number changes [15–17]. Conventional CGH has been widely used in identifying chromosomal imbalances in cancers, but the relatively low mapping resolution (5 to 20 Mb) has limited its use as a discovery tool for novel cancer-associated genes [18]. In contrast, array CGH takes the advantages of CGH but it analyzes genomic alterations using DNA microarrays instead of metaphase chromosomes. In this way, the assay resolution increases as thousands of genomic targets representing different genomic locations can be analyzed simultaneously. In array CGH, total genomic DNA from a tumor and a normal cell population are labeled with different fluorochromes and hybridized to arrayed genomic components of cDNA [16] or large genomic fragments such as bacteria artificial chromosomes and phage artificial chromosome [15]. The ratio of the fluorescence intensities on each spot in the array is proportionally correlated to the copy number of the corresponding sequences in the tumor. Comparison of ratios on overlapping clones should allow amplifications and deletions in DNA copy number to be mapped in the genome. Thus, array CGH is a technique by which variation in relative copy num-

bers between two genomes can be analyzed by competitive hybridization to DNA microarrays [19–21]. Several recent studies have shown the potential of array CGH in detecting DNA copy number alterations in fallopian tube carcinomas [22], oral squamous carcinoma [23], bladder cancer [24], pancreatic cancer [25], chronic lymphocytic leukemia [26], and gastric cancer [27,28]. Although CGH array can provide a number of advantages over the conventional cytogenetics approaches including higher resolution and throughput, it has been previously limited by the availability of genomic clones that can be spotted as targets. Recent attempts, however, have improved the resolution of array CGH to approximately 1 Mb by establishing a high-density array [29••,30]. Furthermore, new analysis tools have been recently developed to provide a more uniform and convenient analysis platform for array CGH [31].

Representational oligonucleotide microarray analysis is another array-based technique for the detection of genome copy number variation. The method is modified from the representational difference analysis [32] by utilizing the microarray format [33••]. The principle of ROMA is based on the concept of genomic representation that is generated by amplifying restriction enzyme (such as Bgl II) digested genomic fragments from samples. The representative genomic fragments hybridize to the oligonucleotides in arrays that are designed from the human genome sequence assembly. The major advantage of using a representation strategy is to minimize the genome complexity and therefore maximize the signal-to-background ratio. Using ROMA, investigators are able to detect regions of copy number variations between cancer and normal genomes and between normal human genomes [33••,34]. Currently, ROMA can reach a resolution up to 30 to 35 kb, and further refinement of ROMA will promise to reveal an even better resolution by designing a higher density array.

High-throughput mutational analysis

Besides DNA copy number changes, somatic point mutation represents another salient feature of molecular genetic changes in cancer because the point mutation can lead to activation of oncogenes and inactivation of tumor suppressor genes. The discovery of somatic point mutations, in the past, has been challenged by an unsatisfied throughput inherent to the traditional DNA sequencing and heteroduplex analysis. Recently, with the advance of human genome assembly, a high-throughput sequencing pipeline is made possible by the application of capillary sequencers and the availability of bioinformatic software. For example, the current capacity of a single capillary nucleotide sequencer with a 384-well format can analyze at least 2304 sequencing reactions per day (384 reactions/plate × 6 plates/d). This high-throughput platform permits a systemic scan of cancer genome at the nucleotide level in a short time [35]. This format has been successfully used to screen protein families that could contain genes critical in tumor development [36–38••].

Identification of the BRAF oncogene is another example of the power of high-throughput mutation analysis in finding new oncogenes. Davies *et al.* [39] used the heteroduplex method and high-throughput capillary sequencers to screen mutations in genes belonging to the RAS-RAF-MEK-ERK (MAP) kinase pathway and found that activating mutations in BRAF occurred in 66% of melanomas. Functional study demonstrates that mutated BRAF proteins have elevated kinase activity and are able to transform NIH3T3 cells. Subsequent studies have further shown frequent BRAF mutations in other specific types of cancer, including papillary thyroid carcinomas (69%) [40] and low-grade ovarian serous tumors (30%) [41•]. Because activating mutations within the protein kinase family may be amenable to therapeutic intervention such as kinase inhibitors, these studies suggest a potential target-based therapy for those patients whose tumors harbor BRAF mutations.

Critical issues in preparation of tumor DNA

As new molecular genetic technologies are emerging, isolation of tumor DNA has become a critical issue because all the above mentioned techniques will not be useful unless the tumor DNA is enriched. Detection of homozygous deletions and point mutations would be equivocal and the folds of amplification obscure in the presence of substantial amounts of contaminated DNA from normal tissues. Genomic DNA is generally obtained from tumor cells isolated by laser capture microdissection on tissue sections, from tumor cell lines/long-term cultures, and from freshly isolated tumor cells (directly from surgical specimens). Laser capture microdissection has become a powerful technique in isolating tumor cells, especially in acquiring the preneoplastic cells in the precursor lesions. However, it can be labor intensive to obtain a sufficient amount of DNA for assays. Tumor cell lines/long-term cultures, on the other hand, provide a convenient source of pure tumor DNA, but they are not ideal for genomic analyses of human cancer because they may acquire a variety of genetic changes as a result of *in vitro* selection, and those genetic changes may not be relevant to tumorigenesis. Accordingly, it is preferable to use the genomic DNA of purified or enriched tumor cells from surgical specimens if fresh tumor samples are available. Many investigators have used immunosorting in which the magnetic beads are bound to antibodies that react to the tumor-associated antigen on cancer cells. The magnet-isolated tumor cells can be directly used to isolate genomic DNA and RNA or they can be cultured for a short term to further expand the tumor cell population. The epithelial origin of the immunosorted carcinoma cells can be confirmed by staining the purified cells with a cytokeratin antibody or by loss of heterozygosity assay. An example

Figure 2. An example of tumor cell isolation from fresh tissue samples

(**A**) Isolated tumor cells using magnetic beads coated with an Epi-CAM antibody (phase contrast). After magnet sorting, almost all tumor cells are bound to the beads (small dark dots). The isolated tumor cells can be directly used for genomic DNA extraction or they can be short-term cultured to expand the tumor cell population. (**B**) Loss of heterozygosity (LOH) assay. This method is to confirm the purity of immunosorted tumor cells because LOH is unique to tumor but not to normal cells. Both tumor cells (T) and the matched normal cells (N) are analyzed in parallel by PCR using four representative microsatellite markers. Attenuation of intensity in one of the two alleles from the tumor sample (T) was observed in microsatellite markers of chromosomes 5, 8, and 22, indicating a highly enriched tumor cell population. Estimation of the percentage of tumor DNA can be performed by comparing the intensity ratio of the two alleles between tumor and normal samples. The marker in chromosome 1 is not informative because the tumor does not have LOH in the particular locus.

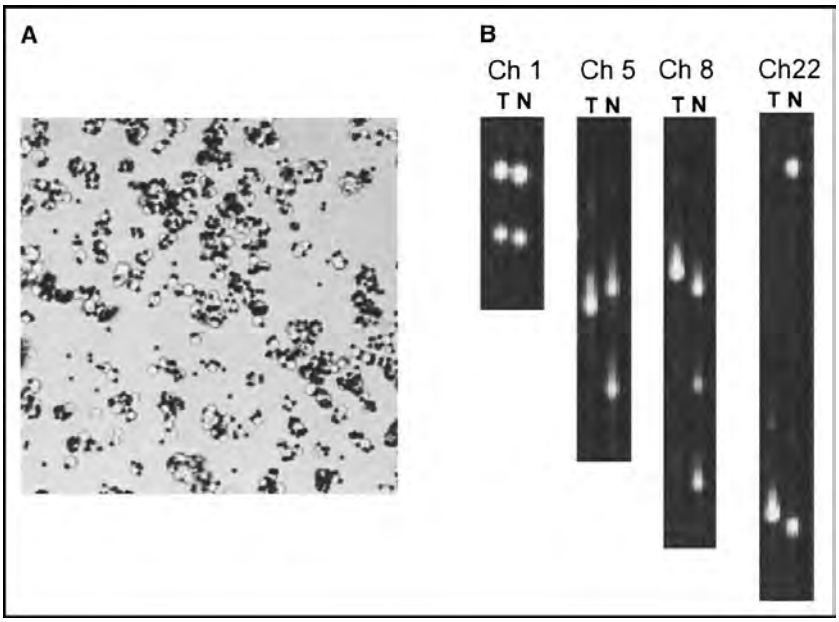

of tumor cell isolation and assessment of its purity is shown in Figure 2.

Combined technical platform for cancer gene discovery

Once amplified or deleted chromosomal regions are identified, the next question is how one can effectively search for the culprit oncogenes and tumor suppressors among an overwhelming number of co-amplified or deleted genes within the same chromosomal region. Because oncogenes within an amplicon almost always overexpress whereas the neighborhood genes may or may not, a rational strategy has been developed by parallel analyses of cancer genome and transcriptome in the same tumors to reveal the profiles of gene expression in the genomically amplified regions. This genome–transcriptome combined approach has allowed several investigators to successfully narrow down the candidate genes [23,42–45]. The other approach expected to significantly facilitate the identification of oncogenes and tumor suppressors is the mutational analysis. Oncogenes and tumor suppressors are characterized not only by DNA copy number changes but also by somatic point mutations because both mechanisms complement each other in tumorigenesis. For example, c-Myc, KRAS, and EGFR are found to be amplified in some tumors and somatically mutated in others of the same tumor type. Similarly, tumor suppressors can be inactivated as a result of homozygous deletion or somatic point mutations. These mechanisms lead to a decrease or a complete abolishment of gene expression. Thus, candidate genes located in the chromosomal regions of interest (identified by digital karyotyping, array CGH and ROMA) can be analyzed for point mutations using a large panel of tumor DNA samples.

Conclusion

The availability of the human genome database creates a new era for biomedical research. New technical platforms that take advantage of the human genome sequences are now available, allowing us to comprehensively analyze complex cancer genomes. The recent development of digital karyotyping, array-based CGH, ROMA, high-throughput mutational analysis, and other emerging techniques provides unprecedented opportunities in discovering new oncogenes, tumor suppressors, and drug-resistant genes, which holds great promise to develop new strategies for diagnosis and treatment of this devastating disease. Further refinement and modification of these techniques will improve their performance including reproducibility, resolution, and throughput in the years to come.

Acknowledgments

The authors thank Mr. Jim M. Yen for preparation of figures, Dr. Victor Velculescu for valuable advice on the figures, and the members of Gynecological Cancer Genomic Laboratory at Johns Hopkins Medical Institutions for their review of the manuscript.

References and recommended reading

Papers of particular interest, published within the annual period of review, have been highlighted as:

- • Of special interest
- •• Of outstanding interest

1 Kinzler KW, Vogelstein B: The Genetic Basis of Human Cancer, edn 2. Edited by Kinzler KW, Vogelstein B. Toronto: McGraw-Hill; 2002:3–821.

2 Onyango P: Genomics and cancer. Curr Opin Oncol 2002, 14:79–85.

3 Keyomarsi K, Tucker SL, Bedrosian I: Cyclin E is a more powerful predictor of breast cancer outcome than proliferation. Nat Med 2003, 9:152.

4 Farley J, Smith LM, Darcy KM, et al.: Cyclin E expression is a significant predictor of survival in advanced, suboptimally debulked ovarian epithelial cancers: a Gynecologic Oncology Group study. Cancer Res 2003, 63:1235–1241.

5 Masood S, Bui MM: Prognostic and predictive value of HER2/neu oncogene in breast cancer. Microsc Res Tech 2002, 59:102–108.

6 Zhang HT, Wang Q, Greene MI, et al.: New perspectives on anti-HER2/neu therapeutics. Drug News Perspect 2000, 13:325–329.

7 Guo QM: DNA microarray and cancer. Curr Opin Oncol 2003, 15:36–43.

8 Velculescu VE, Zhang L, Vogelstein B, et al.: Serial analysis of gene expression. Science 1995, 270:484–487.

9 Wang TL, Maierhofer C, Speicher MR, et al.: Digital karyotyping. Proc Natl Acad Sci USA 2002, 99:16156–16161.

10 Saha S, Sparks AB, Rago C, et al.: Using the transcriptome to annotate the genome. Nat Biotechnol 2002, 20:508–512.

11 King BL, Carter D, Foellmer HG, et al.: Neu proto-oncogene amplification and expression in ovarian adenocarcinoma cell lines. Am J Pathol 1992, 140:23–31.

12 Hauptmann S, Denkert C, Koch I, et al.: Genetic alterations in epithelial ovarian tumors analyzed by comparative genomic hybridization. Hum Pathol 2002, 33:632–641.

13 Rao PH, Harris CP, Yan Lu X, et al.: Multicolor spectral karyotyping of serous ovarian adenocarcinoma. Genes Chromosomes Cancer 2002, 33:123–132.

14 •• Wang TL, Diaz LA Jr, Romans K, et al.: Digital karyotyping identifies thymidylate synthase amplification as a mechanism of resistance to 5-fluorouracil in metastatic colorectal cancer patients. Proc Natl Acad Sci USA 2004, 101:3089–3094.

This article demonstrates an example by using digital karyotyping in searching for DNA copy alteration that is involved in drug resistance. Genome-wide analysis reveals a close association of TYMS gene amplification and clinical 5-FU resistance in colorectal carcinoma. The paper concludes that TYMS may serve as a useful prognosis marker in patients with colorectal cancer.

15 Pinkel D, Segraves R, Sudar D, et al.: High resolution analysis of DNA copy number variation using comparative genomic hybridization to microarrays. Nat Genet 1998, 20:207–211.

16 Pollack JR, Perou CM, Alizadeh AA, et al.: Genome-wide analysis of DNA copy-number changes using cDNA microarrays. Nat Genet 1999, 23:41–46.

17 Lucito R, West J, Reiner A, et al.: Detecting gene copy number fluctuations in tumor cells by microarray analysis of genomic representations. Genome Res 2000, 10:1726–1736.

18 Kallioniemi A, Kallioniemi OP, Sudar D, et al.: Comparative genomic hybridization for molecular cytogenetic analysis of solid tumors. Science 1992, 258:818–821.

19 Albertson DG, Collins C, McCormick F, et al.: Chromosome aberrations in solid tumors. Nat Genet 2003, 34:369–376.

20 Albertson DG, Pinkel D: Genomic microarrays in human genetic disease and cancer. Hum Mol Genet 2003, 12(spec no 2):R145–R152.

21 Paris PL, Albertson DG, Alers JC, et al.: High-resolution analysis of paraffin-embedded and formalin-fixed prostate tumors using comparative genomic hybridization to genomic microarrays. Am J Pathol 2003, 162:763–770.

22 Snijders AM, Nowee ME, Fridlyand J, et al.: Genome-wide-array-based comparative genomic hybridization reveals genetic homogeneity and frequent copy number increases encompassing CCNE1 in fallopian tube carcinoma. Oncogene 2003, 22:4281–4286.

23 Garnis C, Coe BP, Zhang L, et al.: Overexpression of LRP12, a gene contained within an 8q22 amplicon identified by high-resolution array CGH analysis of oral squamous cell carcinomas. Oncogene 2004, 23:2582–2586.

24 Veltman JA, Fridlyand J, Pejavar S, et al.: Array-based comparative genomic hybridization for genome-wide screening of DNA copy number in bladder tumors. Cancer Res 2003, 63:2872–2880.

25 Holzmann K, Kohlhammer H, Schwaenen C, et al.: Genomic DNA-chip hybridization reveals a higher incidence of genomic amplifications in pancreatic cancer than conventional comparative genomic hybridization and leads to the identification of novel candidate genes. Cancer Res 2004, 64:4428–4433.

26 Schwaenen C, Nessling M, Wessendorf S, et al.: Automated array-based genomic profiling in chronic lymphocytic leukemia: development of a clinical tool and discovery of recurrent genomic alterations. Proc Natl Acad Sci USA 2004, 101:1039–1044.

27 Weiss MM, Snijders AM, Kuipers EJ, et al.: Determination of amplicon boundaries at 20q13.2 in tissue samples of human gastric adenocarcinomas by high-resolution microarray comparative genomic hybridization. J Pathol 2003, 200:320–326.

28 Weiss MM, Kuipers EJ, Postma C, et al.: Genomic profiling of gastric cancer predicts lymph node status and survival. Oncogene 2003, 22:1872–1879.

29 •• Ishkanian AS, Malloff CA, Watson SK, et al.: A tiling resolution DNA microarray with complete coverage of the human genome. Nat Genet 2004, 36:299–303.

The investigators in this work demonstrate the feasibility of higher resolution of array CGH, which is made possible by using 32,433 overlapping BAC clones that cover the entire human genome.

30 Greshock J, Naylor TL, Margolin A, et al.: 1-Mb resolution array-based comparative genomic hybridization using a BAC clone set optimized for cancer gene analysis. Genome Res 2004, 14:179–187.

31 Wang J, Meza-Zepeda LA, Kresse SH, et al.: M-CGH: Analysing microarray-based CGH experiments. BMC Bioinformatics 2004, 5:74.

32 Lisitsyn N, Wigler M: Cloning the differences between two complex genomes. Science 1993, 259:946–951.

33 •• Lucito R, Healy J, Alexander J, et al.: Representational oligonucleotide microarray analysis: a high-resolution method to detect genome copy number variation. Genome Res 2003, 13:2291–2305.

This is the original paper that described the principle, development, and application of ROMA.

34 Sebat J, Lakshmi B, Troge J, et al.: Large-scale copy number polymorphism in human genome. Science 2004, 305:525–528.

35 Wang TL, Rago C, Silliman N, et al.: Prevalence of somatic alterations in the colorectal cancer cell genome. Proc Natl Acad Sci USA 2002, 99:3076–3080.

36 Bardelli A, Parsons DW, Silliman N, et al.: Mutational analysis of the tyrosine kinome in colorectal cancers. Science 2003, 300:949.

37 Samuels Y, Wang Z, Bardelli A, et al.: High frequency of mutations of the PIK3CA gene in human cancers. Science 2004, 304:554.

38 •• Wang Z, Shen D, Parsons DW, et al.: Mutational analysis of the tyrosine phosphatome in colorectal cancers. Science 2004, 304:1164–1166.

This article has surveyed the DNA sequences of protein tyrosine phosphatase (PTP) family in colorectal cancers and found somatic mutation in approximately 26% of cancers. Functional studies *in vitro* and *in vivo* further suggest the tumor suppressor function of one of the genes, PTPRT.

39 Davies H, Bignell GR, Cox C, et al.: Mutations of the BRAF gene in human cancer. Nature 2002, 417:949–954.

40 Cohen Y, Xing M, Mambo E, et al.: BRAF mutation in papillary thyroid carcinoma. J Natl Cancer Inst 2003, 95:625–627.

41 • Singer G, Oldt R 3rd, Cohen Y, et al.: Mutations in BRAF and KRAS characterize the development of low-grade ovarian serous carcinoma. J Natl Cancer Inst 2003, 95:484–486.

This paper documents mutations in either BRAF or KRAS genes in 61% of low-grade ovarian serous carcinoma, but none in 72 high-grade ovarian serous carcinomas. The results indicate that low-grade and high-grade ovarian tumors develop through distinct pathways.

42 De Preter K, Pattyn F, Berx G, et al.: Combined subtractive cDNA cloning and array CGH: an efficient approach for identification of overexpressed genes in DNA amplicons. BMC Genomics 2004, 5:11.

43 Pollack JR, Sorlie T, Perou CM, et al.: Microarray analysis reveals a major direct role of DNA copy number alteration in the transcriptional program of human breast tumors. Proc Natl Acad Sci USA 2002, 99:12963–12968.

44 Hyman E, Kauraniemi P, Hautaniemi S, et al.: Impact of DNA amplification on gene expression patterns in breast cancer. Cancer Res 2002, 62:6240–6245.

45 Redon R, Hussenet T, Bour G, et al.: Amplicon mapping and transcriptional analysis pinpoint cyclin L as a candidate oncogene in head and neck cancer. Cancer Res 2002, 62:6211–6217.

A BTB/POZ protein, NAC-1, is related to tumor recurrence and is essential for tumor growth and survival

Kentaro Nakayama*, Naomi Nakayama*, Ben Davidson†, Jim J.-C. Sheu*, Natini Jinawath*, Antonio Santillan‡§, Ritu Salani‡§, Robert E. Bristow‡§, Patrice J. Morin¶, Robert J. Kurman*‡§, Tian-Li Wang‡§, and Ie-Ming Shih*‡§‖

Departments of *Pathology, ‡Oncology, and §Gynecology and Obstetrics, Johns Hopkins Medical Institutions, Baltimore, MD 21231; †Norwegian Radium Hospital, 0310 Oslo, Norway; and ¶Laboratory of Cellular and Molecular Biology, National Institute on Aging, National Institutes of Health, Baltimore, MD 21224

Edited by Joan S. Brugge, Harvard Medical School, Boston, MA, and approved October 8, 2006 (received for review May 18, 2006)

Recent studies have suggested an oncogenic role of the BTB/POZ-domain genes in hematopoietic malignancy. The aim of this study is to identify and characterize BTB/POZ-domain genes in the development of human epithelial cancers, i.e., carcinomas. In this study, we focused on ovarian carcinoma and analyzed gene expression levels using the serial analysis of gene expression (SAGE) data in all 130 deduced BTB/POZ genes. Our analysis reveals that NAC-1 is significantly overexpressed in ovarian serous carcinomas and several other types of carcinomas. Immunohistochemistry studies in ovarian serous carcinomas demonstrate that NAC-1 is localized in discrete nuclear bodies (tentatively named NAC-1 bodies), and the levels of NAC-1 expression correlate with tumor recurrence. Furthermore, intense NAC-1 immunoreactivity in primary tumors predicts early recurrence in ovarian cancer. Both coimmunoprecipitation and double immunofluorescence staining demonstrate that NAC-1 molecules homooligomerize through the BTB/POZ domain. Induced expression of the NAC-1 mutant containing only the BTB/POZ domain disrupts NAC-1 bodies, prevents tumor formation, and promotes tumor cell apoptosis in established tumors in a mouse xenograft model. Overexpression of full-length NAC-1 enhanced tumorigenicity of ovarian surface epithelial cells and NIH 3T3 cells in athymic *nu/nu* mice. In summary, NAC-1 is a tumor recurrence-associated gene with oncogenic potential, and the interaction between BTB/POZ domains of NAC-1 proteins is critical to form the discrete NAC-1 nuclear bodies and essential for tumor cell proliferation and survival.

oncogene | ovarian cancer | serial analysis of gene expression

The BTB (bric-a-brac tramtrack broad complex) (also known as POZ) gene family is composed of several proteins that share a conserved BTB/POZ protein–protein interaction motif at the N terminus that mediates homodimer or heterodimer formation (1–3). These proteins have been demonstrated to participate in a wide variety of cellular functions including transcription regulation, cellular proliferation, apoptosis, cell morphology, ion channel assembly, and protein degradation through ubiquitination (1). A subset of BTB/POZ proteins have been implicated in human cancer, and they include BCL-6 (4, 5), PLZF (promyelocytic leukemia zinc finger) (4, 6), leukemia/lymphoma-related factor (LRF)/Pokemon (7, 8), HIC-1 (hypermethylated in cancer-1), and Kaiso (9, 10). Among them, the *BCL-6* gene is the best characterized oncogene. Frequent gene translocation or mutation has been identified in B cell lymphoma, resulting in constitutive BCL-6 expression in the tumor cells (4, 5). Peptide inhibitors that block interaction between the BCL-6 BTB/POZ domain and corepressors abrogate BCL-6 oncogenic functions in B cells, suggesting that the use of peptide inhibitors of the BTB/POZ domain may represent a therapeutic approach for B cell lymphoma (5). As the role of BTB/POZ proteins in human cancer is emerging, we have analyzed the expression patterns of tumor-associated BTB/POZ genes in ovarian cancer *in silico* using the serial analysis of gene expression (SAGE) database. Ovarian cancer was selected in this study because this disease represents one of the most aggressive cancer types in women. Most patients with ovarian cancer are diagnosed at advanced stages when conventional therapy is less effective. As a result, most ovarian cancer patients suffer from, and eventually succumb to, recurrent disease. New therapeutic agents are urgently needed for effective treatment to improve outcome in these patients. In this study, we focused on a BTB/POZ gene, *NAC-1*, that is overexpressed in ovarian cancer, particularly in recurrent disease. We demonstrated that *NAC-1* plays a critical role in tumorigenesis and in the growth and survival of tumor cells.

Results

NAC-1 Expression Is Associated with Cancer Development. A total of 11 SAGE libraries were used to screen 130 BTB/POZ domain-containing genes for overexpression in high-grade ovarian serous carcinomas as compared with ovarian surface epithelium and benign ovarian cystadenoma. Sixteen genes were selected based on an average tag count per library >10 (Table 2, which is published as supporting information on the PNAS web site). Among these 16 genes, a gene named *NAC-1* (BTBD14B HS.531614) showed the highest ratio of average tag counts in ovarian carcinoma to controls (ovarian surface epithelium and benign ovarian cyst) and was therefore selected for validation and characterization in this study. The SAGE database was also used to analyze *NAC-1* expression in different cancer types and their corresponding normal tissues. As shown in Fig. 1, in addition to ovarian cancer, NAC-1 was upregulated in several tumors from other organs including pancreatic, colorectal, and breast carcinomas, although the sample size of SAGE libraries in most of tumor types was too small for a statistical analysis.

To validate the SAGE results in ovarian cancer, we generated a mouse monoclonal antibody (NAC-1 Ab clone 3) that reacted to the C terminus of the NAC-1 protein and performed immunohistochemistry in 265 ovarian tumors and normal tissue samples (Table 3, which is published as supporting information on the PNAS web site). The specificity of the NAC-1 antibody was evaluated by

Author contributions: K.N., N.N., T.-L.W., and I.-M.S. designed research; K.N., N.J., and N.N. performed research; B.D., J.J.-C.S., R.E.B., P.J.M., and R.J.K. contributed new reagents/analytic tools; K.N., N.N., A.S., R.S., T.-L.W., and I.-M.S. analyzed data; and K.N., T.-L.W. and I.-M.S. wrote the paper.

The authors declare no conflict of interest.

This article is a PNAS direct submission.

Abbreviations: JHMI, Johns Hopkins Medical Institutions; MOSE, immortalized OSE cells; NRH, Norwegian National Radium Hospital; OSE, ovarian surface epithelial cells; SAGE, serial analysis of gene expression.

Data deposition: The sequence reported in this paper has been deposited in the UniGene database, www.ncbi.nlm.nih.gov/entrez/guery.fcgi?db-unigene (accession no. HS.531614).

‖To whom correspondence should be addressed at: Johns Hopkins Hospital, CRB II, Room 305, 1550 Orleans Street, Baltimore, MD 21231. E-mail: ishih@jhmi.edu.

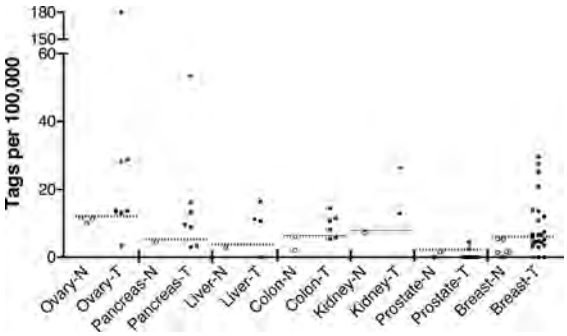

Fig. 1. Scatter plot of NAC-1 tags in several major tumor types. NAC-1 expression level is analyzed by counting NAC-1-specific tags from SAGE libraries in both cancer tissue (T, filled symbols) and the corresponding normal tissues (N, open symbols). The NAC-1 tags are normalized to tags per 100,000 (*y* axis). The dash line in each tumor type indicates the ''ceiling'' tag number in normal tissue libraries. Each symbol represents an individual specimen.

reciprocal immunoprecipitation/Western blot analyses in RK3E cells transfected with pCDNA6-V5/NAC-1 and vector control. A single band with a molecular mass of ≈57 kDa corresponding to NAC-1 protein was detected in *NAC-1*-transfected cells but not in control cells (Fig. 2*A*). Because the immunoreactive tumor cells always exhibited diffuse staining, we used intensity scores to quantify NAC-1 expression in tissues. In contrast to normal ovaries and benign ovarian cystadenomas, both low- and high-grade serous carcinomas demonstrated a higher NAC-1 immunoreactivity, with 27% and 40% of cases showing 2+ and 3+, respectively (χ^2 test, $P < 0.001$) (Fig. 2 *B–D* and Table 3). The number of high-grade cases with high NAC-1 immunointensity (2+ and 3+) was significantly higher than that in low-grade carcinoma ($P < 0.01$). Immunofluorescence revealed that NAC-1 was localized to dot-like structures in those tumors showing strong NAC-1 immunointensity (2+ and 3+) (Fig. 2 *E* and *F*). Ultrastructural analysis using ImmunoGold labeling, and electron microscopy further revealed that NAC-1 was localized to discrete nuclear bodies, tentatively termed "NAC-1 bodies", with a diameter ranging from 0.3 to 1.8 μm (Fig. 2*G*).

Overexpression of NAC-1 Correlates with Recurrent Ovarian Cancer. It is widely accepted that recurrent tumors represent the true "killer" in cancer patients, because the primary tumors are usually removed by surgery. Identification of molecular targets that are present in recurrent tumors would be important in the development of a prognostic test and a novel therapeutic intervention for cancer patients. Thus, we addressed whether NAC-1 expression was related to tumor progression by analyzing primary and recurrent ovarian high-grade serous carcinomas using immunohistochemistry and quantitative real-time PCR. NAC-1 immunohistochemistry was performed at two institutions, Johns Hopkins Medical Institutions (JHMI, solid tumors) and Norwegian National Radium Hospital (NRH, effusions), by using independent sets of ovarian cancer specimens, and the results are presented in a 2 × 2 contingency table (Table 1). Among 182 JHMI high-grade carcinoma cases, we analyzed 166 samples including 110 primary and 56 first recurrent tumors. The remaining 16 specimens that were obtained from second and third recurrence were not included in the analysis. Both JHMI and NRH studies demonstrated that a higher NAC-1 staining intensity (2+ and 3+) was more frequently found in recurrent than in primary tumor tissues ($P < 0.01$ in JHMI and $P = 0.013$ in NRH, χ^2 test). To validate the immunohistochemistry results, we performed quantitative real-time PCR using samples from JHMI to assess the correlation of *NAC-1* mRNA expression levels and the recurrence status. We found that an increased *NAC-1* transcript level significantly correlated with recurrent disease ($P = 0.012$, Mann–Whitney test) (Fig. 3*A*). The association of NAC-1 expression and recurrent status was independent of clinical stage (III versus IV) at diagnosis.

Among 56 recurrent carcinomas from JHMI, there were 21 cases for which the corresponding primary tumors were available from the same patients for comparison. A statistically significant increase in NAC-1 immunointensity (2+ and 3+) was found in recurrent tumors as compared with the primary tumors from the same

Table 1. Increased NAC-1 immunoreactivity correlates with first tumor recurrence

	JHMI (solid tumors)		NRH (effusions)	
	0+/1+	2+/3+	0+/1+	2+/3+
Primary	71	39	62	49
First recurrent	21	35	22	39
Total	92	74	84	88

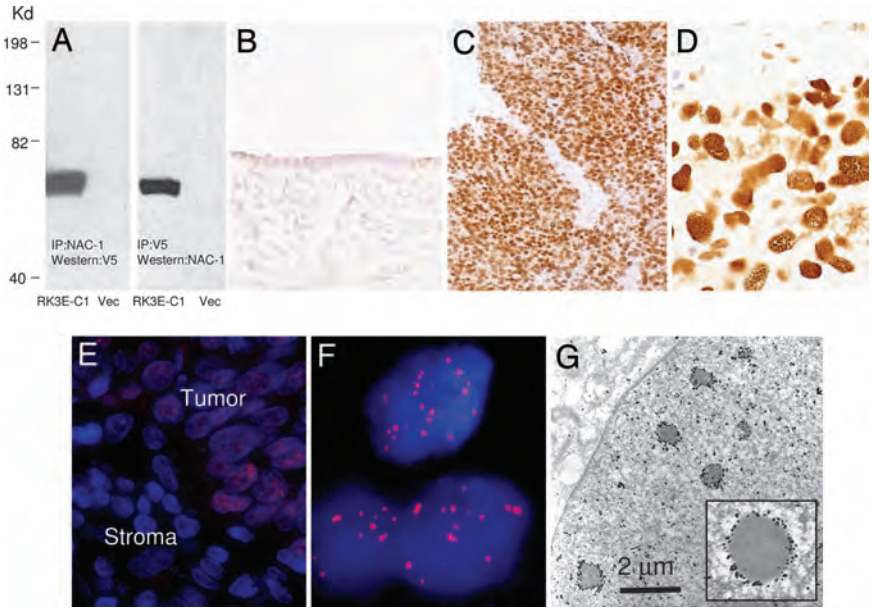

Fig. 2. Immunoreactivity of NAC-1 in ovarian cancer tissues. (*A*) Immunoprecipitation/Western blot analyses using NAC-1 and V5 antibodies in RK3E cells transfected with pCDNA6-NAC-1/V5 (RK3E-C1) or vector-only control (Vec). A discrete band corresponding to NAC-1 protein mass is identified in this reciprocal analysis. (*B–D*) The NAC-1 immunointensity is undetectable or weak in normal ovarian surface epithelium (*B*) but is strong in a high-grade serous carcinoma (*C* and *D*). (*E* and *F*) Immunofluorescence of NAC-1 protein localization in ovarian cancer cells in a tissue section. Tumor cells contain NAC-1 protein, which is located in discrete nuclear bodies (*E*). The adjacent stromal cells are negative for NAC-1 immunoreactivity. A higher magnification demonstrates the NAC-1 nuclear bodies by using a confocal fluorescence microscope (*F*). (*G*) Ultrastructure of NAC-1 bodies. ImmunoGold labeling of NAC-1-expressing RK3E cells demonstrates electron-dense bodies decorated by gold particles in the nuclear matrix.

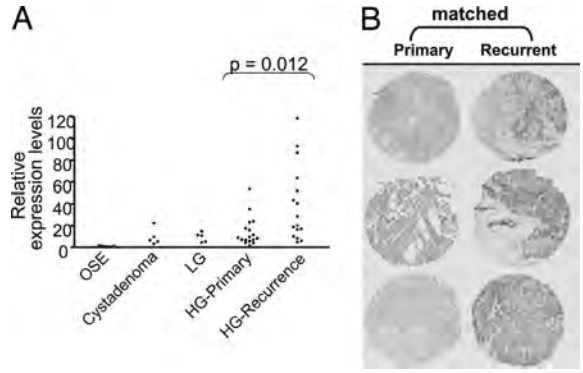

Fig. 3. NAC1 expression correlates with tumor progression in ovarian serous carcinomas. (*A*) Quantitative real-time PCR analysis shows higher NAC-1 expression levels in high-grade carcinomas (HG) than in ovarian surface epithelial cells (OSE), low-grade carcinomas (LG), and cystadenomas. Moreover, recurrent carcinomas have significantly higher expression levels than primary tumors ($P = 0.012$). The data are expressed as fold increase as compared with the average of OSE. (*B*) Immunohistochemistry demonstrates intense immunoreactivity in recurrent tumors as compared with patients' primary tumors in three representative cases.

patients ($P = 0.017$, χ^2 test) (Fig. 3*B*). Based on these findings, we further analyzed to see whether *NAC-1* expression in primary tumors was predicative of disease-free interval (the period between primary surgery and tumor recurrence) in 57 patients with advanced-stage high-grade serous carcinomas who underwent optimal primary debulking surgery, followed by a standard chemotherapeutic regimen in the same institution (JHMI). We found that high NAC-1 immunointensity (2+ and 3+) predicted recurrence within 1 year after diagnosis with an odds ratio of 14.9 (95% CI, 3.00–74.2; $P = 0.0002$, Fisher's exact test). The median disease-free interval with NAC-1 immunointensity of ≥2 was 12 months, whereas when the intensity was <2, the interval was 18 months.

The positive correlation of NAC-1 expression and recurrent disease suggests that NAC-1 plays a role in the development of recurrent ovarian tumors. To test whether NAC-1 expression directly contributes to drug resistance, we correlated NAC-1 immunoreactivity and *in vitro* drug resistance in 60 high-grade serous carcinomas. The *in vitro* drug-resistance results were performed at Oncotech (Tustin, CA) by using the protocol described at www.oncotech.com/pdfs/edr_4_pager.pdf (11, 12). Cases were grouped according to different immunointensity scores, but there was no significant correlation ($P > 0.17$, χ^2 test) between NAC-1 expression and *in vitro* resistance to carboplatin, cisplatin, and taxol, the standard chemotherapeutic agents for ovarian cancer.

Dominant Negative Role of NAC-1 BTB/POZ Domain. Because the BTB/POZ domain has been known to be involved in protein homomerization or heteromerization, we tested whether the NAC-1 BTB/POZ domain participated in protein–protein interaction using deletion mutants of NAC-1 (Fig. 4*A*). Based on coimmunoprecipitation and immunofluorescence colocalization studies (Fig. 4 *B* and *C*), we found that the BTB/POZ domain of NAC-1, corresponding to the 1–129 aa at the N terminus (N130 construct), was the minimal structural motif required for NAC-1 homooligomerization (Fig. 4*B*). The *NAC-1* deletion mutants/Xpress tags were then transfected into RK3E cells that had been stably transfected with a full-length NAC-1/V5 tag expression vector. As shown in Fig. 4*C*, full-length NAC-1/V5 colocalized with the full-length NAC-1/Xpress in the NAC-1 bodies, indicating that NAC-1 interacted with NAC-1. As expected, both *N130* and *N250* deletion mutants containing the BTB/POZ domain also colocalized with full-length *NAC-1*, but interestingly, both mutants disrupted the formation of NAC-1 bodies by transforming them into "cotton candy"-like aggregates or large "noodle"-like structures in the nuclei (Fig. 4*C*). In contrast, *C250* and *M120* deletion mutants that did not contain the BTB/POZ domain failed to colocalize with wild-type NAC-1.

Suppression of Tumor Formation upon Induction of NAC-1 N130 Mutant. To test whether the BTB/POZ domain is involved in tumor growth, we established an inducible (Tet-Off) system by expressing the N130 construct upon removal of doxycycline in two *NAC-1*-positive tumor cell lines, SKOV3, an ovarian cancer cell line, and HeLa, a cervical adenocarcinoma cell line. Cervical adenocarcinomas, like ovarian serous carcinomas, frequently overexpressed NAC-1, because a high level of NAC-1 immunoreactivity (2+ and 3+) occurred in ≈50% (16 of 32) cervical adenocarcinomas, whereas the NAC-1 immunoreactivity in normal endocervical glands were undetectable (Fig. 7, which is published as supporting information on the PNAS web site).

For both SKOV3-N130 and HeLa-N130 cell lines, the efficiency of N130 induction was very high as evidenced by >99% of cells expressing green fluorescence based on flow cytometry (data not shown) and increased copy number of N-terminal mRNA sequence as compared with C-terminal sequence based on quantitative real-time PCR (Fig. 8 *A* and *B*, which is published as supporting information on the PNAS web site) after removal of doxycycline. Like RK3E cells expressing the *N130* mutant (Fig. 4*C*), NAC-1 nuclear bodies were transformed to cotton candy-like aggregates in

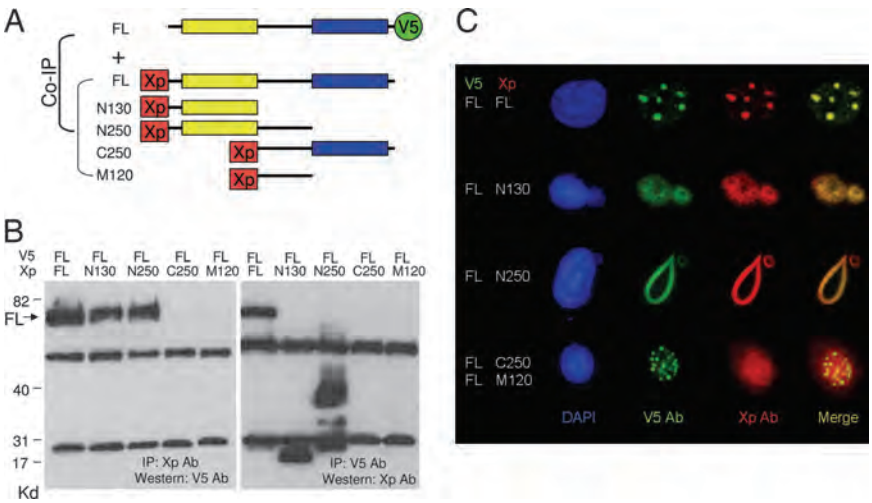

Fig. 4. Coimmunoprecipitation and colocalization of NAC-1 deletion mutants and full-length NAC-1. (*A*) Diagram of NAC-1 and NAC-1 deletion mutants. Full-length (FL) construct contains V5 tag at the C terminus, whereas all of the deletion mutants contain an Xpress (Xp) tag at the N terminus. The yellow box is the BTB/POZ domain; the blue box is the DUF1172 domain. (*B*) Coimmunoprecipitation shows that full-length NAC-1, N130, and N250 bind to NAC-1. The predicted molecular masses, not including the tag sequences, are: full-length NAC-1 (57.3 kDa), N130 (14.4 kDa), N250 (27.8 kDa), C250 (30.3 kDa), and M120 (14 kDa). (*C*) Cells with stable full-length NAC-1/V5 expression were transfected with different deletion mutants with the Xp tag. Double immunofluorescence shows that full-length NAC-1, N130, and N250 deletion mutants colocalize with full-length NAC-1. However, only full-length NAC-1 proteins form discrete round and oval-shaped NAC-1 nuclear bodies ,whereas both N130 and N250 form irregular aggregates with the full-length NAC-1. Neither C250 nor M120 colocalizes with the full-length NAC-1 protein.

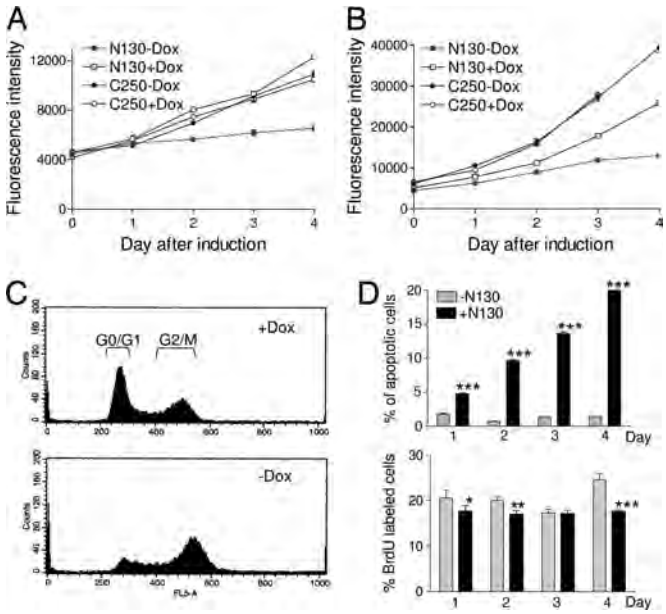

Fig. 5. Effects of N130 induction on cellular proliferation and apoptosis in 96-well plates. (*A* and *B*) Cell growth curves show that after induction of N130 (−Dox), cell growth is significantly suppressed as compared with the noninduced cells (+Dox). In contrast, induction of C250 does not have an apparent effect on cell growth in SKOV3 (*A*) or HeLa (*B*) cells. (*C*) Cell cycle analysis shows an increase in G_2/M fraction in N130-induced HeLa cells (*Lower*) as compared with noninduced cells (*Upper*) 24 h after induction, indicating a G_2/M block. (*D*) Percentages of apoptotic and proliferating cells are determined by counting annexin V- and BrdU-positive cells, respectively, in both N130-induced and -noninduced cells. Data are presented as mean + SD. *, $P < 0.05$; **, $P < 0.001$, ***, $P < 0.0001$, Student's *t* test.

both SKOV3 and HeLa cells after induction of *N130* (Fig. 8*C*). As compared with the control (induction of C250), induction of *N130* expression significantly reduced cell proliferation in both SKOV3 cells (Fig. 5*A*) and HeLa cells (Fig. 5*B*). Induction of the control *C250* mutant did not have significant effects on cellular proliferation in either of the cell lines. Similarly, expression of *N130* significantly suppressed colony formation in both cell lines (Fig. 9, which is published as supporting information on the PNAS web site). The decrease in cellular growth after *N130* induction was associated with cell cycle arrest at G_2/M phase (percentage of cells in G_0/G_1-to-S-to-G_2/M = 50.3%-to-16.5%-to33.2% in noninduced cells vs. 20.1%-to-17.4%-to-62.5% in induced cells) (Fig. 5*C*). *N130* induction significantly increased the number of annexin V-labeled cells and also decreased the number of BrdU-labeled cells (except on day 3), although the level in the decrease of cells with BrdU uptake is not as dramatic as the increase of annexin V-labeled cells (Fig. 5*D*). To further evaluate the effect of N130 on cellular proliferation and apoptosis, we used the miniN130 mutants, N65 and N30-122, in which its BTB/POZ oligomerization activity was deficient. Both N65 and N30-122 showed protein expression but were not able to coimmunoprecipitate with the full-length NAC-1 protein (Fig. 10*A*, which is published as supporting information on the PNAS web site). When transfecting these two constructs into the NAC-1 overexpressing SKOV3 cells, both N65 and N30-122 could not effectively suppress cellular proliferation as compared with N130 (Fig. 10*B*). In addition, we also knocked down NAC-1 using RNAi to determine whether there was a similar inhibitory effect to the expression of the N130 dominant-negative construct. In fact, NAC-1-expressing SKOV3 and HeLa cells had significantly reduced cell numbers after NAC-1 siRNA treatment (Fig. 11 *A* and *B*, which is published as supporting information on the PNAS web site). In contrast, NAC-1 siRNA did not show a significant effect on the cell growth of OVCAR3 cells that did not express abundant NAC-1 (Fig. 11*B*). Furthermore, we found that the apoptosis-inducing effect of the siRNAs used here was potent, but was less pronounced than the N130 dominant-negative NAC-1 (Fig. 11*C*), indicating that the latter approach could be a more effective experimental system to inactivate NAC-1 function. As a control, we expressed N130 in OVCAR3, which expressed only a minimal amount of NAC-1 protein compared with HeLa and SKOV3 cells, and found that N130 expression did not have a significant effect on the growth of OVCAR3 cells (Fig. 11*D*).

Based on the above findings, we investigated whether disrupting interactions between NAC-1 molecules using the N130 dominant-negative approach had a growth-inhibitory effect in HeLa (Fig. 12, which is published as supporting information on the PNAS web site) and SKOV3 (Fig. 13, which is published as supporting information on the PNAS web site) xenografts in nude mice. First, we tested whether expression of N130 could prevent tumorigenesis by inducing N130 expression 2 days after s.c. tumor injection. As shown in Figs. 12*A* and 13*A*, induction of N130 expression in HeLa and SKOV3 cells almost completely prevented the formation of s.c. tumors. In contrast, the control cells grew tumors at all injection sites. Second, we determined whether N130 could limit tumor growth in established HeLa and SKOV3 tumors. The expression of N130 was induced by removing doxycycline, when all of the mice harbor palpable tumors. Five days after discontinuation of doxycycline, induction of N130 expression was evidenced by green fluorescence in the s.c. HeLa tumors because expression of both N130 and EGFP was driven by a bicistronic promoter (Fig. 12*B*). As shown in Figs. 12*C* and 13*B*, tumors continued growing in control mice, whereas the tumors stopped growing or decreased in size after N130 induction. Histological examination of the tumors excised 10 days after N130 induction revealed extensive apoptosis in tumor cells, based on morphology and immunoreactivity with the M30 antibody, which recognizes the apoptosis-specific caspase-cleaved cytokeratin epitope (13, 14) (Fig. 12*D*).

The Oncogenic Potential of NAC-1 Expression. To test whether NAC-1 expression is tumorigenic, we randomly selected two clones from a spontaneously immortalized MOSE cell line and two NIH 3T3 clones that were stably transfected with an NAC-1 expression vector (Fig. 6). When compared with vector-transfected controls, all NAC-1-expressing clones had a higher cellular proliferation, based on growth curves and BrdU-uptake assays (Fig. 6 *A*, *D*, and *F*). S.c. injections of NAC-1-expressing MOSE clones in athymic *nu*/*nu* mice produced larger tumors than the control cells transfected with the vector-only (Fig. 6 *B* and *C*). MOSE clones did not grow i.p. tumors 21 days after i.p. injection. The NAC-1-expressing NIH 3T3 clones produce both s.c. and i.p. tumors in the athymic *nu*/*nu* mice. The i.p. tumors were always multiple, and their combined weights were measured in each mouse (Fig. 6*E*). In contrast, the vector-transfected NIH 3T3 cells did not grow tumors during the course of this study.

Discussion

NAC-1 was first identified and cloned as a transcript induced in the nucleus accumbens from rats treated with cocaine (15). The nucleus accumbens is a unique forebrain structure involved in reward motivation (16) and many addictive behaviors (17–19). Except for its role in cocaine-induced expression in animal brains, the cellular function of NAC-1 is unknown. In this study, we demonstrate that *NAC-1* is a previously uncharacterized cancer-associated gene, because the NAC-1 expression level is significantly increased in several types of cancers including ovarian cancer, cervical adenocarcinoma, and breast cancer. We showed that NAC-1 was required for cell proliferation and survival and was sufficient to enhance tumorigenicity in athymic *nu*/*nu* mice.

Cancer mortality and morbidity are related to recurrent and metastatic disease. Therefore, a positive correlation between

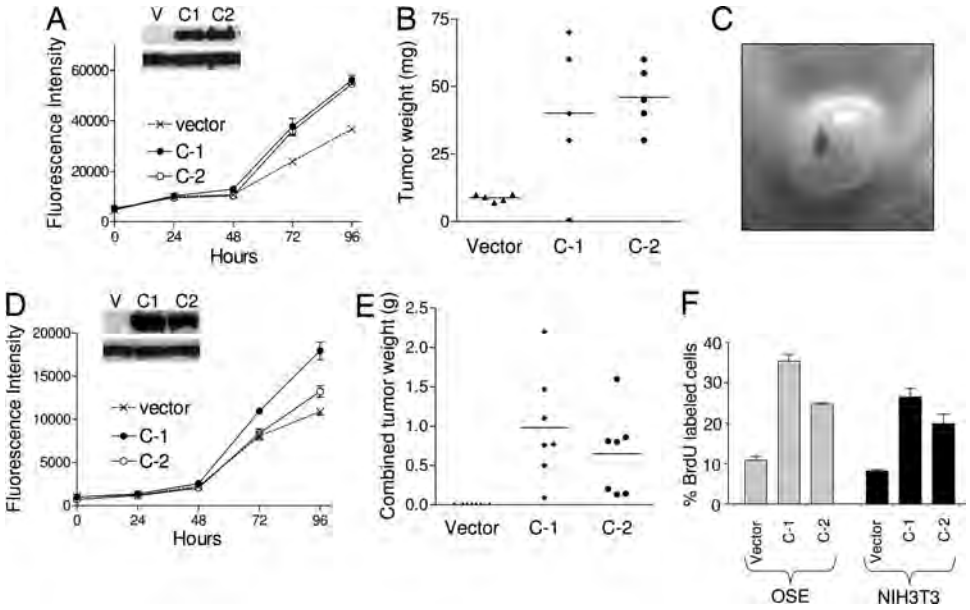

Fig. 6. Effects of constitutive expression of NAC-1 in immortalized ovarian surface epithelial cells (MOSE) and NIH 3T3 cells. Western blot analysis shows NAC-1 expression in stable clones of NAC-1-expressing MOSE cells (*A*) and NIH 3T3 cells (*D*). Upper blots, NAC-1; lower blots, GAPDH. Growth curves show a higher proliferation activity in both NAC-1 clones as compared with vector-transfected control under a low serum (0.5%) culture condition in MOSE cells (*A*) and NIH 3T3 cells (*D*). The weights of s.c. tumors increase in NAC-1-expressing MOSE tumors as compared with control MOSE in nude mice (*B*). A representative photomicrograph shows a s.c. NAC-1-expressing MOSE tumor (*C*). Similarly, the combined tumor weights of tumors in the peritoneal wall of the NAC-1-expressing NIH 3T3 cells are greater than the controls (*E*). (*F*) Cell proliferation was determined by a BrdU-incorporation assay, and all NAC-1-expressing clones have a higher proliferation rate than the vector-only control. Data are presented as mean + SD.

NAC-1 expression and recurrence status in ovarian carcinoma as shown in this study has significant biological and clinical implications. First, NAC-1 expression may directly contribute to tumor recurrence and tumor progression. However, a lack of correlation between NAC-1 expression and *in vitro* drug resistance to taxol, carboplatin, and cisplatin, the primary chemotherapeutic agents used in the treatment of ovarian cancer patients, suggests that NAC-1 may not directly participate in the development of drug resistance. Because the etiology of tumor recurrence is multifactorial, it is likely that NAC-1 overexpression confers a growth advantage to tumor cells by providing them with higher proliferative and lower apoptotic activity as shown in this study. Second, we demonstrated that intense NAC-1 immunoreactivity in primary tumors is highly predictive of a shorter disease-free interval; therefore, NAC-1 expression may potentially be used alone or in combination with other markers as a prognostic test to identify ovarian cancer patients who are likely to develop early recurrence. This finding can have potential clinical implications because at least 60% of advanced-stage ovarian cancer patients who appear to be disease-free after completing primary therapy ultimately develop recurrent disease (20). Thus, patients with NAC-1-positive ovarian serous carcinoma can be monitored more closely to detect recurrent tumor. It has been demonstrated that ovarian carcinoma patients can most benefit from secondary cytoreduction when the recurrent tumor is small and localized (20–24).

Similar to other BTB/POZ members, the NAC-1 BTB/POZ domain is essential and sufficient for NAC-1 homomerization. Based on immunoprecipitation using the NAC-1 antibody and tumor lysates from ovarian cancer tissues that expressed NAC-1, we did not detect other proteins that were pulled down with NAC-1, suggesting that NAC-1 molecules may homooligomerize to each other. The dominant-negative strategy using the *N130* deletion mutant suggests that homooligomerization of NAC-1 is required for formation of NAC-1 nuclear bodies. Although both *N130* and *N250* deletion mutants can be coimmunoprecipitated and colocalized with wild-type (full-length) NAC-1 molecules, they transformed the morphology of NAC-1 bodies, suggesting that both the BTB/POZ domain and the C-terminal motif of the NAC-1 molecule are critical for NAC-1 body formation. This finding is consistent with what has been observed in LAZ3/BCL6 proteins in which the BCL6 BTB/POZ domain has the capability to self-interact and target the protein to form discrete nuclear substructures (25). Furthermore, expression of the *N130* mutant but not miniN130 mutants that failed to bind to NAC-1 suppressed cellular proliferation and induced apoptosis, suggesting that interaction among NAC-1 molecules or between NAC-1 and other partner protein(s) through their BTB/POZ domains is essential for NAC-1-regulated tumor cell growth and survival. This result is similar to BCL-6 in which the peptide inhibitors that block interaction between the BCL-6 BTB/POZ domain and corepressors abrogate BCL-6 oncogenic functions in B cells and suggests that targeting the BTB/POZ domain of a specific BTB/POZ member may provide an approach for cancer therapy (5). Besides its critical role in maintaining cell proliferation and survival, NAC-1 expression could also enhance cellular proliferation and induce tumorigenicity in athymic *nu/nu* mice. These findings suggest that *NAC-1* is a gene with oncogenic potential in ovarian carcinomas.

In conclusion, this study shows that expression of NAC-1, a member of BTB/POZ family, is associated with the development of recurrent ovarian serous carcinoma. Homo-oligomerization of NAC-1 proteins through the BTB/POZ domains is essential for cell survival in carcinomas that express NAC-1. Targeting the BTB/POZ domain of NAC-1 could be a molecular strategy for drug intervention in ovarian cancer and other types of cancer with NAC-1 overexpression.

Materials and Methods

For detailed procedures of quantitative PCR, siRNA knockdown, and tumor xenograft assay, please see *Supporting Material and Methods*, which is published as supporting information on the PNAS web site.

Tag Counts of the BTB/POZ Family Genes from SAGE Libraries. Proteins matching the PS50097 profile of the BTB/POZ domain amino acid

sequence were extracted from the Swiss-Prot/TrEMBL protein databank released on January 16, 2006 (http://us.expasy.org/cgi-bin/get-entries?DR=PS50097&db=tr&db=sp&view=tree). A total of 130 BTB/POZ genes were identified. The expression levels of the BTB/POZ gene family members were determined from the ovarian tumor SAGE libraries by obtaining the SAGE tag counts for each BTB/POZ gene. The libraries included the OSE cells (SV-40 immortalized IOSE29 (26) and short-term cultured HOSE4), benign cystadenoma (ML10), ovarian high-grade serous carcinoma tissues (HG63, HG48, HG92, OVT6, OVT7, and OVT8), and ovarian cancer cell lines (OVCAR3 and A2780). All libraries have been published (27), except HG63, HG48 and HG92 which were established in this study. The NAC-1-specific SAGE tags included TTCCCGGCCC, TGAAGGCAGT, CCTATAATCG, AGTGCCAGGG, AGAATATCAG, GAGGGAGGGA, and GTTCCCCCAC. By using a minimum tag count setting of >1, these NAC-1 tags were tallied and normalized per 100,000 total tags for each SAGE library. To select the candidate gene(s) for further study, we first select those with a high average tag count (>10 tags per 100,000 tags) in ovarian carcinoma libraries, followed by the highest ratio of average tag counts in ovarian carcinoma to the benign controls (IOSE29, HOSE4, and ML10).

To determine the NAC-1 expression levels among different cancer libraries, we compared NAC-1 tag counts among 81 SAGE libraries (http://cgap.nci.nih.gov/SAGE) (28, 29) from carcinomas and normal tissues of ovary, pancreas, liver, colon, kidney, prostate, and breast (30). NAC-1 tag counts for each library were retrieved by filtering for tag sequences that matched uniquely to NAC-1 according to the April 15, 2005 SAGEMap available on the public National Center for Biotechnology Information FTP site (ftp://ftp.ncbi.nlm.nih.gov/pub/sage/map/Hs/NlaIII).

Immunohistochemistry and Immunoelectron Microscopy. Paraffin-embedded tumor tissues were obtained from the Department of Pathology at the Johns Hopkins Hospital and effusion ovarian cancer samples were obtained from the Norwegian Radium National Hospital in Norway. These included 182 high-grade ovarian serous carcinoma tissues (154 stage III and 28 stage IV), 44 low-grade ovarian serous carcinoma tissues (42 stage III and 2 stage IV), 172 high-grade ovarian carcinoma effusion samples (1 stage I, 6 stage II, 97 stage III, and 68 stage IV), and 32 cervical adenocarcinomas. In addition, 21 benign ovarian cystadenomas, 18 normal ovaries, and 8 normal cervical tissues were included for comparison. Acquisition of tissue specimens and clinical information was approved by an institutional review board (Johns Hopkins Medical Institutions) or by the Regional Ethics Committee (Norwegian Radium Hospital).

For immunohistochemistry studies, we generated a mouse NAC-1 monoclonal antibody by immunizing mice with the NAC-1 recombinant protein using a standard hybridoma protocol (31). Immunohistochemistry was performed on deparaffinized sections by using the NAC-1 antibody at a dilution of 1:100 and an EnVision+System peroxidase kit (DAKO, Carpinteria, CA). Immunoreactivity was scored by two investigators as follows: 0, undetectable; 1+, weakly positive; 2+, moderately positive; and 3+, intensely positive. NAC-1 immunoreactivity was not detectable (immunointensity score = 0) or weak (1+) in normal OSE and benign serous cystadenomas. For ultrastructure study of NAC-1 bodies, we applied ImmunoGold labeling on NAC-1-expressing-RK3E cells, followed by electron microscopy.

Coimmunoprecipitation and Double Immunofluorescence Staining. A series of *NAC-1*-deletion mutants including N130 (encoding the amino acids 1–129 at the N terminus), N250 (amino acids 1–263 at the N terminus), M120 (amino acids 123–263 in the middle portion), and C250 (amino acids 257–528 at the C terminus) were generated by PCR. Both N130 and N250 mutants contained the BTB/POZ domain (amino acids 20–122) of NAC-1. In addition, two miniN130 expression constructs were generated, and they included N65 (encoding the first 1–65 aa of the BTB domain) and N30-122 (30–122 aa). PCR products of the *NAC-1*-deletion mutants were cloned into an expression vector, pCDNA4 with an Xpress tag at the N terminus. RK3E cells were first stably transfected with pCDNA6/V5/NAC-1 and then transiently transfected with the pCDNA4/NAC-1-deletion mutants. Coimmunoprecipitation was performed to assess the specific structural motifs that bound to full-length NAC-1. For immunofluorescence staining, cells were incubated with primary antibodies, followed by fluorescence-labeled secondary antibodies.

N130-Inducible Construct, Cell Proliferation, and Apoptosis Assays. The Tet-Off inducible system was used to assess the biological effects of N130. HeLa and SKOV3 cells that constitutively expressed tTA (tetracycline-controlled transactivator) were transfected with pBI-N130/EGFP or pBI-C250/V5-EGFP (control) that bicistronically expressed the products of interest and reporter EGFP upon the binding of tTA to the tetracycline-responsive element in the absence of inducer (doxycycline). Cell proliferation and apoptosis assays were performed as described (32) in 96-well plates.

We thank Mr. David Chu and Mr. M. Jim Yen for editorial assistance and Dr. C.-Y. Hsu for organization of cervical adenocarcinoma tissue microarrays. This study was supported by Department of Defense Grant OC0400600 and National Institutes of Health Grant CA103937.

1. Stogios PJ, Downs GS, Jauhal JJ, Nandra SK, Prive GG (2005) *Genome Biol* 6:R82.1–R82.17.
2. Bardwell VJ, Treisman R (1994) *Genes Dev* 8:1664–1677.
3. Albagli O, Dhordain P, Deweindt C, Lecocq G, Leprince D (1995) *Cell Growth Differ* 6:1193–1198.
4. Chen Z, Brand NJ, Chen A, Chen SJ, Tong JH, Wang ZY, Waxman S, Zelent A (1993) *EMBO J* 12:1161–1167.
5. Polo JM, Dell'Oso T, Ranuncolo SM, Cerchietti L, Beck D, Da Silva GF, Prive GG, Licht JD, Melnick A (2004) *Nat Med* 10:1329–1335.
6. Yeyati PL, Shaknovich R, Boterashvili S, Li J, Ball HJ, Waxman S, Nason-Burchenal K, Dmitrovsky E, Zelent A, Licht JD (1999) *Oncogene* 18:925–934.
7. Maeda T, Hobbs RM, Merghoub T, Guernah I, Zelent A, Cordon-Cardo C, Teruya-Feldstein J, Pandolfi PP (2005) *Nature* 433:278–285.
8. Maeda T, Hobbs RM, Pandolfi PP (2005) *Cancer Res* 65:8575–8578.
9. van Roy FM, McCrea PD (2005) *Nat Rev Cancer* 5:956–964.
10. Park JI, Kim SW, Lyons JP, Ji H, Nguyen TT, Cho K, Barton MC, Deroo T, Vleminckx K, Moon RT, McCrea PD (2005) *Dev Cell* 8:843–854.
11. Fruehauf JP, Alberts DS (2003) *Recent Results Cancer Res* 161:126–145.
12. Eltabbakh GH, Piver MS, Hempling RE, Recio FO, Lele SB, Marchetti DL, Baker TR, Blumenson LE (1998) *Gynecol Oncol* 70:392–397.
13. Leers M, Kolgen W, Bjorklund V, Bergman T, Tribbick G, Persson B, Bjorklund P, Ramaekers FC, Bjorklund B, Schutte B (1999) *J Pathol* 5:567–572.
14. Caulin C, Salvesen GS, Oshima RG (1997) *J Cell Biol* 138:1379–1394.
15. Cha XY, Pierce RC, Kalivas PW, Mackler SA (1997) *J Neurosci* 17:6864–6871.
16. Roitman MF, Wheeler RA, Carelli RM (2005) *Neuron* 45:587–597.
17. Koob GF (1996) *Neuron* 16:893–896.
18. Mackler SA, Korutla L, Cha XY, Koebbe MJ, Fournier KM, Bowers MS, Kalivas PW (2000) *J Neurosci* 20:6210–6217.
19. Kalivas PW, Duffy P, Mackler SA (1999) *Synapse* 33:153–159.
20. Diaz-Montes TP, Bristow RE (2005) *Curr Oncol Rep* 7:451–458.
21. Harter P, du Bois A (2005) *Curr Opin Oncol* 17:505–514.
22. Gadducci A, Iacconi P, Cosio S, Fanucchi A, Cristofani R, Riccardo Genazzani A (2000) *Gynecol Oncol* 79:344–349.
23. Gadducci A, Iacconi P, Fanucchi A, Cosio S, Teti G, Genazzani AR (2000) *Anticancer Res* 20:1959–1964.
24. Zang RY, Li ZT, Tang J, Cheng X, Cai SM, Zhang ZY, Teng NN (2004) *Cancer* 100:1152–1161.
25. Dhordain P, Albagli O, Ansieau S, Koken MH, Deweindt C, Quief S, Lantoine D, Leutz A, Kerckaert JP, Leprince D (1995) *Oncogene* 11:2689–2697.
26. Auersperg N, Pan J, Grove BD, Peterson T, Fisher J, Maines-Bandiera S, Somasiri A, Roskelley CD (1999) *Proc Natl Acad Sci USA* 96:6249–6254.
27. Hough CD, Sherman-Baust CA, Pizer ES, Montz FJ, Im DD, Rosenshein NB, Cho KR, Riggins GJ, Morin PJ (2000) *Cancer Res* 60:6281–6287.
28. Boon K, Osorio EC, Greenhut SF, Schaefer CF, Shoemaker J, Polyak K, Morin PJ, Buetow KH, Strausberg RL, De Souza SJ, Riggins GJ (2002) *Proc Natl Acad Sci USA* 99:11287–11292.
29. Lal A, Lash AE, Altschul SF, Velculescu V, Zhang L, McLendon RE, Marra MA, Prange C, Morin PJ, Polyak K, *et al.* (1999) *Cancer Res* 59:5403–5407.
30. Yen M-J, Hsu CY, Mao TT, Wu TC, Roden R, Wang TL, Shih IM (2006) *Clin Cancer Res* 12:827–831.
31. Shih IM, Elder DE, Speicher D, Johnson JP, Herlyn M (1994) *Cancer Res* 54:2514–2520.
32. Shih IM, Sheu JJ, Santillan A, Nakayama K, Yen MJ, Bristow RE, Vang R, Parmigiani G, Kurman RJ, Trope CG, *et al.* (2005) *Proc Natl Acad Sci USA* 102:14004–14009.

Research Article

Notch3 Gene Amplification in Ovarian Cancer

Joon T. Park,[1,2] Mei Li,[1] Kentaro Nakayama,[2] Tsui-Lien Mao,[2] Ben Davidson,[3] Zhen Zhang,[2] Robert J. Kurman,[1,2] Charles G. Eberhart,[2] Ie-Ming Shih,[1,2] and Tian-Li Wang[1]

Departments of [1]Gynecology and Obstetrics and Oncology, and [2]Pathology, The Johns Hopkins Medical Institutions, Baltimore, Maryland; and [3]Department of Pathology, Norwegian Radium Hospital, University of Oslo, Oslo, Norway

Abstract

Gene amplification is one of the common mechanisms that activate oncogenes. In this study, we used single nucleotide polymorphism array to analyze genome-wide DNA copy number alterations in 31 high-grade ovarian serous carcinomas, the most lethal gynecologic neoplastic disease in women. We identified an amplicon at 19p13.12 in 6 of 31 (19.5%) ovarian high-grade serous carcinomas. This amplification was validated by digital karyotyping, quantitative real-time PCR, and dual-color fluorescence *in situ* hybridization (FISH) analysis. Comprehensive mRNA expression analysis of all 34 genes within the minimal amplicon identified *Notch3* as the gene that showed most significant overexpression in amplified tumors compared with nonamplified tumors. Furthermore, *Notch3* DNA copy number is positively correlated with Notch3 protein expression based on parallel immunohistochemistry and FISH studies in 111 high-grade tumors. Inactivation of Notch3 by both γ-secretase inhibitor and Notch3-specific small interfering RNA suppressed cell proliferation and induced apoptosis in the cell lines that overexpressed Notch3 but not in those with minimal amount of Notch3 expression. These results indicate that Notch3 is required for proliferation and survival of *Notch3*-amplified tumors and inactivation of Notch3 can be a potential therapeutic approach for ovarian carcinomas. (Cancer Res 2006; 66(12): 6312-8)

Introduction

Gene amplification is one of the key mechanisms in activating oncogenes in human cancer (1). Ovarian cancer is the most malignant gynecologic neoplasm. Each year, ~16,000 women will succumb to this disease. In ovarian carcinomas, amplifications of *cyclin E1* (2), *Her2/neu* (3), *AKT2* (4), *L-Myc* (5), and *Rsf-1* (6) have been reported. Because these amplifications occur only in a subset of tumors, it is expected that additional oncogenic amplifications will be identified. Recent developments of molecular genetic techniques that allow a genome-wide exploration of DNA copy number in cancer have provided investigators unprecedented opportunities to analyze cancer genome in great details. For example, single nucleotide polymorphism (SNP) array has been recently shown as an effective tool in discovering amplified chromosomal regions (7, 8). In the current study, we did SNP array analysis on 31 high-grade ovarian serous carcinomas purified from fresh clinical samples and identified a chromosomal region at 19p13.12 that is frequently amplified. One of the genes within this amplicon, *Notch3*, showed the most significant correlation between gene copy numbers and transcript expression in ovarian cancer, suggesting that *Notch3* is a candidate oncogene in the chr19p13.12 amplicon.

Materials and Methods

Tumor specimens. For SNP arrays, tissue samples, including 31 high-grade and 7 low-grade ovarian serous carcinomas, were obtained from the department of pathology at the Johns Hopkins Hospital and the Norwegian Radium Hospital in Norway. Tumor cells were affinity purified by anti-EPCAM–conjugated beads. In addition, genomic DNA from 13 normal ovarian tissues was prepared for controls. For quantitative reverse transcription-PCR (RT-PCR), 89 frozen tumor tissues were used to extract RNA, and nine normal ovarian tissues were also included as controls. Acquisition of tissue specimens and clinical information was approved by an institutional review board (Johns Hopkins University) or by the Regional Ethics Committee (Norway).

SNP array. SNPs were genotyped using 10K arrays (Affymetrix, Santa Clara, CA) in the Microarray Core Facility at the Dana-Farber Cancer Institute (Boston, MA). A detailed protocol is available at the Core center web page.[4] Briefly, genomic DNA was cleaved with the restriction enzyme, *Xba*I, ligated with linkers, followed by PCR amplification. The PCR products were purified and then digested with DNaseI to a size ranging from 250 to 2,000 bp. Fragmented PCR products were then labeled with biotin and hybridized to the array. Arrays were then washed on the Affymetrix fluidics stations. The bound DNA was then fluorescently labeled using streptavidin-phycoerythrin conjugates and scanned using the Gene Chip Scanner 3000.

dChip software version 1.3 was used to analyze the SNP array data as described previously (7, 8). Data was normalized to a baseline array with median signal intensity at the probe intensity level using the invariant set normalization method. A model-based (PM/MM) method was used to obtain the signal values for each SNP in each array. Signal values for each SNP were compared with the average intensities from 13 normal samples. To infer the DNA copy number from the raw signal data, we used the Hidden-Markov model (7) based on the assumption of diploidy for normal samples. Mapping information of SNP locations and cytogenetic band were based on curation of Affymetrix and University of California Santa Cruz hg15. A cutoff of >2.8 copies in more than three consecutive SNPs was defined as amplification.

Digital karyotyping. Purified carcinoma cells as described in the SNP array method were used to generate digital karyotyping library as previously described (9). Approximate 120,000 genomic tags were obtained for each digital karyotyping library. After removing the nucleotide repeats in human genome, the average of filtered tags was 66,000 for each library. We set up a window size of 300 (300 virtual tags) for the analysis in this study. Based on Monte Carlo simulation, the variables used in this study can reliably detect >0.6 Mb amplicon with >5-fold amplification with >99% sensitivity and 100% positive predictive value.

Note: Supplementary data for this article are available at Cancer Research Online (http://cancerres.aacrjournals.org/).

Requests for reprints: Tian-Li Wang, Departments of Gynecology/Obstetrics and Oncology, Johns Hopkins University School of Medicine, CRBII, 1550 East Jefferson Street, Room 306, Baltimore, MD 21231. Phone: 410-502-7774; Fax: 410-502-7943; E-mail: tlw@jhmi.edu.

doi:10.1158/0008-5472.CAN-05-3610

[4] http://chip.dfci.harvard.edu/lab/services.php.

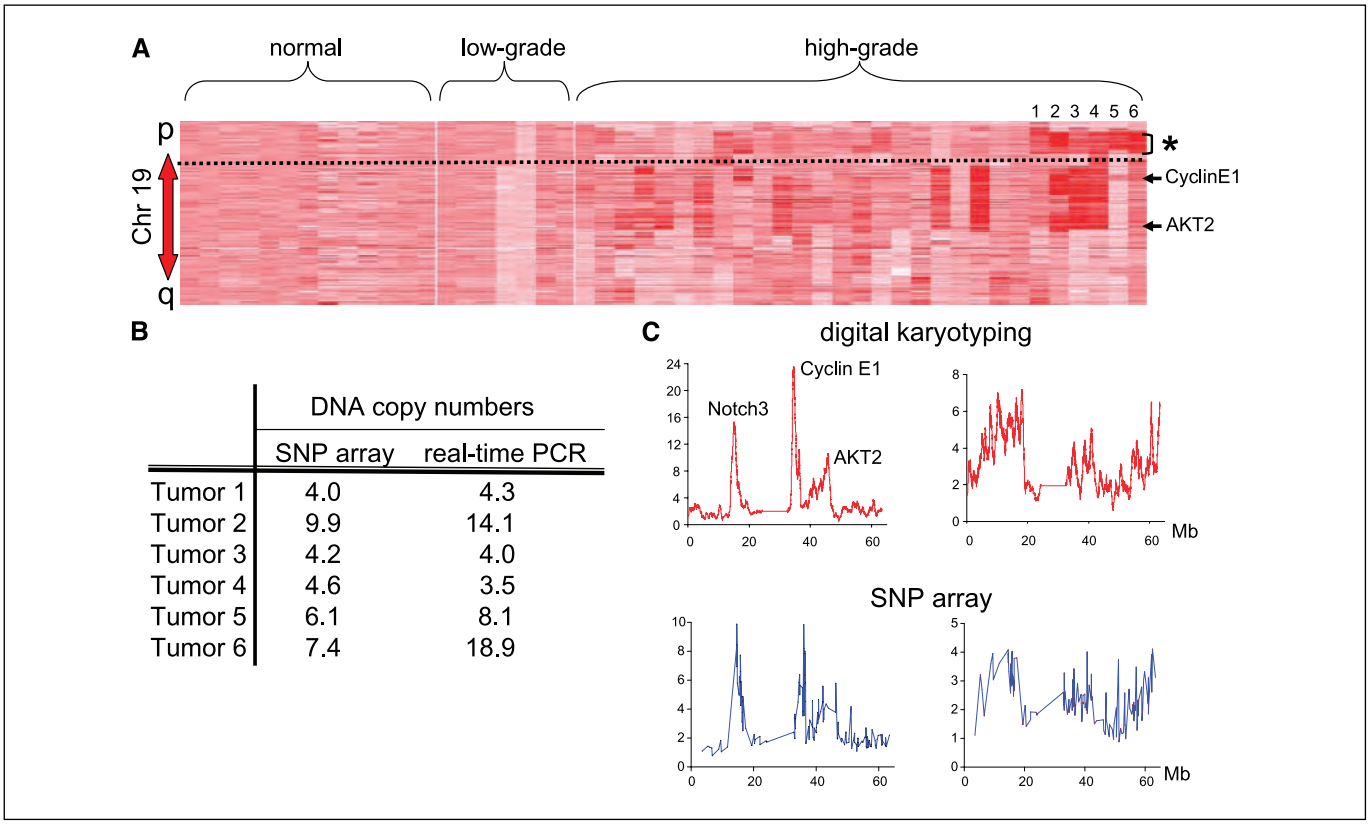

	DNA copy numbers	
	SNP array	real-time PCR
Tumor 1	4.0	4.3
Tumor 2	9.9	14.1
Tumor 3	4.2	4.0
Tumor 4	4.6	3.5
Tumor 5	6.1	8.1
Tumor 6	7.4	18.9

Figure 1. Identification of chr19p13.12 amplification in high-grade ovarian serous carcinomas. *A,* SNP array analysis shows several distinct amplicons on chromosome 19 (*top to bottom,* p to q arm) including the *cyclin E1* and *AKT2* loci and a novel amplicon at chr19p13.12 (*bracket*). An increase in DNA copy number is indicated by a gradient in color with 0 copy in white and five or more copies in red. Each column represents an individual tumor sample. *B,* quantitative real-time PCR on genomic DNA validates the amplification on the six tumors with chr19p13.12 amplification identified by the SNP array analysis. *C,* comparison of DNA copy number using SNP array and digital karyotyping on chromosome 19. The data of SNP array is compared with that of digital karyotyping analysis on two representative specimens. *Left,* tumor 2, which contains a high copy number amplification at chr19p13.12. *Right,* tumor 1, which contains a low copy number gain at chr19p13.12. Both SNP array and digital karyotyping analyses show a similar pattern of DNA copy number alterations.

Fluorescence *in situ* hybridization and quantitative real-time PCR. BAC clones (RP11-937H1 and RP11-319O10) containing the genomic sequences of the 19p13.12 amplicon at 15.00 to 15.25 Mb were purchased from Bacpac Resources (Children's Hospital, Oakland, CA). BAC clone (RP11-752A21), located at 19q13.42 (59.26-59.46 Mb), was used to generate the reference probe. The method for fluorescence *in situ* hybridization (FISH) has been detailed in a previous report (6).

Relative gene expression and genomic amplification levels were measured by quantitative real-time PCR using methods previously described (9, 10). PCR primers were designed using the Primer 3 program and the nucleotide sequences of the primers for determining transcript expression were listed in Supplementary Table S1. The primer sequences to determine the 19p13.12 genomic amplification were 5′-GCCTGTGGCTGAAAATTAAGG-3′ and 5′-TCAATGTCCACCTCGCAATAG-3′.

Immunohistochemistry. A rabbit polyclonal anti-Notch3 antibody was purchased from Santa Cruz Biotechnology (Santa Cruz, CA) and was used in the immunohistochemistry. An EnVision+System peroxidase kit (DAKO, Carpinteria, CA) was used for staining following the protocol provided by the manufacturer. Tissue microarrays (triplicate 1.5 mm cores from each specimen) including 111 high-grade serous carcinomas and 10 normal ovaries were used to facilitate immunohistochemistry. Immunointensity was scored as negative (0), negligible (1+), moderate (2+), and intense (3+), and two investigators independently scored all the samples. For discordant cases, a third investigator scored and the final intensity score was determined by the majority scores.

Cell proliferation and apoptosis assays. Cells were grown in 96-well plates at a density of 4,000 per well. Type 1 γ-secretase inhibitor was purchased from Calbiochem (San Diego, CA) and was dissolved in DMSO as 4 mmol/L stock solution. Cells were treated with γ-secretase inhibitor with DMSO final concentration <0.1%. Notch3-specific small interfering RNA (siRNA) (rGrUrCrArArUrGrUrUrCrArCrUrUrCrGrCrArGrUrU and rGrCrGrUrGrGrArUrUrCrGrGrArCrCrArGrUrCrUrGrArGrArGrGrG) and control siRNA that targets the *Luciferase* gene (rGrArUrUrArArArUrCrUr-UrCrUrArGrCrGrArCrUrGrCrUrUrCrGrC) were synthesized by Integrated DNA Technologies (Coralville, IA). Cells were treated with siRNA at a final concentration of 200 nmol/L.

Cell number was measured by the fluorescence intensity of SYBR green I nucleic acid gel stain (Molecular Probes, Eugene, OR) using a fluorescence microplate reader (Fluostar from BMG, Durham, NC). Data was determined from five replicates and was expressed as the percentage of the inhibitor or Notch3 siRNA-treated cells versus DMSO or control siRNA-treated cells. BrdUrd uptake and staining were done using a cell proliferation kit (Amersham, Buckinghamshire, England, United Kingdom) and apoptotic cells were detected using an Annexin V staining kit (BioVision, Mountain View, CA). The percentage of BrdUrd-positive and Annexin V–positive cells was determined by counting ~400 cells from each well in 96-well plates. The data was expressed as mean ± 1 SD from triplicates.

Results and Discussion

Amplification of chromosome 19 in ovarian serous carcinomas. SNP arrays were used to search for genome-wide DNA copy number alterations in 31 high-grade and 7 low-grade ovarian serous carcinomas. In addition, 13 normal ovarian tissues were analyzed as controls. We found several distinct amplifications on

chromosome 19 specific to high-grade serous carcinomas. Among them, amplification of the *cyclin E1* locus was present in 10 of 31 (32.2%) samples and amplification of *AKT2* locus in 9 of 31 (29%) samples. Both *cyclin E1* and *AKT2* have been previously reported as potential oncogenes that are frequently amplified in ovarian cancer. More importantly, a novel amplification on chr19p13.12 was identified in 6 of 31 (19.5%) high-grade carcinomas. The peak copy number changes in these six amplified tumors ranged from four to nine copies based on SNP array analysis (Fig. 1*A* and *B*). In contrast to high-grade serous carcinomas, no evidence of amplification at 19p13.12, or *cyclin E1* or *AKT2* loci could be detected in low-grade ovarian tumors or normal ovarian tissues.

Three independent methods were used to validate the 19p13.12 amplification. First, digital karyotyping was done on a tumor with low level of gain (four copies) and a tumor with high level of amplification (nine copies) based on SNP array analysis. Digital karyotyping is a recently developed genome-wide technology that allows a precise measurement of DNA copy number at high resolution (9). The method has been used to identify new amplicons in human cancer (6, 11–13) and using digital karyotyping, we found similar location and amplitude of these amplicons detected by SNP arrays (Fig. 1*C*). Second, quantitative real-time PCR was used to measure the copy number of the predicted amplification in all of the six tumors (Fig. 1*B*). The amplification levels based on the SNP arrays were generally in agreement with quantitative PCR but with an underestimation of copy number in those samples with high amplitude of amplifications. This could be due to the saturation of probe hybridization signal associated with array platform. Third, dual-color FISH analysis was done on all six amplified tumors using a BAC clone located at the 19p13.12 amplicon and a BAC clone located at the 19q as the reference. All of the six cases showed increased target signals compared with the reference signals. Among them, four cases showed a pattern of chromosomal gain and two cases showed a pattern of homogenously staining region. Taken together, the above results confirmed amplification of 19p13.12 in high-grade ovarian serous carcinomas.

***Notch3* as the candidate cancer-related gene in the 19p13.12 amplicon.** To select the most promising tumor-associated gene within the minimal amplicon, we aligned the amplicons from these six tumors and delineated a common region of amplification (minimal amplicon), which spanned from 14.60 to 16.47 Mb on chromosome 19p and contained 34 genes (Fig. 2). To identify the candidate-amplified tumor-associated gene within the amplicon, we correlated the gene copy number and gene expression levels for all 34 genes based on the rationale that a tumor-driving gene, when amplified, should overexpress to activate its tumorigenic pathway, whereas coamplified "passenger" genes that are not related to tumor development may or may not do so (14). This approach can be useful to narrow down the candidate gene lists, although some amplification events may not necessarily have overexpression of the gene of interest. The mRNA levels were measured using quantitative RT-PCR on five high-grade carcinomas with 19p13.12

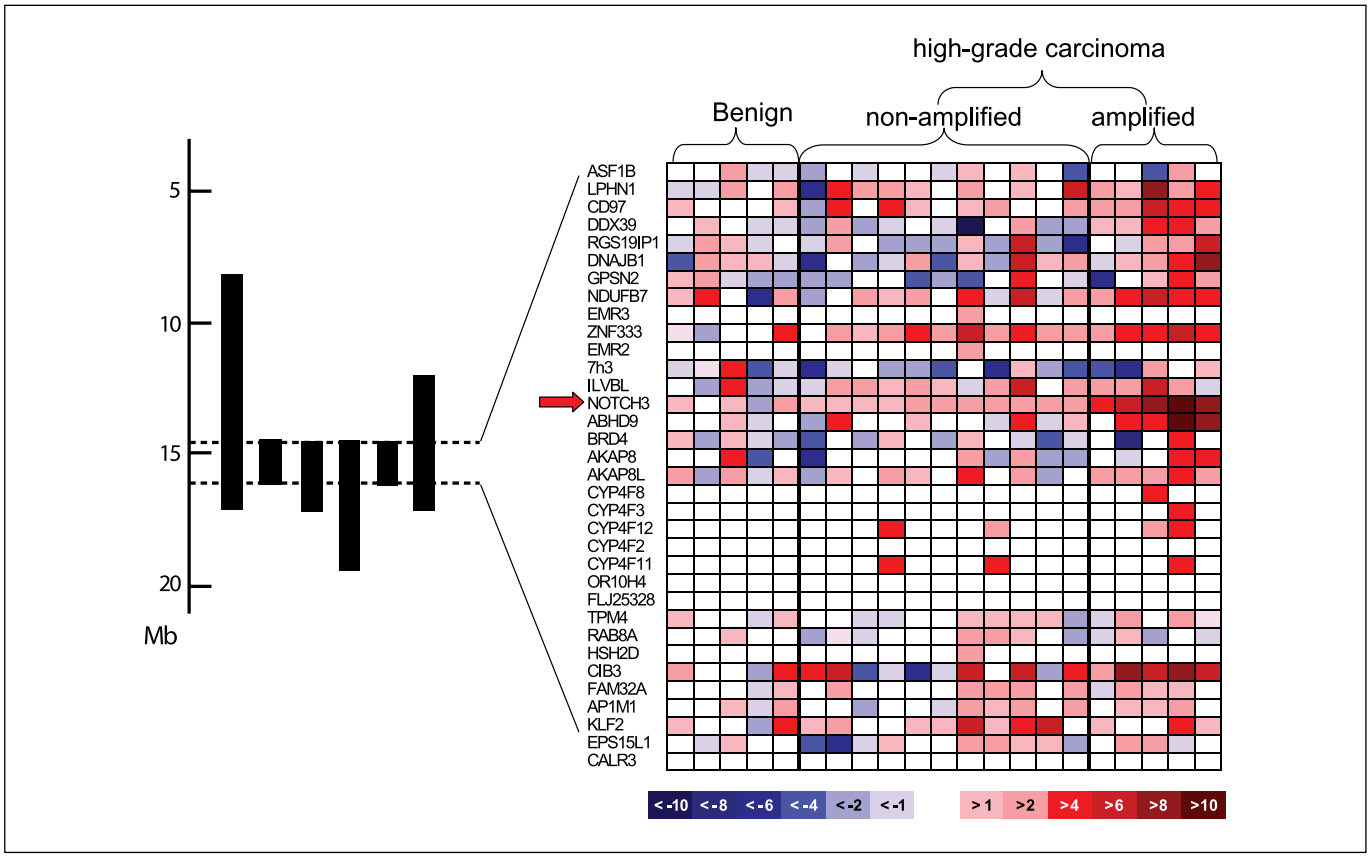

Figure 2. Gene expression analysis of the 19p13.12 amplicon in ovarian tumors. *Left,* alignment of the amplicons from the 19p13.12-amplified tumors reveals a common region of amplification spanning from 14.60 to 16.47 Mb at chromosome 19p. *Right,* quantitative real-time PCR was done for all 34 genes located within the minimal amplicon in high-grade serous carcinomas with or without 19p13.12 amplification and benign OSE cells were used as controls. The expression level of each gene (*top to bottom,* centromeric to telomeric) in individual specimen is shown as a pseudocolor gradient based on the relative expression level of a given specimen to the average value derived from five benign OSE samples.

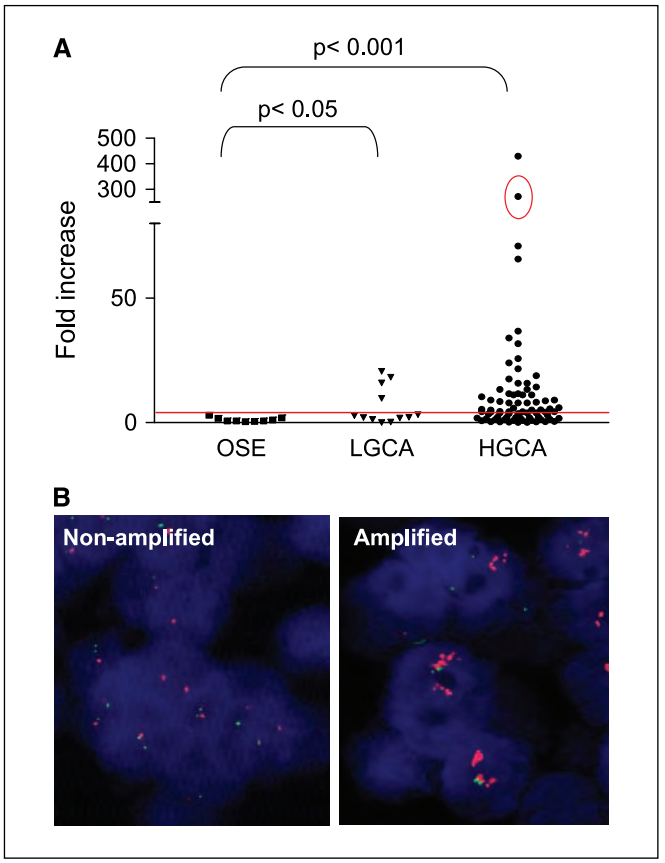

Figure 3. Overexpression and amplification of Notch3 in high-grade ovarian carcinomas. *A,* mRNA expression level of Notch3 for each specimen is measured by quantitative RT-PCR and is expressed as fold increase relative to the average value derived from nine OSE samples. Each symbol represents one specimen. The sample with circle harbored 19p13.12 amplification, which is shown in (*B*). *B,* FISH analysis shows a homogenously stained region in an amplified tumor (*right*) with a high level of mRNA expression. A nonamplified tumor (*left*) is also shown as a control.

amplification, 11 high-grade tumors without such amplification, and five benign ovarian tissues including four OSE samples and a benign ovarian cyst. The expression levels for each gene were normalized to the average value of benign tissues (Fig. 2). Mann-Whitney *U* test was used to compute and compare the difference in gene expression levels between the 19p13.12 amplified versus nonamplified high-grade carcinomas. Among the 34 genes within the minimal amplicon, *Notch3* showed the most consistent and significant up-regulation in 19p13.12-amplified tumors compared with nonamplified tumors (P = 0.0018). Other genes in the amplicon, such as *DDX39* and *ADHD9*, also showed a significant overexpression in the amplified versus nonamplified tumors (P = 0.01 and P = 0.02, respectively). It is plausible that these genes also contribute to the tumorigenesis in ovarian cancer. In this study, we selected *Notch3* for further characterization because it showed the most significant P value. We further correlated *Notch3* DNA and mRNA copy number in a set of 31 samples in which both tissues and RNA samples were available for FISH and quantitative RT-PCR analyses. Our data showed a moderate positive correlation of these two variables with a correlation coefficient of 0.481 (Spearman rank-order test, $P < 0.05$).

The above results, together with previous reports showing that *Notch3* participates in both development and oncogenesis, suggest that *Notch3* is a candidate "driving" gene in the 19p13.12 amplicon. Therefore, *Notch3* was prioritized for further characterization in this study. We then did quantitative RT-PCR on a large panel of ovarian serous tumors to determine *Notch3* mRNA levels. As shown in Fig. 3*A*, *Notch3* was overexpressed in 66% (51 of 77) of high-grade tumors, but only in 33% (4 of 12) of low-grade tumor compared with normal ovarian surface epithelium (OSE). In addition, the top five tumors with the highest Notch3 mRNA expression harbored 19p13.12 amplification (Fig. 3*B*), further supporting *Notch3* as a candidate amplified gene that is important in tumor development. Mann-Whitney *U* test showed that there was a statistically significant difference in the levels of *Notch3* expression between OSE and high-grade serous carcinomas ($P < 0.001$) and between OSE and low-grade serous carcinomas ($P < 0.05$). However, there was no significant difference between low-grade and high-grade carcinomas (P = 0.3187).

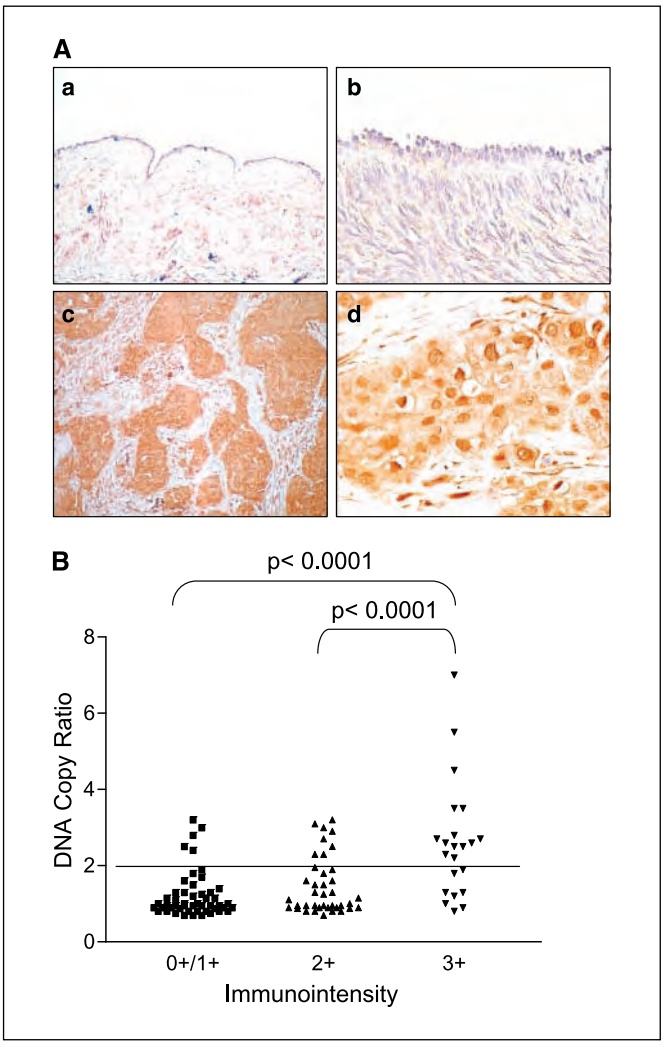

Figure 4. Immunoreactivity of Notch3 in ovarian tumors. *A,* immunoreactivity of Notch3 is not detectable in normal OSE (*a* and *b*) but is overexpressed in 55% of high-grade serous carcinoma. Immunolocalization of Notch3 is detected in both nucleus and cytoplasm in the tumor cells (*c* and *d*). *B,* correlation of Notch3 immunointensity and DNA copy number ratio in high-grade serous carcinomas. The intensity of Notch3 immunoreactivity positively correlates with the Notch3 DNA copy ratio based on FISH analysis. Furthermore, there is a statistically significant difference between tumors with intense staining intensity (3+) and those without (Mann-Whitney *U* test).

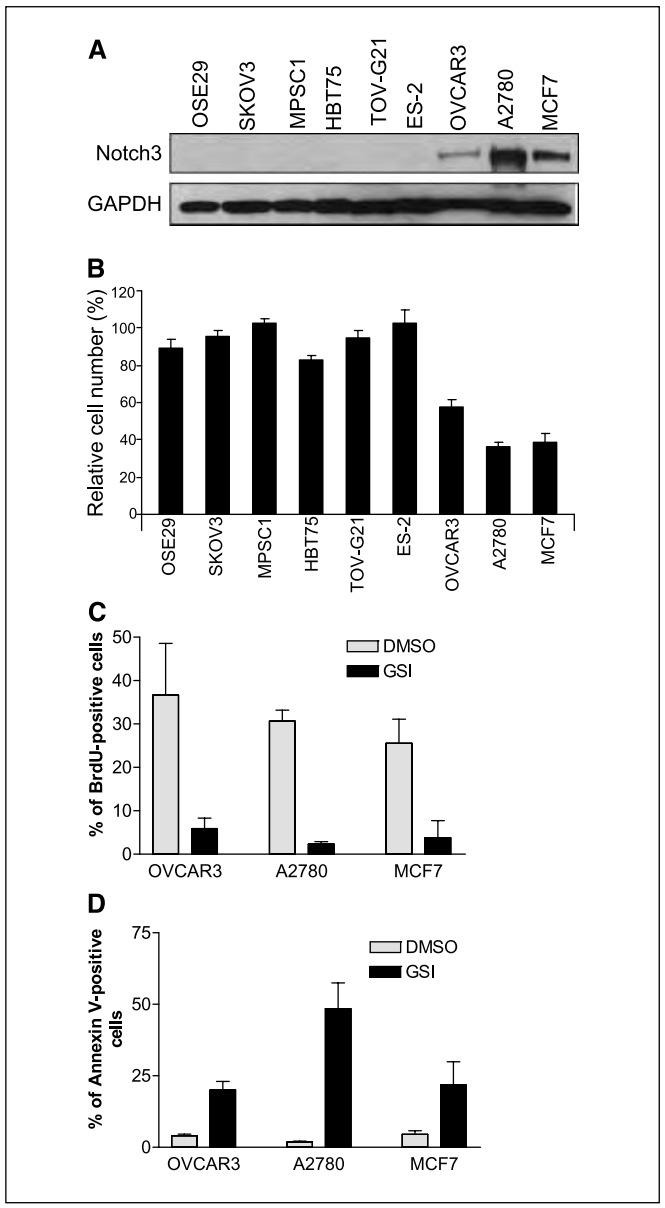

Figure 5. Effects of γ-secretase inhibitor on cell proliferation and apoptosis in cell lines. *A,* Western blot analysis shows a higher expression level of Notch3 protein in OVCAR3, A2780, and MCF-7 cells compared with the other cell lines in which the Notch3 protein is not detectable. *B,* γ-secretase inhibitor significantly reduces the cell number in cell lines with Notch3 overexpression, including OVCAR3, A2780, and MCF-7 compared with those without Notch3 overexpression. γ-Secretase inhibitor decreases DNA synthesis (*C*) and increases apoptosis (*D*) in OVCAR, A2780, and MCF-7 cells based on measurement of BrdUrd uptake and Annexin V labeling assays, respectively.

Immunohistochemistry and FISH were done in parallel on 111 tumor samples to correlate protein expression and *Notch3* DNA copy number. Notch3 immunoreactivity was detected in both nucleus and cytoplasm of tumor cells in 61 of 111 (55%) carcinomas but not in normal ovarian epithelial cells (Fig. 4*A*). Notch3 immunointensity was scored as negative (0), negligible (1+), moderate (2+), and intense (3+) and was correlated with *Notch3* DNA copy number ratio based on FISH analysis (Fig. 4*B*). Specifically, the intensity of Notch3 staining positively correlated with the *Notch3* DNA copy ratio (Spearman rank-order correlation coefficient = 0.4). Furthermore, there is statistically significant difference between tumors with intense staining intensity (3+) and those without (intensity score = 0, 1+, and 2+; Mann-Whitney *U* test, $P < 0.0001$). We observed that 8 of 22 carcinomas are with Notch3 overexpression (3+) but without *Notch3* gene amplification (gene copy ratio ≤2). This finding implies that in addition to gene amplification, mechanisms such as epigenetic activation of the *Notch3* promoter in response to environmental cues may contribute to Notch overexpressing in those tumors. Although a positive correlation of *Notch3* gene copy ratio and protein expression was observed, there are some tumors (5 of 50 tumors)

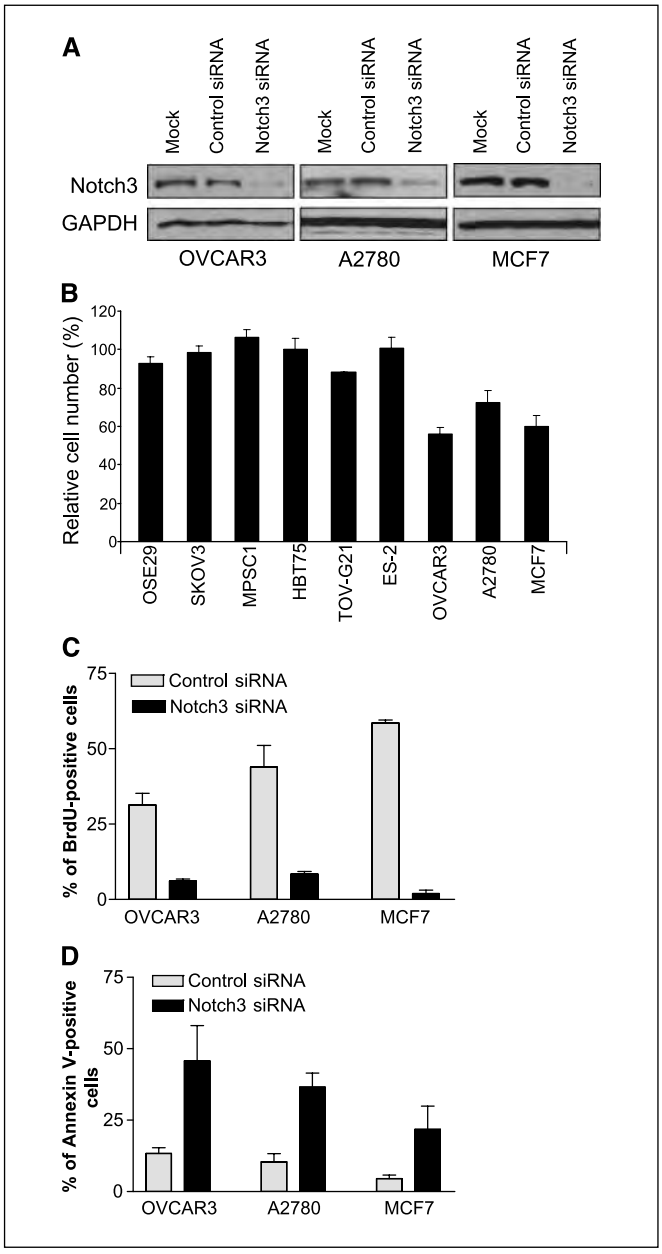

Figure 6. Effects of Notch3 knockdown on cell proliferation and apoptosis in cell lines. *A,* Western blot analysis shows a significant reduction of Notch3 protein in Notch3 siRNA-treated cells compared with the mock or control siRNA-treated cells. *B,* Notch3 siRNA significantly reduces the cell number in cell lines with Notch3 overexpression, including OVCAR3, A2780, and MCF-7 compared with those without. Treatment with Notch3 siRNA decreases DNA synthesis as measured by BrdUrd uptake (*C*) and increases apoptosis as measured by Annexin V labeling (*D*) in OVCAR3, A2780, and MCF-7 cells.

with *Notch3* DNA copy ratio >2 but with only weak Notch3 protein expression (0/1+). This result suggests that these carcinomas may use other oncogene(s) that resides on the same chromosomal arm as the *Notch3* locus to promote tumor progression in ovarian serous carcinomas.

Notch receptors participate in signal transduction by translocating their cytoplasmic domain to the nucleus where it activates an array of downstream effectors that can play important roles in cell proliferation and survival (15). The association of genetic changes in *Notch3* and human cancer has been recently established in lung carcinoma. Translocation of t(15;19) was identified in non–small-cell lung cancer cell lines and the breakpoint has been mapped to 50 bp upstream of the *Notch3* locus. The translocation of chromosome 19p was found to correlate with overexpression of Notch3 full-length mRNA (16). Our data here provide new evidence that besides translocation, gene amplification is another mechanism to activate Notch3 in human cancer.

The genetic findings are supported by mouse models. For example, expression of the intracellular domain (a constitutively active form) of Notch3 in mouse thymus induced T-cell leukemia/lymphoma (17). Furthermore, constitutive expression of activated Notch3 in the central nervous system initiates the formation of brain tumors in the choroid plexus in mice (18), suggesting that deregulation of Notch3 plays a role in neoplastic transformation.

Functional analysis of Notch3 expression. To determine if Notch3 is essential for cell growth and survival in cell lines that overexpress Notch3, we used γ-secretase inhibitor 1, which prevents the activation of Notch3 by inhibiting the proteolysis and translocation of Notch3 cytoplasmic domain to the nucleus. This compound has been shown to be a potent and specific inhibitor of Notch pathway (19, 20). γ-Secretase inhibitor was applied to the culture medium in nine cell lines, including three cancer cell lines with Notch3 overexpression (OVCAR3, A2780, and MCF7), an immortalized OSE cell line (OSE 29), and five cancer cell lines (SKOV3, MPSC1, HTB75, TOV-G21, and ES-2) without Notch3 overexpression (Fig. 5*A*). We first determined the concentration of γ-secretase inhibitor to be used and found that the IC_{50} was lowest in OVCAR3 (1 μmol/L). Therefore, we treated different cell lines with inhibitor at 1 μmol/L in culture and found that there was a substantial reduction in cell number of OVCAR3, A2780, and MCF7 cells that overexpressed Notch3 compared with other cell lines that did not have Notch3 overexpression (Fig. 5*B*, $P < 0.001$, Student's *t* test). To assess the mechanisms underlying the growth inhibition by the γ-secretase inhibitor in OVCAR3, A2780, and MCF-7 cells, we measured the percentage of BrdUrd-labeled cells for cellular proliferation and Annexin V–labeled cells for apoptosis (Fig. 5*C* and *D*). We found that γ-secretase inhibitor significantly reduced cellular proliferation and induced apoptosis in all three cell lines with Notch3 overexpression compared with the DMSO controls ($P < 0.001$, Student's *t* test). siRNA was used to knock down the expression of Notch3 in the same nine cell lines used for the γ-secretase inhibitor assay. The knockdown effect of siRNA was shown by Western blot (Fig. 6*A*). siRNA treatment significantly reduced the Notch3 protein expression compared with the mock or control siRNA-treated groups. Similar to the effects of γ-secretase inhibitor, Notch3 siRNA reduced cell number most significantly in OVCAR3, A2780, and MCF7 cells, which overexpressed Notch3 compared with the other cell lines (Fig. 6*B*, $P < 0.001$, Student's *t* test). The BrdUrd-positive cells decreased and the Annexin V–labeled cells increased in Notch3 siRNA-treated cells compared with control siRNA-treated cells (Fig. 6*C* and *D*, $P < 0.001$, Student's *t* test).

Our *in vitro* data to inactivate Notch3 by γ-secretase inhibitor and siRNA may have clinical implications for ovarian cancer patients and suggest that Notch3 can be a candidate therapeutic target. γ-Secretase inhibitors have been studied in the past several years as a potential therapeutic intervention in Alzheimer's disease. Very recently, γ-secretase inhibitors have been shown to inhibit the epithelial cell proliferation and induce goblet cell differentiation in intestinal adenomas $Apc^{-/-}$ (min) mice (20). Furthermore, γ-secretase was shown to be able to inhibit the growth of Kaposi's sarcoma cells in mouse tumor model (19). Therefore, with the promising effects at both *in vitro* and *in vivo* systems, γ-secretase inhibitors can be used as new target-based therapy for those tumors with Notch3 activation.

The current study suggests that *Notch3* is a strong candidate oncogene among the genes within the ch19p13.12 amplicon in ovarian carcinomas. This is because *Notch3* gene shows a high correlation of gene amplification and overexpression and is functionally essential for tumor growth and survival. Although the above represents our preferred interpretation, other alternative interpretations should be pointed out. For example, *Notch3* may not be the only gene with high correlation of DNA copy number and gene expression level after analyzing a large series of amplified and nonamplified tumors. It is possible that other coamplified gene(s) within the *Notch3* amplicon also plays a role in tumorigenesis and they may cooperate with Notch3 in propelling tumor progression.

In conclusion, we have identified *Notch3* as a candidate amplified oncogene that overexpressed in 66% of ovarian serous carcinomas. Our findings suggest that *Notch3* amplification may play an important role in the development of ovarian carcinomas; moreover, these findings provide a rationale for future development of Notch3-based therapy for ovarian cancer.

Acknowledgments

Received 10/6/2005; revised 3/10/2006; accepted 4/11/2006.

Grant support: Department of Defense grant OC0400600 and NIH grant CA103937.

The costs of publication of this article were defrayed in part by the payment of page charges. This article must therefore be hereby marked *advertisement* in accordance with 18 U.S.C. Section 1734 solely to indicate this fact.

We thank Dr. Edward Fox and Dr. Changzhong Chen at the microarray core facility of the Dana-Farber Cancer Institute for valuable suggestions.

References

1. Meltzer PS, Kallioniemi A, Trent JM. Chromosome alterations in human solid tumors. In: Vogelstein B, Kinzler KW, editors. The genetic basis of human cancer. New York: McGraw-Hill; 2002. p. 93–113.
2. Farley J, Smith LM, Darcy KM, et al. Cyclin E expression is a significant predictor of survival in advanced, suboptimally debulked ovarian epithelial cancers: a Gynecologic Oncology Group study. Cancer Res 2003;63:1235–41.
3. Slamon DJ, Godolphin W, Jones LA, et al. Studies of the HER-2/neu proto-oncogene in human breast and ovarian cancer. Science 1989;244:707–12.
4. Cheng JQ, Godwin AK, Bellacosa A, et al. AKT2, a putative oncogene encoding a member of a subfamily of protein-serine/threonine kinases, is amplified in human ovarian carcinomas. Proc Natl Acad Sci U S A 1992;89:9267–71.
5. Wu R, Lin L, Beer DG, et al. Amplification and overexpression of the L-MYC proto-oncogene in ovarian carcinomas. Am J Pathol 2003;162:1603–10.
6. Shih I-M, Sheu JJ, Santillan A, et al. Amplification of a

chromatin remodeling gene, Rsf-1/HBXAP, in ovarian carcinoma. Proc Natl Acad Sci U S A 2005;102:14004–9.
7. Zhao X, Li C, Paez JG, et al. An integrated view of copy number and allelic alterations in the cancer genome using single nucleotide polymorphism arrays. Cancer Res 2004;64:3060–71.
8. Zhao X, Weir BA, LaFramboise T, et al. Homozygous deletions and chromosome amplifications in human lung carcinomas revealed by single nucleotide polymorphism array analysis. Cancer Res 2005;65:5561–70.
9. Wang TL, Maierhofer C, Speicher MR, et al. Digital karyotyping. Proc Natl Acad Sci U S A 2002;99:16156–61.
10. Buckhaults P, Zhang Z, Chen YC, et al. Identifying tumor origin using a gene expression-based classification map. Cancer Res 2003;63:4144–9.
11. Wang TL, Diaz LA, Jr., Romans K, et al. Digital karyotyping identifies thymidylate synthase amplification as a mechanism of resistance to 5-fluorouracil in metastatic colorectal cancer patients. Proc Natl Acad Sci U S A 2004;101:3089–94.
12. Boon K, Eberhart CG, Riggins GJ. Genomic amplification of orthodenticle homologue 2 in medulloblastomas. Cancer Res 2005;65:703–7.
13. Di C, Liao S, Adamson DC, et al. Identification of OTX2 as a medulloblastoma oncogene whose product can be targeted by *all-trans* retinoic acid. Cancer Res 2005;65:919–24.
14. Hogarty MD, Brodeur GM. Gene amplification in human cancers: biological and clinical significance. In: Vogelstein B, Kinzler KW, editors. The genetic basis of human cancer. New York: McGraw-Hill; 2002. p. 115–28.
15. Allenspach EJ, Maillard I, Aster JC, Pear WS. Notch signaling in cancer. Cancer Biol Ther 2002;1:466–76.
16. Dang TP, Gazdar AF, Virmani AK, et al. Chromosome 19 translocation, overexpression of Notch3, and human lung cancer. J Natl Cancer Inst 2000;92:1355–7.
17. Bellavia D, Campese AF, Alesse E, et al. Constitutive activation of NF-κB and T-cell leukemia/lymphoma in Notch3 transgenic mice. EMBO J 2000;19:3337–48.
18. Dang L, Fan X, Chaudhry A, Wang M, Gaiano N, Eberhart CG. Notch3 signaling initiates choroid plexus tumor formation. Oncogene 2005;25:487–91.
19. Curry CL, Reed LL, Golde TE, Miele L, Nickoloff BJ, Foreman KE. γ-Secretase inhibitor blocks Notch activation and induces apoptosis in Kaposi's sarcoma tumor cells. Oncogene 2005;24:6333–44.
20. van Es JH, van Gijn ME, Riccio O, et al. Notch/γ-secretase inhibition turns proliferative cells in intestinal crypts and adenomas into goblet cells. Nature 2005;435:959–63.

Human Pathology (2006) **37**, 1169–1175

ELSEVIER

Human PATHOLOGY

www.elsevier.com/locate/humpath

Original contribution

Expression of Rsf-1, a chromatin-remodeling gene, in ovarian and breast carcinoma

Tsui-Lien Mao MD[a,b,c,e], Chih-Yi Hsu MD[f], May J. Yen MD[a,b,c], Blake Gilks MD[d], Jim Jinn-Chyuan Sheu PhD[a,b,c], Edward Gabrielson MD[a,b,c], Russell Vang MD[a,b,c], Leslie Cope PhD[a,b,c], Robert J. Kurman MD[a,b,c], Tian-Li Wang PhD[a,b,c], Ie-Ming Shih MD, PhD[a,b,c,*]

[a]*Department of Pathology, Johns Hopkins Medical Institutions, Baltimore, MD 21231, USA*
[b]*Department of Oncology, Johns Hopkins Medical Institutions, Baltimore, MD 21231, USA*
[c]*Department of Gynecology, Johns Hopkins Medical Institutions, Baltimore, MD 21231, USA*
[d]*Department of Pathology, Vancouver General Hospital, Vancouver, Canada V5E1M9*
[e]*Department of Pathology, National Taiwan University Hospital, Taipei 10001, Taiwan*
[f]*Department of Pathology, Taipei Veterans General Hospital and National Yang-Ming University School of Medicine, Taipei 11221, Taiwan*

Received 27 January 2006; revised 6 April 2006; accepted 10 April 2006

Keywords:
Rsf-1;
Ovarian serous carcinoma;
Breast carcinoma

Summary Rsf-1 protein is a member of a chromatin-remodeling complex that plays an important role in regulating gene expression and cell proliferation. Our previous study showed that Rsf-1 was an amplified gene that participated in the development of ovarian serous carcinoma. To further elucidate the role of Rsf-1 in ovarian cancer, we studied Rsf-1 immunoreactivity in 294 ovarian tumors of various histologic types. Because the Rsf-1 amplicon overlaps an amplified region reported in breast cancer, we included 782 neoplastic and normal breast tissues for comparison. Immunohistochemistry was performed on tissue microarrays using a 4-tiered scoring system. Overexpression of Rsf-1 was defined as a nuclear immunointensity of 3+ to 4+ because of a strong correlation between 3+ and 4+ immunointensity and Rsf-1 gene amplification, based on our previous fluorescence in situ hybridization analysis. Rsf-1 overexpression was observed in 25% of high-grade ovarian serous carcinomas and in only rare cases (<7%) of low-grade ovarian serous, ovarian endometrioid, and invasive breast carcinomas but not in any ovarian serous borderline tumors, ovarian clear cell carcinomas, ovarian mucinous carcinomas, intraductal carcinomas of the breast, and normal ovaries and breast tissues. Thus, overexpression of Rsf-1 was significantly associated with high-grade ovarian serous carcinoma ($P < .05$), as compared with other types of ovarian tumors

This study was supported by US Department of Defense grant no. OC040060 and National Cancer Institute/National Institutes of Health grant no. CA103937.

* Corresponding author. Department of Pathology, Johns Hopkins Medical Institutions, Baltimore, MD21231, USA.
E-mail address: ishih@jhmi.edu (I.-M. Shih).

doi:10.1016/j.humpath.2006.04.008

and breast carcinomas. Our results provide evidence that Rsf-1 expression is primarily confined to high-grade serous carcinoma, the most aggressive ovarian cancer. Because Rsf-1 overexpression occurs in only a small number of breast carcinomas, it is unlikely that Rsf-1 is a critical gene in the development of breast carcinoma.

1. Introduction

Identification of new cancer-associated genes not only plays an important role in elucidating the molecular etiology of neoplastic diseases but also has a significant impact in the future development of new diagnostic markers and therapeutic targets. In an effort to search for new amplified tumor-associated genes, we have previously applied a genome-wide technology, digital karyotyping [1,2], to identify novel amplicons that may harbor potential oncogenes in ovarian cancer. Using this methodology, we identified the Rsf-1 gene as a candidate amplified oncogene in ovarian serous carcinoma, a common and aggressive type of ovarian cancer [3].

Rsf-1 encodes a nuclear protein and functions as a histone chaperone that binds to its partner, hSNF2H, which possesses nucleosome-dependent adenosine triphosphatase activity [4]. The Rsf-1/hSNF2H complex (or remodeling and spacing factor [RSF] complex) mediates nucleosome deposition and generates regularly spaced nucleosome arrays. At the cellular level, RSF participates in chromatin remodeling by mobilizing nucleosomes in response to a variety of growth-modifying signals and environmental cues. Such nucleosome remodeling is essential for transcriptional regulation [5], DNA replication [6], and cell cycle progression [7]. A growing body of evidence has highlighted the role of chromatin remodeling in cancer [8,9], and the findings from our previous study support this view [3]. We demonstrated that Rsf-1 was located on chromosome 11q13.5 and that this chromosomal region was amplified in 13.2% of high-grade ovarian serous carcinomas. Patients with Rsf-1 amplification or overexpression have a significantly shorter survival than those without. Rsf-1 gene knockdown inhibited cell growth in OVCAR3 cells, which exhibit Rsf-1 amplification. It is of interest to note that the 11q13.5 amplicon that harbors Rsf-1 gene is also reported in breast carcinomas [10].

Given the potential role of Rsf-1 in the development of ovarian cancer, we extended our studies by performing a comprehensive immunohistochemical analysis of Rsf-1 expression in different histologic types and grades of ovarian carcinoma. Furthermore, to clarify the role of Rsf-1 in breast tumors, we examined the expression of Rsf-1 in a large number of breast carcinomas and compared the frequency of Rsf-1 overexpression between ovarian and breast carcinomas.

2. Materials and methods

2.1. Tissue samples

All the ovarian tissue samples were obtained from the Department of Pathology at the Johns Hopkins Hospital, except clear cell and endometrioid carcinomas, which were obtained from the Department of Pathology at National Taiwan University Hospital (Taipei, Taiwan), and mucinous tumors from Vancouver General Hospital (Vancouver, Canada). Ovarian tissues included normal ovary (n = 19), serous cystadenomas (n = 23), serous borderline tumors (n = 13), low-grade serous carcinomas (n = 31), high-grade serous carcinomas (n = 100), endometrioid carcinomas (n = 45), mucinous carcinomas (n = 29), and clear cell carcinomas (n = 64). Breast tissue samples were obtained from the Johns Hopkins tissue microarray core facility and Taipei Veterans General Hospital and included invasive carcinomas (n = 689), in situ carcinomas (n = 42), and normal breast tissue (n = 51). Most breast carcinomas were of ductal type. All the tissues from the 4 hospitals were fixed in 10% neutral formalin and processed according to standardized procedures. The acquisition of archival anonymous tissues was approved by the local institutional research boards.

2.2. Immunohistochemistry

Tissue microarrays (TMAs) were used to facilitate immunohistochemistry for all specimens. Formalin-fixed, paraffin-embedded tissues were arranged onto TMAs. Three representative cores (1.5-mm diameter) from each tumor were placed on the TMAs at the Johns Hopkins Tissue Microarray Center. Antigen retrieval was performed on deparaffinized sections by boiling them in citrate buffer (pH 6.0) using a microwave oven for 10 minutes. A commercially available monoclonal anti–Rsf-1 antibody, clone 5H2/E4 (Upstate, Lake Placid, NY), was used at an optimal dilution that was previously determined (1:2000) for 2 hours at room temperature, followed by the EnVision+ System (DAKO, Carpinteria, Calif) using the peroxidase method. An isotype-matched control antibody (MN-4) was used as a control. Our previous studies [3] had shown that the distribution of Rsf-1 immunoreactivity was always homogenous in tumor cells for almost all the tumors. Therefore, we applied intensity score ranging from 0 to 4+ to evaluate Rsf-1 immunoreactivity in tumors (Fig. 1) [3]. A positive reaction was defined as discrete localization of the chromagen in the nuclei. Scoring was performed independently by 2 investigators after

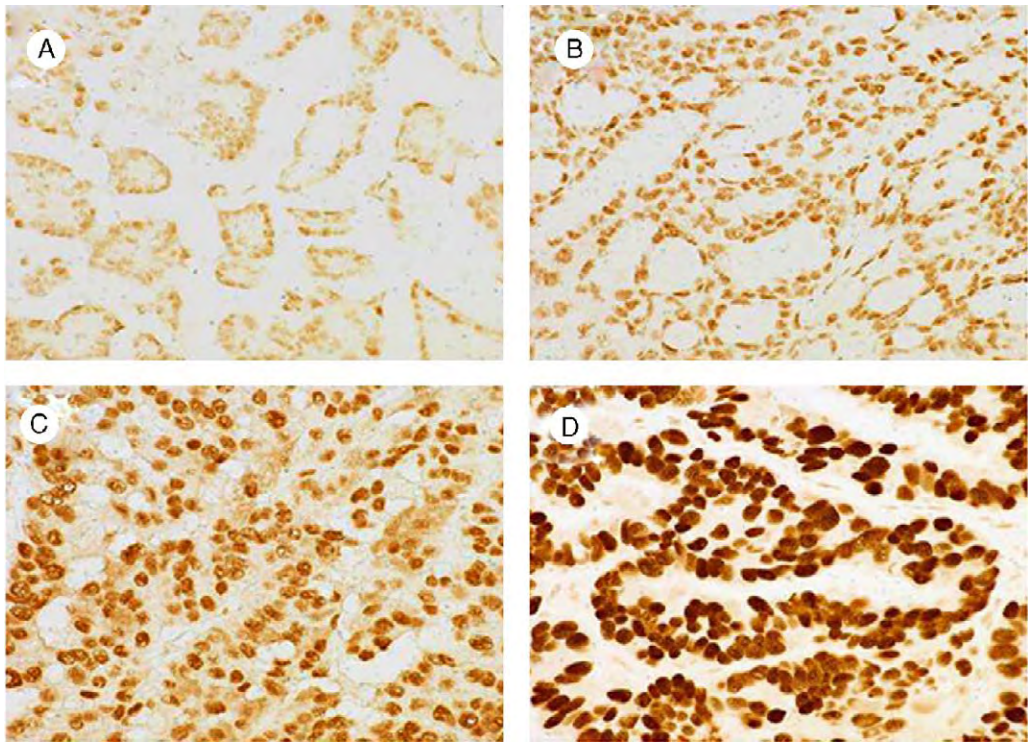

Fig. 1 Immunoreactivity scores for Rsf-1 expression. Examples of ovarian carcinomas are shown to indicate the immunointensity scores of 1+ (A), 2+ (B), 3+ (C), and 4+ (D).

randomly counting approximately 500 tumor cells from 3 different high-power fields (×40) within 1 specimen. For the discordant cases, a third pathologist participated, and the final score was an average of the 2 scores that were the closest. All specimens were anonymized, and the investigators who perform the scoring were blinded to the diagnosis of the specimens.

2.3. Western blot analysis

To confirm the specificity of the anti–Rsf-1 antibody (5H2/E4) in the immunohistochemical analysis, we performed Western blotting on OVCAR3 cells, which are known to amplify and overexpress Rsf-1; on HEK293 cells that have a low level of Rsf-1 expression; and on HEK293 cells stably transfected with an Rsf-1–expressing vector. An equal number of cells (5×10^5 cells) were lysed in a sodium dodecyl sulfate–containing buffer, and cellular proteins were separated by sodium dodecyl sulfate–polyacrylamide gel electrophoresis. The Western blot analysis on Rsf-1 protein has been described in a previous report [3].

2.4. Statistical methods

Overexpression was defined as 3+ and 4+ nuclear immunoreactivity. The frequency of Rsf-1 overexpression in tumors was assessed by the percentage of 3+ and 4+ cases among the group of tumors. The 95% confidence intervals (CIs) were determined. The difference in immunointensity between different groups of tumors was calculated by Fisher exact test. The survival analysis was calculated by the Kaplan-Meier survival curve. A P value (2-tailed) less than .05 was considered statistically significant.

3. Results

To evaluate Rsf-1 expression in tissue sections, we first confirmed the specificity of the anti–Rsf-1 antibody (5H2/E4) by Western blot analysis. The antibody recognized a single protein band at a molecular mass of approximately 215 kd that corresponded to Rsf-1 protein in OVCAR3 cells and in HEK293 cells that were transfected with an Rsf-1–expressing vector. In contrast, the parental HEK293 cells did not show detectable Rsf-1 expression under the same experimental conditions (Fig. 2A). Intense immunoreactivity (3+ to 4+) is frequently associated with a high-fold gain in DNA copy number, as demonstrated by fluorescence in situ hybridization [3]. Accordingly, in this study, we stratified cases into 2 groups: those with a low level of expression (0 to 2+ staining) and those with a high level of expression (3+ to 4+ staining). The staining results for all cases are shown in Table 1. Ovarian surface epithelium from normal ovaries was negative or showed weak Rsf-1 expression (7 cases, negative; 11 cases, 1+; and 1 case, 2+). A similar pattern of Rsf-1 expression was observed in serous cystadenoma (10 cases, negative; 9 cases, 1+; and 4 cases, 2+). Most serous borderline tumors and low-grade serous carcinoma showed 1+ to 2+ immunoreactivity (12/13 cases and 25/33 cases, respectively), whereas only a small number were negative. A high level of Rsf-1 expression (3+ and 4+) was seen

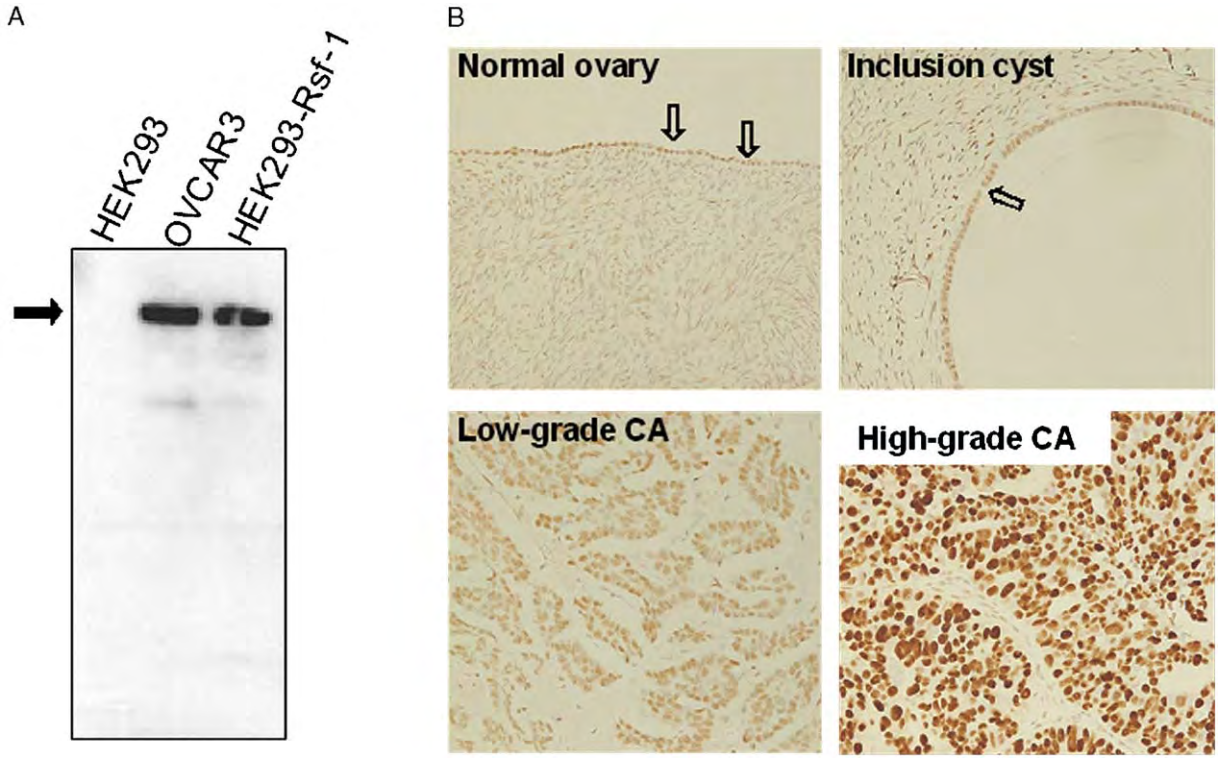

Fig. 2 Expression of Rsf-1 in ovarian tissues and tumors. A, Western blot analysis shows the specificity of the anti–Rsf-1 antibody (5H2/E4). The antibody recognizes a single protein band at the molecular weight of approximately 215 kd (arrow) that corresponded to Rsf-1 protein in OVCAR3 cells and in HEK293 cells that were transfected with an Rsf-1 (HEK293–Rsf-1)–expressing vector. In contrast, the parental HEK293 cells show very weak or undetectable Rsf-1 expression. B, Immunohistochemistry of the Rsf-1 antibody on representative ovarian tissue and tumors. Intense immunoreactivity (3+) is detected in a high-grade serous carcinoma but is only weakly expressed (1+ to 2+) in normal ovarian surface epithelium, an ovarian surface inclusion cyst, and a low-grade serous carcinoma.

predominantly in high-grade serous carcinomas (25/100 cases) and only rarely in low-grade serous (1/33 cases) and endometrioid carcinomas (3/45 cases) but not in other types of ovarian tumors (Table 1). Of 3 endometrioid carcinomas showing 3+ immunoreactivity, 1 was low-grade, and the other 2 were high-grade endometrioid carcinomas. Fisher exact test showed that the frequency of Rsf-1 overexpressed tumors (3+ and 4+) was significantly higher in high-grade serous carcinomas, as compared with other types of ovarian tumors and normal ovaries ($P < .05$). An example of 3+

Table 1 Expression of Rsf-1 in ovarian and breast tissue

Histologic type	Total cases	Immunoreactivity for Rsf-1					*P**
		0	1+	2+	3+	4+	
Ovarian tissue	294						
Serous carcinoma, HG	100	5 (5)[a]	15 (15)	55 (55)	2 (20)	5 (5)	
Serous carcinoma, LG	31	5 (16)	11 (35)	14 (45)	1 (3)	0	.004
Serous borderline tumor	13	1 (8)	9 (69)	3 (23)	0	0	.03
Serous cystadenoma	23	10 (43)	9 (39)	4 (17)	0	0	.029
Normal ovary	19	7 (37)	11 (58)	1 (5)	0	0	.007
Endometrioid carcinoma	45	23 (51)	9 (20)	10 (22)	3 (7)	0	.006
Clear cell carcinoma	34	6 (18)	13 (38)	15 (44)	0	0	<.001
Mucinous carcinoma	29	15 (52)	10 (34)	4 (14)	0	0	<.001
Breast tissue	782						
Invasive carcinoma	689	92 (13)	306 (44)	255 (37)	32 (5)	4 (0.006)	<.0001
In situ carcinoma	42	6 (14)	25 (60)	11 (26)	0	0	
Normal breast	51	20 (39)	30 (59)	1 (2)	0	0	

Abbreviations: HG, high grade; LG, low grade.
[a] Figures in parenthesis represent percentage given of cases.
* *P* value generated by comparing the overexpressed cases (3+ and 4+) between ovarian high-grade serous carcinoma and other groups.

to 4+ Rsf-1 immunoreactivity is shown in Fig. 2B. Although both high-grade and low-grade serous carcinomas are thought to be different types of ovarian cancer because they have distinct molecular and clinicopathologic features and are rarely present in the same tumor [11], there was a tumor in this series demonstrating a morphological continuum of low-grade and high-grade carcinoma in the same tumor. As shown in Fig. 3, Rsf-1 immunoreactivity was confined to the high-grade carcinoma cells but not in the adjacent low-grade counterpart in this tumor, a finding further supporting that Rsf-1 expression is associated with high-grade serous carcinomas.

Normal lobular and ductal breast epithelium was negative or showed a low level of Rsf-1 expression (20 cases, negative; 30 cases, 1+; and 1 case, 2+). A similar immunoreactivity pattern was found in ovarian surface epithelium. In situ carcinoma was negative or exhibited a low level of Rsf-1 expression, with more cases showing 2+ immunoreactivity (6 cases, negative; 25 cases, 1+; and 11 cases, 2+). This expression profile was similar to that of ovarian serous borderline tumors. Only a small number of invasive breast carcinomas (36/689 cases) exhibited a high level (3+ and 4+) of Rsf-1 expression (Fig. 4), whereas most cases demonstrated a low level (0 to 2+) of Rsf-1 expression. The frequency of Rsf-1 overexpressed cases in invasive breast carcinoma (5%; 95% CI, 3.4%-6.6%) was significantly less than that in high-grade ovarian serous carcinomas (25%; 95% CI,17%-33%) ($P < .0001$). There was no significant correlation ($P > .05$) of Rsf-1 expression with clinical stage, tumor grade, or histologic type in breast carcinomas. Rsf-1 immunointensity scores did not correlate with overall survival in breast and high-grade ovarian serous carcinomas by applying different score cutoffs ($P > .05$ by Kaplan-Meier curves and the log-rank test).

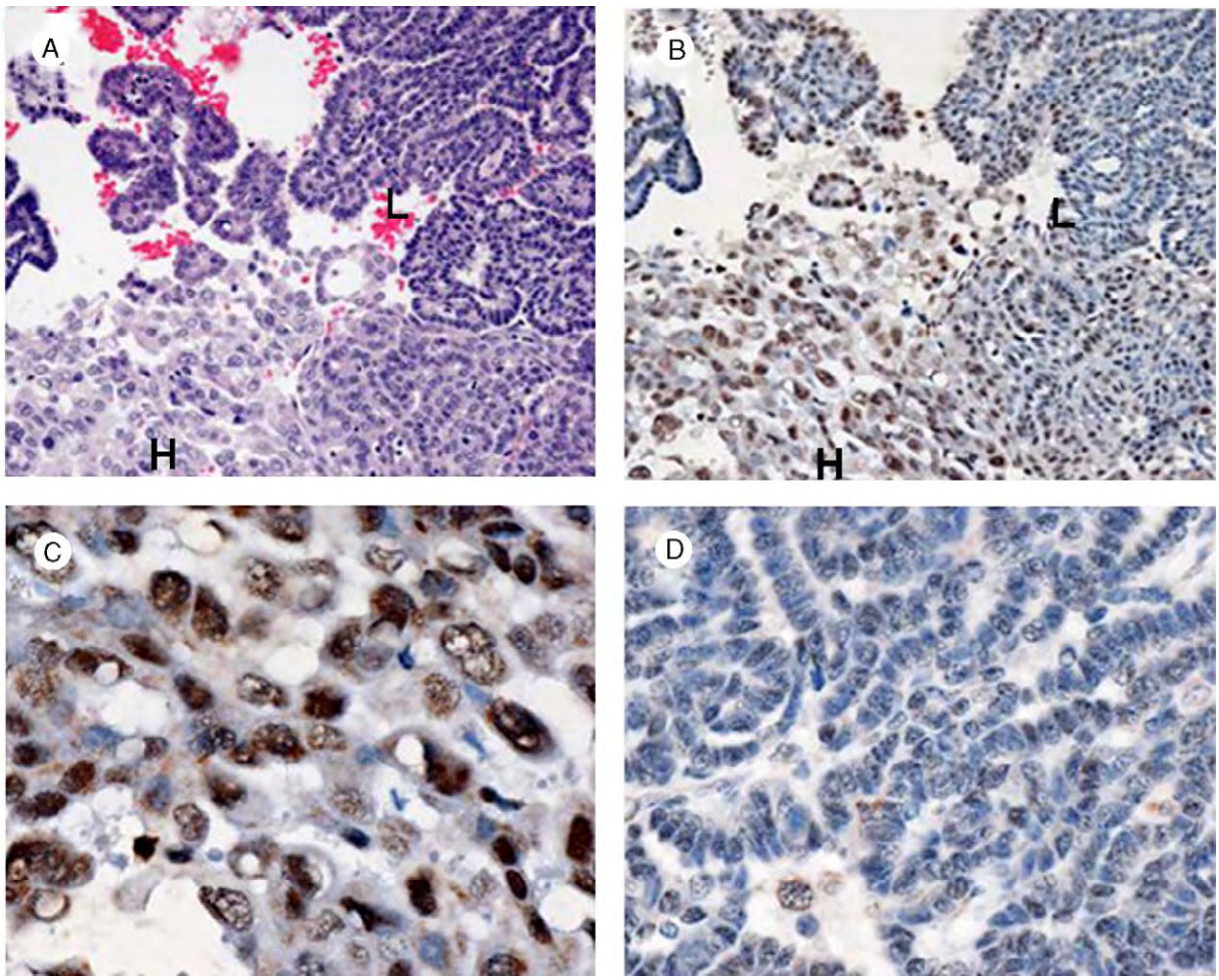

Fig. 3 Rsf-1 immunoreactivity in a serous carcinoma with both low- and high-grade features. A, A hematoxylin and eosin–stained section shows a morphological continuum of low- (L) and high-grade (H) serous carcinomas. The low-grade carcinoma exhibits a papillary architecture, whereas the high-grade carcinoma demonstrates a solid growth pattern. B, Rsf-1 immunoreactivity is present in the nuclei of high-grade carcinoma but not in low-grade carcinoma. C, A high-power view of the high-grade area showing intense Rsf-1 nuclear staining in almost all the tumor cells. D, A high-power view of the low-grade area demonstrating weak Rsf-1 immunoreactivity in tumor cells.

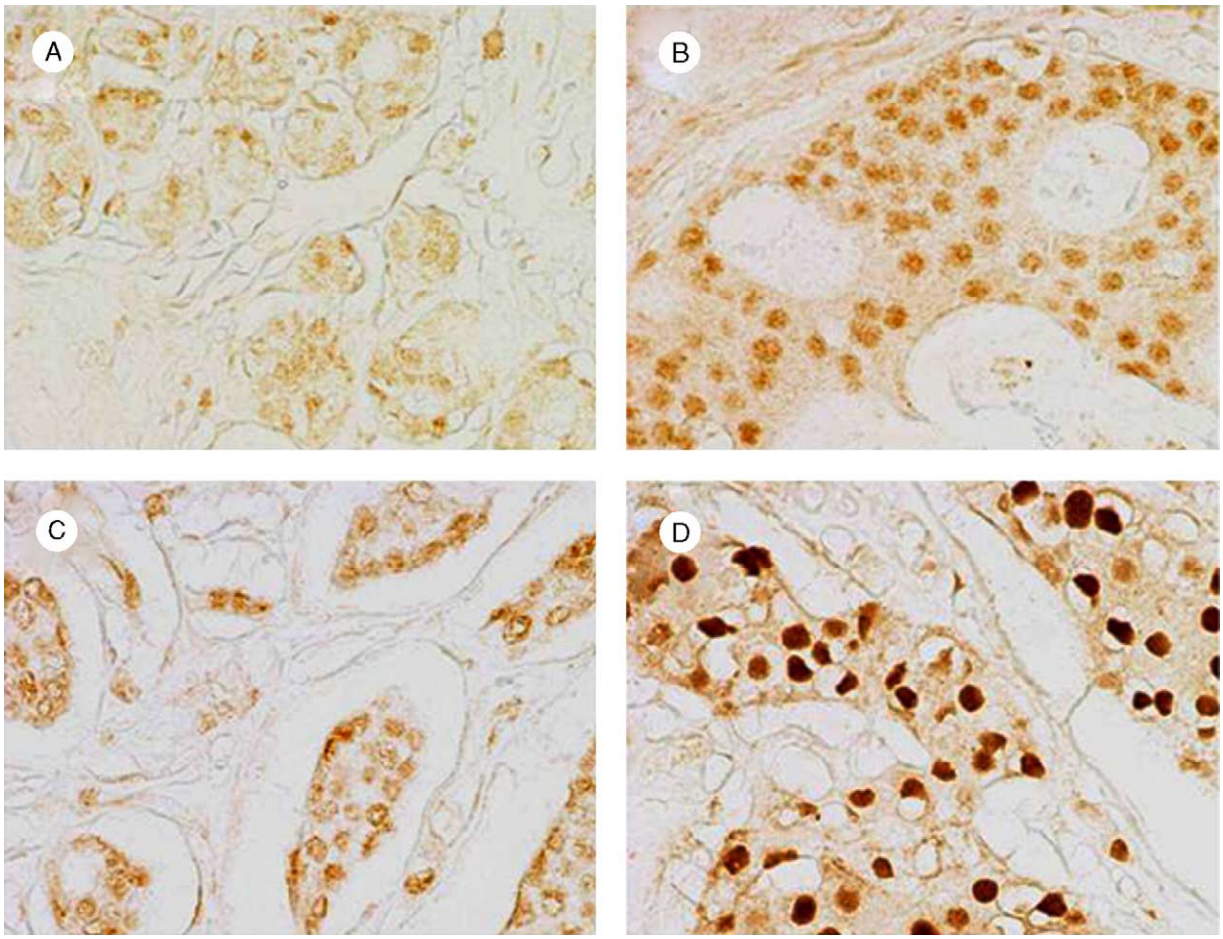

Fig. 4 Expression of Rsf-1 in normal breast tissue and carcinomas. A, Normal breast tissue with weak (1+) Rsf-1 immunostaining in ductal and lobular epithelium. B, Dutal carcinoma in situ showing a low level (2+) of Rsf-1 immunointensity. C, Invasive ductal carcinoma with a low level (2+) of expression. D, A rare invasive carcinoma with a high level (4+) of Rsf-1 expression.

4. Discussion

Chromosomal region 11q13 is one of the most frequently amplified regions in human tumors, including carcinomas arising from ovary, breast, lung, liver, esophagus, head, and neck. Several genes have been implicated as candidate amplified oncogenes in this chromosomal region, including Rsf-1 [3], EMSY [10], PAK1 [12], TAOS1 [13], Rad9 [14], CCND1, FGF3, and FGF4 [15]. Our previous study that focused on high-grade ovarian serous carcinomas identified Rsf-1 as the gene showing the best correlation between gene and transcript copy numbers among all the genes within the minimal 11q13.5 amplicon [3]. In the current study, evaluating a variety of ovarian tumors, we provide new evidence that Rsf-1 overexpression is confined to high-grade ovarian serous carcinoma. Because the 11q13.5 amplicon has also been reported in breast cancer, we analyzed Rsf-1 expression in a large series of breast carcinomas to determine if Rsf-1 is also frequently overexpressed in breast carcinomas. We found that, as compared with high-grade ovarian serous carcinomas, overexpression of Rsf-1 is rare in breast carcinomas, indicating that other gene(s) within the 11q13.5 amplicon may be important for the progression of breast carcinoma.

The finding that immunoreactivity of Rsf-1 is mostly negative or weak in ovarian endometrioid, clear cell, mucinous, and low-grade serous carcinomas suggests that Rsf-1 may not be involved in the pathogenesis of these types of ovarian carcinomas. This finding is consistent with a proposed model of ovarian tumorigenesis that we have previously proposed [11]. In that model, there are 2 main pathways of carcinogenesis, and tumors developing along these pathways have been designated as type I and type II. Type I tumors include low-grade serous, endometrioid, clear cell, and mucinous carcinomas. Those tumors share a common pattern in tumor progression as they develop in a stepwise fashion from well-recognized precursors, namely, "borderline" tumors, which, in turn, develop from cystadenomas/adenofibromas [16,17]. The benign tumors appear to develop from the surface epithelium or inclusion cysts in the case of serous and mucinous tumors and from endometriosis or endometriomas in the case of endometrioid and clear cell

tumors. Type I tumors are slow-growing, as evidenced by the observation that they are large and often confined to the ovary at diagnosis. In contrast, type II tumors are high-grade and usually have spread beyond the ovaries at presentation. Type II carcinomas include what are currently classified as high-grade serous carcinoma ("moderately" and "poorly" differentiated), malignant mixed mesodermal tumors (carcinosarcomas), and undifferentiated carcinoma. Type II carcinomas evolve rapidly, disseminate early in their course, and are highly aggressive. Both type I and type II carcinomas are characterized by distinctive molecular genetic changes. In type I tumors, low-grade serous carcinomas contain frequent activating mutations in KRAS and BRAF, endometrioid carcinomas harbor mutations in PTEN and β-catenin, and clear cell carcinomas show microsatellite instability and KRAS mutations [11]. These genetic changes are rarely found in type II carcinomas, which are characterized by frequent p53 mutations [18] and a high level of chromosomal instability [16]. Thus, Rsf-1 overexpression in type II carcinomas but not in type I carcinomas provides further support that both types of ovarian carcinomas develop along distinct molecular pathways. The lack of correlation of Rsf-1 immunointensity and overall survival in high-grade serous carcinomas contrasts with the previous finding demonstrating that Rsf-1 gene amplification correlated with a shorter survival [3]. This discrepancy can be explained by the insufficient number of high-grade serous carcinomas with scores of 3 and above for survival curve analysis in this study. Alternatively, it is likely that counting Rsf-1 gene copy number by fluorescence in situ hybridization is superior to Rsf-1 immunoreactivity in predicting survival in patients with advanced-stage, high-grade serous carcinomas.

In this report, we also studied Rsf-1 expression in breast carcinomas because the 11q13.5 amplicon has been reported in breast carcinomas [10]. Because Rsf-1 overexpression in breast carcinomas is relatively uncommon (5%), it is not likely that the Rsf-1 gene is important in the development of breast carcinoma. Thus, although both ovarian high-grade serous carcinoma and breast carcinoma harbor amplicons at a similar chromosomal region, that is, 11q13.5, different core amplicons and amplified genes within 11q13.5 may be operative for tumor progression in these 2 tumors. For example, the EMSY gene, which has been suggested as a potential oncogene within the 11q13.5 region, may be more important in the development of breast cancer [10] than in ovarian high-grade serous carcinomas [3]. The findings reported in this study have important implications in studying the roles of Rsf-1 and EMSY genes in the development of different types of cancer.

In conclusion, we have shown that among different types of ovarian carcinomas, Rsf-1 gene is most frequently up-regulated in high-grade serous carcinomas. This finding further supports the view that Rsf-1 gene expression is related to the aggressive type of ovarian cancer. Because Rsf-1 up-regulation occurs uncommonly in breast carcinoma, it is not likely that the Rsf-1 gene is as important in driving tumor progression in breast cancer as it is in ovarian high-grade serous carcinoma.

References

[1] Wang TL, Diaz Jr LA, Romans K, et al. Digital karyotyping identifies thymidylate synthase amplification as a mechanism of resistance to 5-fluorouracil in metastatic colorectal cancer patients. Proc Natl Acad Sci U S A 2004;101:3089-94.
[2] Wang TL, Maierhofer C, Speicher MR, et al. Digital karyotyping. Proc Natl Acad Sci U S A 2002;99:16156-61.
[3] Shih I-M, Sheu JJ, Santillan A, et al. Amplification of a chromatin remodeling gene, Rsf-1/HBXAP, in ovarian carcinoma. Proc Natl Acad Sci U S A 2005;102:14004-9.
[4] Loyola A, Huang JY, LeRoy G, et al. Functional analysis of the subunits of the chromatin assembly factor RSF. Mol Cell Biol 2003;23:6759-68.
[5] Vignali M, Hassan AH, Neely KE, Workman JL. ATP-dependent chromatin-remodeling complexes. Mol Cell Biol 2000;20:1899-910.
[6] Flanagan JF, Peterson CL. A role for the yeast SWI/SNF complex in DNA replication. Nucleic Acids Res 1999;27:2022-8.
[7] Cosma MP, Tanaka T, Nasmyth K. Ordered recruitment of transcription and chromatin remodeling factors to a cell cycle- and developmentally regulated promoter. Cell 1999;97:299-311.
[8] Wolffe AP. Chromatin remodeling: why it is important in cancer. Oncogene 2001;20:2988-90.
[9] Klochendler-Yeivin A, Muchardt C, Yaniv M. SWI/SNF chromatin remodeling and cancer. Curr Opin Genet Dev 2002;12:73-9.
[10] Hughes-Davies L, Huntsman D, Ruas M, et al. EMSY links the BRCA2 pathway to sporadic breast and ovarian cancer. Cell 2003;115:523-35.
[11] Shih I-M, Kurman RJ. Ovarian tumorigenesis—a proposed model based on morphological and molecular genetic analysis. Am J Pathol 2004;164:1511-8.
[12] Schraml P, Schwerdtfeger G, Burkhalter F, et al. Combined array comparative genomic hybridization and tissue microarray analysis suggest PAK1 at 11q13.5-q14 as a critical oncogene target in ovarian carcinoma. Am J Pathol 2003;163:985-92.
[13] Huang X, Gollin SM, Raja S, Godfrey TE. High-resolution mapping of the 11q13 amplicon and identification of a gene, TAOS1, that is amplified and overexpressed in oral cancer cells. Proc Natl Acad Sci U S A 2002;99:11369-74.
[14] Cheng CK, Chow LW, Loo WT, Chan TK, Chan V. The cell cycle checkpoint gene Rad9 is a novel oncogene activated by 11q13 amplification and DNA methylation in breast cancer. Cancer Res 2005;65:8646-54.
[15] Zaharieva BM, Simon R, Diener PA, et al. High-throughput tissue microarray analysis of 11q13 gene amplification (CCND1, FGF3, FGF4, EMS1) in urinary bladder cancer. J Pathol 2003;201:603-8.
[16] Singer G, Kurman RJ, Chang H-W, Cho SK, Shih IEM. Diverse tumorigenic pathways in ovarian serous carcinoma. Am J Pathol 2002;160:1223-8.
[17] Ho C-L, Kurman RJ, Dehari R, Wang T-L, Shih IEM. Mutations of BRAF and KRAS precede the development of ovarian serous borderline tumors. Cancer Res 2004;64:6915-8.
[18] Singer G, Stohr R, Cope L, et al. Patterns of p53 mutations separate ovarian serous borderline tumors and low- and high-grade carcinomas and provide support for a new model of ovarian carcinogenesis: a mutational analysis with immunohistochemical correlation. Am J Surg Pathol 2005;29:218-24.

CANCER

Mol Diag Ther 2006; 10 (4): 231-237
1177-1062/06/0004-0231/$39.95/0

Digital Karyotyping

An Update of its Applications in Cancer

Ritu Salani,[1,2] *Chao-Ling Chang*,[2] *Leslie Cope*[2] and *Tian-Li Wang*[1,2]

1 Department of Gynecology and Obstetrics, Johns Hopkins University School of Medicine, Baltimore, Maryland, USA
2 Department of Oncology, Johns Hopkins University School of Medicine, Baltimore, Maryland, USA

Contents

Abstract

DNA copy number alterations, including entire chromosomal changes and small interstitial DNA amplifications and deletions, characterize the development of cancer. These changes usually affect the expression of target genes and subsequently the function of the target proteins. Since the completion of the human genome project, the capacity to comprehensively analyze the human cancer genome has expanded significantly. Techniques such as digital karyotyping have been developed to allow for the detection of DNA copy number alterations in cancer at the whole-genome scale. When compared with conventional methods such as spectral karyotyping, representational difference analysis, comparative genomic hybridization (CGH), or the more recent array CGH; digital karyotyping provides an evaluation of copy number of genetic material at higher resolution. Digital karyotyping has therefore promised to enhance our understanding of the cancer genome. This article provides an overview of digital karyotyping including the principle of the technology and its applications in identifying potential oncogenes and tumor suppressor genes.

1. The Principle of Digital Karyotyping

Digital karyotyping, which was first developed in 2002, allows for the quantitative analysis of DNA copy number at high resolution. This technique provides a comprehensive examination of gene dosage of the entire genome by DNA sequencing of representative fragments (known as tags) contained within the whole genome, and enumerating the relative numbers of these tags.[1] The tags, which are extracted from the genomic DNA of each sample, are 21 base pair (bp) in length. They contain sufficient information to uniquely identify the genomic loci of derivation. Digital karyotyping is closely related to serial analysis of gene expression (SAGE).[2] However, unlike SAGE, which measures frequencies of the poly-A-tagged RNAs, digital karyotyping measures tag densities throughout the whole genome.

Compared with microarray analysis, the unique features of digital karyotyping are (i) its information is independent of existing databases, so it has the capability of identifying chromosomal regions of amplifications and deletions at previously unreported human genome loci, as well as DNA sequences foreign to the human genome, such as viral sequences;[1] and (ii) the signal is based on digital tag count obtained from genome sequencing, which is different from the analog signal intensity from hybridization for microarrays.

In practice, digital karyotyping requires detailed steps in order to isolate representative sequence tags. Briefly, the genomic DNA is fragmented into ~4000bp fragments by a mapping endonuclease enzyme, usually a 6bp-cutter such as a *Sac*I (figure 1). The DNA fragments are then ligated to biotinylated linkers and digested with the fragmenting enzyme that recognizes even more frequent sequences, such as the 4bp-cutter *Nla*III. The biotinylated and *Nla*III cut DNA fragments are isolated by binding the fragments to streptavidin-coated magnetic beads. Linkers containing a 6bp site recognized by *Mme*I (a type IIS restriction endonuclease) are ligated to the captured DNA fragments. The fragments are then digested by *Mme*I and 21bp tags are released. The 21bp tags are then ligated to each other to form ditags, which are isolated to form concatemers. Similar to SAGE, the concatemers are then cloned into plasmid vectors and sequenced.[2] These tags are computationally extracted from the sequence data and matched to the corresponding chromosomal locations.[2] In addition, digital enumeration of tag observations along each chromosome can be used to provide a quantitative evaluation of the DNA content. As tag counts are directly proportional to the amount of genetic material present in a given sample, digital karyotyping acts as a reliable tool for analysis of genetic dosage.

2. Resolution of Digital Karyotyping: Comparison with Other Genome-Wide Technologies

The size of alterations that can be identified by digital karyotyping is dependent on the combination of the mapping and fragmenting enzymes, and the number of tags that are obtained through sequencing. The ability to modify the mapping and fragmenting enzymes can change the sensitivity of this technique. In addition, it can overcome the potential caveat of incompletely analyzing the genome due to lower density mapping/fragmenting enzyme restriction sites at certain genome loci. The resolution can also be effectively improved by increasing the number of tags sampled by sequencing. Table I summarizes the sensitivity of digital karyotyping deduced by parametric power calculation

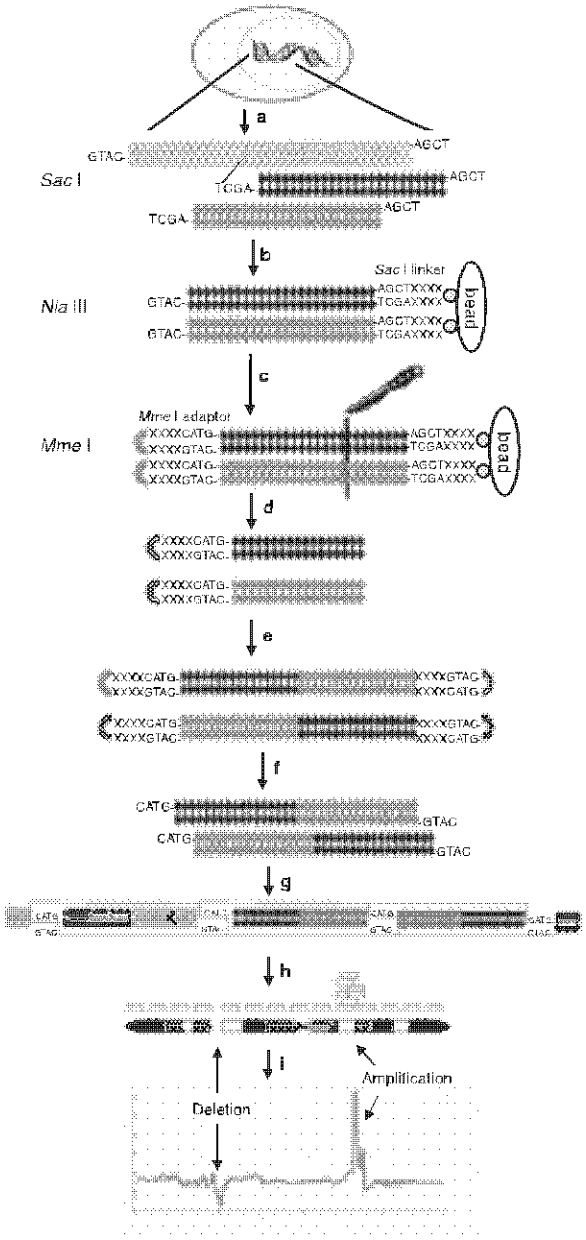

Fig. 1. The process of digital karyotyping. Digital karyotyping is based on the extraction of the 21bp sequence tags that represent unique locations in the genome. Intact genomic DNA is fragmented by *Sac*I, ('mapping' enzyme), to create small DNA pieces (**a**). The *Sac*I sites are linked to linkers that can be immobilized to beads. DNA fragments bound to the beads are digested with a frequently cutting enzyme, *Nla*III ('tagging' enzyme), leaving the 3′GTAC overhang (**b**). The new *Nla*III sites are linked to adaptors with *Mme*I enzyme binding sites. *Mme*I binds to the adaptors and cuts 21bp from the adaptor (**c**). DNA fragments including the *Mme*I adaptor and 21bp unique tags are released (**d**). These are ligated to form ditags (**e**), then amplified by PCR and released by *Nla*III digestion (**f**). Ditags are concatenated (**g**), cloned and sequenced (**h**). Finally, tags are computationally extracted from sequence data and matched to precise chromosomal locations and tag densities are evaluated to determine abnormalities in DNA copy number (**i**).

Table I. Theoretical resolutions of digital karyotyping determined by Poisson test

Size of alteration		The probability that a detected mutation represents a real mutation (%)			
No. of base pairs	No. of virtual tags	amplification (copy number = 10)		subchromosomal gain (copy number = 3)	
		100 000 tags	1 000 000 tags	100 000 tags	1 000 000 tags
100 000	30	>95	>95	0.09	25
200 000	50	95	95	0.30	66
600 000	150	95	95	10.88	>95
2 000 000	500	95	95	80.99	95
4 000 000	1000	95	95	93.84	95
6 000 000	1500	95	95	>95.00	95

based on an assumption that tag counts follow a Poisson distribution. The data derived from power calculation are similar to those obtained by Monte Carlo simulation published previously by our research group.[1] Both methods demonstrate that increasing the number of tags, for example a 10-fold increase of tag counts, will significantly enhance the resolution and positive predictive values.

In addition to digital karyotyping, several high-resolution genome-wide technologies are currently available to detect DNA copy number alterations, including array comparative genomic hybridization (CGH), representational oligonucleotide microarray analysis (ROMA) and single nucleotide polymorphism (SNP) arrays. In contrast to digital karyotyping, which uses representative sequencing of the genome, the above technologies use hybridization strategies on array formats. The detailed description of these technologies can be found in several reviews.[3,4] Two of the major factors concerning the resolution of array-based technologies are the density of the spotted probes (the coverage) and the nature (sequence) of the selected probe. The current genome coverage of each array-based technology is 44 000 probes for array CGH (available from Agilent Technologies [Palo Alto, CA, USA]), 100 000 probes for ROMA and 500 000 probes for SNP array (available from Affymetrix [Santa Clara, CA, USA]). Oligonucleotide array platform is currently the leader in the hybridization array market because oligonucleotide array gives a better signal-to-noise ratio than cDNA or bacterial artificial chromosomes (BACs) as probes. The theoretical limit of resolution for each technique is calculated by simply dividing the whole human genome size (3×10^9bp) by the number of spotted oligonucleotide probes (0.068Mb for array CGH, 0.03Mb for ROMA, and 0.006Mb for SNP arrays). Compared with these hybridization-based technologies, digital karyotyping has the highest genome coverage. This is because the current platform mapping enzyme (*Sac*I) and fragmenting enzyme (*Nla*III) produce 842 202 virtual tags and thus the theoretical limit of resolution is 0.004Mb.

It should be emphasized that probe coverage does not represent the actual resolution for the above mentioned technologies. For hybridization-based assays, the actual resolution will potentially be hampered by factors including the non-specific hybridization signal, non-linear relationships between hybridization and gene dosage, and the unpredictable reproducibility across different array platforms. The actual resolution limit of each method will be determined by the systemic experimental implementations to test its limitation in detecting genetic alterations with various sizes and magnitudes. Since the specificity of the array-based technologies is not well established, it is recommended that data be interpreted with caution and that independent methods are used, such as fluorescent *in situ* hybridization (FISH) or quantitative real-time PCR, to validate the inferred copy number alterations.

In contrast to the hybridization-based technologies where the actual resolution is currently not known, digital karyotyping has an advantage in providing the statistical confidence of detected genomic alterations. This is because of its unique data output that allows a detailed analysis of predicted resolution by computer simulation using the Monte Carlo method or power calculation. In the original report of digital karyotyping,[1] the Monte Carlo method was used to determine the sensitivity and positive predictive value (PPV) of various sizes of genetic alterations. The PPV indicates the probability of a detected alteration being a true one, and therefore can help researchers determine the need to design validation experiments.

In addition, to help determine the number of experimental tags required to confidently detect different sizes and folds of DNA copy number alterations, we performed power calculations, which are provided in table II. A detailed method of the power calculation is discussed in the appendix. Based on table II, with 82 114 tags, we expect to reliably detect a 5-fold amplification of 200kb in size, but if 941 160 tags are obtained, we expect to reliably detect a 5-fold amplification covering 20kb.

Table II. Experimental tag requirements for different folds of amplification

Size of alteration		No. of experimental tags required to achieve ≥95% PPV				
No. of base pairs	No. of virtual tags	1.5-fold[a]	2-fold[a]	3-fold[a]	5-fold[a]	10-fold[a]
7724	2	87 961 682	24 861 803	7 626 139	2 448 702	768 509
19 320	5	33 300 667	9 489 511	2 861 381	941 160	286 348
38 640	10	10 352 768	2 949 813	890 628	286 348	88 431
193 200	50	2 869 803	812 725	248 449	82 114	25 266
579 600	150	882 207	252 660	80 009	27 372	8422
1 930 000	500	242 133	67 376	21 055	8422	2106
3 860 000	1100	100 222	29 477	10 528	4211	2106

a Fold of amplification.

PPV = the probability that a detected mutation represents a real mutation.

3. Limitation of Digital Karyotyping

It should be noted that digital karyotyping can assess DNA copy number changes, but it is not well suited for revealing the physical location of the genetic arrangements. Therefore, digital karyotyping does not allow detection of translocations and cannot reveal the topological alteration of gene duplication, such as distinguishing between a tandem or inverted repeat. On the other hand, its sensitivity of detecting gene duplication is not affected by the topological arrangements.

In practice, DNA polymorphisms will affect the resolution of digital karyotyping. For example, polymorphisms at the mapping or tagging enzyme sites that affect the efficiency of the restriction enzyme digestions, as well as polymorphisms at the 21bp tags, will reduce the numbers of extractable tags and thus compromise the resolution digital karyotyping. Similarly, polymorphism in the genome will also affect hybridization-based technologies. For example, DNA polymorphism at the probe site will affect the efficiency of hybridization and thus hamper the resolution.

3.1 Cost of Digital Karyotyping

Despite the great reliability and sensitivity achievable by digital karyotyping, the current cost of each digital karyotyping library remains high, mostly attributed to the cost of the dideoxy sequencing method. It is estimated to range from $US10 000 to $US20 000 to obtain a library with 100 000–200 000 tags. Therefore, before performing the expensive procedures, careful selection of the tumor cell cultures and tumor specimens to be analyzed is recommended. If a cell culture is chosen, it is better to use low passage cell cultures instead of long-term culture (e.g. a cell line). This is because long-term culture has a higher risk of harboring accumulated genetic alterations during *in vitro* propagation that are not relevant to the pathogenesis of tumors. If a tumor specimen is to be used, a careful review of tumor histological types and tumor cell enrichment methods, such as microdissection or tumor cell purification using antibody-conjugated magnetic beads, are recommended.

Although expensive, the high-quality and high-resolution data from a small set of tumors at the discovery phase will likely justify the expense of digital karyotyping. The successful examples using digital karyotyping to identify causal genes for a variety of cancer types that will be described in this review are proof of the cost-effectiveness of digital karyotyping. In addition, with the development of cheaper and more reliable sequencing technologies,[5,6] it is foreseeable that in the near future the cost of digital karyotyping may reduce substantially and be comparable to array-based technologies.

4. Online Database of Digital Karyotyping

Public deposit of digital karyotyping data is available from the CGAP (Cancer Genome Anatomy Project) website.[7] All the sequence tags from each digital karyotyping library can be retrieved. The web browser provides bioinformatics tools for analysis of the DNA copy number alterations using varying parameters, including window scales, and size and fold of alterations. Currently, there have been 23 libraries deposited and it can be expected that in the future, with the accumulated digital karyotyping database, this centralized web deposit will provide scientists with a valuable resource to study the cancer genome in detail.

This website also provides free software to analyze new data. Text files containing the experimental tag data with observed frequencies can be uploaded, then the software in the web browser can analyze the data with varying window size and parameters for amplification and deletion.

5. Methylation-Specific Digital Karyotyping

By applying the mapping enzyme that is sensitive to DNA methylation, digital karyotyping can also be used to assess methylation changes in the cancer genome.[8] This modification, named methylation-specific digital karyotyping (MS-DK), was demonstrated in breast cancer and normal tissues using the methylation sensitive mapping enzyme *Asc*I.[8] The findings of this study showed more tags in the tumor epithelial cells, consistent with an overall hypomethylation of the cancer genome. MS-DK has also demonstrated distinct epigenetic changes at the different stages in tumor progression.[8]

MS-DK inherits the unique features of digital karyotyping, unlike other array-based technologies, and it can therefore be envisaged that MS-DK will be one of the most powerful methods to permit the analysis of cancer methylome at a genome-wide scale. Compared with methylation-specific PCR, which is a candidate approach to analyze methylation patterns at each gene locus, the advantage of MS-DK is that it only requires a small amount of DNA (≤1μg) for analysis of the entire human genome, while the same amount of DNA can only be used to analyze a handful of genes by methylation-specific PCR.

6. Applications of Digital Karyotyping in Identifying Genomic Alterations

6.1 Identifying Deleted Genes

Detection of a homozygous deletion has historically led to the identification of genes that are important in cancer development. Genes reported to be homozygously deleted in cancer include *DPC4* (*SMAD4*),[9] *BRCA2*[10] and $p16^{INK4A}$ (*CDKN2A*).[11] However, genome-wide detection of homozygous deletion is fraught with technical difficulties when compared with the discovery of amplified genes. In contrast to several-fold (generally >5-fold) increases of DNA copy number for an amplified gene, a homozygous deletion usually occurs in chromosomal regions with hemizygous deletion. The change in DNA copy number in homozygous deleted genes is usually from 1–2 copies/genome to 0 copy/genome, making its identification challenging. Therefore, it requires a method with sufficient sensitivity for the discovery of homozygous deletion. Digital karyotyping has been shown to be able to identify novel homozygous deletions including the one at the 5q locus in the colorectal cancer cell line DiFi.[1] More recently, digital karyotyping has identified a discrete deletion at chromosome 17p, harboring a putative tumor suppressor, *MKK4* (*MAP2K4*)[12,13] in two of the purified ovarian serous carcinomas.[14] Thus, digital karyotyping can potentially identify the existence of a previously unknown genetic deletion that contributes to the development of cancer.

6.2 Identifying Amplified Genes

An increase in genomic DNA copy number is one of the major mechanisms to activate an oncogene. With an increase in DNA copies, the encoded transcript and functional protein of a specific gene are consequently up regulated, which may contribute to tumorigenesis. In addition to identifying deletions in a cancer genome, digital karyotyping has been employed to recognize amplifications of oncogenes. The identification of orthodenticle homologue 2 (*OTX2*) as an oncogene in medulloblastomas is the product of digital karyotyping.[15] Analysis of five digital karyotyping libraries generated from medulloblastomas identified a novel amplicon, the *OTX2* gene, on chromosome14q. OTX2 is responsible for the fate of neuroectoderm in various regions of the developing brain.[15] The role of OTX2 in the development of the brain is consistent with its proposed role as a medulloblastoma oncogene.[15] Another study also identified *OTX2* amplification in permanent medulloblastoma cell lines using digital karyotyping.[16] Functional analysis of OTX2 by small interstitial RNA knock-down strategy was shown to result in the inhibition of *in vitro* medulloblastoma cell growth, supporting the pathogenesis of *OTX2* as an oncogene.[16]

A recent study has applied digital karyotyping to survey the DNA copy number alterations in purified ovarian carcinomas and has identified a region on chromosome 11q13.12 to be frequently amplified in patients with advanced ovarian cancer. This amplification was also found to correlate with a poor overall survival.[17] A candidate oncogene, remodeling and spacing factor 1 (*RSF1*; also known as *HBXAP*), was pinpointed in this study by its concurrent amplification and over-expression characteristics. This oncogene was amplified in 13.2% of high-grade serous ovarian carcinomas studied and was not detected in any cases of low-grade serous carcinomas, serous borderline tumors, benign cystadenomas, or normal ovaries. This study has not only utilized digital karyotyping to identify a new oncogene in ovarian carcinoma, but also recognized its role as a prognostic factor and a potential drug target.

6.3 Identifying Chemotherapeutic Targets

The purpose of identifying genetic alterations lies in the potential to provide improved diagnostic tests at an earlier stage, as well as the ability to administer a more effective treatment regimen.

Digital karyotyping has also been used with the intention of discovering potential chemotherapeutic targets. As noted earlier, digital karyotyping identified the oncogene *OTX2* in medulloblastomas.[15,16] Cell lines that expressed OTX2 were noted to respond to all-trans retinoic acid, which represses OTX2 expression and induces apoptosis; thus, providing a possible therapeutic modality for medulloblastomas expressing this gene.[16] In a study by Wang et al.,[18] digital karyotyping was used to identify an amplified 100kb region on chromosome 18p11.32 in patients with colorectal cancer that demonstrated resistance to 5-fluorouracil (5-FU) therapy. This area was identified as a region encoding thymidylate synthase (TYMS), which is a target of 5-FU. The study was able to correlate this amplification with a shorter mean survival, and proposed that *TYMS* gene amplification may be used to identify patients with 5-FU resistance. The discovery of this 5-FU resistance marker may lead to the development of a different treatment regimen for patients who develop resistance, which will likely result in a more efficacious drug regimen and eliminate unnecessary adverse effects.[18] These applications indicate that digital karyotyping may be used amongst patients with evidence of drug resistance or other profiles to identify loci that may be altered resulting in a changed drug response.

7. Conclusion

In summary, digital karyotyping has been developed to detect gross and interstitial chromosomal changes, including amplifications and deletions that may potentially harbor oncogenes and tumor suppressor genes, respectively. It provides a high-resolution evaluation of genomic DNA content and has proven to be a useful method to evaluate genomic changes with a digital readout. Digital karyotyping has been successfully applied to explore the DNA copy contents in colorectal carcinoma, medulloblastoma, melanoma and ovarian serous carcinomas, and it has facilitated the identification of potential tumor-associated genes involved in tumorigenesis. However, current cost and labor associated with this new technology remain high, limiting its practical applications. It is foreseeable that in the near future, with the reduction of sequencing costs, digital karyotyping will become a more feasible technology. The modified version of digital karyotyping, MS-DK, which holds the unique and comprehensive features, will likely play a role in revealing the genome-wide methylation profile in cancer and will advance our understanding of the cancer genome.

Acknowledgements

This study was supported by the US Department of Defense grant (W81XWH-05-1-0004).

The authors have no conflicts of interest that are directly relevant to the content of this review.

Appendix

1. Method for Table I and Table II

In order to identify DNA copy number alterations, we slide a window along each chromosome, looking for places where the sum of tag counts within a window is higher or lower than expected by chance alone. If we assume that the tag counts have a Poisson distribution, then the sum has a Poisson distribution as well, and we can perform hypothesis tests based on that distribution. If the Poisson assumption is correct, these tests are equivalent to the permutation tests usually used for analysis of digital karyotyping data. As shown in table I, we compared the results produced by Poisson test with the results from Monte Carlo simulation in the original digital karyotyping paper.[1] They appear consistent when requiring the PPV to be >95%. We include a p-value adjustment for the multiple tests that arise when scanning the genome and the exact value was determined by extensive simulation.

If there is exactly one mutation on a chromosome, the PPV can be approximated as power/(α + power), where α represents a type I error. We set power to be 0.95 and α to be 0.05, so the PPV will be approximately 0.95 in each cell of the table. More mutations will lead to a higher PPV, so this is in some sense, the most stringent criteria. The calculation was based on a total of 842 202 virtual tags deduced from the entire human genome, and for convenience, an 'average' chromosome of 40 000 tags were used for all the calculations, although results may vary slightly between chromosomes of different lengths.

References

1. Wang TL, Maierhofer C, Speicher MR, et al. Digital karyotyping. Proc Natl Acad Sci U S A 2002; 99 (25): 16156-61
2. Velculescu VE, Zhang L, Vogelstein B, et al. Serial analysis of gene expression. Science 1995 Oct 20; 270 (5235): 484-7
3. Parrett TJ, Yan H. Digital karyotyping technology: exploring the cancer genome. Expert Rev Mol Diagn 2005 Nov; 5 (6): 917-25
4. Feuk L, Carson AR, Scherer SW. Structural variation in the human genome. Nat Rev Genet 2006 Feb; 7 (2): 85-97
5. Margulies M, Egholm M, Altman WE, et al. Genome sequencing in microfabricated high-density picolitre reactors. Nature 2005 Sep 15; 437 (7057): 376-80
6. Shendure J, Porreca GJ, Reppas NB, et al. Accurate multiplex polony sequencing of an evolved bacterial genome. Science 2005 Sep 9; 309 (5741): 1728-32

7. The Cancer Genome Anatomy Project. Digital karyotyping data viewer [online]. Available from URL: http://cgap-stage.nci.nih.gov/SAGE/DKViewHome [Accessed 2006 Jun 9]
8. Hu M, Yao J, Cai L, et al. Distinct epigenetic changes in the stromal cells of breast cancers. Nat Genet 2005 Aug; 37 (8): 899-905
9. Hahn SA, Hoque AT, Moskaluk CA, et al. Homozygous deletion map at 18q21.1 in pancreatic cancer. Cancer Res 1996 Feb 1; 56 (3): 490-4
10. Schutte M, da Costa LT, Hahn SA, et al. Identification by representational difference analysis of a homozygous deletion in pancreatic carcinoma that lies within the BRCA2 region. Proc Natl Acad Sci U S A 1995 Jun 20; 92 (13): 5950-4
11. Kamb A, Gruis NA, Weaver-Feldhaus J, et al. A cell cycle regulator potentially involved in genesis of many tumor types. Science 1994 Apr 15; 264 (5157): 436-40
12. Teng DH, Perry WL, Hogan JK, et al. Human mitogen-activated protein kinase kinase 4 as a candidate tumor suppressor. Cancer Res 1997 Oct 1; 57 (19): 4177-82
13. Su GH, Hilgers W, Shekher MC, et al. Alterations in pancreatic, biliary, and breast carcinomas support MKK4 as a genetically targeted tumor suppressor gene. Cancer Res 1998 Jun 1; 58 (11): 2339-42
14. Nakayama K, Nakayama N, Davidson B, et al. Homozygous deletion of MKK4 in ovarian serous carcinoma. Cancer Biol Ther 2006 Jun 9, 5 (6) Epub ahead of print
15. Boon K, Eberhart CG, Riggins GJ. Genomic amplification of orthodenticle homologue 2 in medulloblastomas. Cancer Res 2005 Feb 1; 65 (3): 703-7
16. Di C, Liao S, Adamson DC, et al. Identification of OTX2 as a medulloblastoma oncogene whose product can be targeted by all-trans retinoic acid. Cancer Res 2005 Feb 1; 65 (3): 919-24
17. Shih IeM, Sheu JJ, Santillan A, et al. Amplification of a chromatin remodeling gene, Rsf-1/HBXAP, in ovarian carcinoma. Proc Natl Acad Sci U S A 2005 Sep 27; 102 (39): 14004-9
18. Wang TL, Diaz LA, Romans K, et al. Digital karyotyping identifies thymidylate synthase amplification as a mechanism of resistance to 5-fluorouracil in metastatic colorectal cancer patients. Proc Natl Acad Sci U S A 2004 Mar 2; 101 (9): 3089-94

Correspondence and offprints: Dr *Tian-Li Wang*, Departments of Gynecology and Oncology, Johns Hopkins University School of Medicine, 1550 Orleans Street, Room: 306, Baltimore, MD 21231, USA.
E-mail: tlw@jhmi.edu

[Cancer Biology & Therapy 5:6, 630-634, June 2006]; ©2006 Landes Bioscience

Appendix #7

Research Paper

Homozygous Deletion of *MKK4* in Ovarian Serous Carcinoma

Kentaro Nakayama[1,†]
Naomi Nakayama[1,†]
Ben Davidson[4]
Hidetaka Katabuchi[5]
Robert J. Kurman[1,2,3]
Victor E. Velculescu[2]
Ie-Ming Shih[1,2,3]
Tian-Li Wang[2,3,*]

Departments of [1]Pathology, [2]Oncology and [3]Gynecology and Obste trics; Johns Hopkins Medical Institutions; Baltimore, Maryland USA

[4]Department of Pathology; the Norwegian Radium Hospital; University of Oslo; Montebello, Norway

[5]Department of Gynecology and Obstetrics; Kumamoto University School of Medicine; Kumamoto, Japan

[†]These authors contributed equally to this work.

*Correspondence to: Tian-Li Wang; Departments of Gynecology/Obstetrics and Oncology; Johns Hopkins University School of Medicine; 1550 Orleans Street, Rm: 306; Baltimore, Maryland 21231 USA; Tel.: 410.502.7774; Fax: 410.502.7943; Email: tlw@jhmi.edu

Received 12/25/05; Accepted 03/09/06

Previously published online as a *Cancer Biology & Therapy* E-publication: http://www.landesbioscience.com/journals/cbt/abstract.php?id=2675

KEY WORDS

digital karyotyping, ovarian cancer, homozygous deletion, loss of heterozygosity, tumor suppressor

ABBREVIATIONS

HD	homozygous deletion
FISH	fluorescent in situ hybridization
MKK4	mitogen-activated protein kinase kinase-4
LOH	loss of heterozygosity

ACKNOWLEDGEMENTS

This study was supported by the US Department of Defense grant (OC040060) and the National Cancer Institute grant (RO1 CA103937). The authors thank Dr. May J. Yen for preparation of the figure illustrations.

ABSTRACT

Analysis of deleted chromosomal regions in tumors has historically led to the identification of tumor suppressor genes. In this study, we used digital karyotyping, a genome-wide, high-resolution technology, to search for chromosomal deletions in ovarian serous carcinoma, the most lethal gynecological malignancy in women. Five purified ovarian serous carcinomas were analyzed by digital karyotyping and small interstitial deletions at chromosome 17p were identified in two tumor samples. Aligning these two deletions identified an overlapping region that spanned 2.4 Mb which harbored a candidate tumor suppressor gene, *mitogen-activated protein kinase kinase-4* (*MKK4*). Dual-color FISH analysis confirmed homozygous deletion of the *MKK4* locus in both samples and RT-PCR demonstrated that both carcinomas lacked *MKK4* transcript expression. Loss of heterozygosity of 17p occurred in 24 (86%) of 28 high-grade serous carcinomas including both cases with homozygous *MKK4* deletion. Additionally, downregulation of *MKK4* expression was found in 96 (75%) of 128 ovarian serous carcinomas as compared to benign ovarian tissues. These findings suggest that homozygous deletion or reduced expression of *MKK4* may contribute to the development of ovarian serous carcinoma.

INTRODUCTION

Functional inactivation or loss of expression of tumor suppressor genes is important in cancer development. Traditionally, tumor suppressor genes have been identified by detection of homozygous deletions in a chromosomal region. Several tumor suppressor genes with homozygous deletion have been reported in human cancers including DPC-4,[1] p16[2] and BRCA2[3] and it is expected that more will be discovered. However, genome-wide identification of homozygous deletion is fraught with technical difficulties as compared to discovery of gene amplification. First, gene amplification usually shows greater than 3-fold increase of DNA copy number while homozygous deletion usually occurs in chromosomal regions with hemizygous deletion (or loss of heterozygosity) and the absolute change in DNA copy number in the homozygous deleted region is smaller (usually a change from one copy to zero copy per genome) and may be difficult to detect using the current methods. Furthermore, the size of homozygous deletions may be small (<500 kb) while the size of amplified chromosomal regions generally ranges from 1 to several Mb. Thus, a highly sensitive genome-wide method is required to detect homozygous deletion. Second, although contamination of normal DNA in the tumor samples can obscure detection of amplification as well as homozygous deletions, it is a much greater problem in the detection of deletions. Therefore, tumor cell lines have been successfully used as alternatives to characterize homozygous deletions in cancer although cell lines can acquire molecular genetic changes as a result of long-term culture that are not relevant to tumor development.

To overcome these technical difficulties, we applied a new genome-wide technology, digital karyotyping,[4] to identify deleted chromosomal regions in ovarian serous carcinoma, one of the most aggressive malignancies in women. Digital karyotyping is based on extracting and counting 21 bp sequence tags that represent unique loci in the human genome. Populations of tags can be directly matched to the genome assembly and digital enumeration of tags is then used to quantitatively evaluate DNA content along each chromosome. The major advantage of digital karyotyping is that it directly counts sequence tags, thus providing an unbiased digital readout of DNA copy numbers. Digital karyotyping has been demonstrated to be a sensitive method of detecting DNA copy number changes and has been used successfully to identify novel genomic deletions and amplifications and in human cancer.[4-8]

In order to minimize contamination from normal DNA, we applied an affinity immunosorting method using EpCAM antibody-conjugated magnetic beads[9] to isolate pure tumor cells from fresh surgical specimens. As a result of employing digital karyotyping on purified ovarian serous carcinomas, we found interstitial deletions of a region on chromosome 17p containing the *MKK4* gene.

MATERIALS AND METHODS

Digital karyotyping. Tissue samples were obtained from the Department of Pathology at the Johns Hopkins Hospital and ascites samples from the Norwegian Radium Hospital in Oslo, Norway. The acquisition of specimens was approved by the institutional research review boards of both institutions. All the tumor samples were high-grade, FIGO stage III or IV ovarian serous carcinomas. Tumor cells were affinity purified from tissue specimens using anti-EpCAM-conjugated beads and genomic DNA was isolated using a DNeasy kit (Qiagen, Chatsworth, CA). Digital karyotyping libraries were constructed from five serous carcinoma tissues and were analyzed as previously described.[4] Approximate 120,000 genomic tags were obtained from each library. After removing the nucleotide repeats in the human genome, the average number of filtered tags was 66,000 for each library. A window size of 150 virtual tags was used for analysis. The sensitivity and specificity of the analysis have been described in a previous report.[4]

Dual-color fluorescence in situ hybridization (FISH). Tissue microarrays consisting of 48 high-grade ovarian serous carcinomas were used in the FISH analysis. BAC clones (RP11-1112M11, CTD-3045M24 and CTD-2331E5), containing the genomic sequences harboring the *MKK4* gene located at 17p12, were labeled with biotin by nick translation. BAC clone (CTD-2506E12), located at 17q11.2, was used to generate the reference probe. The FISH method and the scoring criteria have been detailed in a previous report.[5]

Loss of heterozygosity (LOH) analysis. LOH was determined using fluorescent-labeled microsatellite markers located at 17p: D17S1298, D17S974 and D17S969 (Invitrogen, Carlsbad,CA). PCR was performed using DNA isolated from purified tumor cells and their matched normal cells obtained from stromal cells. PCR products were separated and analyzed using a capillary electrophoresis system (SpectruMedix, State College, PA).

Mutational analysis of *MKK4*. Sequences for exons and adjacent introns containing the kinase domain of *MKK4* were extracted from the public database of the human genome sequences (http://genome.ucsc.edu/). Primers for PCR amplification and sequencing were designed using the Primer 3 program (http://frodo.wi.mit.edu/cgi-bin/primer3/primer3_www.cgi), and were synthesized by IDT (Coralville, IA). PCR amplification and sequencing were performed on tumor DNA from purified primary tumors using a 96 capillary ABI 3700 instrument at Agencourt Biosciences (Beverly, MA). Sequence traces were assembled and analyzed to identify potential genomic alterations using the Mutation Surveyor software package (SoftGenetics, State College, PA). Sequences of all primers used for PCR amplification and sequencing are provided in Supplementary Table 1.

Quantitative real-time PCR. For quantitative RT-PCR, a total of 128 high-grade ovarian serous carcinomas (75 tissue samples and 58 ascites samples) and 12 samples of benign ovarian epithelial cells (2 from brushed ovarian surface epithelium, 4 from brushed cystadenomas and 6 primary cultures) were analyzed. Relative gene expression was determined by quantitative real-time PCR using methods previously described.[10] PCR reactions were performed using an iCycler (Bio-Rad Lab, Hercules, CA) and the PCR primers used to amplify *MKK4* transcript were: 5'-GCCTGTG-GCTGAAAATTAAGG-3' and 5;-TCAATGTCCACCTCGCAATAG-3'. The results were expressed as the difference between the Ct of the *MKK4* and the Ct of a control gene (APP) for which expression is relatively constant among the SAGE libraries analyzed.[10]

Immunohistochemistry. A total of 52 paraffin-embedded tissues including 35 high-grade ovarian serous carcinomas, five low-grade ovarian serous carcinomas, eight benign ovarian cysts and four normal ovaries were analyzed for immunoreactivity of total JNK1 and phosphorylated (activated) JNK1. The antibodies used included a rabbit polyclonal anti-JNK1 pan antibody (44-690G) and a rabbit polyclonal anti-JNK1&2 ($pTpY^{183/185}$) phosphorylation-specific antibody (44-682G) which were purchased from Biosource (Camarillo, CA). Immunohistochemistry was performed by incubating the slides with antibodies at 1:100 dilutions at 4°C overnight followed by chromagen development using the Envision kit (DAKO, Carpinteria, CA).

RESULTS AND DISCUSSION

Purified tumor cells from five fresh high-grade serous carcinomas were used for digital karyotyping. A discrete interstitial deletion on chromosome 17p was identified in two specimens with an inferred copy number of <0.5 copy/haploid genome (Fig. 1A). In contrast, the inferred number for the normal diploid genome is 1 copy/haploid genome and for hemizygous deletion was 0.5 copy/haploid genome. Using a cutoff of 0.5, we deduced that the smallest deleted region in these two tumors spanned 10.535 to 12.960 Mb (Fig. 1B). Twelve genes were located in this region, including *MKK4*, a candidate tumor suppressor gene previously reported to be homozygously deleted in pancreatic and breast carcinomas.[11,12] Based on the properties of *MKK4* and its localization within this homozygous deletion, we focused on *MKK4* in this study.

To validate the digital karyotyping results, we employed a dual-color FISH analysis because it is generally acknowledged that FISH analysis which is based on directly counting probe signals on single cells, provides a highly sensitive and specific approach of assessing gene copy number.[13-15] Three different BACs with different sizes that covered the *MKK4* genomic locus were selected to generate the FISH probes (Fig. 2A). FISH demonstrated that only one probe derived from the BAC clone, CTD-2331E5, was able to detect *MKK4* deletion in both cases with the deletion defined by digital karyotyping. This probe hybridized to the genomic region close to the 5' portion of *MKK4*, including its 5' promoter and the first 2 exons. As shown in (Fig. 2B), the carcinoma cells showed signals only of the reference probe, indicating a homozygous deletion. In contrast, signals of both *MKK4* and reference probes were observed with a similar count ratio in stromal cells adjacent to the carcinoma cells. Using this BAC clone, FISH analyses were performed on 48 high-grade serous carcinoma samples including those used in the digital karyotyping analysis. Except for the two cases with homozygous deletion detected by digital karyotyping, there were no additional cases showing a homozygous deletion. Therefore, the frequency of *MKK4* homozygous deletion in high-grade ovarian serous carcinomas was 4.2%. This was similar to that observed in pancreatic (2%) and breast (4.5%) carcinoma.[11,12]

LOH of 17p is frequently identified in ovarian carcinomas and is thought to be one of the mechanism to inactivate p53 or other tumor suppressor located on 17p.[16] To determine the relationship of 17p LOH and *MKK4* deletion, we analyzed the LOH status of 17p on 28 serous carcinomas using fluorescent-labeled microsatellite markers, D17S1298, D17S974 and D17S969, located at 3.87, 10.72 and 12.05 Mb on 17p, respectively. Our results demonstrated that 17p LOH in at least one of the markers occurred in 24 (86%) of 28 high-grade serous carcinomas including both carcinomas with *MKK4* homozygous deletion (Fig. 3). This result supports the view that LOH is one of the mechanisms that inactivates *MKK4* alleles. To further assess somatic inactivating mutations in the retained allele, we sequenced *MKK4* from the same 48 ovarian serous carcinomas. None of them showed somatic mutations, suggesting that sequence mutation of *MKK4* is a rare or non-existent event in ovarian serous carcinomas.

Appendix #7

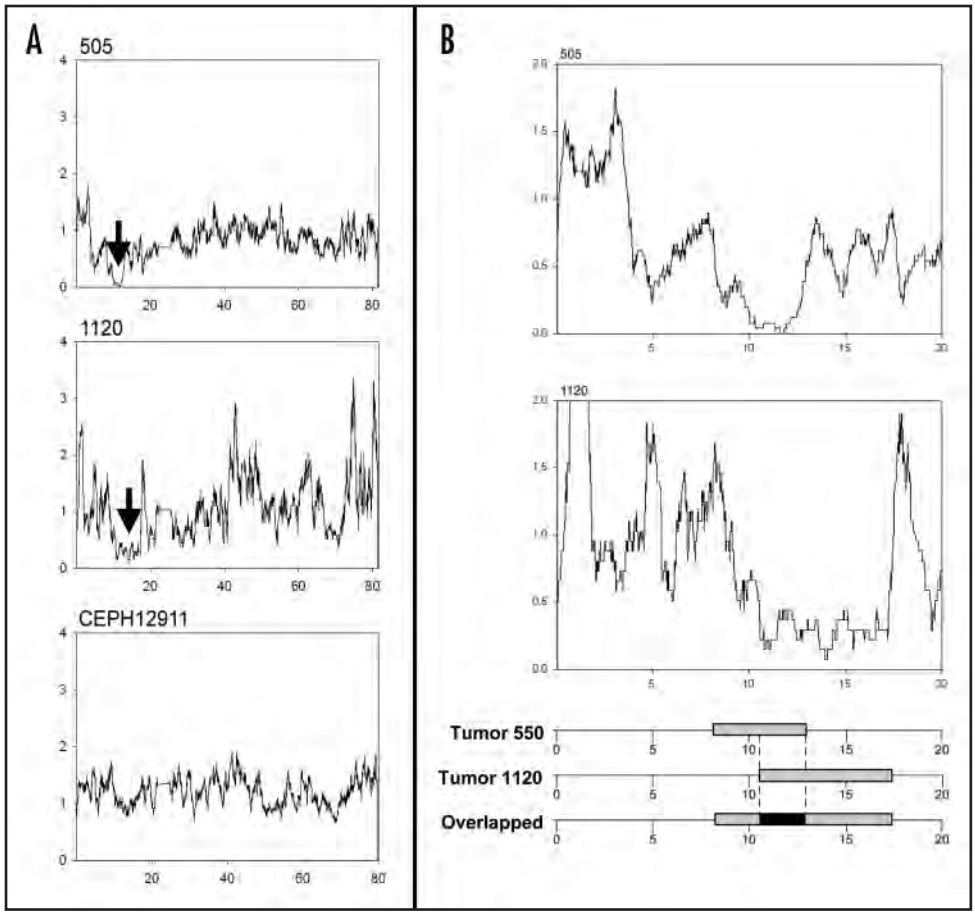

Figure 1. Detection of genomic deletion on chromosome 17p by digital karyotyping. (A) Digital karyotyping detects a decrease of DNA copy number (<0.5 copy/haploid genome) on 17p in two purified ovarian serous carcinomas labeled as 505 and 1120 but not in a control diploid lymphoblastoid cell line (CEPH129111) which demonstrates an inferred copy number of 1 across the whole chromosome. (B) Aligning the deletions in 505 and 1120 carcinomas defines the overlapped deletion region. Using a cutoff of 0.5 copy/haploid genome, the minimally deleted region is predicted to span from 10.535 to 12.960 Mb on 17p.

The presence of homozygous deletion of *MKK4* in ovarian carcinomas supports its role as a tumor suppressor in ovarian cancer. In addition, we attempted to determine if the gene expression level of *MKK4* decreased in high-grade serous carcinomas. First, we measured the *MKK4* mRNA levels in 38 ovarian serous carcinomas in which the status of genomic DNA copy number was known and compared this to benign control tissues. There was no detectable amplified PCR product in either of the two cases with homozygous deletion (Fig. 4A). In contrast, in the remaining 36 tumors without homozygous deletion, MKK4 PCR products were demonstrated (Fig. 4A). In addition, MKK4 expression in carcinomas compared to benign ovarian tissues was performed using quantitative RT-PCR. The results showed that as compared to benign ovarian tissues, the *MKK4* transcript level in high-grade serous carcinoma tissues and ascites was significantly decreased (Fig. 4B, $p < 0.001$, t-test). The lowest expression level (cycle threshold, Ct) in the benign group was 24.25 and it was used as the cutoff to evaluate *MKK4* downregulation in the carcinoma group. Fifty-eight (77.3%) of 78 ovarian carcinoma tissue samples and 38 (71.7%) of 53 ovarian carcinoma ascites samples had a *MKK4* expression level below the cutoff. Clinical follow up was available in the patients with ascites. Kaplan-Meier survival analysis demonstrated no significant correlation between *MKK4* expression levels and overall survival or disease-free interval ($p > 0.1$).

MKK4 has been shown to phosphorylate and activate *JNK*; therefore we performed immunohistochemistry to determine if total and phosphorylated *JNK* proteins were present in tumors with *MKK4* homozygous deletion. Our result demonstrated that the immunoreactivity of total and phosphorylated (active) *JNK* was present in both *MKK4*-null tumors; however, their immuno-intensity of phosphorylated *JNK* was reduced as compared to benign cyst epithelium (Fig. 5). Previous studies have demonstrated that the levels of active *JNK* in $MKK4^{-/-}$ ES cells were at reduced but comparable levels to those of $MKK4^{+/+}$ cells after treatment with UV irradiation and osmolarity shock.[17,18] Therefore it has been proposed that other kinase, such as *MKK7*, was required in conjunction with *MKK4* for a full activation of *JNK*.[19] Based on our finding in this report, it is plausible that the similar mechanism is employed by ovarian tumor cells.

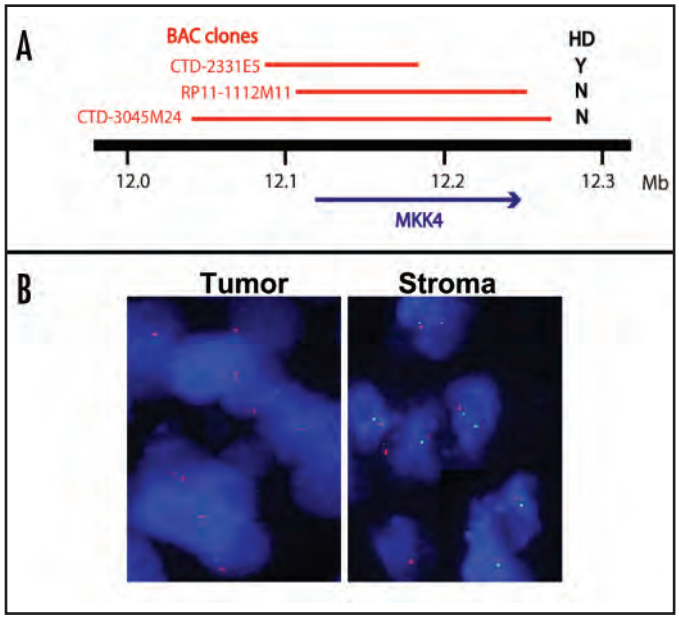

Figure 2. Dual-color FISH validates homozygous deletion of the *MKK4* gene. (A) The physical location of *MKK4* and three BAC clones used for FISH probes. Only the CTD-2331E5 FISH probe detects the *MKK4* homozygous deletion. HD: homozygous deletion. (B) In the 505 carcinoma cells (left), FISH detects a complete loss of *MKK4* gene (green) while retaining the signals of the control reference probe (red). In contrast, stromal cells on the same tissue section of the 505 specimen contain signals for both *MKK4* and reference probes with approximately 1:1 ratio (right).

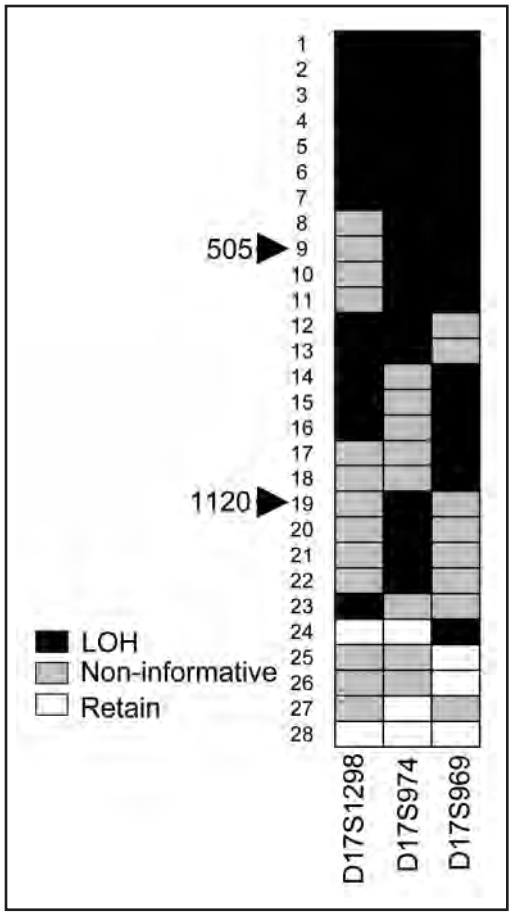

Figure 3. LOH analysis of 17p in high-grade ovarian serous carcinomas. LOH of 17p was analyzed using fluorescent-labeled microsatellite markers, D17S1298, D17S974 and D17S969, located at 3.87, 10.72 and 12.05 Mb on 17p, respectively. The majority of serous carcinomas demonstrate LOH in at least one of the markers. Arrows indicate the two tumors harboring *MKK4* deletion.

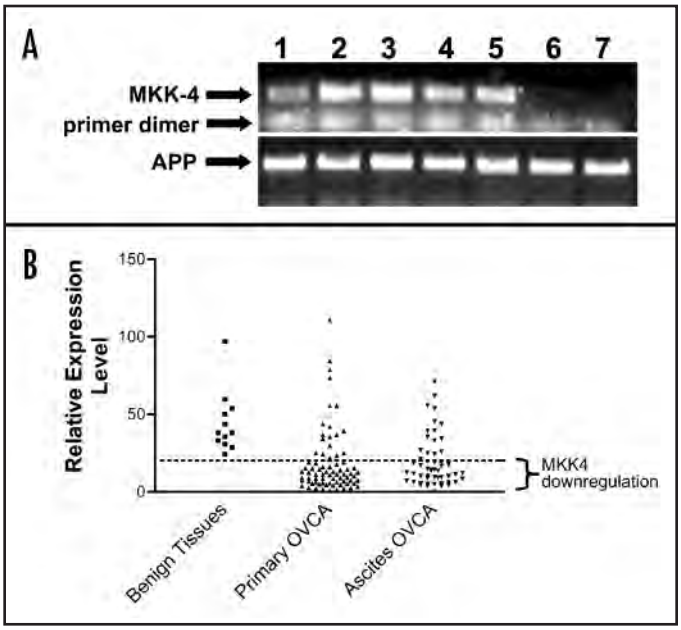

Figure 4. *MKK4* transcript levels in high-grade ovarian serous carcinomas. (A) RT-PCR of the *MKK4* mRNA demonstrates that the two samples harboring MKK4 homozygous deletion (lanes 6 and 7) do not show detectable *MKK4* transcript expression while the 36 tumors without MKK4 homozygous deletion expressed robust *MKK4* mRNA (representatives shown in lanes 1 through 5). RT-PCR of the APP gene was performed on the same cDNA panels as controls (bottom). (B) Quantitative RT-PCR of *MKK4* expression in a panel of ovarian benign tissues, high-grade serous carcinoma tissues and high-grade serous carcinomas ascites. As compared to benign ovarian tissues, *MKK4* was significantly down-regulated in high-grade carcinomas and ascites tumors ($p < 0.001$, t-test).

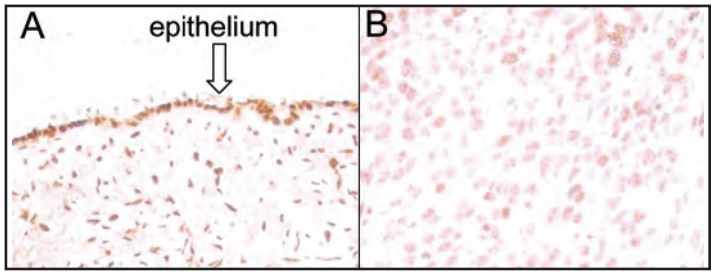

Figure 5. Immunoreactivity of phosphorylated JNK in benign ovarian epithelium and ovarian serous carcinoma with *MKK4* homozygous deletion. (A) Benign ovarian cyst shows diffuse and intense phosphorylated JNK immunoreactivity in the nuclei of epithelial cells. (B) Carcinoma tissue with known MKK4 deletion demonstrates weaker immunoreactivity than the benign cyst epitheliums.

MKK4 is a component of the stress-activated protein kinase signaling cascade involving the *MEKK1/MAPKKK1*, *SEK1/MKK4/JNKK*, and *SAPK/JNK* pathway. A variety of extracellular signals including environmental stress, growth factors and inflammatory cytokines activate *MKK4* and the *JNK/p38* signaling cascades.[20-21] *MKK4* plays a major role during normal development[22,18-23] and tumorigenesis.[12,24-26] Biallelic inactivation of *MKK4* such as an inactivating mutation of one allele and loss of the other has been identified in cancer cell lines of the breast, colon, testis, and pancreas.[11,12] In ovarian cancer, *MKK4* has been shown to act as a metastasis suppressor gene.[25] Engineered expression of *MKK4* in the SKOV3 ovarian cancer cells suppressed metastasis in mice and engineered *MKK4* expression in tumor cells prolonged the life span of mice by 70%.

As in other types of human carcinomas, the prevalence of homozygous deletion of *MKK4* in ovarian carcinoma is low with a frequency of 4.2%. However, downregulation of *MKK4* expression was detected in the majority of ovarian carcinomas. The wild-type nucleotide sequence of *MKK4* in 48 ovarian carcinomas analyzed suggests that the decrease in *MKK4* expression may operate by transcriptional regulation rather than sequence mutations that affect *MKK4* protein function.

In summary, our findings provide the first molecular genetic evidence of *MKK4* alteration in ovarian serous carcinoma. Despite a low frequency of *MKK4* homozygous deletion, we found that down-regulation of *MKK4* expression was present in the majority of ovarian serous carcinomas. These findings together with a previous study showing that inactivation of *MKK4* led to cell transformation[26] suggest that *MKK4* is a tumor suppressor gene in ovarian high-grade serous carcinomas. These results shed new light on the pathogenesis of ovarian serous carcinoma and may have important therapeutic implications.

References

1. Hahn SA, Hoque AT, Moskaluk CA, da Costa LT, Schutte M, Rozenblum E, Seymour AB, Weinstein CL, Yeo CJ, Hruban RH, Kern SE. Homozygous deletion map at 18q21.1 in pancreatic cancer. Cancer Res 1996; 56:490-4.
2. Kamb A, Gruis NA, Weaver-Feldhaus J, Liu Q, Harshman K, Tavtigian SV, Stockert E, Day RSr, Johnson BE, Skolnick MH. A cell cycle regulator potentially involved in genesis of many tumor types. Science 1994; 264:436-40.
3. Schutte M, da Costa LT, Hahn SA, Moskaluk C, Hoque AT, Rozenblum E, Weinstein CL, Bittner M, Meltzer PS, Trent JM, et al. Identification by representational difference analysis of a homozygous deletion in pancreatic carcinoma that lies within the BRCA2 region. Proc Natl Acad Sci USA 1995; 92:5950-4.
4. Wang TL, Maierhofer C, Speicher MR, Lengauer C, Vogelstein B, Kinzler KW, Velculescu VE. Digital karyotyping. Proc Natl Acad Sci USA 2002; 99:16156-61.
5. Wang TL, Diaz Jr LA, Romans K, Bardelli A, Saha S, Galizia G, Choti M, Donehower R, Parmigiani G, Shih Ie M, Iacobuzio-Donahue C, Kinzler KW, Vogelstein B, Lengauer C, Velculescu VE. Digital karyotyping identifies thymidylate synthase amplification as a mechanism of resistance to 5-fluorouracil in metastatic colorectal cancer patients. Proc Natl Acad Sci USA 2004; 101:3089-94.
6. Shih IM, Sheu JJ, Santillan A, Nakayama K, Yen MJ, Bristow RE, Vang R, Parmigiani G, Kurman RJ, Trope CG, Davidson B, Wang TL. Amplification of a chromatin remodeling gene, *Rsf-1/HBXAP*, in ovarian carcinoma. Proc Natl Acad Sci USA 2005; 102:14004-9.
7. Boon K, Eberhart CG, Riggins GJ. Genomic amplification of orthodenticle homologue 2 in medulloblastomas. Cancer Res 2005; 65:703-7.
8. Di C, Liao S, Adamson DC, Parrett TJ, Broderick DK, Shi Q, Lengauer C, Cummins JM, Velculescu VE, Fults DW, McLendon RE, Bigner DD, Yan H. Identification of OTX2 as a medulloblastoma oncogene whose product can be targeted by all-trans retinoic acid. Cancer Res 2005; 65:919-24.
9. Shih Ie M, Wang TL. Apply innovative technologies to explore cancer genome. Curr Opin Oncol 2005; 17:33-8.
10. Buckhaults P, Zhang Z, Chen YC, Wang TL, St Croix B, Saha S, Bardelli A, Morin PJ, Polyak K, Hruban RH, Velculescu VE, Shih Ie M. Identifying tumor origin using a gene expression-based classification map. Cancer Res 2003; 63:4144-9.
11. Teng DH, Perry IIIrd WL, Hogan JK, Baumgard M, Bell R, Berry S, Davis T, Frank D, Frye C, Hattier T, Hu R, Jammulapati S, Janecki T, Leavitt A, Mitchell JT, Pero R, Sexton D, Schroeder M, Su PH, Swedlund B, Kyriakis JM, Avruch J, Bartel P, Wong AK, Tavtigian SV, et al. Human mitogen-activated protein kinase kinase 4 as a candidate tumor suppressor. Cancer Res 1997; 57:4177-82.
12. Su GH, Hilgers W, Shekher MC, Tang DJ, Yeo CJ, Hruban RH, Kern SE. Alterations in pancreatic, biliary, and breast carcinomas support *MKK4* as a genetically targeted tumor suppressor gene. Cancer Res 1998; 58:2339-42.
13. Cox MC, Maffei L, Buffolino S, Del Poeta G, Venditti A, Cantonetti M, Aronica G, Aquilina P, Masi M, Amadori S. A comparative analysis of FISH, RT-PCR, and cytogenetics for the diagnosis of bcr-abl-positive leukemias. Am J Clin Pathol 1998; 109:24-31.
14. Pauletti G, Godolphin W, Press MF, Slamon DJ. Detection and quantitation of *HER-2/neu* gene amplification in human breast cancer archival material using fluorescence in situ hybridization. Oncogene 1996; 13:63-72.
15. Swiger RR, Tucker JD. Fluorescence in situ hybridization: A brief review. Environ Mol Mutagen 1996; 27:245-54.
16. Kinzler KW, Vogelstein B. The Genetic Basis of Human Cancer. 2nd ed. Toronto: McGraw-Hill, 2002.
17. Nishina H, Fischer KD, Radvanyi L, Shahinian A, Hakem R, Rubie EA, Bernstein A, Mak TW, Woodgett JR, Penninger JM. Stress-signalling kinase Sek1 protects thymocytes from apoptosis mediated by CD95 and CD3. Nature 1997; 385:350-3.
18. Yang D, Tournier C, Wysk M, Lu HT, Xu J, Davis RJ, Flavell RA. Targeted disruption of the *MKK4* gene causes embryonic death, inhibition of c-Jun NH2-terminal kinase activation, and defects in AP-1 transcriptional activity. Proc Natl Acad Sci USA 1997; 94:3004-9.
19. Nishina H, Wada T, Katada T. Physiological roles of SAPK/JNK signaling pathway. J Biochem (Tokyo) 2004; 136:123-6.
20. Atfi A, Djelloul S, Chastre E, Davis R, Gespach C. Evidence for a role of Rho-like GTPases and stress-activated protein kinase/c-Jun N-terminal kinase (SAPK/JNK) in transforming growth factor beta-mediated signaling. J Biol Chem 1997; 272:1429-32.
21. Roulston A, Reinhard C, Amiri P, Williams LT. Early activation of c-Jun N-terminal kinase and *p38* kinase regulate cell survival in response to tumor necrosis factor alpha. J Biol Chem 1998; 273:10232-9.
22. Ganiatsas S, Kwee L, Fujiwara Y, Perkins A, Ikeda T, Labow MA, Zon LI. SEK1 deficiency reveals mitogen-activated protein kinase cascade crossregulation and leads to abnormal hepatogenesis. Proc Natl Acad Sci USA 1998; 95:6881-6.
23. Nishina H, Vaz C, Billia P, Nghiem M, Sasaki T, De la Pompa JL, Furlonger K, Paige C, Hui C, Fischer KD, Kishimoto H, Iwatsubo T, Katada T, Woodgett JR, Penninger JM. Defective liver formation and liver cell apoptosis in mice lacking the stress signaling kinase *SEK1/MKK4*. Development 1999; 126:505-16.
24. Chae KS, Ryu BK, Lee MG, Byun DS, Chi SG. Expression and mutation analyses of *MKK4*, a candidate tumour suppressor gene encoded by chromosome 17p, in human gastric adenocarcinoma. Eur J Cancer 2002; 38:2048-57.
25. Yamada SD, Hickson JA, Hrobowski Y, Vander Griend DJ, Benson D, Montag A, Karrison T, Huo D, Rutgers J, Adams S, Rinker-Schaeffer CW. Mitogen-activated protein kinase kinase 4 (*MKK4*) acts as a metastasis suppressor gene in human ovarian carcinoma. Cancer Res 2002; 62:6717-23.
26. Cazillis M, Bringuier AF, Delautier D, Buisine M, Bernuau D, Gespach C, Groyer A. Disruption of *MKK4* signaling reveals its tumor-suppressor role in embryonic stem cells. Oncogene 2004; 23:4735-44.

[Cancer Biology & Therapy 5:7, 779-785, July 2006]; ©2006 Landes Bioscience

Appendix #8

Research Paper

Sequence Mutations and Amplification of PIK3CA and AKT2 Genes in Purified Ovarian Serous Neoplasms

Kentaro Nakayama[1,†]
Naomi Nakayama[1,†]
Robert J. Kurman[1-3]
Leslie Cope[2]
Gudrun Pohl[1]
Yardena Samuels[2]
Victor E. Velculescu[2]
Tian-Li Wang[2,3,*]
Ie-Ming Shih[1-3,*]

Departments of [1]Pathology, [2]Oncology and [3]Gynecology and Obstetrics; Johns Hopkins Medical Institutions; Baltimore, Maryland USA

[†]These authors contibuted equally to this manuscript.

*Correspondence to:Ie-Ming Shih; Johns Hopkins Medical Institutions; 550 Orleans Street, Room 305; Baltimore, Maryland 21231 USA; Tel.: 410.502.7774; Fax: 410.502.7943; Email: ishih@jhmi.edu/ Tian-Li Wang; Johns Hopkins Medical Institutions; 1503 E. Jefferson Street, Room: B-315; Baltimore, Maryland 21231 USA; Tel.: 410.502.0863; Fax: 410.502.7943; Email: tlw@jhmi.edu

Received 02/27/06; Accepted 03/26/06

Previously published online as a *Cancer Biology & Therapy* E-publication:
http://www.landesbioscience.com/journals/cbt/abstract.php?id=2751

KEY WORDS

mutation, amplification, FISH, digital karyotyping, ovarian cancer

ACKNOWLEDGEMENTS

This study was supported by the US Department of Defense grant (OC04-0060) and the National Cancer Institute grant (RO1 CA103937). The authors thank Dr. May J. Yen for preparation of the figure illustrations.

NOTES

Supplemental information can be found at:
http://www.landesbioscience.com/journals/cbt/supplement/nakayama5-7-supp.pdf

ABSTRACT

Sequence mutations and gene amplifications lead to activation of the *PIK3CA-AKT2* signaling pathway and have been reported in several types of neoplasms including ovarian cancer. Analysis of such genetic alterations, however, is usually complicated by contamination of normal cell DNA, artifacts associated with formalin-fixed tissues and the sensitivity of the techniques employed. In this study, we analyzed the sequence mutations in *PIK3CA* and *AKT2* genes using purified tumor cells that were isolated from high-grade ovarian serous carcinomas and serous borderline tumors (SBTs) and assessed gene amplification using a dual-color FISH on tissue microarrays. Somatic sequence mutations in the kinase domain of *AKT2* were not detected in any of the 65 ovarian tumors analyzed. Mutations of *PIK3CA* were rare, occurring only in one (2.3%) of 44 high-grade serous carcinomas and in only one (4.8%) of 21 SBTs. Dual-color FISH demonstrated that *PIK3CA* and *AKT2* were not amplified in SBTs but amplified in 13.3% and 18.2% high-grade carcinomas, respectively. High-level amplification (>3 fold) was more frequently observed in *AKT2* than in *PIK3CA*. Unlike mutations in *ERBB2*, *KRAS* and *BRAF* which are mutually exclusive in SBTs, coamplification of *PIK3CA* and *AKT2* was present in five high-grade carcinomas including the OVCAR3 cells. Amplification in either of the genes occurred in 27% high-grade serous carcinomas. In conclusion, the methods we employed provide unambiguous evidence that somatic sequence mutations of *PIK3CA* and *ATK2* are rare in ovarian serous tumors but amplification of both genes may play an important role in the development of high-grade ovarian serous carcinoma.

INTRODUCTION

Ovarian cancer is the most lethal gynecologic malignancy and serous tumors are the most common type of ovarian cancer.[1,2] Ovarian serous neoplasms are heterogeneous and can be divided into high- and low-grade tumors that are characterized by distinctive molecular, histopathological and clinical features.[3-6] High-grade tumors are the usual type of ovarian serous carcinoma. They are aggressive and have a high mortality rate. Low-grade tumors are composed mainly of serous borderline tumors (SBTs) and invasive low-grade serous carcinomas. SBTs may progress to invasive low-grade carcinomas which are indolent neoplasms with a better outcome than high-grade serous carcinomas. Mutations of *KRAS* and *BRAF* occur in approximately two thirds of low-grade serous tumors but are rare in high-grade serous carcinomas.[5-8] In contrast, somatic *TP53* mutations are detected in greater than 60% of high-grade serous carcinoma and only rarely (8%) in low-grade serous tumors.[9] Furthermore, both high-grade carcinomas and low-grade tumors are characterized by distinctive gene expression profiles.[10-12] Based on these findings, a dualistic model of ovarian serous carcinogenesis in which high-grade and low-grade ovarian serous tumors develop along distinctly different molecular pathways has been proposed.[3]

Activating mutations and amplification of genes in kinase signaling pathways play a critical role in tumorigenesis. Moreover, the mutated kinase proteins can potentially provide new targets for a kinase inhibitor or antibody-based therapy. In this study, we focused on somatic mutations and gene amplifications of the phosphoinositide 3-kinase (PIK3CA)-AKT2 signaling pathway because *PIK3CA* gene and its downstream gene, *AKT2*, are thought to be important in ovarian cancer development and therefore are potential molecular targets for new therapeutics.[8,13-16] The PI3K-AKT2 signaling pathway regulates diverse cellular functions including cellular proliferation, survival and migration.[17-19] Somatic mutations within the *PIK3CA* kinase domains have been reported in colorectal, brain, ovarian and breast cancers.[20-24] In addition, increased *PIK3CA* and *AKT2* gene copy numbers have been detected in pancreatic, ovarian, cervical, head and neck, and lung

Appendix #8

carcinomas.[13,14,25-27] Although molecular genetic analysis has been performed in ovarian cancer,[23,28,29] none of the reports employed purified tumor samples to determine sequence mutations and fluorescence in situ hybridization (FISH) analysis on surgical specimens to assess gene copy number. Finally, simultaneous analyses of copy number changes in both *PIK3CA* and *AKT2* have not been performed on the same tumor tissues. In order to clarify the mutational profiles of *PIK3CA* and *AKT2* genes in surgical specimens, we obtained genomic DNA from purified high-grade serous carcinomas and SBTs in which the high purity of tumor cells was confirmed by cytokeratin staining and identification of heterozygous somatic mutations in control genes. We also analyzed DNA copy number changes of *PIK3CA* and *AKT2* genes in the same archival tumor specimens using a dual-color FISH which is an accurate method of assessing gene amplification especially for those with a low-level gain.

MATERIALS AND METHODS

Tissue samples and tumor cell isolation. High-grade (conventional) ovarian serous carcinomas and ovarian serous borderline tumors (SBTs) [atypical proliferative serous tumors and intraepithelial (micropapillary) low-grade serous carcinomas] were obtained from the Department of Pathology at the Johns Hopkins Hospital between 2000 and 2005. All high-grade ovarian tumors were advanced stage (FIGO stage III and IV). Acquisition of tissue specimens was approved by the institutional review board at the Johns Hopkins Hospital.

For sequencing analysis, tumor cells from 65 serous tumors (44 high-grade serous carcinomas and 21 serous borderline tumors) were isolated using the following protocol illustrated in Figure 1. Frozen section examination was performed by a surgical pathologist (IS) on all specimens to confirm the diagnosis before tissue harvesting. For high-grade carcinomas, fresh tumor tissues were washed in cold phosphate buffered saline (PBS), minced to ~1 mm^3 fragments and digested with collagenase A (10 mg/ml) with mild agitation at 37°C for 40 min. Single tumor cells or small tumor cell clusters (<10 cells) were collected from the top portion of centrifuge tubes after the large incompletely digested tissue fragments descended to the bottom of the tube. The tumor cells were washed with PBS and then isolated using magnetic beads coated with an Ep-CAM antibody (Dynal, Oslo, Norway). The tumor cells were either directly harvested for genomic DNA isolation or cultured in RPMI1640 containing 10% fetal bovine serum for three days to expand the tumor cell population for those samples with only limited amounts of tumor tissue. For SBTs, the fresh tumor fragments were harvested directly into centrifuge tubes containing 0.05% trypsin and 200 μg/ml EDTA in HBSS (Invitrogen) without mincing and collagenase digestion. This approach allowed epithelial (tumor) cells that covered the surface of papillary structures of borderline tumors to detach from the basement membrane without digesting the underlying stromal cells, thus minimizing possible stromal cell contamination. After incubation at 37°C for 20 min, the SBT fragments were agitated at room temperature for 1 min to allow complete separation of epithelial cells from the tissue fragments. The epithelial cells were washed with culture medium twice and cultured for 3 days. Purity of the tumor cells was confirmed by immunostaining with an anti-cytokeratin antibody, CAM 5.2 (Becton Dickinson, San Jose, CA). The genomic DNA from normal uterus or colonic mucosa from the same patient was also obtained for all cases.

For dual-color FISH analysis, formalin-fixed, paraffin-embedded tissues were used. A total of 124 specimens consisting of 74 high-grade serous carcinomas, 37 SBTs and 13 normal ovaries were arranged onto tissue microarrays for FISH analysis. Three representative cores (1.5 mm diameter) from each tumor block were placed on the tissue microarrays.

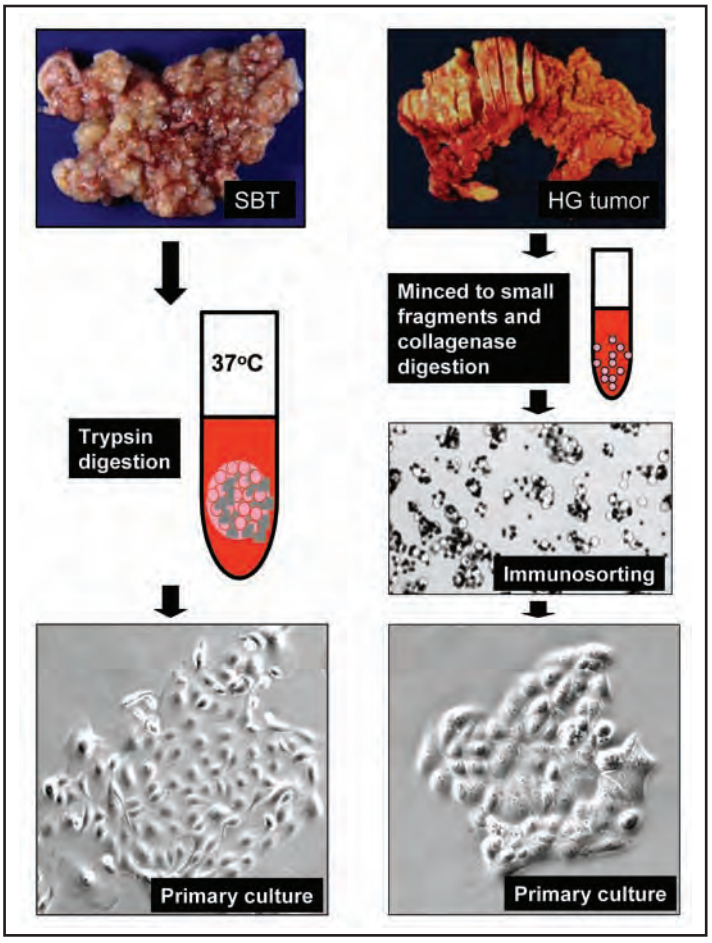

Figure 1. Tumor cell purification from surgical specimens in a serous borderline tumor SBT) and a high-grade (HG) ovarian serous carcinoma.

Mutational analysis. Nucleotide sequencing was used to analyze the mutational status of *PIK3CA* and *AKT2* in tumor cells isolated from the ovarian serous tumors. In addition, *KRAS*, *BRAF*, *ERBB2* and *TP53* genes were also analyzed in the same panel for comparison. In this study, we focused on analyzing the exons that have been reported to harbor the majority of mutations for each of the genes. The primer sequences and the PCR protocol have been previously described.[6,9,20,30-35] Supplement Table 1 listed PCR and sequencing primers of all the exons that were sequenced in this study. PCR products were purified and sequenced at Agencourt Bioscience (Beverly, MA).

Fluorescence in situ hybridization (FISH). For the *PIK3CA* locus, bacterial artificial chromosome clones containing the target (RP11-245C23) and referenced (RP11-69N24) chromosomal regions hybridized to 3q26.32 and 3q13.11, respectively. For the *AKT2* locus, bacterial artificial chromosome clones containing the target (CTC-425O23) and referenced (RP11-75H6 and CTD-3195E18) chromosomal regions hybridized to 19q13.2 and the reference probe to 19p13.13, respectively. The bacterial artificial chromosome clones were purchased from Bacpac Resources (Children's Hospital Oakland, CA) and Invitrogen.

Table 1 **Mutational status of kinase genes in ovarian serous tumors**

Case No.	Tumor	PIK3CA	AKT2	ERBB2	KRAS	BRAF
1	SBT	WT	WT	12 bp ins**	WT	WT
2	SBT	WT	WT	WT	WT	T1976A:V600E
3	SBT	WT	WT	WT	G35T:G12V	WT
4	SBT	WT	WT	WT	G35A:G12D	WT
5	SBT	WT	WT	WT	G35A:G12D	WT
6	SBT	WT	WT	WT	WT	T1976A:V600E
7	SBT	WT	WT	WT	WT	WT
8	SBT	WT	WT	WT	WT	WT
9	SBT	WT	WT	WT	WT	WT
10	SBT	WT	WT	WT	WT	T1976A:V600E
11	SBT	A3140G:H1047R	WT	WT	G35T:G12V	WT
12	SBT	WT	WT	WT	G38T:G13V	WT
13	SBT	WT	WT	WT	WT	WT
14	SBT	WT	WT	WT	G35T:G12V	WT
15	SBT	WT	WT	WT	WT	WT
16	SBT	WT	WT	WT	WT	T1976A:V600E
17	SBT	WT	WT	12 bp ins	WT	WT
18	SBT	WT	WT	WT	WT	T1976A:V600E
19	SBT	WT	WT	WT	WT	WT
20	SBT	WT	WT	WT	WT	WT
21	SBT	WT	WT	WT	G35T:G12V	WT
22–63	HG1-42	WT	WT	WT	WT	WT
64	HG43	WT	WT	WT	WT	T1976A:V600E
65	HG44	A3140G:H1047R	WT	WT	WT	WT

SBT, serous borderline tumor; HG, high-grade serous carcinoma. *12 bp insertion at 2313–2324.

The method for FISH on tissue sections has been detailed in a previous report.[36] Target and reference probes were labeled with biotin and digoxigenin, respectively. To detect biotin-labeled and digoxigenin-labeled signals, slides were first incubated with FITC-avidin (Vector, Burlingame, CA) and anti-digoxigenin sheep Fab fragment (Roche, Indianapolis, IN); then incubated with a biotinylated anti-avidin antibody (Vector, Burlingame, CA) and TRITC-conjugated rabbit anti-sheep $F(ab)_2$ (Jackson ImmunoResearch, West Grove, PA); followed by incubation with FITC-avidin and TRITC-conjugated goat anti-rabbit $F(ab)_2$ (Jackson ImmunoResearch). Two investigators (TLW and IS) who were not aware of the tumor grade and clinical information evaluated the FISH signals. Approximately 100 tumor cells were examined for each specimen. Gain of DNA copy number of a gene was defined as the ratio of the gene probe signal to the control probe signal exceeding 1.5. High-level of amplification was defined as a signal ratio greater than 3.

RESULTS

Our method for tumor cell purification yielded a sample in which tumor cells comprised greater than 99% of the sample for all high-grade carcinomas and SBTs based on immunostaining for cytokeratin. Both high-grade carcinoma and SBT cells formed cohesive epithelial nests in short term primary cultures (Fig. 1). The mutational status of *PIK3CA, AKT2, ERBB2, KRAS* and *BRAF* in all 65 purified ovarian serous tumors is summarized in Table 1. Somatic mutations of *PIK3CA* were identified in one (2.3%) of 44 high-grade serous carcinomas and in one (4.8%) of 21 SBTs. Both mutations were heterozygous and were located at A3140G of a kinase domain (Fig. 2 and Table 1). Neither SBTs nor high-grade serous carcinomas demonstrated a somatic mutation in the *AKT2* kinase domain. Since mutations of both kinase genes in either high-grade carcinomas or SBTs were so infrequent, we used *TP53* gene as a positive control for high-grade serous carcinomas because *TP53* mutation is the most frequent molecular genetic change known so far in high-grade ovarian

Appendix #8

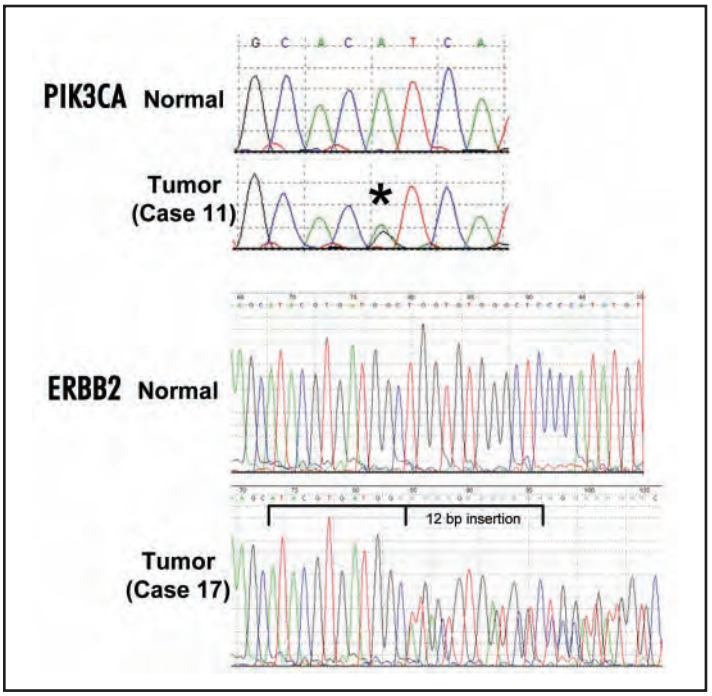

Figure 2. Chromatograms of *PIK3CA* and *ERBB2* mutational status in two representative serous borderline tumors (case number 11 and 17). Case 11 shows a heterozygous somatic mutation at the nucleotide 3140 (A to G). Case 17 demonstrates a heterozygous 12 bp in-frame insertion mutation at the nucleotide of 2313–2324.

serous carcinomas.[3,9,35] Two kinase genes including *KRAS* and *BRAF* were used as controls for SBTs because they are the most common mutations in SBTs.[37] As *ERBB2* may regulate the *KRAS* signaling pathway, we also analyzed the mutational status of this gene in SBTs. Among 44 high-grade carcinomas, 34 (77%) tumors harbored TP53 nonsynonymous mutations or deletions and the majority of the mutations were homozygous changes (data not shown). Somatic mutations of either *ERBB2*, *KRAS* and *BRAF* occurred in 9.5%, 33% and 24% of SBTs, respectively. Most KRAS mutations were located at codon 12 and all *BRAF* mutations at codon 600, the hot spots of mutations for both genes. *ERBB2* mutations occurred as a 12-bp insertion at the nucleotide 2313-2324 (Fig. 2 and Table 1). The mutations of *ERBB2*, *KRAS* and *BRAF* mutations were not shared in any of the SBTs. The high frequency of somatic mutations detected in those control genes with an unambiguous chromatogram tracing indicated that the purified samples used in this study had a high fraction of tumor cells and that the rare mutation of *PIK3CA* and lack of mutation in the *AKT2* genes were not likely to be an artifact due to sample preparation or methods of PCR and nucleotide sequencing.

In addition to somatic sequence mutations, gene amplification provides another mechanism to activate a kinase oncogenic pathway. Accordingly, we performed dual-color FISH to determine the amplification status of *PIK3CA* and *AKT2* in both high-grade serous carcinomas and SBTs. Dual-color FISH was used because this method provides high sensitivity and specificity in counting gene copy number. *PIK3CA* and *AKT2* gene copy numbers were assessed in the same tumor tissues to determine if there was a correlation of DNA copy number gain between both genes. FISH was first performed in the OVCAR3 ovarian cancer cell line and 6 representative high-grade serous carcinoma tissues in which the DNA copy

Table 2 **DNA copy number changes of the *PIK3CA* locus in ovarian tumors based on FISH analysis**

PIK3CA Locus	OSE	SBT	HG
No gain or amplified	13	37	52
Low gain (1.5–3 fold)	0	0	7
High gain (> 3 fold)	0	0	1
polyploidy	0	0	14
Total	13	37	74

OSE, ovarian surface epithelium from normal ovaries; SBT, serous borderline tumor; HG, high-grade serous carcinoma.

number changes in *PIK3CA* and *AKT2* had been detected by digital karyotyping.[38] The latter is a genome-wide technology to assess gene copy number by counting sequencing tags that represent different genomic loci.[39] Digital karyotyping analysis showed that all samples lacked a discrete gain or amplification (< 5 Mb) in the 3q *PIK3CA* locus including the OVCAR3 cells which demonstrated a two-fold gain along the whole 3q arm (Fig. 3 and supplementary Fig. 1). Dual-color FISH was performed on the metaphase OVCAR3 cells and demonstrated a low level gain (~2 fold) at the *PIK3CA* locus in OVCAR3 cells (Fig. 3) which was consistent with a previous report.[25] We correlated the PIK3CA gene copy number and mRNA expression levels and found only a marginal correlation ($p = 0.04$). Among those cases with gain of the PIK3CA region, four specimens showed downregulation of PIK3CA mRNA as compared to ovarian surface epithelial cultures. In contrast to this low level gain of *PI3KCA*, digital karyotyping showed a discrete 10 fold amplification spanning ~3 Mb of the *AKT2* locus in the OVCAR3 cells (Fig. 2) and a 5 fold amplification in the other carcinoma tissues (Park et al, unpublished data). FISH analysis of this region showed a homogenously staining region (HSR) in tumor cells in both cases (Fig. 3). In the remainder of the cases, both target and reference probes showed equal signals in both *PIK3CA* and *AKT2* loci. The analysis correlating digital karyotyping and FISH results validated the FISH method to determine DNA copy number of *PIK3CA* and *AKT2* in archival paraffin tissues.

Using the same probes, we performed dual-color FISH on a panel of paraffin tissues from different types of ovarian serous tumors and normal ovaries that were arranged in tissue microarrays. Based on the FISH analysis, we did not identify gain of *PIK3CA* gene copy number in 37 SBTs and 13 cases of surface epithelium from normal ovaries (Table 2). In contrast, *PIK3CA* amplification was detected in 8 of the 60 (13.3%) high-grade serous carcinomas in addition to 14 other cases with a polyploid pattern (same increased number of signals between *PIK3CA* and control probes) as these tumors were not considered to have amplification specific to *PIK3CA*. Among the amplified cases, only one showed a high level of amplification manifested as HSR and the other six cases were of low level gains (1.5-3 fold). FISH analysis also demonstrated that *AKT2* did not amplify in any of the normal ovarian surface epithelial samples and SBTs (Table 3). In contrast, *AKT2* amplification was observed in 12 of 66 (18.2%) high-grade serous carcinomas, the majority of which demonstrated high-level amplification as manifested by HSR. In addition, there were 8 cases showing a polyploid pattern (Table 3). Performing FISH analysis on the same tissues allowed us to assess the relationship of *PIK3CA* and *AKT2* amplification in high-grade ovarian serous carcinomas. Four high-grade serous carcinomas and the OVCAR3 cell line showed coamplification of *PIK3CA* and *AKT2*.

Appendix #8

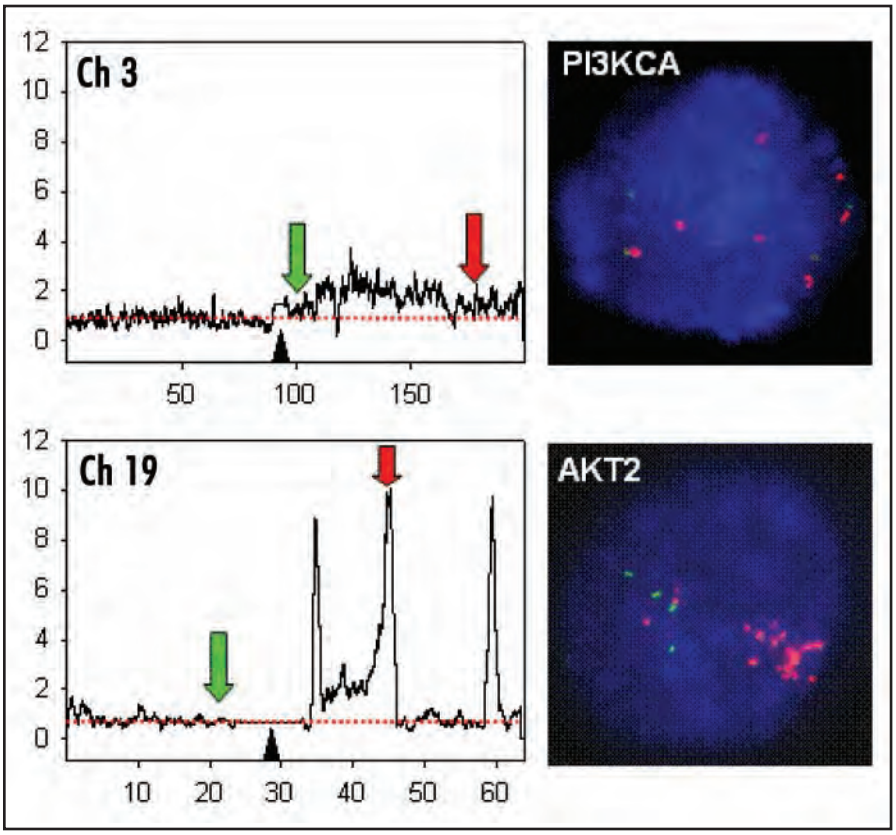

Figure 3. Digital karyotyping and dual-color FISH analysis of the *PIK3CA* and *AKT2* copy number in OVCAR3 cells. Digital karyotyping of OVCAR3 cell line shows a two-fold increase in the entire 3q arm that harbors *PIK3CA*. FISH probes are designed to hybridize to the *PIK3CA* locus (red arrow) and a reference chromosomal region (green arrow). The centromeres are indicated by triangles. FISH analysis demonstrated an increase in the signals of *PIK3CA* with a ratio of *PIK3CA*/reference probe signal counts of 2. In contrast, the *AKT2* region which is located on chromosome 19q is highly amplified in OVCAR3 cells and FISH shows a homogenously stained region pattern in tumor cells.

Amplification in either *PIK3CA* and/or *AKT2* occurred in 16 of 59 (27%) nonpolyploid cases.

DISCUSSION

In this study, we performed a comprehensive mutational analysis of exons 1, 9 and 20 of *PIK3CA* and the kinase domain of *AKT2* in purified ovarian serous neoplasms including high-grade (conventional) serous carcinomas and serous borderline tumors (SBTs). In contrast to previous studies which analyzed nonpurified tumors,[23,28,29] only purified tumor samples from surgical specimens were analyzed for sequence mutations in this study. Purified tumor cells are far superior for mutational analysis as DNA contamination from normal cells and the PCR/sequencing artifacts from formalin-fixed paraffin- embedded tissue are minimized. In addition, dual-color FISH provides a clear assessment of DNA copy number gains of *PIK3CA* and *AKT2* in the same tumor tissues thereby allowing a determination of the relationship of amplification between both genes. Our findings demonstrate that compared to high-grade serous carcinomas, SBTs are characterized by mutations in the ERBB2-KRAS-BRAF signaling pathway while high-grade ovarian serous carcinomas have an increased gene copy number of the PIK3CA-AKT2 signaling pathway. These results shed new light on the pathogenesis of serous carcinoma of the ovary and may have important therapeutic implications.

The low frequency (3%) of mutations of *PIK3CA* in both purified high-grade serous carcinomas and SBTs confirms what has been reported previously.[23,28] These data and the lack of somatic mutations in the *AKT2* kinase domain in all the samples tested indicates that activating sequence mutations of the PIK3CA-AKT2 pathway most likely do not play a significant role in the development of ovarian serous tumors. We also analyzed the copy number changes of *PIK3CA* and *AKT2* in ovarian serous tumors using dual-color FISH, a method thought to provide a more sensitive and specific assessment of gene copy number in tissues. We found a low level gain (1.5-3 fold increase) in *PIK3CA* in the majority of *PIK3CA* amplified specimens. This is consistent with a previous report using FISH that showed a low copy number gain (1.5–2.5 fold) of *PIK3CA* in the majority of ovarian cancer cell lines.[25] These results differ from another study reporting high level amplification (>7 fold) in 24.5% of ovarian cancers based on genomic real-time PCR.[23] The discrepancy is probably due to the different methods used to measure the *PIK3CA* copy number. It is generally acknowledged that FISH analysis which is based on directly counting probe signals provides the most sensitive and specific method of assessing gene copy number, especially for samples with low copy number gains.[40-42] In contrast, analysis of DNA copy number using genomic real-time PCR can be complicated by the primer selection, the presence of genomic repeats/pseudogenes that can lead to spurious results because of inappropriate primer set, as well as background noise inherent in real-time PCR. The frequency of high copy number gain in the *PIK3CA* gene is much lower than in the *AKT2* gene which is known to be a frequently amplified oncogene in ovarian cancer.[13] The molecular genetic findings in this report imply that amplification of the genes in the PIK3CA-AKT2 pathway may play an important role in the development of ovarian high-grade serous carcinoma. However, it is also likely that *PIK3CA* contributes to tumor development through another downstream mediator, other than *AKT2*, because amplification of *AKT2* and gain of *PIK3CA* were found in a small set of 4 high-grade carcinomas and in the OVCAR3 cell line. The low level gains of *PIK3CA* may not have significant biological significance as the increased DNA copy number of *PIK3CA* only marginally correlates with its RNA copy number. In this study, we have shown overexpression of *PIK3CA* in some of ovarian high-grade serous carcinomas, a finding similar to a previous report demonstrating that *PIK3CA* protein (p110α) overexpression could be detected in of ovarian carcinomas.[43]

The identification of a 12 bp in-frame insertion mutation of *ERBB2* in this study is of interest since sequence mutations have not been reported in ovarian neoplasms although amplification of *ERBB2* has been extensively studied in ovarian carcinomas. The frequency and type of *ERBB2* insertion mutation in SBTs are similar to those reported in lung adenocarcinomas[31] but are different from gastric, colorectal and breast carcinomas.[44] Although the number of tumors with *ERBB2* mutations in this study was small, the mutually

Table 3 **DNA copy number changes of the AKT2 locus in ovarian tumors based on FISH analysis**

AKT2 locus status	OSE	SBT	HG
No gain or amplified	13	34	54
Low gain (1.5-3 fold)	0	0	4
High gain (> 3 fold)	0	0	8*
Polyploidy	0	3	8
Total	13	37	74

OSE, ovarian surface epithelium from normal ovaries; SBT, serous borderline tumor; HG, high-grade serous carcinoma. *Cases show high-level amplification as manifested by homogenous staining region.

exclusive pattern among *ERBB2*, *KRAS* and *BRAF* mutations suggests that each of the kinase genes has a similar effect in the development of SBTs.

In conclusion, our findings indicate that amplification of genes in the PIK3CA-AKT2 pathway occurs in high-grade ovarian serous carcinomas and somatic mutations in the ERBB2-KRAS-BRAF pathway occur in SBTs. These findings provide further support for the dualistic model of ovarian serous tumorigenesis which proposes that low-grade serous carcinomas arise from a well characterized precursor, namely SBTs, whereas high grade serous carcinoma arises along an entirely different pathway in which morphologically characterized precursor lesions have not yet been identified.[3,37] As small molecule kinase inhibitors show promise for the treatment of tumors with specific kinase activation,[15,45,46] the findings in this study have potential clinical application for target-based therapy in patients with different types of ovarian serous neoplasms.

References

1. Banks E, Beral V, Reeves G. The epidemiology of epithelial ovarian cancer: A review. Int J Gynecol Cancer 1997; 7:425-38.
2. Parkin DM, Muir CS, Whelan SF. Cancer incidence in five continents. Lyon, France: IARC Scientif., 1992.
3. Shih IM, Kurman RJ. Ovarian tumorigenesis—A proposed model based on morphological and molecular genetic analysis. Am J Pathol 2004; 164:1511-8.
4. Malpica A, Deavers MT, Lu K, Bodurka DC, Atkinson EN, Gershenson DM, Silva EG. Grading ovarian serous carcinoma using a two-tier system. Am J Surg Pathol 2004; 28:496-504.
5. Singer G, Kurman RJ, Chang HW, Cho SKR, Shih IM. Diverse tumorigenic pathways in ovarian serous carcinoma. Am J Pathol 2002; 160:1223-8.
6. Singer G, Oldt IIIrd R, Cohen Y, Wang BG, Sidransky D, Kurman RJ, Shih Ie M. Mutations in *BRAF* and *KRAS* characterize the development of low-grade ovarian serous carcinoma. J Natl Cancer Inst 2003; 95:484-6.
7. Sieben NL, Macropoulos P, Roemen GM, Kolkman-Uljee SM, Jan Fleuren G, Houmadi R, Diss T, Warren B, Al Adnani M, De Goeij AP, Krausz T, Flanagan AM. In ovarian neoplasms, *BRAF*, but not *KRAS*, mutations are restricted to low-grade serous tumours. J Pathol 2004; 202:336-40.
8. Hu L, Hofmann J, Jaffe RB. Phosphatidylinostol 3-kinase mediates angiogenesis and vascular permeability associated with ovarian carcinoma. Clin Cancer Res 2005; 11:8208-12.
9. Singer G, Stohr R, Cope L, Dehari R, Hartmann A, Cao DF, Wang TL, Kurman RJ, Shih IM. Patterns of *p53* mutations separate ovarian serous borderline tumors and low- and high-grade carcinomas and provide support for a new model of ovarian carcinogenesis: A mutational analysis with immunohistochemical correlation. Am J Surg Pathol 2005; 29:218-24.
10. Gilks CB, Vanderhyden BC, Zhu S, van de Rijn M, Longacre TA. Distinction between serous tumors of low malignant potential and serous carcinomas based on global *mRNA* expression profiling. Gynecol Oncol 2005; 96:684-94.
11. Meinhold-Heerlein I, Bauerschlag D, Hilpert F, Dimitrov P, Sapinoso LM, Orlowska-Volk M, Bauknecht T, Park TW, Jonat W, Jacobsen A, Sehouli J, Luttges J, Krajewski M, Krajewski S, Reed JC, Arnold N, Hampton GM. Molecular and prognostic distinction between serous ovarian carcinomas of varying grade and malignant potential. Oncogene 2005; 24:1053-65.
12. Bonome T, Lee JY, Park DC, Radonovich M, Pise-Masison C, Brady J, Gardner GJ, Hao K, Wong WH, Barrett JC, Lu KH, Sood AK, Gershenson DM, Mok SC, Birrer MJ. Expression profiling of serous low malignant potential, low-grade, and high-grade tumors of the ovary. Cancer Res 2005; 65:10602-12.
13. Cheng JQ, Godwin AK, Bellacosa A, Taguchi T, Franke TF, Hamilton TC, Tsichlis PN, Testa JR. AKT2, a putative oncogene encoding a member of a subfamily of protein-serine/threonine kinases, is amplified in human ovarian carcinomas. Proc Natl Acad Sci USA 1992; 89:9267-71.
14. Cheng JQ, Ruggeri B, Klein WM, Sonoda G, Altomare DA, Watson DK, Testa JR. Amplification of AKT2 in human pancreatic cells and inhibition of AKT2 expression and tumorigenicity by antisense RNA. Proc Natl Acad Sci USA 1996; 93:3636-41.
15. Tang HJ, Jin X, Wang S, Yang D, Cao Y, Chen J, Gossett DR, Lin J. A small molecule compound inhibits AKT pathway in ovarian cancer cell lines. Gynecol Oncol 2005.
16. Dan HC, Jiang K, Coppola D, Hamilton A, Nicosia SV, Sebti SM, Cheng JQ. Phosphatidylinositol-3-OH kinase/AKT and survivin pathways as critical targets for geranylgeranyltransferase I inhibitor-induced apoptosis. Oncogene 2004; 23:706-15.
17. Vogelstein B, Kinzler KW. Cancer genes and the pathways they control. Nat Med 2004; 10:789-99.
18. Dancey JE. Molecular targeting: PI3 kinase pathway. Ann Oncol 2004; 15:iv233-9.
19. Stokoe D. The phosphoinositide 3-kinase pathway and cancer. Expert Rev Mol Med 2005; 7:1-22.
20. Samuels Y, Velculescu VE. Oncogenic mutations of *PIK3CA* in human cancers. Cell Cycle 2004; 3:1221-4.
21. Samuels Y, Wang Z, Bardelli A, Silliman N, Ptak J, Szabo S, Yan H, Gazdar A, Powell SM, Riggins GJ, Willson JK, Markowitz S, Kinzler KW, Vogelstein B, Velculescu VE. High frequency of mutations of the *PIK3CA* gene in human cancers. Science 2004; 304:554.
22. Broderick DK, Di C, Parrett TJ, Samuels YR, Cummins JM, McLendon RE, Fults DW, Velculescu VE, Bigner DD, Yan H. Mutations of *PIK3CA* in anaplastic oligodendrogliomas, high-grade astrocytomas, and medulloblastomas. Cancer Res 2004; 64:5048-50.
23. Campbell IG, Russell SE, Choong DY, Montgomery KG, Ciavarella ML, Hooi CS, Cristiano BE, Pearson RB, Phillips WA. Mutation of the *PIK3CA* gene in ovarian and breast cancer. Cancer Res 2004; 64:7678-81.
24. Bachman KE, Argani P, Samuels Y, Silliman N, Ptak J, Szabo S, Konishi H, Karakas B, Blair BG, Lin C, Peters BA, Velculescu VE, Park BH. The *PIK3CA* gene is mutated with high frequency in human breast cancers. Cancer Biol Ther 2004; 3:772-5.
25. Shayesteh L, Lu Y, Kuo WL, Baldocchi R, Godfrey T, Collins C, Pinkel D, Powell B, Mills GB, Gray JW. PIK3CA is implicated as an oncogene in ovarian cancer. Nat Genet 1999; 21:99-102.
26. Ma YY, Wei SJ, Lin YC, Lung JC, Chang TC, Whang-Peng J, Liu JM, Yang DM, Yang WK, Shen CY. PIK3CA as an oncogene in cervical cancer. Oncogene 2000; 19:2739-44.
27. Redon R, Muller D, Caulee K, Wanherdrick K, Abecassis J, du Manoir S. A simple specific pattern of chromosomal aberrations at early stages of head and neck squamous cell carcinomas: *PIK3CA* but not *p63* gene as a likely target of 3q26-qter gains. Cancer Res 2001; 61:4122-9.
28. Wang Y, Helland A, Holm R, Kristensen GB, Borresen-Dale AL. *PIK3CA* mutations in advanced ovarian carcinomas. Hum Mutat 2005; 25:322.
29. Levine DA, Bogomolniy F, Yee CJ, Lash A, Barakat RR, Borgen PI, Boyd J. Frequent mutation of the *PIK3CA* gene in ovarian and breast cancers. Clin Cancer Res 2005; 11:2875-8.
30. Ho CL, Kurman RJ, Dehari R, Wang TL, Shih IM. Mutations of *BRAF* and *KRAS* precede the development of ovarian serous borderline tumors. Cancer Res 2004; 64:6915-8.
31. Shigematsu H, Takahashi T, Nomura M, Majmudar K, Suzuki M, Lee H, Wistuba II, Fong KM, Toyooka S, Shimizu N, Fujisawa T, Minna JD, Gazdar AF. Somatic mutations of the *HER2* kinase domain in lung adenocarcinomas. Cancer Res 2005; 65:1642-6.
32. Davies H, Bignell GR, Cox C, Stephens P, Edkins S, Clegg S, Teague J, Woffendin H, Garnett MJ, Bottomley W, Davis N, Dicks E, Ewing R, Floyd Y, Gray K, Hall S, Hawes R, Hughes J, Kosmidou V, Menzies A, Mould C, Parker A, Stevens C, Watt S, Hooper S, Wilson R, Jayatilake H, Gusterson BA, Cooper C, Shipley J, Hargrave D, Pritchard-Jones K, Maitland N, Chenevix-Trench G, Riggins GJ, Bigner DD, Palmieri G, Cossu A, Flanagan A, Nicholson A, Ho JW, Leung SY, Yuen ST, Weber BL, Seigler HF, Darrow TL, Paterson H, Marais R, Marshall CJ, Wooster R, Stratton MR, Futreal PA. Mutations of the *BRAF* gene in human cancer. Nature 2002; 417:949-54.
33. Cohen Y, Xing M, Mambo E, Guo Z, Wu G, Trink B, Beller U, Westra WH, Ladenson PW, Sidransky D. *BRAF* mutation in papillary thyroid carcinoma. J Natl Cancer Inst 2003; 95:625-7.
34. Downward J. Targeting RAS signalling pathways in cancer therapy. Nat Rev Cancer 2003; 3:11-22.
35. Leitao MM, Soslow RA, Baergen RN, Olvera N, Arroyo C, Boyd J. Mutation and expression of the *TP53* gene in early stage epithelial ovarian carcinoma. Gynecol Oncol 2004; 93:301-6.
36. Wang TL, Diaz Jr LA, Romans K, Bardelli A, Saha S, Galizia G, Choti M, Donehower R, Parmigiani G, Shih Ie M, Iacobuzio-Donahue C, Kinzler KW, Vogelstein B, Lengauer C, Velculescu VE. Digital karyotyping identifies thymidylate synthase amplification as a mechanism of resistance to 5-fluorouracil in metastatic colorectal cancer patients. Proc Natl Acad Sci USA 2004; 101:3089-94.
37. Shih Ie M, Kurman RJ. Molecular pathogenesis of ovarian borderline tumors: New insights and old challenges. Clin Cancer Res 2005; 11:7273-9.
38. Shih IM, Sheu JJ, Santillan A, Nakayama K, Yen MJ, Bristow RE, Vang R, Parmigiani G, Kurman RJ, Trope CG, Davidson B, Wang TL. Amplification of a chromatin remodeling gene, *Rsf-1/HBXAP*, in ovarian carcinoma. Proc Natl Acad Sci USA 2005; 102:14004-9.
39. Wang TL, Maierhofer C, Speicher MR, Lengauer C, Vogelstein B, Kinzler KW, Velculescu VE. Digital karyotyping. Proc Natl Acad Sci USA 2002; 99:16156-61.

Appendix #8

40. Cox MC, Maffei L, Buffolino S, Del Poeta G, Venditti A, Cantonetti M, Aronica G, Aquilina P, Masi M, Amadori S. A comparative analysis of FISH, RT-PCR, and cytogenetics for the diagnosis of bcr-abl-positive leukemias. Am J Clin Pathol 1998; 109:24-31.
41. Pauletti G, Godolphin W, Press MF, Slamon DJ. Detection and quantitation of *HER-2/neu* gene amplification in human breast cancer archival material using fluorescence in situ hybridization. Oncogene 1996; 13:63-72.
42. Swiger RR, Tucker JD. Fluorescence in situ hybridization: A brief review. Environ Mol Mutagen 1996; 27:245-54.
43. Wang Y, Kristensen GB, Helland A, Nesland JM, Borresen-Dale AL, Holm R. Protein expression and prognostic value of genes in the *erb-b* signaling pathway in advanced ovarian carcinomas. Am J Clin Pathol 2005; 124:392-401.
44. Lee JW, Soung YH, Seo SH, Kim SY, Park CH, Wang YP, Park K, Nam SW, Park WS, Kim SH, Lee JY, Yoo NJ, Lee SH. Somatic mutations of *ERBB2* kinase domain in gastric, colorectal, and breast carcinomas. Clin Cancer Res 2006; 12:57-61.
45. Solit DB, Garraway LA, Pratilas CA, Sawai A, Getz G, Basso A, Ye Q, Lobo JM, She Y, Osman I, Golub TR, Sebolt-Leopold J, Sellers WR, Rosen N. *BRAF* mutation predicts sensitivity to MEK inhibition. Nature 2005.
46. Pohl G, Ho CL, Kurman RJ, Bristow R, Wang TL, Shih Ie M. Inactivation of the mitogen-activated protein kinase pathway as a potential target-based therapy in ovarian serous tumors with *KRAS* or *BRAF* mutations. Cancer Res 2005; 65:1994-2000.

Measurement of Cyclin E Genomic Copy Number and Strand Length in Cell-Free DNA Distinguish Malignant versus Benign Effusions

Ritu Salani,[1] Ben Davidson,[3] Michael Fiegl,[4] Christian Marth,[5] Elisabeth Müller-Holzner,[5] Guenther Gastl,[4] Han-Yao Huang,[2] Jui-Chi Hsiao,[6] Her-Sheng Lin,[6] Tian-Li Wang,[1] Bai-Ling Lin,[6] and Ie-Ming Shih[1]

Abstract

Purpose: Previous studies have shown that the concentration of cell-free DNA was higher and its strand length longer in body fluids obtained from patients with cancer as compared to patients with benign diseases. We hypothesized that analysis of both DNA copy number and strand length of cell-free DNA from an amplified chromosomal region could improve the diagnosis of malignant diseases in body fluids.

Experimental Design: To test this hypothesis, we used ovarian cancer effusion as an example and applied a quantitative real-time PCR to measure the relative copy number and strand length of DNA fragments from one of the most frequently amplified genes, cyclin E, in ovarian serous carcinomas.

Results: As compared with nonamplified chromosomal loci, including β-actin, p53, 2p24.1, and 4p15.31, measurement of cyclin E DNA copy number (100 bp) had the best performance in distinguishing malignant (n = 88) from benign (n = 70) effusions after normalization to effusion volume or Line-1 DNA with areas under the receiver operating characteristics curve (AUC) of 0.832 and 0.847, respectively. Different DNA lengths of the cyclin E locus were further analyzed and we found that the AUC was highest by measuring the 400-bp cyclin E locus (AUC = 0.896). The AUC was improved to 0.936 when it was combined with the length integrity index as defined by the relative abundance of 400 bp cyclin E to 100 bp p53 loci. Cyclin E real-time PCR assay had a higher sensitivity (95.6%) than routine cytology examination (73.9%) and was able to diagnose false-negative cytology cases in this study.

Conclusions: The above findings indicate that measurement of the DNA copy number and strand length of the cyclin E locus is a useful cancer diagnostic tool.

The development of tumor biomarkers that can be clinically applicable in body fluids for cancer diagnosis is useful for clinical management in patients with cancer (1). It is well recognized that several solid malignant tumors release a significant amount of genomic DNA into body fluids including blood, urine, saliva, and effusion from cellular necrosis and apoptosis (2–5). Tumor-released DNA can be detected as a result of specific genetic and epigenetic alterations including point mutations, microsatellite alterations, allelic imbalance, translocation, promoter methylation, and the presence of viral sequences (6–9). In addition to those specific molecular genetic alterations, elevated DNA concentration and increased DNA strand integrity in cell-free DNA have been reported in plasma samples from patients with cancer. As compared with nonneoplastic controls, cell-free DNA concentration was higher in ovarian (7, 8), breast (10), prostate (11), esophageal, and lung (12) carcinomas, as well as in melanoma (13, 14). Furthermore, increased DNA strand length (integrity) of cell-free DNA was found in plasma samples from patients with ovarian cancer (15) and in the stool of patients with colorectal tumors (16).

Increased DNA copy number or genomic amplification at certain loci are frequently present in a variety of human cancers (17). As genomic amplification occurs only in cancer but not in normal tissues, measurement of a certain amplified chromosomal region may likely increase both the sensitivity and specificity of the DNA copy number and DNA strand integrity assays. In this study, we hypothesize that measurements of both DNA copy number and strand integrity of an amplified chromosomal locus in cancer could provide a highly sensitive and specific approach to diagnose malignant versus benign clinical samples in body fluids. To test this hypothesis, we used ovarian carcinoma effusion as an example because ovarian carcinoma is one of the most common causes of malignant effusion in women. Furthermore, the differential diagnosis of malignant from benign effusions would have a significant effect

Authors' Affiliations: Departments of [1]Pathology, Gynecology, and Oncology, and [2]Epidemiology, Johns Hopkins Medical Institutions, Baltimore, Maryland; [3]Department of Pathology, Rikshospitalet-Radiumhospitalet Medical Center, Oslo, Norway; Departments of [4]Internal Medicine, Hemato-Oncology, [5]Obstetrics and Gynecology, Innsbruck Medical University, Innsbruck, Austria; and [6]Development Center for Biotechnology, Taipei, Taiwan

Received 4/11/07; revised 7/6/07; accepted 7/17/07.

Grant support: U.S. Department of Defense grant (OC04-0060), Ovarian Cancer Research Fund, Inc. (POE01.06), and National Cancer Institute grant (CA103937). Work at the Development Center for Biotechnology was supported by Technology Development Program Funds from the Ministry of Economic Affairs, Taiwan.

The costs of publication of this article were defrayed in part by the payment of page charges. This article must therefore be hereby marked *advertisement* in accordance with 18 U.S.C. Section 1734 solely to indicate this fact.

Requests for reprints: Ie-Ming Shih, Johns Hopkins Medical Institutions, 1550 Orleans Street, Room 305, Baltimore, MD 21231. Phone: 410-502-7774; E-mail: ishih@jhmi.edu.

doi:10.1158/1078-0432.CCR-07-0853

Table 1. Clinical diagnosis of benign effusions

Diagnosis	No. of patients
Cardiomyopathy	26
Liver cirrhosis	21
Pneumonia/tuberculosis	15
Others	
Renal failure	3
Pulmonary embolus	2
Meigs syndrome	1
Congenital chylothorax	1
Arthritis	1
Total	70

on the clinical management of patients (18). Based on our single nucleotide polymorphism array analysis (19), we identified cyclin E as the most frequently amplified chromosomal region in ovarian carcinomas which occur in nearly 40% of high-grade ovarian serous carcinomas. Thus, we measured the DNA copy number and strand length of the cyclin E locus and several other control regions that are rarely amplified in ovarian cancer. Our results showed that such an approach showed promise toward diagnosing ovarian cancer effusions.

Materials and Methods

Samples and genomic DNA isolation. The effusion samples were collected at the Innsbruck University Hospital in Austria and the Rikshospitalet-Radiumhospitalet Medical Center in Oslo, Norway. All specimens used were approved by the local institutional review boards or ethics committee and included a total of 268 anonymous effusions (140 ascites samples and 128 pleural effusions). The samples included 88 ovarian carcinoma effusions, 70 benign effusions (Table 1), and 110 effusions from other cancer types (34 lung carcinomas, 21 breast carcinomas, 10 endometrial carcinomas, 8 gastrointestinal carcinomas, 7 pancreatic carcinomas, 6 hepatocellular carcinomas, and 24 other miscellaneous cases). The diagnoses of effusions were based on clinical diagnosis and final pathology reports. There was no statistical significance in ages among the cancer and benign groups ($P > 0.5$, two-way ANOVA analysis). Effusion samples (3 mL-2 L) were collected from patients and samples were centrifuged for 5 min and the supernatants were aliquoted and frozen immediately. Before genomic DNA extraction, the effusion supernatant was centrifuged again and 200 μL of the supernatant, containing the cell-free DNA, was collected from tubes. The genomic DNA was extracted using a Qiagen DNA Blood Kit (Qiagen) according to the manufacturer's instructions. All samples were analyzed in a blinded fashion without prior knowledge of the specimen's identity.

Primer selection and real-time PCR. The primers that amplified each genomic locus were designed based on the Santa Cruz web site.[7] The sequences of all PCR primers used in this study are listed in Table 2. The genomic loci were selected based on the frequency of amplification in ovarian serous carcinomas (19). Among them, cyclin E locus was the most frequently amplified whereas the TP53 locus was commonly deleted (20, 21). Semiquantitative real-time PCR was done using locus-specific primers to obtain the cycle threshold and to calculate the DNA length integrity, which was defined as the ratio of the longer (400 bp) PCR products and the 100 bp PCR products. All samples were done in duplicate. For semiquantitative real-time PCR, an aliquot of 1 μL of the purified cell-free DNA was used in an 11.5 μL PCR mixture containing PCR buffer, 10 μmol/L of deoxynucleotide triphosphate, and 0.125 units/μL of Platinum Taq (Invitrogen). The PCR protocol for iCycler was denaturation for 1 min at 94°C followed by 40 cycles of denaturation at 94°C for 30 s, annealing at 57°C for 30 s, and extension at 70°C for 5 min. The Bio-Rad iCycler software monitored the changes in fluorescence of SYBR Green I dye (Molecular Probe) in each cycle. The cycle threshold (Ct) value for each reaction was calculated by the iCycler software package. Alternatively, the real-time PCR was done in ABI PRISM 7000 with Power SYBR Green PCR Master Mix (2×, Applied Biosystems) and the default program: 50°C for 2 min, 95°C for 10 min, and 40 cycles of the two-step reaction; 95°C for 15 s and 60°C for 1 min. Cyclin E DNA integrity index was modified from a previous report (15) and was defined as Ct of cyclin E (400 bp) - Ct of p53 (100 bp).

Statistical analysis. The results of the real-time PCR were analyzed using receiver operating characteristics (ROC) curves. ROC curves were constructed for cycle threshold of a given genomic locus and DNA integrity index as a diagnostic marker by plotting sensitivity versus 1- specificity, followed by the calculation of the area under the curve (AUC), which was done by a statistics program, MedCalc version 8.1.1.0.[8] Reproducibility of the real-time PCR assay was done by evaluating the coefficient of variation (CV) for each primer and disease subgroup. Linear regression was used to correlate the cyclin E copy number between ascites cell–free DNA and matched tumor cell pellets in 10 representative ovarian cancer effusions. The DNA copy number of a specific locus was normalized to the effusion volume or the level of the Line-1 DNA element because Line-1 represented the abundant repetitive sequences dispersed in the human genome and was thought to be a reliable reference marker to quantify specific genomic DNA fragments. Fisher exact test was used to determine the significance of the differences between cases and controls. CV was used to determine assay reproducibility between two institutions.

Results

We first tested whether the DNA copy number was different between cancer cases and nonneoplastic controls using primers that amplified 100 bp of cyclin E, β-actin, p53, 2p24.1, 4p15.31, and Line-1 (as the normalization control). We found that the copy numbers of all the genomic loci were higher in ovarian cancer effusions ($n = 88$) than in benign samples ($n = 70$) after normalization to effusion volume or Line-1 DNA ($P < 0.0001$; Table 3). ROC curves were used to compare the performance of the DNA copy number between cyclin E and nonamplified chromosomal loci in distinguishing ovarian cancer effusions from benign samples. As shown in Table 3, cyclin E primers demonstrated the highest performance in distinguishing ovarian cancer versus benign effusion samples with an AUC of 0.832 [95% confidence interval (95% CI), 0.762-0.889] when normalized to plasma volume and 0.847 (95% CI, 0.738-0.923) when normalized to Line-1 DNA.

We then assessed if a DNA length (integrity) index could improve the performance of cyclin E DNA copy number in the differential diagnosis of malignant effusions. We tested the performance of different lengths of cyclin E DNA fragments using different reverse primers that were located 100, 400, 600, and 800 bp downstream from the anchored forward primer. The AUC of the abundance PCR product in distinguishing ovarian cancer versus benign effusions was the highest using the 400 bp (AUC = 0.896) as compared with the 100 bp (AUC = 0.832), 600 bp (AUC = 0.813), and 800 bp (AUC = 0.825; Table 4). Thus,

[7] http://genome.ucsc.edu/

[8] http://www.medcalc.be/

Table 2. Primer nucleotide sequences used in the study

Gene	Product size (bp)	Forward primer	Reverse primer
β-Actin	100	5′-GCACCACACCTTCTACAATGA-3′	5′-GTCATCTTCTCGCGGTTGGC-3′
β-Actin	400	5′-GCACCACACCTTCTACAATGA-3′	5′-TGTCACGCACGATTTCCC-3′
Cyclin E	100	5′-TCATTTACAGCCTTGGGACAA-3′	5′-CTTGCACGTTGAGTTTGGGTA-3′
Cyclin E	400	5′-TCATTTACAGCCTTGGGACAA-3′	5′-AGCGAACAGGAAGACTCAAGC-3′
Cyclin E-DCB	400	5′-GTCCAAAGGCCTGCTCTCAG-3′	5′-AAAGTGGAAACTCGGGCTGTAAG′-3
Cyclin E	600	5′-TCATTTACAGCCTTGGGACAA-3′	5′-GCCAATTTTAAAACATCTGAAGGA-3′
Cyclin E	800	5′-TCATTTACAGCCTTGGGACAA-3′	5′-GGCCAGGAAAGTCACTTGAAC-3′
Line-1	100	5′-AAAGCCGCTCAACTACATGG-3′	5′-TGCTTTGAATGCGTCCCAGAG-3′
p53	100	5′-TCAGATAGCGATGGTGAGCAG-3′	5′-GGCCAGACCTAAGAGCAATCA-3′
p53-DCB	100	5′-TGCAATAGGTGTGCGTCAGAA-3′	5′-AAACCTTAAAATCTAAGCTGGTATGTCCTACT-3′
2p24.1	100	5′-TTCACTCAGGAAACCACATGC-3′	5′-ATTGAACACGGCTCTCCTCTC-3′
4p15.31	100	5′-GGGATCTGACAAACAATCGAA-3′	5′-TGGCTTCTATAACCCCTACAGTTG-3′

we defined the cyclin E DNA strand length (integrity) index as the difference of Ct of cyclin E (400 bp) and Ct of p53 (100 bp). The cyclin E integrity index was significantly higher in malignant effusions than in benign effusions ($P = 0.0014$). As compared with the DNA length integrity index using β-actin (400 bp) - β-actin (100 bp) as we previously described (15), we found that the AUC of cyclin E DNA integrity index defined in this study (cyclin E 400 bp - p53 100 bp) was higher (0.921) than the β-actin DNA integrity index (0.851). Furthermore, combining the cyclin E copy number and length index, we found that the AUC for the cyclin E integrity index increased to 0.936 (95% CI, 0.868-0.975; $P < 0.0001$), with a sensitivity of 73% and a specificity of 97% (Fig. 1).

In the ovarian carcinoma group, 74 samples were obtained from ascites and 14 samples were from pleural effusions. There was no difference in cyclin E copy number and strand length index according to sample origins ($P > 0.5$). Similarly, in the benign disease groups, our results also showed no difference between ascites ($n = 23$) and pleural effusions ($n = 47$; $P > 0.3$). Twenty-three effusion cases were selected in consecutive sequences of collections regardless of their cytology diagnoses and the remaining ovarian cancer cases were selected based on positive cytology. Therefore, only the former group of specimens were used to compare the results of the cyclin E assay with the traditional cytology. The cyclin E real-time PCR was able to identify 22 (95.6%) of 23 cases of ovarian carcinomas that were confirmed by clinical and surgical pathology findings using the cutoff value of 30.705, which was selected as the best value in distinguishing malignant cases versus benign controls based on the ROC curve analysis. In the same group, cytology results were positive in 17 (73.9%) of 23 cases. Therefore, the cyclin E assay was able to diagnose five additional cases of ovarian carcinoma which were not diagnosed by routine cytology. Combining the cyclin E assay with traditional cytology, all 23 cases of ovarian cancer were correctly identified, achieving 100% sensitivity in the diagnosis of malignant effusions.

Ten representative pairs of ascites samples and matched ascites tumor cell pellets from the same patients were compared to determine if there was a correlation in the cyclin E DNA copy number (normalized to Line-1 DNA copy number) between ascites cell–free DNA and the corresponding tumor cell DNA. Linear regression showed a significant correlation ($r = 0.946$) of the cyclin E copy number between ascites cell–free DNA and the genomic DNA from tumor cell pellets of the matched cases.

To determine whether the cyclin E assay was specific to ovarian carcinoma, the effusion specimens of ovarian carcinoma were compared with 110 malignant effusion samples of other cancer types. Using a cyclin E Ct of 30.705, which was used as a cutoff to distinguish ovarian carcinoma from benign samples, the percentage of cases with Ct below the cutoff (i.e., higher copy number) was significantly higher in ovarian cancer cases (88.6%; 95% CI, 95.6-81.6%) than in non–ovarian cancer cases (47.2%; 95% CI, 58.7-35.7%; $P < 0.001$). The reproducibility of the real-time PCR assay was assessed and the overall mean CV for the cyclin E and p53 PCRs were 1.31% and 1.02%, respectively. The reproducibility assay remained consistent and showed minimal variation between samples evaluated from day to day or batch to batch; CV for cyclin E ranged from 0.84% to 1.75% and CV for p53 ranged from 0.59% to 1.52%. Furthermore, the real-time PCR in representative specimens were analyzed in a separate institution (Development Center for Biotechnology, DCB) to assess the reproducibility of the assay for DNA integrity. A different experimental protocol was used for real-time PCR, including different primers, reagent composition, reaction programs, and instruments. We found that the CV for cyclin E was within 3.19 ± 2.3%, whereas for Line-1 it was 8.4 ± 4.8%.

Discussion

In this study, we show that the measurement of quantity and quality of a specific amplified genomic region in cell-free DNA of body fluids can be a useful approach to distinguish a cancerous specimen from a benign one. We showed that the copy number of the cyclin E genomic fragments and its DNA

Table 3. DNA copy number (100 bp) of different loci in the diagnosis of ovarian cancer effusions

Locus	AUC (effusion volume)*	AUC (Line-1) †	*P*
Cyclin E	0.832	0.847	<0.0001
β-Actin	0.816	0.811	<0.0001
p53	0.815	0.807	<0.0001
2p	0.693	0.685	<0.0001
4p	0.657	0.703	<0.0005

*Normalized to plasma volume.
† Normalized to Line-1 DNA copy number.

Table 4. Results of the DNA copy number and DNA length index in the diagnosis of malignant effusions

PCR product	Cycle threshold	DNA length index	AUC (95% CI)	*P*
Cyclin E 100	31		0.832 (0.762-0.889)	<0.0001
Cyclin E 100*	27.42	<0.35	0.879 (0.781-0.944)	<0.0001
Cyclin E 400	30.93		0.896 (0.838-0.939)	<0.0001
Cyclin E 400*	30.705	<0.90	0.936 (0.868-0.975)	<0.0001
Cyclin E 600	31.865		0.813 (0.741-0.872)	<0.0001
Cyclin E 600*	30.82	<0.32	0.914 (0.813-0.971)	<0.0001
Cyclin E 800	31.11		0.825 (0.752-0.883)	<0.0001
Cyclin E 800*	31.11	<0.75	0.905 (0.812-0.962)	<0.0001

*Combination of cyclin E copy number and DNA length index.

length integrity were significantly higher in effusion samples of ovarian cancer than in benign effusions. This finding suggests that increased DNA levels and strand length (integrity) of a specific amplified genomic locus in body fluid are unique characteristics of tumor-released DNA besides molecular genetic changes such as sequence mutations, microsatellite alterations, and allelic imbalance. Our results also imply that measurement of cyclin E DNA fragments using real-time PCR provides a simple diagnostic test for malignant effusions.

Effusions in the abdominal cavity (ascites) and the pleural compartment are associated with a variety of clinical conditions, including inflammatory disorders, infectious diseases, cardiac, liver, and renal diseases, as well as malignant neoplasms (22–24). Cytologic examination is routinely done to distinguish malignant from benign diseases. Although the sensitivity and specificity of cytology, when combined with immunocytochemistry, are generally high in the diagnosis of malignant effusions, they can be variable in some cases (25). This can be a result of a small number of tumor cells in some of the effusion samples or the presence of a large amount of leukocytes, mesothelial cells, and blood which obscure the detection of malignant cells. For example, inflammation, which is commonly associated with a malignant effusion, could result in reactive changes in mesothelial cells that make their morphologic distinction from carcinoma cells difficult. Thus, the cyclin E real-time PCR assay described here may provide an adjunct molecular test to distinguish malignant from benign effusions and could have potential clinical utility.

We first compared DNA copy number of cyclin E and other nonamplified chromosomal loci in effusion DNA samples using a quantitative real-time PCR assay of the 100 bp products. We showed that measurement of the cyclin E DNA copy number has the best performance in the diagnosis of ovarian cancer effusions. Next, we focused on the cyclin E locus to improve its diagnostic efficacy by testing different lengths of PCR products and by combining the DNA copy number and the DNA integrity index of cyclin E. The significant correlation of cyclin E copy number between cell-free DNA from effusion and DNA from the corresponding tumor cell pellets supports the view that a significant amount of cell-free DNA in body fluids was likely derived from tumor cells (7, 8). Results showing that measurement of the cyclin E DNA copy number was better than other genomic loci that are rarely amplified in ovarian cancer suggests that the amplified genomic region was a better marker for cancer diagnosis, as it was released at higher levels from tumor cells into body fluids than the nonamplified chromosomal regions. Based on our previous report, we found that increased DNA copy number in the cyclin E locus was observed in 43.3% of high-grade ovarian serous carcinomas (36.1% of cases showed amplification and 7.2% showed low copy number gain; ref. 19). Thus, many ovarian serous carcinomas we analyzed presumably did not have increased cyclin E DNA copy number and this could explain a mild increase of AUC by analyzing cyclin E as compared with the *β-actin* gene. The current finding was also consistent with our previous report showing that the level of total cell-free DNA was higher in malignant effusions than in benign effusions; however, the performance of total cell-free DNA concentration as a marker was not satisfactory as a sensitive or specific stand-alone assay to differentiate malignant from benign effusions (7). The selection of the cyclin E locus also facilitated a differential diagnosis in malignant effusions which resulted from different types of cancer because cyclin E was more frequently amplified in ovarian cancer than in other types of

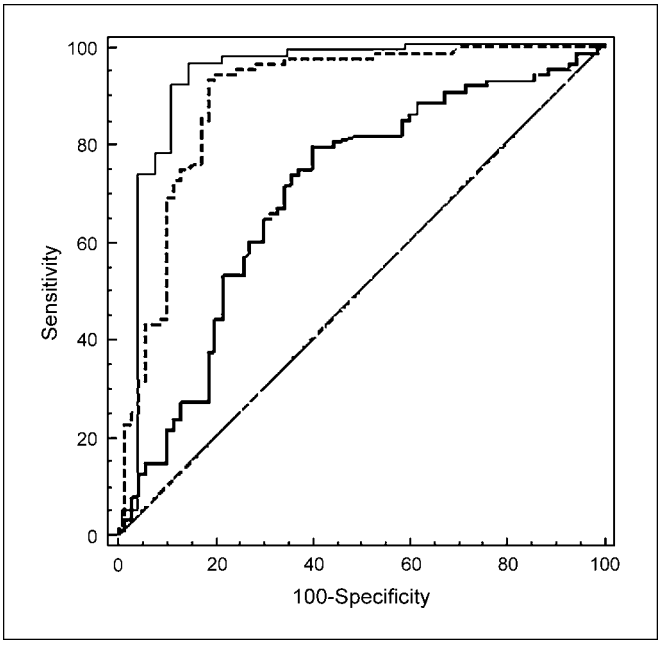

Fig. 1. ROC curve comparison in the diagnosis of ovarian cancer cases versus benign controls. Using cyclin E copy number and strand length integrity index (——), the AUC is 0.936; cyclin E copy number only (– – –), AUC is 0.896; and DNA strand length integrity index only (——), AUC is 0.698.

cancer analyzed in this study. As the current report is a proof-of-concept study, future efforts are required to extend the current findings by analyzing an array of amplified loci in a specific type of cancer to determine if such approaches have value in differential diagnosis among cancer types.

In this study, we combined the cyclin E DNA copy number and the integrity index to improve performance in the diagnosis of ovarian cancer effusions. This is based on the hypothesis that malignant effusions contain longer DNA fragments than benign effusion because tumor cell necrosis may release a spectrum of DNA strand lengths including the longer ones. Indeed, the AUC in differential diagnosis of ovarian versus benign effusions was improved to 0.936 by combining the cyclin E copy number (400 bp) and DNA length index (Ct of cyclin E-p53, 400 - 100 bp; Fig. 1). The use of the longer cyclin E PCR products such as 600 and 800 bp might be seemingly more specific to differentiate cancer cases versus benign controls (Table 2). However, the longer the DNA strands, the lower their abundance in effusion supernatants because of DNA fragmentation, which may decrease the overall assay sensitivity.

In summary, malignant effusions of ovarian cancer contained a much higher copy number of longer cyclin E DNA fragments than benign effusions. There are several molecular approaches that were previously reported to be useful in the diagnosis of malignant effusions and they included fluorescence *in situ* hybridization to detect aneuploidy cells, reverse transcription-PCR to detect mammaglobin expression (26), and digital PCR to detect allelic imbalance (7). Compared with other molecular techniques, the method described here would likely provide a simple assay system that would facilitate the differential diagnosis of malignant effusion besides conventional cytology. In order for this new assay to have clinical utility, several issues should be addressed. Although the sensitivity and specificity of the assay in diagnosing ovarian cancer effusion seemed satisfactory, higher sensitivity and specificity would be desirable. Sensitivity and specificity could be improved by combining the measurement of cyclin E DNA fragments with other amplified genomic loci, secretory tumor-associated markers (27–29), and other molecular assays (26). It seems necessary to compare the performance of the cyclin E real-time PCR assay and routine cytology by prospectively testing a large number of cytology-negative but clinically positive samples. It is also important to address how age, menopausal status, histologic grade, and other clinical variables affect cyclin E copy number and length integrity in effusions. Lastly, the potential use of cyclin E copy number and strand length in other body fluids such as plasma should be investigated.

References

1. Diamandis EP. Tumor markers: past, present and future. In: Diamandis EP, editor. Tumor markers, 1st ed. Washington (DC): American Association for Clinical Chemistry; 2002. p. 3–8.
2. Leon SA, Shapiro B, Sklaroff DM, Yaros MJ. Free DNA in the serum of cancer patients and the effect of therapy. Cancer Res 1977;37:646–50.
3. Anker P, Mulcahy H, Chen XQ, Stroun M. Detection of circulating tumour DNA in the blood (plasma/serum) of cancer patients. Cancer Metastasis Rev 1999;18:65–73.
4. Jahr S, Hentze H, Englisch S, et al. DNA fragments in the blood plasma of cancer patients: quantitations and evidence for their origin from apoptotic and necrotic cells. Cancer Res 2001;61:1659–65.
5. Esteller M, Sanchez-Cespedes M, Rosell R, et al. Detection of aberrant promoter hypermethylation of tumor suppressor genes in serum DNA from non-small cell lung cancer patients. Cancer Res 1999;59:67–70.
6. Diehl F, Li M, Dressman D, et al. Detection and quantification of mutations in the plasma of patients with colorectal tumors. Proc Natl Acad Sci U S A 2005; 102:16368–73.
7. Chang HW, Ali SZ, Cho SK, Kurman RJ, Shih I-M. Detection of allelic imbalance in ascitic supernatant by digital single nucleotide polymorphism analysis. Clin Cancer Res 2002;8:2580–5.
8. Chang HW, Lee SM, Goodman SN, et al. Assessment of plasma DNA levels, allelic imbalance, and CA 125 as diagnostic tests for cancer. J Natl Cancer Inst 2002; 94:1697–703.
9. Muller M, Krause H, Goessl C. Circulating cancer cells and cell-free nucleic acids as tumor markers. In: Diamandis EP, Fritsche H, Lilja H, Chan CCW, Schwartz MK, editors. Tumor markers, 1st ed. Washington (DC): American Association for Clinical Chemistry; 2002. p. 107–22.
10. Huang ZH, Li L, Hua D. Quantitative analysis of plasma circulating DNA at diagnosis and during follow-up of breast cancer patients. Cancer Lett 2006.
11. Allen D, Butt A, Cahill D, et al. Role of cell-free plasma DNA as a diagnostic marker for prostate cancer. Ann N Y Acad Sci 2004;1022:76–80.
12. Herrera LJ, Raja S, Gooding WE, et al. Quantitative analysis of circulating plasma DNA as a tumor marker in thoracic malignancies. Clin Chem 2005;51:113–8.
13. Taback B, Fujiwara Y, Wang HJ, et al. Prognostic significance of circulating microsatellite markers in the plasma of melanoma patients. Cancer Res 2001; 61:5723–6.
14. Taback B, O'Day SJ, Hoon DS. Quantification of circulating DNA in the plasma and serum of cancer patients. Ann N Y Acad Sci 2004;1022:17–24.
15. Wang BG, Huang HY, Chen YC, et al. Increased plasma DNA integrity in cancer patients. Cancer Res 2003;63: 3966–8.
16. Boynton KA, Summerhayes IC, Ahlquist DA, Shuber AP. DNA integrity as a potential marker for stool-based detection of colorectal cancer. Clin Chem 2003;49:1058–65.
17. Kinzler KW, Vogelstein B. The genetic basis of human cancer. 2nd ed. Toronto: McGraw-Hill; 2002.
18. Parrella P, Zangen R, Sidransky D, Nicol T. Molecular analysis of peritoneal fluid in ovarian cancer patients. Mod Pathol 2003;16:636–40.
19. Nakayama K, Nakayama N, Jinawath N, et al. Amplicon profiles in ovarian serous carcinomas. Int J Cancer 2007;120:2613–7.
20. Kmet LM, Cook LS, Magliocco AM. A review of p53 expression and mutation in human benign, low malignant potential, and invasive epithelial ovarian tumors. Cancer 2003;97:389–404.
21. Schuijer M, Berns EM. TP53 and ovarian cancer. Hum Mutat 2003;21:285–91.
22. Nagy JA, Herzberg KT, Dvorak JM, Dvorak HF. Pathogenesis of malignant ascites formation: initiating events that lead to fluid accumulation. Cancer Res 1993;53:2631–43.
23. Garrison RN, Galloway RH, Heuser LS. Mechanisms of malignant ascites production. J Surg Res 1987;42: 126–32.
24. Davidson B. Malignant effusions: from diagnosis to biology. Diagn Cytopathol 2004;31:246–54.
25. Davidson B, Risberg B, Reich R, Berner A. Effusion cytology in ovarian cancer: new molecular methods as aids to diagnosis and prognosis. Clin Lab Med 2003;23:729–54, viii.
26. Fiegl M, Haun M, Massoner A, et al. Combination of cytology, fluorescence *in situ* hybridization for aneuploidy, and reverse-transcriptase polymerase chain reaction for human mammaglobin/mammaglobin B expression improves diagnosis of malignant effusions. J Clin Oncol 2004;22:474–83.
27. Borgono CA, Michael IP, Diamandis EP. Human tissue kallikreins: physiologic roles and applications in cancer. Mol Cancer Res 2004;2:257–80.
28. Shih I-M. Application of HLA-G expression in the diagnosis of human cancer. Hum Immunol 2007;68: 272–6.
29. Shih I-M, Salani R, Fiegl M, et al. Ovarian cancer specific kallikrein profile in effusions. Gynecol Oncol 2007;105:501–7.

Int. J. Cancer: **120,** 2613–2617 (2007)

Amplicon profiles in ovarian serous carcinomas

Kentaro Nakayama[1], Naomi Nakayama[2,3], Natini Jinawath[1], Ritu Salani[2,3], Robert J. Kurman[1,2,3], Ie-Ming Shih[1,2,3] and Tian-Li Wang[2,3]*

[1]*Department of Pathology, Johns Hopkins Medical Institutions, Baltimore, MD*
[2]*Department of Gynecology and Obstetrics, Johns Hopkins Medical Institutions, Baltimore, MD*
[3]*Department of Oncology, Johns Hopkins Medical Institutions, Baltimore, MD*

Ovarian serous carcinoma is the most common and lethal type of ovarian cancer and its molecular etiology remains poorly understood. As an ongoing effort to elucidate the pathogenesis of ovarian serous carcinomas, we assessed the DNA copy number changes in 33 high-grade serous carcinomas and 10 low-grade serous tumors by using a genome-wide technique, single nucleotide polymorphism array, performed on affinity-purified tumor cells from fresh surgical specimens. Compared to low-grade tumors, high-grade serous carcinomas showed widespread DNA copy number changes. The most frequent alterations were in loci harboring candidate oncogenes: *cyclin E1 (CCNE1)*, *AKT2*, *Notch3* and *PIK3CA* as well as in novel loci, including 12p13, 8q24, 12p13 and 12q15. Seven amplicons were selected for dual color fluorescence *in situ* hybridization analysis in ~90 high-grade serous carcinomas and 26 low-grade serous tumors, and a high level of DNA copy number gain (amplification) was found in *CCNE1*, *Notch3*, *HBXAP/Rsf-1*, *AKT2*, *PIK3CA* and chr12p13 occurring in 36.1%, 7.8%, 15.7%, 13.6%, 10.8% and 7.3% of high-grade serous carcinomas. In contrast, we did not observe high level of *ERBB2* amplification in any of the samples. Low-grade tumors did not show DNA copy number gain in any of the loci, except in 2 (8%) of 24 low-grade tumors showing low copy number gain in the *Notch3* locus. Taken together, our results provide the first comprehensive analysis of DNA copy number changes in highly pure ovarian serous carcinoma. These findings may have important biological and clinical implications.

Key words: oncogene; amplification; ovarian cancer; karyotyping; genetics

DNA copy number alterations, including amplification, deletion and aneuploidy in chromosomes, are the hallmarks of neoplasia.[1] Amplification of chromosomal regions plays a critical role in tumor development. Increase in copy number of oncogenes promotes initiation and progression of a variety of solid tumors, while amplification of genes that modify or detoxify chemotherapeutic drugs can cause drug resistance and is associated with tumor recurrence.[2,3] Well-known amplified oncogenes include *c-myc*, *ERBB2*, *EGFR*, *AKT2*, *CCND1* and *cyclin E1 (CCNE1)*.[4] Studies on these genes not only have provided new insights on how cancer develops but also have significant translational implications. For example, *ERBB2* and *EGFR* are the molecular targets for the humanized antibodies Trastuzumab (Herceptin) and Matuzumab respectively, which are used in the treatment of breast and lung cancer. The completion of the human genome database has accelerated cancer genome study, as it provides precise and detailed maps to facilitate localization of genes potentially important in cancer. Several genome-wide technologies, including digital karyotyping, array comparative genomic hybridization (CGH), ROMA and single nucleotide polymorphism (SNP) array, have recently been developed and applied to explore the molecular genetic landscape of cancer in the postgenomic era.[5]

Epithelial ovarian cancer is the most lethal gynecologic neoplastic disease and one of the leading causes of cancer mortality in women. It comprises a diverse group of tumors, and among them, serous carcinoma is the most common and the most lethal type. Among serous neoplasms, 70% are high-grade and 30% are low grade tumors (including invasive low-grade carcinoma and its precursor lesion, serous borderline tumor). Despite considerable efforts aimed at elucidating the molecular etiology of ovarian serous carcinoma, its pathogenesis is still largely unknown. Although many genes have been previously reported to be amplified and deleted in ovarian cancer,[6–13] the overall profile of DNA copy number alterations in high-grade serous carcinomas has not been well described. One of the reasons is that most previous studies have combined different histological types of ovarian cancer, and therefore the specific alterations in the different histological types of ovarian serous carcinoma are not known. Furthermore, in most studies the tumor samples were not enriched by microdissection or affinity purification, which could also have obfuscated the interpretation of the results. Therefore, in this study, we analyzed a total of 43 affinity-purified ovarian serous tumors by using 10K SNP array to identify the chromosomal regions that show the most frequent DNA copy number changes. SNP array was used because it has been recently demonstrated to be feasible and robust and, most important, this technology provides high resolution which facilitates detection of DNA copy number changes.[14–16] In this study, we focused on amplified regions because it appeared more feasible to validate amplicons rather than deletions in regions in which the DNA copy number changes were usually subtle (from 2 to 1 or 0 copy). Our results demonstrate that *CCNE1*, *Notch3*, *HBXAP/Rsf-1, AKT2* and *PIK3CA* are among the most frequently amplified loci in high-grade serous carcinomas. In addition, novel amplifications and subchromosomal deletions were also detected by the SNP array analysis.

Material and methods

Tumor specimens

For SNP arrays, tissue samples from 33 high-grade ovarian serous carcinomas and 10 low-grade ovarian serous tumors (8 serous borderline tumors and 2 low-grade serous carcinomas) were freshly collected from the Department of Pathology at the Johns Hopkins Hospital from 2003 to 2006. The 33 high-grade serous carcinomas were all Stage III or IV and 5 of them were recurrent tumors. In addition, 15 normal ovaries served as controls. Tumor cells were affinity purified by anti-EPCAM-conjugated beads as previously described.[5,13] The acquisition of the anonymous tissue specimens for this study was approved by the Johns Hopkins Institutional Review Board.

Single nucleotide polymorphism array

SNPs were genotyped using 10K arrays (Affymetrix, Santa Clara, CA) in the Microarray Core Facility at the Dana-Farber

Grant sponsor: US Department of Defense Research Council; Grant number: OC0400600; Grant sponsor: NIH; Grant number: CA103937; Grant sponsor: Ovarian Cancer Research Fund; Grant number: POE01.06.
***Correspondence to:** Departments of Gynecology/Obstetrics and Oncology, Johns Hopkins University School of Medicine, CRBII, 1550 Orleans Street, Room 306, Baltimore, MD 21231, USA. Fax: 410-502-7943.
E-mail: tlwang21212@yahoo.com
Received 16 November 2006; Accepted after revision 27 December 2006
DOI 10.1002/ijc.22609
Published online 9 March 2007 in Wiley InterScience (www.interscience.wiley.com).

TABLE I – BAC CLONES USED FOR FISH STUDY

Gene name	BAC clone name	Location
PIK3CA	RP11-245C23 and RP11 -355N16	3q26.32
Rsf-1 (HBXAP)	RP11-45G10 and RP11-1107J12	11q14.1
Chr12p	RP11-62E21 and RP11-35017	12q13.32
ERBB2	RP11-94L15 and CTD-2019C10	17q12
Notch3	RP11-937H1 and RP11-319O10	19p13.12
Cyclin E1	RP11-345J21 and CTD-3005A16	19q12
AKT2	RP11-639F21 and CTC-425O23	12q13.2
Control	RP11-127K18 and RP11-629A22	2q11.2

Cancer Institute (Boston, MA). A detailed protocol is available at the Core center webpage (http://chip.dfci.harvard.edu/lab/services.php). Briefly, genomic DNA was cleaved with the restriction enzyme XbaI and ligated with linkers, followed by PCR amplification. The PCR products were purified and then digested with DNaseI to a size ranging from 250–2,000 bp. Fragmented PCR products were then labeled with biotin and hybridized to the array. Arrays were then washed on the Affymetrix fluidics stations. The bound DNA was then fluorescently labeled using streptavidin–phycoerythrin conjugates and scanned using the Gene Chip Scanner 3000.

dChip software (version 1.3) was used to analyze the SNP array data as described previously.[7,8] Data were normalized to a baseline array with median signal intensity at the probe intensity level using the invariant set normalization method. A model-based (PM/MM) method was employed to obtain the signal values for each SNP in each array. Signal values for each SNP were compared with the average intensities from 15 normal samples. To infer the DNA copy number from the raw signal data, we used the Hidden Markov Model,[7] based on the assumption of diploidy for normal samples. Mapping information of SNP locations and cytogenetic band were based on curation of Affymetrix and University of California Santa Cruz hg15. A cutoff of >3.5 copies in more than 3 consecutive SNPs was defined as amplification.

Fluorescence in situ *hybridization*

BAC clones were purchased from Bacpac Resources (Children's Hospital, Oakland, CA) or Invitrogen (Carlsbad, CA). The BAC clones used in this study are summarized in Table I. Bac clones (RP11-127K18 and RP11-629A22), located at Chr2q11.2, were used to generate the reference probes. The method for fluorescence *in situ* hybridization (FISH) has been detailed in previous reports.[3] The hybridization signals were counted by 2 individuals. The signal ratio of experimental probe/reference probe greater than 2 is considered as gain, and the signal ratio of experimental probe/reference probe greater than 3 is considered as high-fold amplification.

Results

Wide spread DNA copy number changes in high-grade serous carcinomas

The results of DNA copy number changes in all tumor specimens are shown in Figure 1. Compared to low-grade serous tumors (serous borderline tumors and invasive low-grade micropapillary serous carcinomas), the high-grade serous carcinomas demonstrated DNA copy number alterations in the majority of chromosomes. The number and amplitude of changes were much higher in high-grade than in low-grade serous tumors. The DNA copy number alterations in high-grade serous carcinomas involved gain or loss of discrete subchromosomal regions, chromosomal arms and whole chromosomes. In contrast, the low-grade tumors were characterized by a relatively "flat" chromosomal landscape with only a few chromosomal losses and low copy number gains. On the basin SNP array analysis, the regions with high prevalence of copy number gain (>3.5 copies) in high-grade serous carcinomas included regions that contain known putative oncogenes *CCNE1* at chr19q13.1 (33.3%), *AKT2* at chr19q13.2 (27.3%), *Notch3* at chr19p13.12 (21.2%) and *PIK3CA* at chr3q26.32 (9.1%), and novel amplicons 12p13, 8q24, 12p13 and 12q15. Interestingly, the *HBXAP*/*Rsf-1* region at chr11q13.5, which was previously reported to be amplified in ovarian serous carcinomas,[10] was found rarely amplified in this study, as *HBXAP*/*Rsf-1* amplification was only identified in 1 of 33 in this series of tumor samples. This is likely due to the relatively smaller sample size in the SNP array analysis, since FISH analysis in a larger number of specimens in the current study demonstrated an amplification frequency of 15.7%, close to previous reports.[10,11] Another well-known amplified oncogene in breast carcinoma, *ERBB2*, which is located at chr17q12, was not found to be amplified at high levels in any of the high-grade serous carcinomas and low-grade serous tumors.

In addition to the genomic amplification, there were many chromosomal regions demonstrating decrease in DNA copy number in small discrete regions or the whole arm, notably in chr8p, chr16, chr17p and chrX.

Dual-color FISH analysis of CCNE1, Notch3, HBXAP/Rsf-1, AKT2 and PIK3CA amplification in high-grade serous carcinomas

To independently validate the results of SNP arrays, we performed FISH on 98 paraffin-embedded high-grade ovarian tumors and 26 low-grade serous tumors. FISH was used because the method allowed a direct count of the DNA copy number in tumor cells. FISH probes were designed to hybridize *CCNE1*, *Notch3*, *AKT2*, *HBXAP*/*Rsf-1* and *PI3KCA* loci (Fig. 3). In addition, the frequency of *ERBB2* amplification in serous carcinoma was also determined. Chr12p13 was also analyzed because it was the most common amplicon in which the amplified oncogene(s) was unknown. In this study, we used the chr2q11.2 as the reference locus for FISH because the DNA copy number in this specific chromosomal region was relatively constant among the tumors (Fig. 2) that facilitated the quantification of the DNA copy number in the targeted loci. Using this approach, we demonstrated that *CCNE1* was amplified at a high amplitude (>3-fold in ratio of experimental probe *versus* reference probe) in 36.1%, *Notch3* in 7.8%, *AKT2* in 13.6%, *HBXAP*/*Rsf-1* in 15.7%, *PIK3CA* in 10.8% and *chr12p13* in 7.3% of high-grade carcinomas (Table II). Amplification in at least one of the aforementioned genes was found in 64% of cases. An increased DNA copy number was not observed for any loci in low-grade tumors except 2 cases showing *Notch3* low copy number gain (<3 copy ratio). Interestingly, consistent with the above SNP array analysis, this large-scale FISH analysis did not detect high levels of *ERBB2* amplification in any high-grade or low-grade serous tumors.

To determine whether the amplifications of CCNE1, AKT2, Notch3, HBXAP/Rsf-1, PIK3CA and chr12p13 loci were independent or related to each other, we performed Fisher's exact test to determine the significance of correlation. The results in Table III demonstrated that *CCNE1* amplification was significantly correlated with *AKT2* amplification ($p = 0.014$), *Notch3* amplification ($p = 0.042$) and chr12p13 amplification ($p = 0.022$). In addition, there was a marginal correlation between *AKT2* and chr12p13 amplifications ($p = 0.049$).

Discussion

Serous ovarian carcinoma represents ~60% of ovarian epithelial carcinomas. It is one of the most lethal malignancies in women, with a 5-year survival rate less than 30%. This dismal outcome is in part due to the lack of known molecular genetic markers that can be potentially targeted for therapy. The most common genetic alteration known to date in high-grade serous carcinoma is p53 mutation, which occurs in >50% of tumors[17,18] (Salani, unpublished results). In this study, we explored the DNA copy number alterations in ovarian serous carcinoma and identified the gene amplification profiles and subchromosomal deletions in ovarian serous tumors.

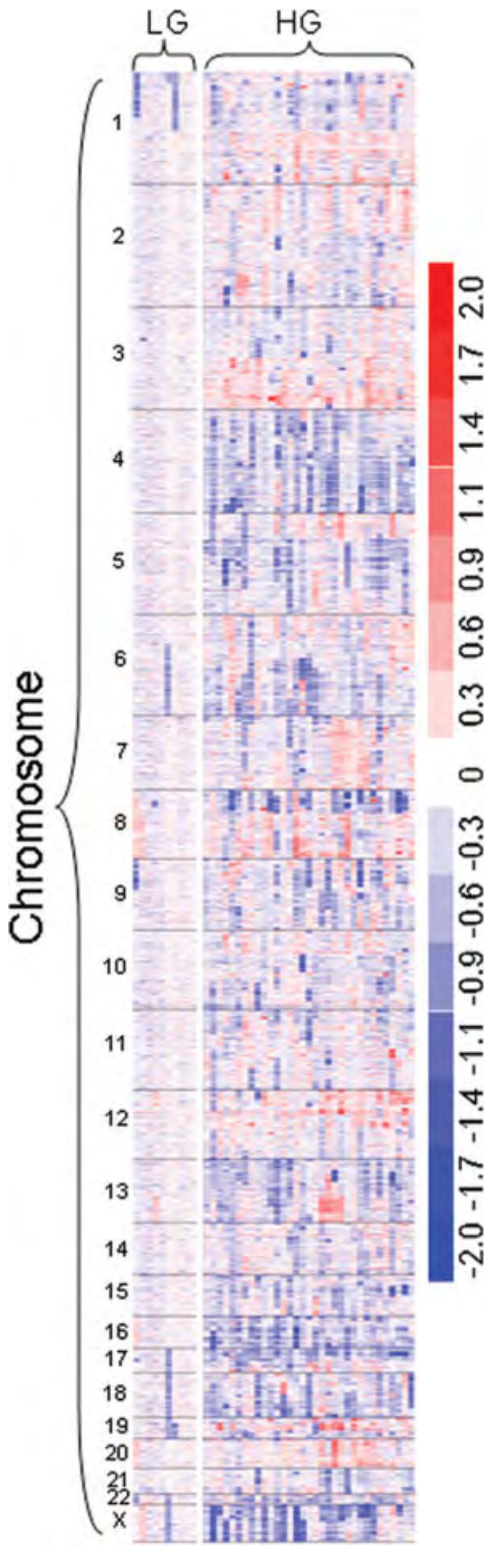

FIGURE 1 – Genome-wide distribution of DNA copy number changes in low-grade and high-grade ovarian serous carcinomas. Each column represents an individual tumor sample. DNA copy number changes are represented as pseudocolor gradients corresponding to the folds of increase (red boxes) and decrease (blue boxes), as compared to pooled normal samples. Compared to low-grade tumors, high-grade carcinomas demonstrate diffuse and sometimes, discrete DNA copy number gain (red boxes) and loss (blue boxes) in many of the chromosomes. Chromosomal numbers are shown in left column.

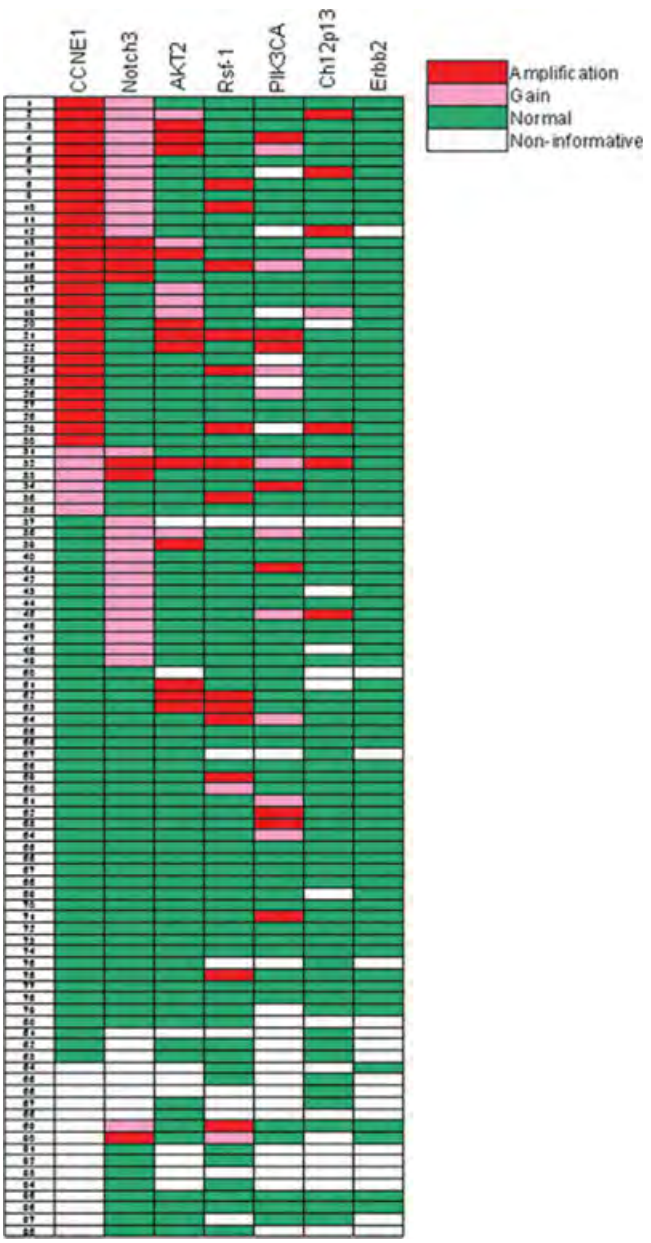

FIGURE 2 – Summary of fluorescence *in situ* hybridization (FISH) results of chromosomal regions harboring CCNE1, AKT2, Notch3, Rsf-1, PIK3CA, ERBB2 and a locus at chr12p13. A total of 98 high-grade serous carcinomas (case numbers shown in the left column) were evaluated using two-color FISH. Red boxes: amplification >3 folds (ratio of target gene signals *versus* reference gene signals greater than 3); pink boxes: DNA copy number increase between 2 and 3 folds; green boxes: normal (DNA copy ratio <2 fold); empty boxes: noninformative cases because either tumor cells are not available or FISH signal is not detectable in tissue sections. Chr2q11.2 was used as the reference locus for FISH because the DNA copy number in this specific chromosomal region was relatively constant among the tumors.

Compared to previous studies using conventional and array CGH,[19–23] the current study utilized 4 distinctly new approaches in the analysis of DNA copy number changes in ovarian cancer. First, we analyzed only serous carcinoma and did so in a relatively large number of cases. Indeed, the current analysis is to the best of our knowledge the largest study of DNA copy number alterations in ovarian serous carcinomas. Second, we used affinity-purified tumor cells directly isolated from surgical specimens for SNP

TABLE II – SUMMARY OF FISH RESULTS FOR OVARIAN SEROUS TUMORS

	Cyclin E1	*Notch3*	*AKT2*	*Rsf-1*	*PIK3CA*	Chr12p13	*ERBB2*
HG							
Normal	47 (56.6)	57 (63.3)	70 (79.5)	73 (82.1)	56 (75.7)	74 (90.2)	79 (100)
Gain	6 (7.2)	26 (28.9)	6 (6.8)	2 (2.2)	10 (13.5)	2 (2.4)	0 (0)
Amp	30 (36.1)	7 (7.8)	12 (13.6)	14 (15.7)	8 (10.8)	6 (7.3)	0 (0)
Total	83	90	88	89	74	79	82
LG							
Normal	26 (100)	22 (91.7)	24 (100)	25 (100)	20 (100)	23 (100)	24 (100)
Gain	0	2 (8.3)	0	0	0	0	0
Amp	0	0	0	0	0	0	0
Total	26	24	24	25	20	23	24

Amp, amplification. Values in parantheses indicate percentage of cases.

TABLE III – CORRELATION OF DIFFERENT AMPLICONS IN OVARIAN HIGH-GRADE SEROUS CARCINOMAS

	Cyclin E	*Notch 3*	*AKT2*	*Rsf-1*	*PI3KCA*	*Chr12p13*
Cyclin E		0.042	0.014	0.386	0.586	0.022
Notch 3	0.042		0.415	1.000	1.000	0.052
AKT2	0.014	0.415		0.741	0.335	0.049
Rsf-1	0.386	1.000	0.741		0.502	0.653
PI3KCA	0.586	1.000	0.335	0.502		0.291
Chr12p13	0.022	0.052	0.049	0.653	0.291	

The number in each box indicates the *p*-value based on the Fisher exact test.

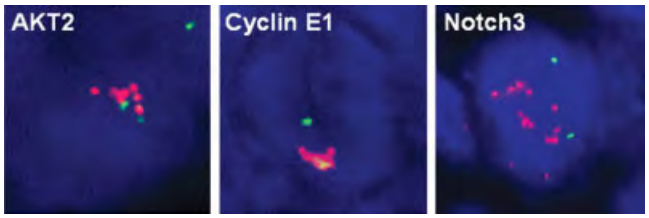

FIGURE 3 – Examples of two-color FISH for amplification in AKT2, Cyclin E1 and Notch3 loci. The numbers of red signals that represent the target gene in each case are more than those of the green signals (control probes). The nuclei are counterstained with DAPI (blue).

arrays. We believe that this approach will allow us to accurately measure the DNA copy number changes. Third, we analyzed high-grade (conventional) serous carcinomas and low-grade serous tumors separately, providing a new dimension to the molecular signatures of ovarian serous carcinoma. Fourth, in addition to SNP array analysis, we performed FISH on an independent set of tumor tissues. Our FISH results further validated the amplicon profiles based on SNP array analysis.

Using these approaches, we were able to characterize detailed amplicon profiles of ovarian serous carcinomas. It has been proposed that both high-grade and low-grade ovarian serous tumors develop along distinct molecular pathways.[24,25] Our results showing marked DNA copy number alterations in high-grade carcinoma when compared to low-grade tumors are consistent with the conclusion based on previous works using the CGH approach.[23,26] The widespread changes in DNA copy number in high-grade carcinoma suggest a high level of chromosomal instability in this type of tumor, while low-grade tumor is relatively stable. Previous studies have shown that low-grade tumors rarely harbor p53 mutation but have frequent ERBB2/KRAS/BRAF mutations.[13,27] In contrast, high-grade carcinomas are characterized by frequent p53 mutations but only rarely harbor ERBB2/KRAS/BRAF mutations. These results, together with the current findings, suggest significant different genetic/genomic profiles for these 2 types of serous ovarian serous carcinoma and further support the dualistic model of ovarian serous tumorigenesis.

Of the different amplified chromosomal regions in high-grade serous carcinomas, the most frequently amplified chromosomal loci were *CCNE1*, *Notch3*, *HBXAP*/*Rsf-1*, *AKT2* and *PIK3CA*. We did not observe amplification of the *ERBB2* locus or detect an increase in its DNA copy number by both SNP array and FISH analyses. The only sample in which we ever have *ERBB2* amplification is the SKOV3 cell line based on digital karyotyping analysis.[5] Our results suggest that *ERBB2* amplification is probably a rare event in high-grade ovarian serous carcinoma. *CCNE1* is the most commonly amplified gene in high-grade ovarian serous carcinomas based on both SNP array and FISH analyses. Amplification of *CCNE1* has been reported in several human cancers, including ovarian carcinoma.[28,29] Furthermore, *CCNE1* expression is correlated with tumor progression and predicts a poor outcome in patients with ovarian carcinoma.[6,30] *Notch3* amplicon has been recently reported in ovarian serous carcinomas based on fine mapping of the chr19p13.12 amplicon from high-grade serous carcinomas using a part of the SNP array results reported here.[16] *HBXAP*/*Rsf-1* functions as a chromatin remodeling protein by partnering with hNSF2H. The resulting complex plays an important role in a variety of cellular functions. *HBXAP*/*Rsf-1* gene has been identified as an amplified gene in ovarian cancer by digital karyotyping,[10] and its amplification was found to be associated with a shorter overall survival in patients with high-grade ovarian serous carcinoma. The PIK3CA–AKT2 signaling pathway regulates diverse cellular functions in response to extracellular milieu. Increased gene copy number of both genes has been found in lung, pancreatic, ovarian, cervical, head and neck carcinomas. Activation of the PIK3CA–AKT2 pathway either by gene amplification or by activating somatic point mutations has been implied to contribute to tumor development. Amplification of these genes may have biological and clinical significance. For example, expression of *AKT2* and *PIK3CA* genes is required for cell growth and survival in cancer cells that amplify or overexpress *AKT2* and *PIK3CA* genes.[31,32] These amplified genes may serve as the molecule targets for future therapeutic strategies in ovarian cancer.

SNP array analysis provides a whole-genome view of DNA copy number alterations in tumor specimen. Among the loci that we identified using both SNP array and FISH analyses, *CCNE1*, *PIK3CA* and chr12p13 showed closer call of amplification, while *NOTCH3* and *AKT2* had a wider deviation of amplification frequency between these 2 different techniques. Several factors could attribute to this discrepancy, including sampling differences between the 2 different analyses, different normalization methods used by each method, relatively subjective call in FISH analysis *etc*.; thus it is advisable to validate DNA copy number alteration results by at least 2 independent methods.

Some genes were found to be coamplified in the same tumor. For example, *CCNE1* frequently coamplifies with *AKT2*, *Notch3* and chr12p13. Coamplification of *CCNE1* and *AKT2* probably occurs because both genes are located in the same chr19q arm which is amplified. Likewise, coamplification of *CCNE1* and chr12p13 may be due to an unbalanced translocation followed by an amplification event. Alternatively, coamplification can be due to tumor evolution by selecting for clones with coamplification of

the genes that provide the cells with growth advantages. Whether these genes cooperate molecularly to propel tumorigenesis in ovarian cancer remains to be investigated. Besides the known candidate oncogenes, we also identified several chromosomal regions that are frequently amplified in ovarian cancer but do not harbor any known (potential) oncogenes. For example, chr12p13 was found to be amplified in 7.3% of high-grade serous tumors. Future studies are required to identify the novel gene(s) within a new amplicon. However, it is important to note that DNA copy number alteration does not necessarily indicate that the amplification plays a causal role in tumor development.

In conclusion, our SNP array and FISH analyses have shown what the prevalence of specific amplicons is in ovarian serous carcinomas. Our findings suggest that *CCNE1*, *Notch3, AKT2*, *HBXAP*/*Rsf-1* and *PIK3CA* are frequently amplified potential oncogenes in high-grade serous carcinomas. In contrast to high-grade carcinoma, low-grade serous tumors did not show high copy number gain, a finding that supports the view that high-grade serous carcinoma is characterized by pronounced chromosomal instability. These results shed light on the molecular features of ovarian carcinoma and provide candidates for molecular targeting in the treatment of ovarian cancer.

References

1. Kinzler KW, Vogelstein B. The genetic basis of human cancer, 2nd edn. Toronto: McGraw-Hill, 2002.
2. Albertson DG, Collins C, McCormick F, Gray JW. Chromosome aberrations in solid tumors. Nat Genet 2003;34:369–76.
3. Wang TL, Diaz LA, Jr, Romans K, Bardelli A, Saha S, Galizia G, Choti M, Donehower R, Parmigiani G, Shih Ie M, Iacobuzio-Donahue C, Kinzler KW, et al. Digital karyotyping identifies thymidylate synthase amplification as a mechanism of resistance to 5-fluorouracil in metastatic colorectal cancer patients. Proc Natl Acad Sci USA 2004;101:3089–94.
4. Brodeur GM, Hogarty MD. Gene amplificaton in human cancers: biological and clinical significance. In: Kinzler KW, Vogelstein B, eds. The genetic basis of human cancer, 1st edn., vol. 1. New York: McGraw-Hill, 1998. 161–79.
5. Shih Ie M, Wang TL. Apply innovative technologies to explore cancer genome. Curr Opin Oncol 2005;17:33–8.
6. Farley J, Smith LM, Darcy KM, Sobel E, O'Connor D, Henderson B, Morrison LE, Birrer MJ. Cyclin E expression is a significant predictor of survival in advanced, suboptimally debulked ovarian epithelial cancers: a gynecologic oncology group study. Cancer Res 2003;63:1235–41.
7. Slamon DJ, Godolphin W, Jones LA, Holt JA, Wong SG, Keith DE, Levin WJ, Stuart SG, Udove J, Ullrich A, Press MF. Studies of the HER-2/neu proto-oncogene in human breast and ovarian cancer. Science 1989;244:707–12.
8. Cheng JQ, Godwin AK, Bellacosa A, Taguchi T, Franke TF, Hamilton TC, Tsichlis PN, Testa JR. *AKT2*, a putative oncogene encoding a member of a subfamily of protein- serine/threonine kinases, is amplified in human ovarian carcinomas. Proc Natl Acad Sci USA 1992; 89:9267–71.
9. Wu R, Lin L, Beer DG, Ellenson LH, Lamb BJ, Rouillard JM, Kuick R, Hanash S, Schwartz DR, Fearon ER, Cho KR. Amplification and overexpression of the *L-MYC* proto-oncogene in ovarian carcinomas. Am J Pathol 2003;162:1603–10.
10. Shih Ie M, Sheu JJ, Santillan A, Nakayama K, Yen MJ, Bristow RE, Vang R, Parmigiani G, Kurman RJ, Trope CG, Davidson B, Wang TL. Amplification of a chromatin remodeling gene, *Rsf-1*/*HBXAP*, in ovarian carcinoma. Proc Natl Acad Sci USA 2005;102:14004–9.
11. Hughes-Davies L, Huntsman D, Ruas M, Fuks F, Bye J, Chin SF, Milner J, Brown LA, Hsu F, Gilks B, Nielsen T, Schulzer M, et al. EMSY links the BRCA2 pathway to sporadic breast and ovarian cancer. Cell 2003;115:523–35.
12. Nakayama K, Nakayama N, Davidson B, Katabuchi H, Kurman RJ, Velculescu VE, Shih Ie M, Wang TL. Homozygous deletion of MKK4 in ovarian serous carcinoma. Cancer Biol Ther 2006;5:630–4.
13. Nakayama K, Nakayama N, Kurman RJ, Cope L, Pohl G, Samuels Y, Velculescu V, Wang TL, Shih IM. Sequence mutations and amplificatin of *PIK3CA* and *AKT2* genes in purified ovarian serous neoplasms. Cancer Biol Ther 2006;5:779–85.
14. Janne PA, Li C, Zhao X, Girard L, Chen TH, Minna J, Christiani DC, Johnson BE, Meyerson M. High-resolution single-nucleotide polymorphism array and clustering analysis of loss of heterozygosity in human lung cancer cell lines. Oncogene 2004;23:2716–26.
15. Huang J, Wei W, Zhang J, Liu G, Bignell GR, Stratton MR, Futreal PA, Wooster R, Jones KW, Shapero MH. Whole genome DNA copy number changes identified by high density oligonucleotide arrays. Hum Genomics 2004;1:287–99.
16. Park JT, Li M, Nakayama N, Davidson B, Eberhart CG, Kurman RJ, Shih I-M, Wang T-L. Notch-3 gene amplification in ovarian cancer. Cancer Res 2006;66:6312–18.
17. Milner BJ, Allan LA, Eccles DM, Kitchener HC, Leonard RC, Kelly KF, Parkin DE, Haites NE. p53 mutation is a common genetic event in ovarian carcinoma. Cancer Res 1993;53:2128–32.
18. Singer G, Stohr R, Cope L, Dehari R, Hartmann A, Cao DF, Wang TL, Kurman RJ, Shih IM. Patterns of p53 mutations separate ovarian serous borderline tumors and low- and high-grade carcinomas and provide support for a new model of ovarian carcinogenesis: a mutational analysis with immunohistochemical correlation. Am J Surg Pathol 2005;29:218–24.
19. Schraml P, Schwerdtfeger G, Burkhalter F, Raggi A, Schmidt D, Ruffalo T, King W, Wilber K, Mihatsch MJ, Moch H. Combined array comparative genomic hybridization and tissue microarray analysis suggest PAK1 at 11q13.5-q14 as a critical oncogene target in ovarian carcinoma. Am J Pathol 2003;163:985–92.
20. Tsuda H, Birrer MJ, Ito YM, Ohashi Y, Lin M, Lee C, Wong WH, Rao PH, Lau CC, Berkowitz RS, Wong KK, Mok SC. Identification of DNA copy number changes in microdissected serous ovarian cancer tissue using a cDNA microarray platform. Cancer Genet Cytogenet 2004;155:97–107.
21. Bernardini M, Lee CH, Beheshti B, Prasad M, Albert M, Marrano P, Begley H, Shaw P, Covens A, Murphy J, Rosen B, Minkin S, et al. High-resolution mapping of genomic imbalance and identification of gene expression profiles associated with differential chemotherapy response in serous epithelial ovarian cancer. Neoplasia 2005;7:603–13.
22. Israeli O, Gotlieb WH, Friedman E, Korach J, Friedman E, Goldman B, Zeltser A, Ben-Baruch G, Rienstein S, Aviram-Goldring A. Genomic analyses of primary and metastatic serous epithelial ovarian cancer. Cancer Genet Cytogenet 2004;154:16–21.
23. Meinhold-Heerlein I, Bauerschlag D, Hilpert F, Dimitrov P, Sapinoso LM, Orlowska-Volk M, Bauknecht T, Park TW, Jonat W, Jacobsen A, Sehouli J, Luttges J, et al. Molecular and prognostic distinction between serous ovarian carcinomas of varying grade and malignant potential. Oncogene 2005;24:1053–65.
24. Shih Ie M, Kurman RJ. Molecular pathogenesis of ovarian borderline tumors: new insights and old challenges. Clin Cancer Res 2005;11: 7273–9.
25. Shih I-M, Kurman RJ. Ovarian tumorigenesis—a proposed model based on morphological and molecular genetic analysis. Am J Pathol 2004;164:1511–8.
26. Staebler A, Heselmeyer-Haddad K, Bell K, Riopel M, Perlman E, Ried T, Kurman RJ. Micropapillary serous carcinoma of the ovary has distinct patterns of chromosomal imbalances by comparative genomic hybridization compared with atypical proliferative serous tumors and serous carcinomas. Hum Pathol 2002;33:47–59.
27. Singer G, Oldt R, III, Cohen Y, Wang BG, Sidransky D, Kurman RJ, Shih Ie M. Mutations in BRAF and KRAS characterize the development of low-grade ovarian serous carcinoma. J Natl Cancer Inst 2003;95:484–6.
28. Schraml P, Bucher C, Bissig H, Nocito A, Haas P, Wilber K, Seelig S, Kononen J, Mihatsch MJ, Dirnhofer S, Sauter G. Cyclin E overexpression and amplification in human tumours. J Pathol 2003;200:375–82.
29. Marone M, Scambia G, Giannitelli C, Ferrandina G, Masciullo V, Bellacosa A, Benedetti-Panici P, Mancuso S. Analysis of cyclin E and CDK2 in ovarian cancer: gene amplification and RNA overexpression. Int J Cancer 1998;75:34–9.
30. Rosen DG, Yang G, Deavers MT, Malpica A, Kavanagh JJ, Mills GB, Liu J. Cyclin E expression is correlated with tumor progression and predicts a poor prognosis in patients with ovarian carcinoma. Cancer 2006;106:1925–32.
31. Cheng JQ, Ruggeri B, Klein WM, Sonoda G, Altomare DA, Watson DK, Testa JR. Amplification of AKT2 in human pancreatic cells and inhibition of AKT2 expression and tumorigenicity by antisense RNA. Proc Natl Acad Sci USA 1996;93:3636–41.
32. Samuels Y, Diaz LA, Jr, Schmidt-Kittler O, Cummins JM, Delong L, Cheong I, Rago C, Huso DL, Lengauer C, Kinzler KW, Vogelstein B, Velculescu VE. Mutant PIK3CA promotes cell growth and invasion of human cancer cells. Cancer Cell 2005;7:561–73.

Review

Notch Signaling, γ-Secretase Inhibitors, and Cancer Therapy

Ie-Ming Shih and Tian-Li Wang

Departments of Gynecology, Oncology, and Pathology, Johns Hopkins Medical Institutions, Baltimore, Maryland

Abstract

The Notch signaling pathway represents a critical component in the molecular circuits that control cell fate during development. Aberrant activation of this pathway contributes to tumorigenesis. The role of Notch in human cancer has been highlighted recently by the presence of activating mutations and amplification of Notch genes in human cancer and by the demonstration that genes in the Notch signaling pathway could be potential therapeutic targets. It has become clear that one of the major therapeutic targets in the Notch pathway are the Notch receptors, in which γ-secretase inhibitors prevent the generation of the oncogenic (intracellular) domain of Notch molecules and suppress the Notch activity. This review article summarizes the biological roles of Notch molecules in cancer development with special emphasis on the promise and challenges in applying γ-secretase inhibitors as a new line of targeted therapeutic agents. [Cancer Res 2007;67(5):1879–82]

Background

The Notch signaling pathway is evolutionarily conserved and the basic molecular players in this pathway are ligands (Delta and Jagged), Notch receptors, and the transcription factors (reviewed in ref. 1). Notch is a transmembrane heterodimeric receptor and there are four distinct members (Notch1 to Notch4) in humans and rodents. In a physiologic condition, binding of the Notch ligand to its receptor initiates Notch signaling by releasing the intracellular domain of the Notch receptor (Notch-IC) through a cascade of proteolytic cleavages by both α-secretase (also called tumor necrosis factor-α–converting enzyme) and γ-secretase (Fig. 1*A*). The released intracellular Notch-IC then translocates into the nucleus where it modulates gene expression primarily by binding to a ubiquitous transcription factor, CBF1, suppressor of hairless, Lag-1 (CSL). This binding recruits transcription activators to the CSL complex and converts it from a transcriptional repressor into an activator, which turns on several downstream effectors. The physiologic functions of Notch signaling are multifaceted, including maintenance of stem cells, specification of cell fate, and regulation of differentiation in development as well as in oncogenesis (2, 3).

In cancers, molecular genetic alterations, such as chromosomal translocation, point mutations, and chromosomal amplification at the Notch receptor loci, are the known mechanisms for constitutive activation of Notch pathway. Despite the different mechanisms, they all result in increased levels of intracellular Notch-IC. The oncogenic potential of Notch was first discovered in human T-cell acute lymphoblastic leukemia (T-ALL). While Notch1 signaling is essential for normal development of T-cell progenitors (4), constitutive activation of Notch1 signaling due to molecular genetic alterations is associated with T-ALL. For example, interstitial deletions of the extracellular portion of human Notch1 due to (7;9) chromosomal translocation are associated with ∼10% of T-ALL cases and activating point mutations of Notch1 are present in ∼50% of T-ALL cases (5, 6). Constitutive activation of nuclear factor-κB and formation of T-cell leukemia/lymphoma were observed in a Notch-IC transgenic mouse model (7), which indicates a causal role of Notch activation in T-ALL development. In non–small cell lung cancer, chromosomal translocation (15;19) has been identified in a subset of tumors, and the translocation is thought to elevate Notch3 transcription in tumors (8). In ovarian cancer, *Notch3* gene amplification was found to occur in ∼19% of tumors, and overexpression of Notch3 was found in more than half of the ovarian serous carcinomas (9). Similarly, Notch signaling activation has been shown in the development of breast cancer. In animal models, constitutively active Notch4 expression causes mammary tumors in mice (10) and Notch1-activating mutations contribute to the development of T-ALL. A recent study further shows that overexpression of activated Notch1 and Notch3 in transgenic mice blocks mammary gland development and induces mouse breast tumors (11). Overexpression of Notch3 is sufficient to induce choroid plexus tumor formation in a mouse model, suggesting a role of Notch3 in the development of certain types of brain tumors (12).

γ-Secretase as a Key Mediator of Notch Signaling

Because the Notch-IC signaling plays an important role in cancer development, it is plausible that targeting the Notch signaling steps, including receptor/ligand binding, release of Notch-IC, interaction of Notch-IC and downstream targets, as well as Notch-IC protein stability, can have antitumor effects (13, 14). Currently, one of the emerging approaches for blocking Notch signaling is to suppress the proteolytic step that leads to the generation of intracellular Notch-IC (Fig. 1*B*). On ligand binding, Notch receptors undergo a series of programmed proteolytic events, first by α-secretase at the extracellular surface, which leads to liberation of the extracellular fragment, and then by intramembranous cleavage mediated by γ-secretase. Notch-IC is then released from the inner surface of cell membrane and is translocated into nucleus where it activates transcription of the target genes. The proteolytic events in Notch signaling activation are comparable with the processes involving amyloid precursor protein (APP) cleavage (Fig. 1*B*), in which sequential cleavages by β-secretase and γ-secretase release the amyloid β-peptide (the precursor of amyloid plaques found in the brain of Alzheimer's disease).

γ-Secretase is a large protease complex and is composed of a catalytic subunit (presenilin-1 or presenilin-2) and accessory subunits (Pen-2, Aph1, and nicastrin). All these subunits contain transmembrane domains and thus they are membrane proteins. The pivotal role of γ-secretase in the Notch activation cascade has been well shown in an elegant knockin experiment, showing that introduction of a single point mutation near the transmembrane cleavage site in Notch1 molecules results in an embryonic lethality in mice, which is similar to the effects observed in Notch1

Requests for reprints: Tian-Li Wang, Johns Hopkins Medical Institutions, Cancer Research Building-II, Room 306, 1550 Orleans Street, Baltimore, Maryland 21231. Phone: 410-502-7774; Fax: 410-502-7943; E-mail: tlw@jhmi.edu.

doi:10.1158/0008-5472.CAN-06-3958

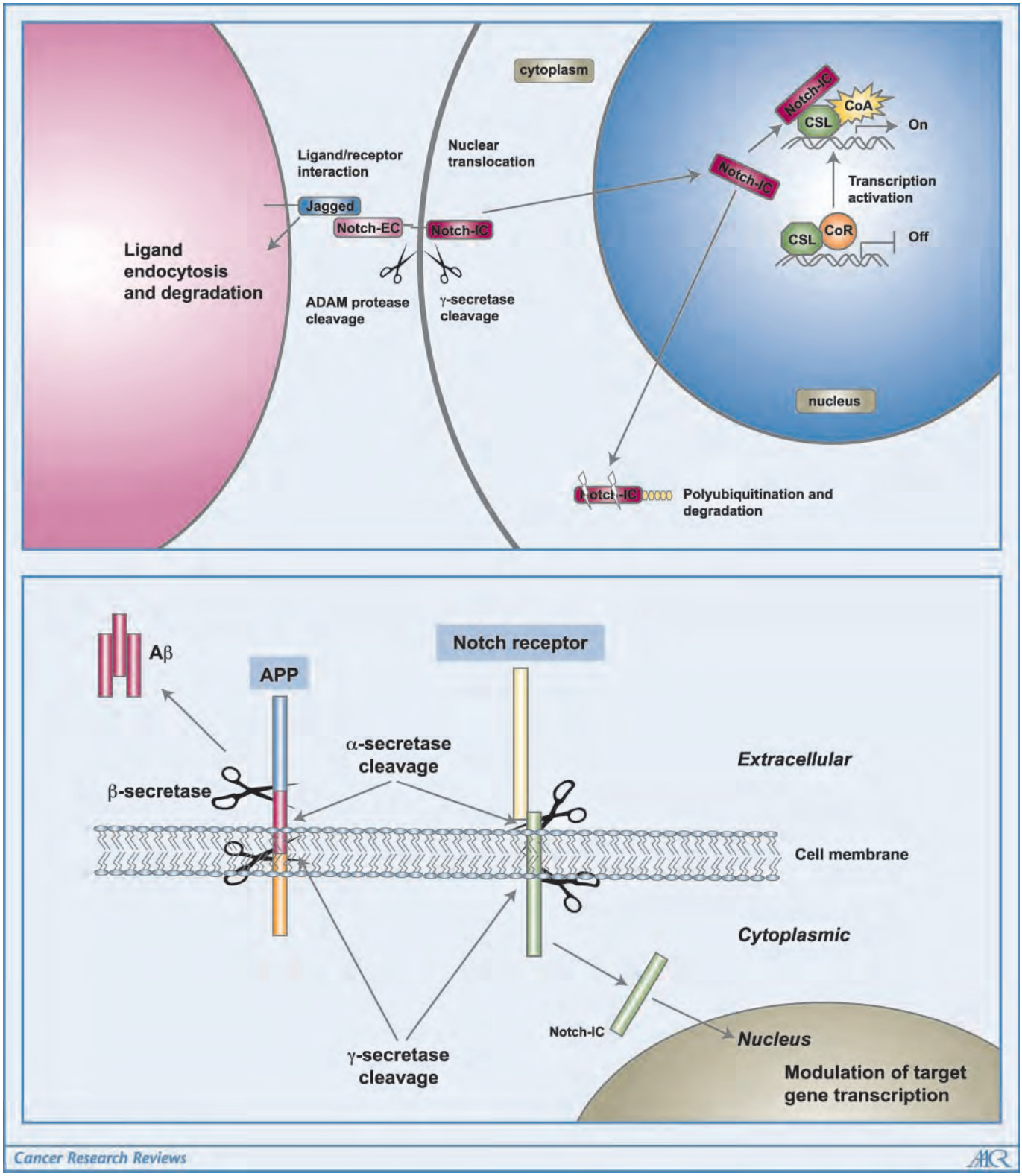

Figure 1. An overview of Notch signaling and proteolytic processing. *Top,* Notch receptor is a cell surface protein. Interaction with the Notch ligand, such as Jagged, initiates proteolytic cleavage at the extracellular site by α-secretase followed by cleavage at the intracellular site by γ-secretase, resulting in the release of Notch-IC from the cytoplasmic side of the cell membrane. Notch-IC is then translocated into the nucleus where it interacts with CSL and recruits coactivators (CoA) to form a transcription-activating complex. Notch-IC can be polyubiquitylated and targeted for degradation in a proteasome-dependent manner. However, the location of degradation is currently not clear. *Bottom,* the proteolytic events involving Notch receptor and APP are similar. APP is an integral membrane protein and is cleaved at the extracellular site by β-secretase followed by γ-secretase to release Aβ peptides. Aβ is the major constituent of amyloid plaques and its accumulation is thought to play a central role in Alzheimer's disease. APP can be also cleaved by α-secretase and γ-secretase, which leads to liberation of P3 peptides with unknown functions.

knockout (15). Furthermore, the presenilin-1–deficient and presenilin-1/presenilin-2 double knockout mice had a marked decrease in Notch-IC generation (16, 17).

Over the past decades, inhibitors for γ-secretase have been actively investigated for their potential to block the generation of Aβ peptide that is associated with Alzheimer's disease (18). Because γ-secretase inhibitors are also able to prevent Notch receptor activation, several forms of γ-secretase inhibitors have been tested for antitumor effects. First, an original γ-secretase inhibitor, IL-X (cbz-IL-CHO), was shown to have Notch1-dependent antineoplastic activity in Ras-transformed fibroblasts. More recently, tripeptide γ-secretase inhibitor (z-Leu-leu-Nle-CHO) was reported to suppress tumor growth in cell lines and/or xenografts in mice from melanoma and Kaposi sarcoma (19). Treatment with dipeptide γ-secretase inhibitor N-[N-(3,5-difluorophenacetyl)-L-alanyl]-S-phenylglycine t-butyl ester (DAPT) also resulted in a marked reduction in medulloblastoma growth and induced G_0-G_1 cell cycle arrest and apoptosis in a T-ALL animal model (20, 21). Another γ-secretase inhibitor, dibenzazepine, has been shown to inhibit epithelial cell proliferation and induce goblet cell differentiation in intestinal adenomas in $Apc^{-/-}$ (min) mice (22). More recently, functional inactivation of Notch3 either by tripeptide γ-secretase inhibitor or Notch3-specific small interfering RNA results in suppression of cell proliferation and induction of apoptosis in the tumor cell lines that overexpressed Notch3 but not in those with minimal amounts of Notch3 expression (9). Futhermore, a phase I clinical trial for a Notch inhibitor, MK0752 (developed by Merck, Whitehouse Station, NJ), has been launched for relapsed or refractory T-ALL patients and advanced breast cancers.[1] As discussed above, Notch signaling and APP metabolism are triggered by the similar proteolytic process; it is foreseeable that γ-secretase inhibitors that are currently tested in clinical trials for Alzheimer's disease may be applicable to treat neoplastic diseases, especially those tumors known to harbor constitutive Notch activation. Besides the evidence of γ-secretase inhibitors in directly inactivating Notch signaling on cancer cells, γ-secretase inhibitors may also suppress angiogenesis in solid tumors by interfering in the cross-talk between the tumor and vasculature through the Notch signaling (23).

The exciting studies summarized above strongly suggest a potential clinical application of γ-secretase inhibitors in cancer therapeutics. However, one of the major challenges on the way toward this goal is the untoward side effects associated with the inhibitors, especially the cytotoxicity in the gastrointestinal tract (24), which can be exacerbated by conventional chemotherapeutic drugs. Therefore, balancing efficacy and toxicity of γ-secretase inhibitors must be considered in future clinical applications. The possible mechanisms underlying the unwanted cytotoxicity are multifactorial. First, Notch signaling pathway is known to widely participate in cellular physiology in normal tissues, including hematopoiesis and maintenance of arterial smooth muscle (25); therefore, it is plausible that inactivation of γ-secretase may lead to dysfunction of vital organs. Second, it is likely that γ-secretase inhibitors do not exclusively target the Notch signaling pathways. This is because γ-secretase has many substrates in addition to Notch receptors, such as several Notch ligands, ErbB4, syndecan (an extracellular matrix), and CD44 (1). Additionally, γ-secretase inhibitors may target proteases other than γ-secretase. As proteases participate in a wide variety of cellular functions, γ-secretase inhibitors may have other widespread adverse effects *in vivo*. Some of the concerns of the nonselectivity of the inhibitors will be addressed based on the results of the ongoing clinical trials. Nevertheless, it may prove possible to identify a therapeutic window, in which partial inhibition of γ-secretase is sufficient to suppress Notch signaling in cancer cells, whereas the dosage will not significantly affect the functions in normal tissues. It is thought that the differential killing between cancer and normal cells can be exaggerated in treating those tumors with constitutive Notch activation, in which cancer cells are "addicted" to the Notch signaling.

Implications and Future Directions

The findings discussed above have at least two major biological and clinical implications. First, like wingless (wnt) and Hedgehog (shh), the Notch signaling pathway is important in controlling both developmental processes and tumorigenesis. Tumor cells sabotage the Notch signaling pathway for tumor initiation and/or progression through constitutive activation by ways of chromosomal translocation, point mutation, gene amplification, and other epigenetic events. Second, recent studies suggest that one of the most promising targets in inactivating the Notch signaling is γ-secretase complex, the molecular switch for Notch signaling activation. Recently, there has been an increased enthusiasm in targeting this pathway using γ-secretase inhibitors for new cancer therapeutics because accumulating preclinical studies have shown that γ-secretase inhibitors hold promise as a new target-based therapy for those tumors with Notch activation. However, before Notch-based therapy becomes a reality, future studies should primarily focus on the issues of target specificity and address the possible side effects that may affect cancer patients who receive this new treatment regimen. Furthermore, the clinical promise of γ-secretase inhibitors in cancer therapeutics depends on careful correlation studies between the molecular genetic alterations in the *Notch* gene (e.g., mutations and gene amplification) and clinical response to γ-secretase inhibitors. To maximize the therapeutic effects (together with conventional therapeutics) and minimize the adverse side effects in cancer patients, it is essential to show the "tumor dependency" of Notch activation experimentally and clinically. Despite several challenges on the way, it is expected that in the coming years, there will be substantial efforts in identifying new specific γ-secretase inhibitors and in opening new clinical trials to test the potential of this new line of cancer therapeutic agents.

Acknowledgments

Received 10/25/2006; revised 12/21/2006; accepted 1/5/2007.
Grant support: Department of Defense grant OC0400600 and NIH grant CA103937.
We thank Jook Park for the editorial assistance.

[1] http://www.clinicaltrials.gov/ct/show/NCT00100152

References

1. Nickoloff BJ, Osborne BA, Miele L. Notch signaling as a therapeutic target in cancer: a new approach to the development of cell fate modifying agents. Oncogene 2003;22:6598–608.
2. Artavanis-Tsakonas S, Rand MD, Lake RJ. Notch signaling: cell fate control and signal integration in development. Science 1999;284:770–6.
3. Greenwald I. LIN-12/Notch signaling: lessons from worms and flies. Genes Dev 1998;12:1751–62.
4. Radtke F, Wilson A, Stark G, et al. Deficient T cell fate specification in mice with an induced inactivation of Notch1. Immunity 1999;10:547–58.
5. Grabher C, von Boehmer H, Look AT. Notch 1 activation in the molecular pathogenesis of T-cell acute lymphoblastic leukaemia. Nat Rev Cancer 2006;6:347–59.

6. Aster JC. Deregulated NOTCH signaling in acute T-cell lymphoblastic leukemia/lymphoma: new insights, questions, and opportunities. Int J Hematol 2005;82:295–301.
7. Bellavia D, Campese AF, Alesse E, et al. Constitutive activation of NF-κB and T-cell leukemia/lymphoma in Notch3 transgenic mice. EMBO J 2000;19:3337–48.
8. Dang TP, Gazdar AF, Virmani AK, et al. Chromosome 19 translocation, overexpression of Notch3, and human lung cancer. J Natl Cancer Inst 2000;92:1355–7.
9. Park JT, Li M, Nakayama N, et al. Notch-3 gene amplification in ovarian cancer. Cancer Res 2006;66: 6312–8.
10. Gallahan D, Callahan R. The mouse mammary tumor associated gene INT3 is a unique member of the NOTCH gene family (NOTCH4). Oncogene 1997;14: 1883–90.
11. Hu C, Dievart A, Lupien M, Calvo E, Tremblay G, Jolicoeur P. Overexpression of activated murine notch1 and notch3 in transgenic mice blocks mammary gland development and induces mammary tumors. Am J Pathol 2006;168:973–90.
12. Dang L, Fan X, Chaudhry A, Wang M, Gaiano N, Eberhart CG. Notch3 signaling initiates choroid plexus tumor formation. Oncogene 2006;25:487–91.
13. Nam Y, Aster JC, Blacklow SC. Notch signaling as a therapeutic target. Curr Opin Chem Biol 2002; 6:501–9.
14. Miele L, Miao H, Nickoloff BJ. NOTCH signaling as a novel cancer therapeutic target. Curr Cancer Drug Targets 2006;6:313–23.
15. Huppert SS, Le A, Schroeter EH, et al. Embryonic lethality in mice homozygous for a processing-deficient allele of Notch1. Nature 2000;405:966–70.
16. Armogida M, Petit A, Vincent B, Scarzello S, da Costa CA, Checler F. Endogenous β-amyloid production in presenilin-deficient embryonic mouse fibroblasts. Nat Cell Biol 2001;3:1030–3.
17. De Strooper B, Annaert W, Cupers P, et al. A presenilin-1-dependent γ-secretase-like protease mediates release of Notch intracellular domain. Nature 1999; 398:518–22.
18. Selkoe D, Kopan R. Notch and presenilin: regulated intramembrane proteolysis links development and degeneration. Annu Rev Neurosci 2003;26:565–97.
19. Curry CL, Reed LL, Golde TE, Miele L, Nickoloff BJ, Foreman KE. γ Secretase inhibitor blocks Notch activation and induces apoptosis in Kaposi's sarcoma tumor cells. Oncogene 2005;24:6333–44.
20. Hallahan AR, Pritchard JI, Hansen S, et al. The SmoA1 mouse model reveals that notch signaling is critical for the growth and survival of sonic hedgehog-induced medulloblastomas. Cancer Res 2004;64:7794–800.
21. O'Neil J, Calvo J, McKenna K, et al. Activating Notch1 mutations in mouse models of T-ALL. Blood 2006;107: 781–5.
22. van Es JH, van Gijn ME, Riccio O, et al. Notch/γ-secretase inhibition turns proliferative cells in intestinal crypts and adenomas into goblet cells. Nature 2005;435: 959–63.
23. Zeng Q, Li S, Chepeha DB, et al. Crosstalk between tumor and endothelial cells promotes tumor angiogenesis by MAPK activation of Notch signaling. Cancer Cell 2005;8:13–23.
24. Barten DM, Meredith JE, Jr., Zaczek R, Houston JG, Albright CF. γ-Secretase inhibitors for Alzheimer's disease: balancing efficacy and toxicity. Drugs R D 2006;7:87–97.
25. Joutel A, Corpechot C, Ducros A, et al. Notch3 mutations in CADASIL, a hereditary adult-onset condition causing stroke and dementia. Nature 1996; 383:707–10.

Research Article

NAC-1 Controls Cell Growth and Survival by Repressing Transcription of Gadd45GIP1, a Candidate Tumor Suppressor

Kentaro Nakayama,[1] Naomi Nakayama,[1] Tian-Li Wang,[2] and Ie-Ming Shih[1,2]

Departments of [1]Pathology and [2]Oncology, Gynecology and Obstetrics, Johns Hopkins Medical Institutions, Baltimore, Maryland

Abstract

Cancer mortality and morbidity are primarily related to recurrent tumors, and characterization of recurrence-associated genes should illuminate fundamental properties of tumor progression and provide new therapeutic targets. We have previously identified *NAC-1*, a member of the BTB/POZ gene family and a transcription repressor, as a gene associated with recurrent ovarian carcinomas after chemotherapy. We further showed that homodimerization of NAC-1 proteins is essential for tumor growth and survival. In this study, we applied serial analysis of gene expression and identified growth arrest and DNA-damage–inducible 45-γ interacting protein (*Gadd45GIP1*) as one of the downstream genes negatively regulated by NAC-1. *NAC-1* knockdown in both SKOV3 and HeLa cells that expressed abundant endogenous NAC-1 induced Gadd45GIP1 expression transcriptionally; on the other hand, engineered expression of NAC-1 in NAC-1–negative RK3E and HEK293 cells suppressed endogenous Gadd45GIP1 expression. In NAC-1–expressing tumor cells, induction of dominant negative NAC-1 conferred a growth-inhibitory effect that can be partially reversed by *Gadd45GIP1* knockdown. Induced Gadd45GIP1 expression resulted in growth arrest in SKOV3 and HeLa cells both *in vitro* and *in vivo*. In summary, NAC-1 contributes to tumor growth and survival by at least inhibiting Gadd45GIP1 expression, which has a tumor suppressor effect in cancer cells. [Cancer Res 2007;67(17):8058–64]

Introduction

The genes of the BTB/POZ family act as ubiquitous transcription repressors and participate in several cellular functions, including proliferation, apoptosis, transcription control, and cell morphology maintenance (1). The BTB/POZ proteins share an evolutionally conserved BTB/POZ protein-protein interaction motif at the NH_2-terminal that mediates either homodimer or heterodimer formation (1–3). The POZ domain also facilitates the recruitment of corepressor proteins including histone deacetylases (4), SMRT (5), N-CoR (6), mSin3A (6), and BcoR (7). The roles of BTB/POZ proteins in human cancer have been recently revealed because several of the BTB/POZ proteins have been shown to be involved in cancer development, and they include BCL-6 (8, 9), PLZF (promyelocytic leukemia zinc finger; refs. 8, 10), leukemia/lymphoma related factor (LRF)/Pokemon (11, 12), HIC-1 (hypermethylated in cancer-1), and Kaiso (13, 14). For example, BCL-6 translocations and mutations frequently occur in B-cell lymphoma, resulting in constitutive BCL-6 activation that contributes to the development of B-cell lymphoma. Peptide inhibitors that block interaction between the BCL-6 BTB/POZ domain and its corepressor suppress BCL-6 oncogenic functions in neoplastic B lymphocytes, suggesting a potential of that peptide inhibitor of the BTB/POZ domain may provide a novel therapeutic agent for B-cell lymphoma (9). Besides, LRF directly represses transcription of the tumor suppressor gene ARF, thus enhancing tumor development (11).

Based on analyzing gene expression levels in all 130 deduced human BTB/POZ genes using the serial analysis of gene expression (SAGE) data, we have recently identified NAC-1 as a carcinoma-associated BTB/POZ gene (15). NAC-1 is a transcription repressor and is involved in self-renewal and maintenance of pluripotency in embryonic stem cells (16). In human cancer, our previous study reveals that NAC-1 is significantly overexpressed in several types of carcinomas including ovarian serous carcinomas, the most malignant and common type of ovarian cancer (15). The levels of NAC-1 expression correlate with tumor recurrence in ovarian serous carcinomas, and intense NAC-1 immunoreactivity in primary ovarian tumors predicts early recurrence (15). Based on co-immunoprecipitation and double immunofluorescence assays, we show that NAC-1 proteins homo-oligomerize through the BTB/POZ domain. Induced expression of the NAC-1 mutant containing only the BTB/POZ domain (N130) disrupts NAC-1 bodies, prevents tumor formation, and enhances apoptosis in mouse tumor xenografts. Overexpression of full-length NAC-1 is sufficient to increase tumorigenicity of ovarian surface epithelial cells and NIH3T3 cells in athymic *nu/nu* mice. Taken together, our previous studies suggest that NAC-1 is a tumor recurrence–associated gene with oncogenic potential, and the interaction between BTB/POZ domains of NAC-1 proteins is essential for tumor cell proliferation and survival in those tumors with NAC-1 overexpression.

To determine the molecular mechanisms underlying how NAC-1 expression contributes to growth and survival in tumor cells that overexpress NAC-1, we used the NAC-1 dominant negative N130 model to identify the differentially expressed genes in cells with and without N130 induction. Based on SAGE, we identified and validated several genes whose expression was up-regulated by N130 protein induction and, thus, was negatively regulated by NAC1 molecules. One of the NAC-1 negatively regulated genes is the growth arrest and DNA-damage–inducible 45-γ interacting protein (Gadd45GIP1), also known as CR6-interacting factor 1 (CRIF1), which has been shown to bind to the Gadd45 family proteins based on glutathione *S*-transferase pull-down, mammalian

Note: Supplementary data for this article are available at Cancer Research Online (http://cancerres.aacrjournals.org/).

Requests for reprints: Ie-Ming Shih, Room 305, Cancer Research Building II, Johns Hopkins Medical Institutions, 1550 Orleans Street, Baltimore, MD 21231. Phone: 410-502-7774; E-mail: ishih@jhmi.edu.

doi:10.1158/0008-5472.CAN-07-1357

cell two-hybrid, and co-immunoprecipitation assays (17). In this study, we provide new evidence that Gadd45GIP1 is one of the NAC-1 downstream targets in which down-regulation by NAC-1 is a possible mechanism that NAC-1 contributes to tumor growth and survival.

Materials and Methods

LongSAGE library construction. Total RNA was isolated from 1×10^7 HeLa cells with the Tet-off N130 inducible system 28 h after removal of doxycyclin and from 1×10^7 control cells in the presence of doxycyclin. This time point of tumor cell harvesting was determined according to our previous study showing that 28 h after N130 induction, cell cycle arrest in the induced cells first became obvious (15). LongSAGE was done with 2 μg mRNA using a standard SAGE protocol.[3]

Quantitative PCR analysis and promoter activity assay. The transcript levels of candidate NAC-1–regulated genes as listed in Table 1, including Gadd45GIP1, were determined by quantitative real-time PCR using an iCycler (Bio-Rad) with the SYBR Green dye (Molecular Probes). Averages in the threshold cycle number (C_t) of duplicate measurements were obtained. The results were expressed as the difference between the C_t of the gene of interest and the C_t of a control gene (APP) for which expression is relatively constant among the SAGE libraries analyzed (19). For the promoter activity assay of the *Gadd45GIP1*, we cloned a 1.5-kb fragment of the *Gadd45GIP1* promoter region into the pGL3-Enhancer vector (Promega). The construct was then used to transfect HeLa cells in a 96-well plate using LipofectAMINE. *Renilla* construct was used as a normalization control. The luciferase intensity that reflected the promoter activity was measured using the Dual-Glo Luciferase Reagent (Promega). The ratio of luminescence from the experimental reporter and the control reporter (the *Renilla* vector) was determined.

Effects of *Gadd45GIP1* expression. The Tet-off inducible system was used to assess the biological effects of Gadd45GIP1. SKOV3 ovarian cancer cell line and HeLa cervical adenocarcinoma cell line, which constitutively expressed tetracycline-controlled transactivator (tTA), were transfected with pBI-Gadd45GIP1/enhanced green fluorescent protein (EGFP) that bicistronically expressed Gadd45GIP1 and the reporter EGFP upon the binding of rTA to the tetracyclin-responsive element (TRE). The Gadd45GIP1 cDNA was prepared from the OVCAR3 cells, amplified by PCR and cloned into the pBI vector. Both Gadd45GIP1 and EGFP proteins were not expressed in the presence of doxycyclin, which bound to tTA and prevented it from interacting with TRE on a pBI vector. Both proteins were induced upon removal of doxycyclin.

To assess if constitutive expression of Gadd45GIP1 could counteract the growth stimulatory effect of NAC-1 proteins, we constructed a mammalian expression vector, pcDNA4/Gadd45GIP1, with an Xpress tag at the NH_2-terminal. The Gadd45GIP1 cDNA was prepared from the OVCAR3 cells, amplified by PCR and cloned into a mammalian expression vector, pcDNA4/His-Max C (Invitrogen). The clone was sequenced to ensure a wild-type coding sequence of Gadd45GIP1. pcDNA/Gadd45GIP1 was then stably transfected into the RK3E/NAC-1 and HEK293/NAC-1 clones using the Nucleofector II electroporator (Amaxa). Cell growth and apoptosis assays were done as previously described (20).

Small interfering RNA knockdown of NAC-1 and Gadd45GIP1 gene expression. The small interfering RNA (siRNA) that targeted Gadd45GIP1 was GGCGGCGCCGUAACGCGCGAACUGCUU. Control siRNA (off-target control) was purchased from IDT. The sequences of NAC-1 siRNA were previously reported (15). Cells were seeded onto 96 wells and transfected with siRNAs using OligofectAMINE (Invitrogen).

Tumor xenograft in nude mice. To determine if Gadd45GIP1 induction could prevent tumor formation, we injected 3×10^6 SKOV3 and HeLa cells with Gadd45GIP1 inducible constructs into the subcutaneous tissue of *nu/nu* mice. For controls, doxycyclin (125 μg/mouse) was injected i.p. daily to suppress Gadd45GIP1 expression, whereas doxycyclin was not given into the mice to induce gene expression. Tumor volume was measured every other day for 14 days. To determine if Gadd45GIP1 has tumor suppressor effects on established tumors, we injected the same number of SKOV3 and HeLa cells and induced Gadd45GIP1 expression 9 days after subcutaneous tumors had formed. The tumors were monitored for induction based on green fluorescence using a small animal fluoroscope imaging device. Tumor volume was measured daily for 9 days after induction, and tumors were prepared for histopathologic examination and immunohistochemistry study using an anti-M30 antibody (Roche).

Results

Identification and validation of NAC-1 regulated genes. To elucidate the mechanisms underlying the effects of NAC-1 in promoting tumor growth and survival, we used the N130 dominant negative system because N130 was a truncated protein of NAC-1 containing only the BTB/POZ domain (amino acids 1–129 from the NH_2-terminal), and induction of N130 was shown to be more potent in inactivating NAC-1 than gene knockdown using siRNA (15). In this study, we did long SAGE and compared the gene expression profiles in N130-induced and non-induced HeLa cells. We found that N130 induction affected transcript levels in only a few genes. There were a total of seven genes that were significantly up-regulated (≥3-fold in tag counts) after N130 induction and could be validated (≥2-fold) by quantitative real-time PCR using the same RNA samples that were used to generate long SAGE libraries (Table 1). The up-regulation of the seven genes by N130 could also be observed in SKOV3 ovarian cancer cells after N130 induction based on real-time PCR analysis. As a control, we induced the expression of C250, the deletion mutant of NAC-1 containing the COOH-terminal 250 amino acids of the NAC-1 protein, in HeLa cells but did not observe a significant fold increase (<1.5-fold) in any of the seven genes. The transcript level of Gadd45GIP1 increased as soon as 9 h after N130 induction and sustained a similar level of expression thereafter. In addition, there were three genes showing marginal down-regulation (2- to 3-fold) in N130-induced cells as compared with non-induced controls based on LongSAGE, but none of them could be validated by real-time PCR (<1.5-fold). Among the seven up-regulated genes, Gadd45GIP1 was selected for further study because it had been shown to be a potential gene that suppresses cellular proliferation and participate in the Gadd45 tumor suppressor pathway (17).

NAC-1–dependent Gadd45GIP1 expression. Induction of N130 expression significantly enhanced the *Gadd45GIP1* promoter activity ($P < 0.001$) and elevated the Gadd45GIP1 mRNA level in HeLa cells (Fig. 1*A*) as well as the Gadd45GIP1 protein level in both HeLa and SKOV3 cells (Fig. 1*B*). In contrast, C250 induction did not show any significant effect on the expression levels of Gadd45GIP1 because the Gadd45GIP1 transcript level increased to only 1.094-fold based on quantitative real-time PCR. To further show that Gadd45GIP1 expression depends on NAC-1 proteins, we used two independent but complementary approaches. First, we knocked down NAC-1 in HeLa and SKOV3 cells using siRNA and observed a decrease in the NAC-1 transcript level with a concomitant increase in the Gadd45GIP1 level (Fig. 1*C* and *D*). Second, we ectopically expressed NAC-1 tagged with V5 in HEK293 and RK3E cells with undetectable NAC-1 expression and analyzed the change in the Gadd45GIP1 expression levels and cell proliferation (Fig. 2*A–C*). The NAC-1/V5 stable clones showed higher proliferation activity as compared with the vector-transfected clones at low (0.5%) serum concentration. The transcript and protein levels

[3] This has been detailed at http://www.sagenet.org/sage_protocol.htm with the modifications previously described (18).

Table 1. Differentially expressed genes after induction of N130 NAC-1

Gene name	Unigene number	Gene description	Tag number N130+	Tag number N130−	Real-time PCR
CHCHD2	389996	Coiled-coil-helix-coiled-coil-helix domain	41	17	9.5-fold up
DUT	527980	Essential enzyme of nucleotide metabolism	13	2	3.3-fold up
UBE2J2	191987	E2 ubiquitin-conjugating enzyme family	7	0	2.1-fold up
CAPNS1	515371	Calpain families related to oxidative stress	6	0	2.4-fold up
GADD45GIP1	515164	Growth arrest and DNA-damage-inducible	11	2	3.9-fold up
COL4A1	17441	Major type IV α collagen chain of basement membranes	13	3	2.6-fold up
TFE3	274184	Transcription factor binding to IGHM enhancer 3	5	0	3.9-fold up

of Gadd45GIP1 were significantly reduced in NAC-1 clones as compared with the control cells without NAC-1 expression.

Functional effects of Gadd45GIP1 expression *in vitro*. The above findings suggest that Gadd45GIP1 mediates the growth-inhibitory effect of the dominant negative NAC-1, N130, and is one of the downstream genes negatively regulated by NAC-1. To test this hypothesis, we established an inducible (Tet-off) system in HeLa and SKOV3 cells by expressing the Gadd45GIP1 in tumor cells upon removal of doxycyclin. Because the inducible system drove the expression of Gadd45GIP1 as well as EGFP, we were able to determine the efficiency of gene induction by counting the green fluorescent cells. Based on flow cytometry, we found that the induction efficiency in both SKOV3 and HeLa cell lines was high because more than 90% of cells became green fluorescent 24 h after induction. Based on Western blot analysis, expression of Gadd45GIP1 in SKOV3 and HeLa cells was first detected 24 (although weak) and 48 h after induction, respectively (Fig. 3*A*). For both cell lines, induction of Gadd45GIP1 expression significantly suppressed cell growth as evidenced by the insignificant increase of cell number in a time course of the induced group as compared with the non-induced group (Fig. 3*B*). Similarly, the colony formation was remarkably reduced in the induced group (Fig. 3*C*), and the percentage of apoptotic cells was increased in the induced SKOV3 and HeLa cells (Fig. 3*D*). In addition to determining the effects of Gadd45GIP1 in SKOV3 and HeLa, we further extended the above finding to RK3E and HEK293 clones that were engineered to express NAC-1. Constitutive Gadd45GIP1 expression (driven by a cytomegalovirus promoter) significantly reduced the growth rate of NAC-1 clones as compared with the control cells without Gadd45GIP1 expression (Supplementary Fig. S1). The above results strongly suggested that the overexpression of NAC-1 in tumor cells contributed to tumor growth by negatively controlling the expression of Gadd45GIP1. Thus, we further determined if Gadd45GIP1 knockdown could rescue growth suppression conferred by N130. We treated HeLa cells with siRNA targeting Gadd45GIP1, and as shown in the Supplementary Fig. S2, Gadd45GIP1 siRNA partially restored cellular proliferation from N130 induction in HeLa cells, whereas the control siRNA did not show any effects on cell growth.

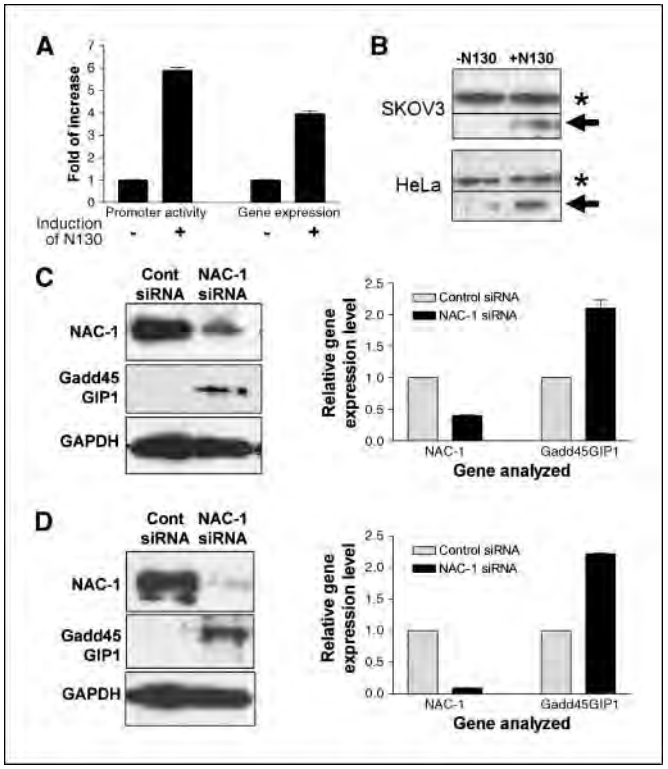

Figure 1. Inactivation of NAC-1 up-regulates Gadd45GIP1 expression. *A,* expression of N130, the dominant negative of NAC-1, enhances the Gadd45GIP1 promoter activity (*left*) and gene transcript level (*right*) in HeLa cells as compared with non-induced controls. The assays were done 48 h after N130 induction, and the data are expressed as the fold increase as normalized to the non-induced group. *B,* Western blots show that N130 expression increases Gadd45GIP1 proteins (*arrows,* ~28 kDa) in both SKOV3 and HeLa cells. Glyceraldehyde-3-phosphate dehydrogenase (GAPDH) was used as the loading control (*, ~37 kDa). *C,* NAC-1 gene knockdown reduces NAC-1, but increases Gadd45GIP1 protein expression (*left*) and mRNA expression (*right*) in HeLa cells. *D,* NAC-1 gene knockdown reduces NAC-1, but increases Gadd45GIP1 protein expression (*left*) and mRNA expression (*right*) in both protein (*left*) and mRNA (*right*) levels in SKOV3 cells. The data of siRNA experiments were obtained 72 h after siRNA treatment and were expressed as fold change as compared with control siRNA-treated cells.

Induction of Gadd45GIP1 expression results in tumor suppression *in vivo*. Based on the above findings, we determined if Gadd45GIP1 expression had a growth-inhibitory effect in tumor formation and development *in vivo*. Tumor xenografts from both SKOV3 and HeLa cell lines were established in the *nu/nu* mouse model. First, we tested if Gadd45GIP1 expression could prevent tumorigenesis by inducing Gadd45GIP1 expression 2 days after s.c. injection of tumor cells. As shown in Fig. 4, induction of Gadd45GIP1 expression almost completely prevented the formation of subcutaneous SKOV3 tumors (Fig. 4*A*) and HeLa tumors (Fig. 4*B*). In contrast, the non-induced cells without Gadd45GIP1 expression grew tumors at all injection sites, which progressively enlarged in size. Representative mice bearing the SKOV3 tumors were shown in Fig. 4*C*. Second, we determined if Gadd45GIP1 could limit tumor growth in established tumors by expressing

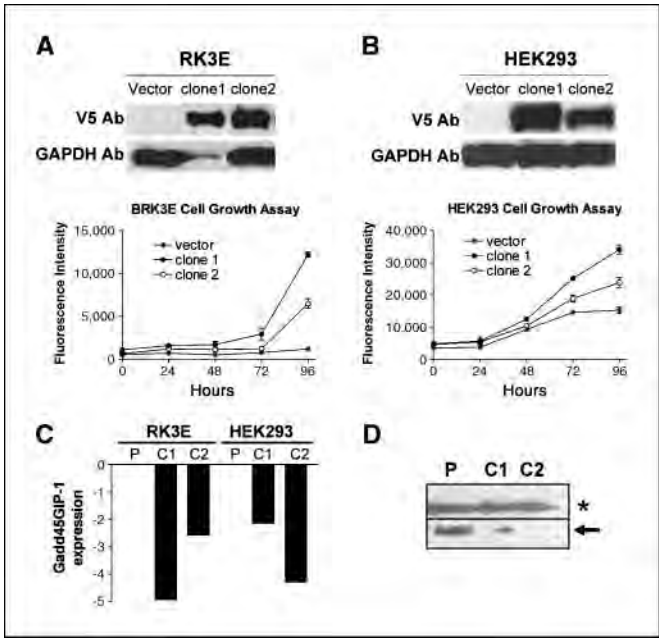

Figure 2. Ectopic expression of NAC-1 increases cellular proliferation and decreases Gadd45GIP1 expression. *A, top,* NAC-1/V5 protein expression from two RK3E clones (*clone 1* and *clone 2*) in Western blot analysis using a V5 antibody. Clone 1 expresses a very high level of NAC-1; therefore, only a small amount of cellular lysate was loaded. GAPDH was used as the loading control. *Bottom,* growth curves of RK3E clones. As compared with vector-transfected clone, cells from both NAC-1 clone 1 and clone 2 show increased proliferation. *B, top,* NAC-1/V5 protein expression from two stable clones of HEK293. *Bottom,* growth curves of HEK293 clones. As compared with vector-transfected clone, cells from both NAC-1 clone 1 and clone 2 show increased proliferation. *C,* quantitative real-time PCR shows reduction of Gadd45GIP1 mRNA levels in NAC-1 clones (*C1* and *C2*) from RK3E and HEK293 cells. *Y*-axis, fold of decrease as compared with parental (*P*) control cells. *D,* Western blot analysis shows a reduced Gadd45GIP1 protein expression (*arrows,* 28 kDa) in both HEK293 clones. GAPDH was used as a loading control (*, 37 kDa).

Gadd45GIP1 9 days after the tumors were formed (30 ± 3.8 mm^3 for SKOV3 tumors and 120 ± 32 mm^3 for HeLa tumors; Supplementary Fig. S3). Five days after discontinuation of doxycyclin, induction of Gadd45GIP1 expression was evidenced by green fluorescence in the subcutaneous tumors in which the tumor cells were previously engineered to express both Gadd45GIP1 and EGFP by a bicistronic promoter. As shown in Supplementary Fig. S3*A*, both SKOV3 and HeLa subcutaneous tumors continued growing in control mice (i.p. injection with doxycyclin), whereas the tumors either stopped growing or decreased in size after Gadd45GIP1 induction (i.p. injection with PBS instead of doxycyclin). The tumor size between induced and non-induced groups was statistically significant ($P < 0.001$) in the end of experiments for both SKOV3 and HeLa cells. Histologic examination of the tumors excised 10 days after Gadd45GIP1 induction revealed extensive apoptosis in tumor cells based on morphology (Supplementary Fig. S3*B*) and immunoreactivity with the M30 antibody, which recognizes an apoptosis-specific caspase-cleaved cytokeratin epitope (refs. 21, 22; Supplementary Fig. S3*C*).

Discussion

Using LongSAGE as a discovery tool and real-time PCR as a validation method, we identified and validated seven genes that were up-regulated after NAC-1 inactivation by the dominant negative NAC-1 (N130) but were unable to validate any genes that were down-regulated by NAC-1 inactivation, a finding consistent with transcription repressor roles of the BTB/POZ family members (23, 24). The demonstration of Gadd45GIP1 as one of the downstream effectors that are negatively regulated by NAC-1 is of great interest. Gadd45GIP1, also known as CRIF1 (17), interacts with the growth arrest and DNA damage–inducible protein 45 (Gadd45) family, which plays an important role in genomic stability, DNA repair, cell cycle regulation, and apoptosis (25–27). It has been previously reported that Gadd45GIP1 expression is detected in normal tissues, including thyroid, heart, lymph node, trachea, and adrenal glands, and its expression level is lower in neoplastic tissues, including adrenal adenomas and papillary thyroid carcinoma (17). Gadd45GIP1 co-localized with Gadd45γ in the nuclei, and recombinant Gadd45GIP1 proteins inhibited histone H1 kinase activity of immunoprecipitated Cdc2/cyclin B1 and Cdk2/cyclin E. The inhibitory effects were synergistic by Gadd45 proteins. In addition, Gadd45GIP1 interacts with the

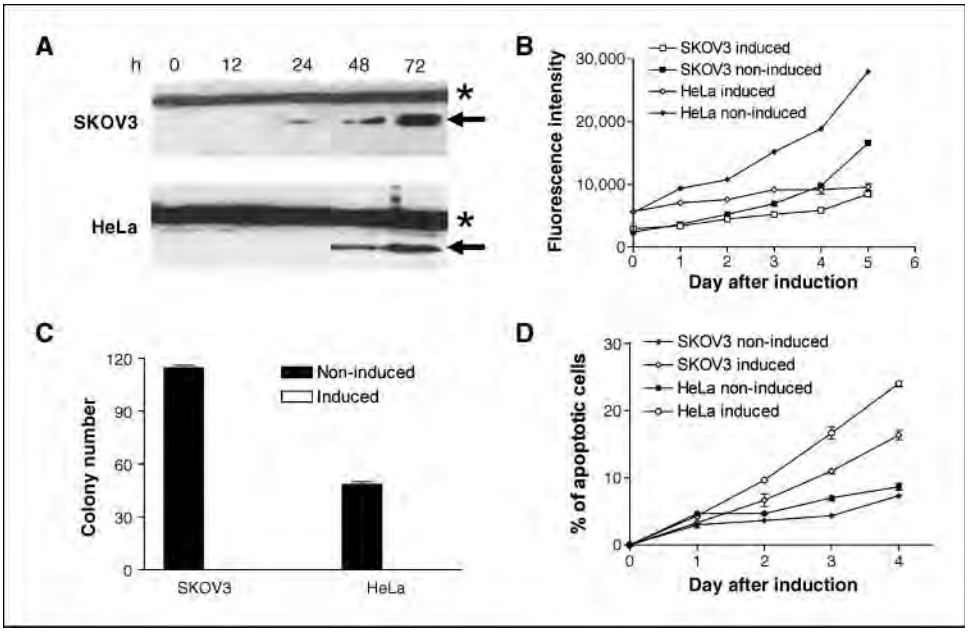

Figure 3. Effects of Gadd45GIP1 on cells with NAC-1 expression. *A,* Western blot analysis shows increasing protein level of Gadd45GIP1 (*arrows,* 28 kDa) in both SKOV3 and HeLa cells after induction. GAPDH was used as the loading control (*, 37 kDa). *B,* cell growth curves show that after induction of Gadd45GIP1 by removing doxycyclin from culture medium, cell growth in both SKOV3 and HeLa cells is significantly suppressed as compared with the non-induced cells (with doxycyclin in the medium). *C,* colony formation is significantly reduced in Gadd45GIP1-induced SKOV3 and HeLa cells. There are essentially no colonies detected in the induced groups. *D,* percentage of apoptotic cells are determined by counting annexin V–positive cells in both Gadd45GIP1-induced and non-induced SKOV3 and HeLa cells. A time-dependent increase in apoptotic cells is observed in Gadd45GIP1-induced cells.

Orphan nuclear receptor, Nur77, and inhibits its transactivation (28). Biologically, overexpression of Gadd45GIP1 inhibited cellular proliferation in NIH3T3 cells, and Gadd45GIP1 gene knockdown led to the inactivation of the Rb pathway (17).

The evidence to support a direct role of NAC-1 in regulating expression of Gadd45GIP1 in this study came from the findings based on two experimental systems. First, inactivation of NAC-1 either by dominant negative NAC-1 (N130) expression or RNA interference enhanced Gadd45GIP1 promoter activity and gene expression levels. Second, engineered expression of NAC-1 inhibited Gadd45GIP1 expression in cells without detectable NAC-1 expression. In this study, we observed that ectopic expression of Gadd45GIP1 proteins in NAC-1–expressing tumor cells was associated with growth suppression in both *in vitro* and *in vivo* systems, a finding consistent with a previous report demonstrating Gadd45GIP1-induced growth inhibition in NIH3T3 cells (17). Furthermore, Gadd45GIP1 gene knockdown could partially rescue NAC-1 dominant negative (N130)–induced growth suppression, suggesting that additional factors other than Gadd45G1P1 are required for NAC1-mediated increase in cell proliferation. The above results suggest that NAC-1 mediates its function in maintaining cell proliferation and survival at least in part through the inhibition of Gadd45GIP1 expression. Although this is the interpretation that we favor, other alternatives should be considered. For example, it is possible that Gadd45GIP1, which was the focus in this study, may not be the only downstream target that is regulated by NAC-1. Our LongSAGE data provide a list of candidate markers (Table 1) for future exploration to determine if there is a synergistic or additive effect between Gadd45GIP1 and other genes in mediating NAC-1 function.

This report also suggests that the NAC-1-Gadd45GIP1 is involved in a protein network that sustains a survival signal to cancer cells. Figure 5 is a simplified scheme to illustrate that survival signals from two oncogenic pathways converge to one of the molecular hubs, which is the Gadd45/Gadd45GIP1. nuclear factor-κB (NF-κB) is a multifunctional protein, and the NF-κB pathway represents a well-known surviving signal in cancer. For example, inhibition of NF-κB sensitizes ovarian cancer cells to cisplatin and paclitaxel-induced apoptosis (29, 30). Upon activation, NF-κB translocates to nuclei and is associated with c-myc up-regulation, which in turn down-regulates Gadd45 proteins (31–33). Gadd45 interacts with Gadd45GIP1 and up-regulates MKK4 through mitogen-activated protein kinase kinase kinase 4/MTK1 activation (34), and Gadd45 has been shown as a functional tumor suppressor (35). The enhanced MKK4 activity activates the proapoptotic c-jun-NH_2-kinase (JNK)/p38 signaling, which results in growth arrest and apoptosis (32, 36, 37). Therefore, during tumor development, turning off the Gadd45 pathway seems to be critical for cancer cells to survive under cellular stress and to facilitate tumor growth. In this study, we propose that in addition to the established NF-κB–c-myc–Gadd45 pathway, down-regulation of Gadd45GIP1 by NAC-1 overexpression represents another molecular switch to turn off the Gadd45 death signals (Fig. 5). Gadd45GIP1 has been shown to directly bind to all Gadd45 isoforms, and more importantly, the interaction between Gadd45GIP 1 and Gadd45 members enhances the Gadd45 function in a cell culture system (17). Therefore, NAC-1 contributes to tumor progression by suppressing Gadd45GIP1 expression, thus inhibiting Gadd45 activity, preventing activation of MKK4 and proapoptotic p38/JNK activity.

It is likely that in the evolution of cancer cell species, tumor cells acquire multiple strategies to inactivate the Gadd45 cell suppressor signaling. In fact, overexpression of NF-κB (29, 30), gene amplification and transcription up-regulation of *c-myc* (38–40), and *Gadd45* promoter methylation (35, 41, 42) have been reported in human cancers, including ovarian cancer cells. Furthermore, our recent study also showed that homozygous deletion and down-regulation of MKK-4 were detected in ovarian carcinomas (43). The above data, together with the results reported in this study,

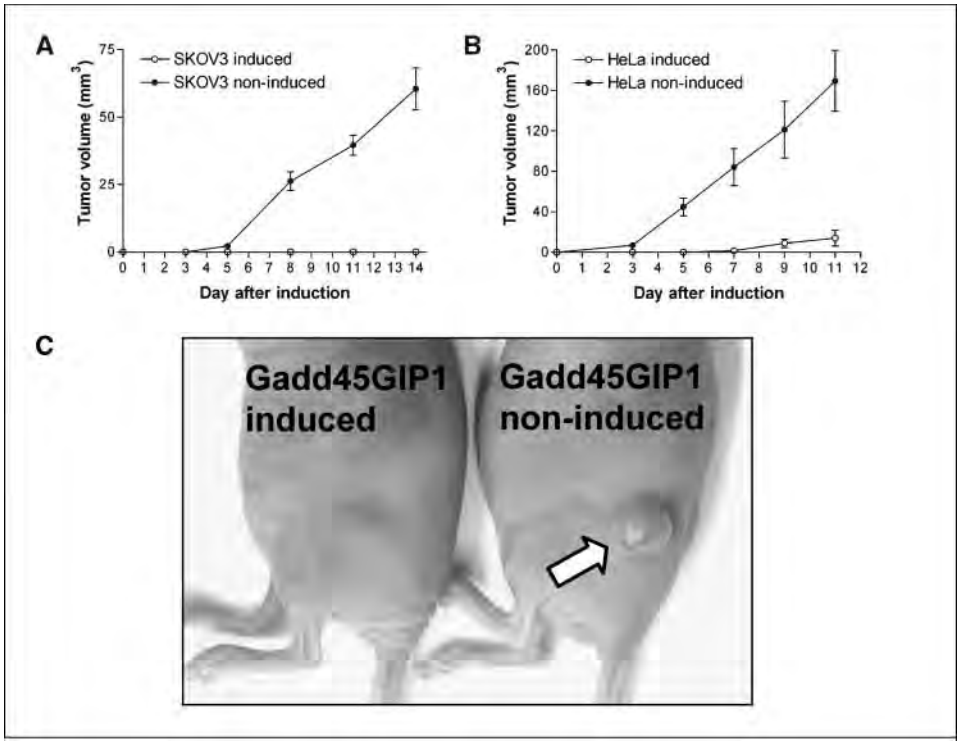

Figure 4. The *in vivo* effects of Gadd45GIP1 expression in SKOV3 and HeLa xenografts. *A,* induction of Gadd45GIP1 expression in SKOV3 cancer cells completely prevents tumor formation in all eight *nu/nu* mice (○), whereas the tumor volumes continue increasing in non-induced control group (●). *B,* induction of Gadd45GIP1 expression in HeLa cells almost completely prevents tumor formation in eight *nu/nu* mice (○), whereas the tumor volumes continue increasing in the non-induced control group (●). *C,* representative mouse from Gadd45GIP1-induced and non-induced group. No visible or palpable tumor can be detected in Gadd45GIP1-induced mouse, whereas a discrete subcutaneous tumor (*arrow*) is detected in a non-induced control mouse. The photograph was taken 14 d after Gadd45GIP1 induction.

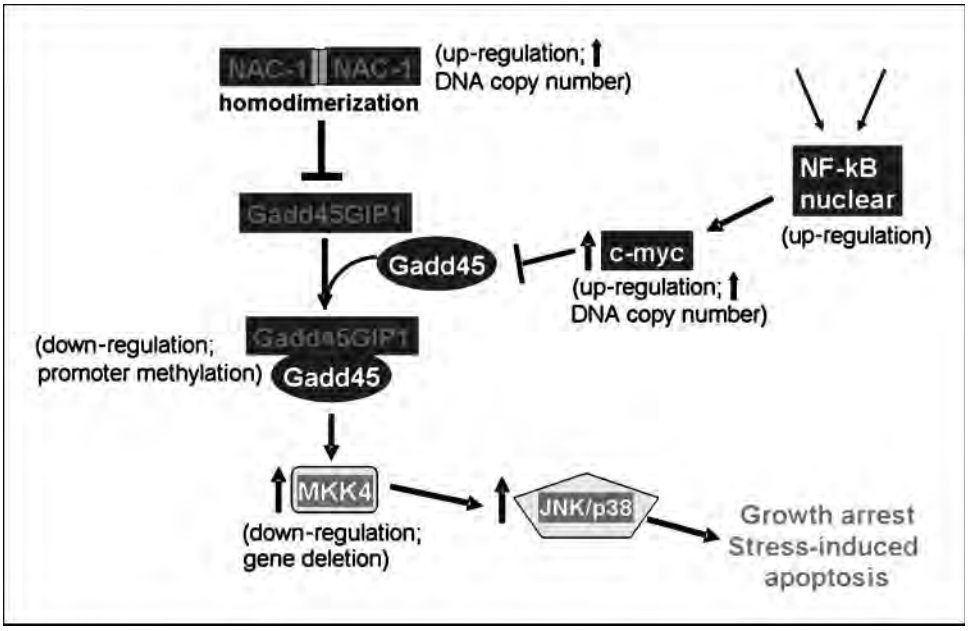

Figure 5. A simplified scheme to illustrate the participation of NAC-1/Gadd45GIP1 in the Gadd45 tumor suppressor pathway. Escape from the Gadd45 tumor suppressor pathway is important for tumor cells to survive especially under a cellular stress such as hypoxia and the presence of chemotherapeutic agents. It has been known that NF-κB/c-myc inactivates Gadd45. As shown in this study, down-regulation of Gadd45GIP1 by overexpression and homodimerization of a transcription repressor, NAC-1, represents another molecular switch to turn off the Gadd45 cell death pathway. Cancer cells thus evolve to evade Gadd45/Gadd45GIP1-induced growth arrest and apoptosis by several molecular mechanisms affecting different genes as highlighted in parenthesis beside the gene names. The green boxes of NAC-1 molecule indicate the BTB/POZ domain.

suggest that cancer cells may likely employ at least a dual molecular system to switch off the Gadd45-mediated growth suppression and apoptosis, i.e., the NF-κB/c-myc/Gadd45 pathway and the NAC-1/Gadd45GIP1 pathway. This hypothesis can explain the clinical findings we observed in which NAC-1 is overexpressed in post-chemotherapy–recurrent tumor samples as compared with the primary untreated specimens and also highlights the critical role of inactivating the Gadd45 pathway in tumor development.

Cancer mortality and morbidity are mainly related to recurrent diseases. Because NAC-1 has been shown to be more frequently overexpressed in recurrent chemoresistant ovarian carcinomas then in the primary untreated counterparts, the findings from the current study may have clinical implications. For example, Gadd45GIP1 expression resulted in the inhibition of cellular proliferation *in vitro* and suppression of tumor growth in mice. Therefore, Gadd45GIP1 can be further studied as a new therapeutic target in which Gadd45GIP1 can be combined with N130 in treating tumors with NAC-1 overexpression. Targeting both NAC-1 and Gadd45GIP1 at the same time may provide a more effective therapy because tumor resistance may likely develop after targeting single agents.

In conclusion, the results from this study show that Gadd45GIP1 expression is negatively regulated by NAC-1, a transcription repressor. Induction of Gadd45GIP1 expression leads to growth suppression in tumor cells with NAC-1 overexpression. Therefore, NAC-1 contributes to tumor growth and survival by inhibiting Gadd45GIP1 expression, which has a tumor suppressor effect in cancer cells. Our observations provide new molecular insight into how NAC-1 proteins contribute to tumor development and suggest that enhancing Gadd45GIP1 expression can be a new potential therapeutic approach in human cancer.

Acknowledgments

Received 4/12/2007; revised 6/16/2007; accepted 6/27/2007.

Grant support: U.S. Department of Defense (OC0400600) and NIH (CA103937).

The costs of publication of this article were defrayed in part by the payment of page charges. This article must therefore be hereby marked *advertisement* in accordance with 18 U.S.C. Section 1734 solely to indicate this fact.

References

1. Stogios PJ, Downs GS, Jauhal JJ, Nandra SK, Prive GG. Sequence and structural analysis of BTB domain proteins. Genome Biol 2005;6:R82.
2. Bardwell VJ, Treisman R. The POZ domain: a conserved protein-protein interaction motif. Genes Dev 1994;8:1664–77.
3. Albagli O, Dhordain P, Deweindt C, Lecocq G, Leprince D. The BTB/POZ domain: a new protein-protein interaction motif common to DNA- and actin-binding proteins. Cell Growth Differ 1995;6:1193–8.
4. Lemercier C, Brocard MP, Puvion-Dutilleul F, Kao HY, Albagli O, Khochbin S. Class II histone deacetylases are directly recruited by BCL6 transcriptional repressor. J Biol Chem 2002;277:22045–52.
5. Wong CW, Privalsky ML. Components of the SMRT corepressor complex exhibit distinctive interactions with the POZ domain oncoproteins PLZF, PLZF-RARα, and BCL-6. J Biol Chem 1998;273:27695–702.
6. Dhordain P, Lin RJ, Quief S, et al. The LAZ3(BCL-6) oncoprotein recruits a SMRT/mSIN3A/histone deacetylase containing complex to mediate transcriptional repression. Nucleic Acids Res 1998;26:4645–51.
7. Huynh KD, Fischle W, Verdin E, Bardwell VJ. BCoR, a novel corepressor involved in BCL-6 repression. Genes Dev 2000;14:1810–23.
8. Chen Z, Brand NJ, Chen A, et al. Fusion between a novel Kruppel-like zinc finger gene and the retinoic acid receptor-α locus due to a variant t(11;17) translocation associated with acute promyelocytic leukaemia. EMBO J 1993;12:1161–7.
9. Polo JM, Dell'Oso T, Ranuncolo SM, et al. Specific peptide interference reveals BCL6 transcriptional and oncogenic mechanisms in B-cell lymphoma cells. Nat Med 2004;10:1329–35.
10. Yeyati PL, Shaknovich R, Boterashvili S, et al. Leukemia translocation protein PLZF inhibits cell growth and expression of cyclin A. Oncogene 1999;18:925–34.
11. Maeda T, Hobbs RM, Merghoub T, et al. Role of the proto-oncogene *Pokemon* in cellular transformation and ARF repression. Nature 2005;433:278–85.
12. Maeda T, Hobbs RM, Pandolfi PP. The transcription factor Pokemon: a new key player in cancer pathogenesis. Cancer Res 2005;65:8575–8.
13. van Roy FMMcCrea PD. A role for Kaiso-p120ctn complexes in cancer? Nat Rev Cancer 2005;5:956–64.
14. Park JI, Kim SW, Lyons JP, et al. Kaiso/p120-catenin and TCF/β-catenin complexes coordinately regulate canonical Wnt gene targets. Dev Cell 2005;8:843–54.
15. Nakayama K, Nakayama N, Davidson B, et al. A BTB/POZ protein, NAC-1, is related to tumor recurrence and is essential for tumor growth and survival. Proc Natl Acad Sci U S A 2006;103:18739–44.
16. Wang J, Rao S, Chu J, et al. A protein interaction network for pluripotency of embryonic stem cells. Nature 2006;444:364–8.
17. Chung HK, Yi YW, Jung NC, et al. CR6-interacting factor 1 interacts with Gadd45 family proteins and modulates the cell cycle. J Biol Chem 2003;278:28079–88.

18. Saha S, Sparks AB, Rago C, et al. Using the transcriptome to annotate the genome. Nat Biotechnol 2002;20:508–12.
19. Buckhaults P, Zhang Z, Chen YC, et al. Identifying tumor origin using a gene expression-based classification map. Cancer Res 2003;63:4144–9.
20. Shih Ie M, Sheu JJ, Santillan A, et al. Amplification of a chromatin remodeling gene, Rsf-1/HBXAP, in ovarian carcinoma. Proc Natl Acad Sci U S A 2005;102:14004–9.
21. Leers M, Kolgen W, Bjorklund V, et al. Immunocytochemical detection and localization of a cytokeratin 18 epitope exposed during early apoptosis. J Pathol 1999;5: 567–72.
22. Caulin C, Salvesen GS, Oshima RG. Caspase cleavage of keratin 18 and reorganization of intermediate filaments during epithelial cell apoptosis. J Cell Biol 1997;138:1379–94.
23. Mackler SA, Korutla L, Cha XY, et al. NAC-1 is a brain POZ/BTB protein that can prevent cocaine-induced sensitization in the rat. J Neurosci 2000;20:6210–7.
24. Mackler SA, Homan YX, Korutla L, Conti AC, Blendy JA. The mouse nac1 gene, encoding a cocaine-regulated Bric-a-brac Tramtrac Broad complex/Pox virus and Zinc finger protein, is regulated by AP1. Neuroscience 2003; 121:355–61.
25. Smith ML, Chen IT, Zhan Q, et al. Interaction of the p53-regulated protein Gadd45 with proliferating cell nuclear antigen. Science 1994;266:1376–80.
26. Zhang W, Bae I, Krishnaraju K, et al. CR6: A third member in the MyD118 and Gadd45 gene family which functions in negative growth control. Oncogene 1999;18: 4899–907.
27. Wang XW, Zhan Q, Coursen JD, et al. GADD45 induction of a G_2-M cell cycle checkpoint. Proc Natl Acad Sci U S A 1999;96:3706–11.
28. Park KC, Song KH, Chung HK, et al. CR6-interacting factor 1 interacts with orphan nuclear receptor Nur77 and inhibits its transactivation. Mol Endocrinol 2005;19: 12–24.
29. Mabuchi S, Ohmichi M, Nishio Y, et al. Inhibition of NFκB increases the efficacy of cisplatin in *in vitro* and *in vivo* ovarian cancer models. J Biol Chem 2004;279: 23477–85.
30. Liu GH, Wang SR, Wang B, Kong BH. Inhibition of nuclear factor-κB by an antioxidant enhances paclitaxel sensitivity in ovarian carcinoma cell line. Int J Gynecol Cancer 2006;16:1777–82.
31. Tang G, Minemoto Y, Dibling B, et al. Inhibition of JNK activation through NF-κB target genes. Nature 2001; 414:313–7.
32. De Smaele E, Zazzeroni F, Papa S, et al. Induction of gadd45β by NF-κB downregulates pro-apoptotic JNK signalling. Nature 2001;414:308–13.
33. Zerbini LF, Wang Y, Czibere A, et al. NF-κ B–mediated repression of growth arrest- and DNA-damage-inducible proteins 45α and γ is essential for cancer cell survival. Proc Natl Acad Sci U S A 2004;101: 13618–23.
34. Mita H, Tsutsui J, Takekawa M, Witten EA, Saito H. Regulation of MTK1/MEKK4 kinase activity by its N-terminal autoinhibitory domain and GADD45 binding. Mol Cell Biol 2002;22:4544–55.
35. Ying J, Srivastava G, Hsieh WS, et al. The stress-responsive gene GADD45G is a functional tumor suppressor, with its response to environmental stresses frequently disrupted epigenetically in multiple tumors. Clin Cancer Res 2005;11:6442–9.
36. Zerbini LFLibermann TA. Life and death in cancer. GADD45α and γ are critical regulators of NF-κB mediated escape from programmed cell death. Cell Cycle 2005;4:18–20.
37. Verheij M, Bose R, Lin XH, et al. Requirement for ceramide-initiated SAPK/JNK signalling in stress-induced apoptosis. Nature 1996;380:75–9.
38. Baker VV, Borst MP, Dixon D, Hatch KD, Shingleton HM, Miller D. c-myc amplification in ovarian cancer. Gynecol Oncol 1990;38:340–2.
39. Abeysinghe HR, Cedrone E, Tyan T, Xu J, Wang N. Amplification of C-MYC as the origin of the homogeneous staining region in ovarian carcinoma detected by micro-FISH. Cancer Genet Cytogenet 1999;114:136–43.
40. Dimova I, Raitcheva S, Dimitrov R, Doganov N, Toncheva D. Correlations between c-myc gene copy-number and clinicopathological parameters of ovarian tumours. Eur J Cancer 2006;42:674–9.
41. Zerbini LFLibermann TA. GADD45 deregulation in cancer: frequently methylated tumor suppressors and potential therapeutic targets. Clin Cancer Res 2005;11: 6409–13.
42. Qiu W, Zhou B, Zou H, et al. Hypermethylation of growth arrest DNA damage-inducible gene 45β promoter in human hepatocellular carcinoma. Am J Pathol 2004;165:1689–99.
43. Nakayama K, Nakayama N, Davidson B, et al. Homozygous deletion of MKK4 in ovarian serous carcinoma. Cancer Biol Ther 2006;5:630–4.

Int J Gynecol Cancer 2008, **18,** 487–491

Assessment of *TP53* mutation using purified tissue samples of ovarian serous carcinomas reveals a higher mutation rate than previously reported and does not correlate with drug resistance

R. SALANI*, R.J. KURMAN*†, R. GIUNTOLI, II*, G. GARDNER*, R. BRISTOW*, T.-L. WANG* & I.-M. SHIH*†

**The Kelly Gynecologic Oncology Service, Department of Gynecology and Obstetrics, The Sidney Kimmel Comprehensive Cancer Center, The Johns Hopkins Medical Institutions, Baltimore, Maryland and †Division of Gynecologic Pathology, Department of Pathology, The Johns Hopkins Hospital, Baltimore, Maryland*

Abstract. Salani R, Kurman RJ, Giuntoli R, II, Gardner G, Bristow R, Wang T-L, Shih I-M. Assessment of *TP53* mutation using purified tissue samples of ovarian serous carcinomas reveals a higher mutation rate than previously reported and does not correlate with drug resistance. *Int J Gynecol Cancer* 2008;**18:**487–491.

The *TP53* mutation frequency in ovarian serous carcinomas has been reported to range between 50% and 80%, but a stringent analysis of *TP53* using purified epithelial samples has not yet been performed to accurately assess the mutation frequency and to correlate it with the histologic grade. The purpose of this study was to assess the *TP53* mutational profile in a relatively large series of high-grade (53 primary and 18 recurrent) and 13 low-grade ovarian serous tumors using DNA isolated from affinity-purified tumor cells and to correlate it with *in vitro* drug resistance. All samples were affinity purified, and the tumor DNA was analyzed for *TP53* mutations in exons 4–9. *In vitro* drug resistance assays to carboplatin, cisplatin, paclitaxel, and taxotere were performed on the same tumor samples and correlated with the *TP53* mutation status. *TP53* mutations were detected in 57 (80.3%) of 71 high-grade carcinomas and in one (7.8%) of 13 low-grade serous tumors (an invasive low-grade serous carcinoma). The mutations were predominantly missense mutations (59.6%). *TP53* mutations were associated with high-grade serous carcinomas and recurrent disease ($P < 0.0001$). There was no statistically significant correlation between *TP53* mutation status and drug resistance assays or clinical stage ($P > 0.25$). The frequency of *TP53* mutations using purified tumor DNA from ovarian serous carcinomas was 80.3%, which is much higher than previously reported. Furthermore, we found that *TP53* is not directly involved in the development of drug resistance in high-grade ovarian serous carcinomas.

KEYWORDS: drug resistance assays, serous ovarian carcinomas, *TP53* mutation.

Ovarian carcinoma is the most lethal gynecological malignancy in the United States. Despite an initial response to primary treatment, the vast majority of ovarian carcinomas recur and eventually result in death. It has been thought that the high mortality of ovarian carcinoma is a direct result of resistance to chemotherapeutic agents. In an effort to maximize chemotherapeutic effects and minimize side effects, *in vitro* assays that measure extreme drug resistance have been developed to determine the sensitivity of specific drugs on individual tumors. It has been reported that the accuracy of this assay for predicting chemoresponsiveness is better than 90%[(1)].

Although it has been thought that somatic mutations of *TP53* could be involved in drug resistance[(2)], studies addressing this issue have been conflicting. For example, it was reported that tumors with *TP53* mutations were more responsive to paclitaxel, whereas other studies have reported that tumors with

Address correspondence and reprint requests to: Ritu Salani, MD, 600 N Wolfe Street, Phipps 281, Baltimore, MD 21287, USA. Email: rsalani1@jhmi.edu

Presented at the International Gynecologic Cancer Society 2006 Annual Meeting and awarded Best Abstract presentation.

doi:10.1111/j.1525-1438.2007.01039.x

TP53 mutations were less sensitive to platinum-based chemotherapy[3–6]. On the other hand, other reports have failed to demonstrate any relationship between *TP53* mutation and chemoresistance[7–9]. The purpose of the present study was to reassess this critical issue using nucleotide sequencing on affinity-purified ovarian tumor cells on a relatively large number of specimens. We focused our analysis on high-grade serous carcinoma because this is the most common and most aggressive ovarian cancer. Tumor recurrence is multifactorial and is influenced by a variety of factors including residual tumor volume after cytoreductive surgery, emergence of chemoresistant tumor subclones, and the acquisition of new malignant phenotypes, for example, enhanced proliferation and escape of immune surveillance during tumor progression. Accordingly, rather than using tumor recurrence as the outcome measure, *TP53* mutation status was correlated with *in vitro* drug resistance assays.

Materials and methods

Tissue selection and processing

All tumor specimens were collected from The Kelly Gynecologic Oncology Service at The Johns Hopkins Hospital between November 2003 and March 2006. Approval to conduct this study was obtained from The Johns Hopkins Medical Institutional Review Board. All specimens were anonymous. We analyzed 71 consecutive high-grade ovarian serous carcinomas and 12 low-grade serous tumors (three serous borderline tumors, five intraepithelial low-grade carcinomas, and four invasive low-grade carcinomas). The method of isolation and affinity purification of tumor cells from fresh tumor samples has been previously described[10]. Briefly, fragments of high-grade carcinoma were first minced into small pieces ($\sim$1 mm^3) and digested with collagenase A (2 mg/mL) at 37°C for 40 min. After removing the undigested tissue fragments, the digested specimen containing single tumor cells and small tumor cell clusters was collected, washed in cold phosphate-buffered saline and immunosorted using an anti-Ep-CAM antibody bound to Dynabeads Epithelial Enrich (Dynal Biotech, Oslo, Norway) according to manufacturer's instructions. Samples were evaluated and estimated to be >97% pure. Genomic DNA was purified using the Qiagen DNA blood mini kit (Qiagen, Valencia, CA).

Drug resistance assays

The results of *in vitro* drug resistance assays for carboplatin, cisplatin, paclitaxel, and docetaxel were obtained from the patients' clinical records. For this assay, a small piece of fresh tumor tissue was sent to Oncotech, Inc. (Tustin, CA) for *in vitro* drug resistance assays. Drug sensitivity was determined by an agar-based cell culture system with radioactive thymidine incorporation as the end point. The protocol of the assay has been detailed at http://www.oncotech.com/innovation/PublicationDetails.asp?id=28. There were 60 cases in which the results of this assay were available for the correlation with the *TP53* mutational status. Drug resistance was classified as follows: 1) low if tumor cells were inhibited by the tested agent and demonstrated less than median growth, 2) intermediate if there was moderate tumor growth, and 3) extreme if tumor cell growth was virtually unaffected by the chemotherapeutic agent. As in previous reports, in this study extreme drug resistance was interpreted as drug resistant, and the intermediate and low drug resistance were interpreted as drug sensitive[1,11].

Mutational analysis

The genomic DNA isolated from the enriched tumor samples was analyzed for sequence mutations of the *TP53* using primers for exons 4–9. The polymerase chain reaction (PCR) sequencing primers are listed in Table 1. PCR was first performed using the following protocol. An aliquot of 1 μL of the purified DNA was used in a 25 μL PCR mixture containing PCR buffer, 10 μM deoxyribonucleotide triphosphate, and 0.25 U/μL Platinum Taq (Invitrogen, Carlsbad, CA). The PCR protocol was as follows: denaturation for 2 min at 94°C followed by 35 cycles of denaturation at 94°C for 30 sec, annealing at 57°C for 30 sec, and extension at 70°C for 5 min. The PCR products were then purified followed by sequencing reactions (Agencourt Inc., Beverly, MA). The nucleotide sequences were then analyzed using the Mutation Surveyor program (Soft Genetics LLC, State College, PA). The sequencing data were analyzed by two investigators independently. To confirm the mutations, we resequenced the exons with p53 mutations using reverse primers. The sequence data were filtered out for the well-known *TP53* polymorphism at codon 72 (Arg/Pro), which was not considered as a mutation in this study.

Statistical analysis

Statistical analysis was performed using the standard Chi-square test to determine if *TP53* mutations correlated with tumor grade and drug resistance assays.

Table 1. Nucleotide sequences of primers used in the study

Exon	Forward primer	Reverse primer
4	5′-ACCTGGTCCTCTGACTGCT-3′	5′-CCCAAGTTCCAAACAAAAGA-3′
4S[a]	5′-AAGAATGCAGGGGGATACG-3′	
5	5′-GGTGCTTAGCATGTTTGTTTC-3′	5′-GGCCAGACCTAAGAGCAATCAG-3′
5S[a]	5′-GCCGTCTTCCAGTTGCTTTA-3′	
6	5′-CATGAGCGCTGCTCAGATAG-3′	5′-TTGCACATCTCATGGGGTTA-3′
6S[a]	5′-GAGAGACGACAGGGCTGGTT-3′	
7	5′-CGACAGAGCGAGATTCCATC-3′	5′-TGGAAGAAATCGGTAAGAGGTG-3′
7S[a]	5′-CTGCTTGCCACAGGTCTCC-3′	
8 and 9	5′-GGTGGTTGGGAGTAGATGGA-3′	5′-AAGAAAACGGCATTTTGAGTG-3′
8 and 9S[a]	5′-ATGGGACAGGTAGGACCTGATT-3′	

[a]Indicates sequencing primer.

Results

A total of 71 high-grade ovarian serous carcinomas and 13 low-grade tumors were evaluated in this study. The median age of the patients with high-grade serous carcinoma and low-grade serous tumors (invasive low-grade micropapillary serous carcinoma and serous borderline tumor) was 61.5 years (range 36–88 years) and 45.3 years, respectively. Fifty-three specimens were collected at the time of primary cytoreduction and 18 were obtained at the time of secondary cytoreductive surgery. Functional mutations were defined as any somatic changes in nucleotide sequence that led to structural changes of the encoded p53 protein. Of the 71 high-grade carcinomas, 57 (80.3%) demonstrated *TP53* mutations. All the mutations are listed in Table 2 after screening for all known polymorphisms of the *TP53* gene using the database from the International Agency for Research on Cancer[12]. In contrast, of the 13 low-grade tumors, only one *TP53* mutation was detected (an invasive low-grade micropapillary serous carcinoma [1 bp deletion at 212]). The mutations in high-grade serous carcinomas were grouped as follows: 3 splice site mutations (5.3%), 7 nonsense mutations (12.3%), 1 insertion and 12 deletions (22.8%), and 34 missense mutations (59.6%). Representative chromatograms are shown in Figure 1. Seven mutations were on exon 4, 14 mutations on exon 5, 15 mutations on exon 6, 14 mutations on exon 7, 6 mutations on exon 8, and 1 mutation on exon 9. Accordingly, the majority (>98%) of mutations were located in exons 4–8 which correspond to the highly conserved DNA-binding domain of the *TP53* protein. The difference in the *TP53* mutation frequency comparing high-grade and low-grade tumors is highly significant ($P < 0.0001$, Chi-square test).

The data for *in vitro* drug resistance assays were available on 60 patients. Of these, 44 were from primary cytoreduction samples and 16 from cytoreductive surgery for recurrent tumors. Fifty tumors harbored *TP53* mutations and ten contained wild-type *TP53*. The drug resistance patterns were analyzed according to the locations of the mutations, that is, the exon involved in the mutation, and the types of mutations including deletion/insertion, missense, nonsense or splice site mutations. We were unable to find any statistically significant association between the *TP53* mutational status and the drug resistance assays for carboplatin ($P > 0.8$), cisplatin ($P = 0.58$), paclitaxel ($P = 0.26$), and docetaxel ($P = 0.62$).

Discussion

We have previously proposed a dualistic model for the development of ovarian carcinoma in which mutation of p53 plays an important role. In that model, ovarian carcinomas are broadly divided into two categories designated type I and type II, which correspond to two main pathways of tumorigenesis. Type I tumors are composed of low-grade micropapillary serous carcinomas, mucinous carcinomas, endometrioid carcinomas, malignant Brenner tumors, and clear cell carcinomas[13]. With the exception of clear cell carcinoma which is typically high-grade, they tend to be low-grade neoplasms that arise in a stepwise fashion from borderline tumors. Mutation of *TP53* is rarely found in these tumors. In contrast, type II tumors are high-grade aggressive neoplasms. Morphologically recognizable precursor lesions have not been identified, and therefore, they have been described as developing "*de novo*"[14]. Mutation of p53 has been frequently detected in these tumors. Thus, the high frequency (80.3%) of *TP53* mutations in high-grade serous carcinomas and rare mutations in low-grade serous tumors (7.7%) as reported in this study further supports this dualistic model.

Table 2. *TP53* mutation status in high-grade ovarian serous carcinomas

Case no.	Mutated exon	Nucleotide change	Amino acid change
HG1	E4	3′Intron-1st bp G to A	Splicing site
HG2	E4	136-1 bp insertion	46; Insertion
HG3	E4	159; TGG to TGA	53; W to stop
HG4	E4	159; TGG to TGA	53; W to stop
HG5	E4	264-1 bp deletion	89; deletion
HG6	E4	400; TTT to GTT	134; F to V
HG7	E5	5′Intron-1st bp G to T	Splicing site
HG8	E5	416-1 bp deletion	139; deletion
HG9	E5	434; CTG to CGG	145; L to R
HG10	E5	438; TGG to TGA	147; W to stop
HG11	E5	452; CCC to CAC	151; P to H
HG12	E5	466-486-21 bp deletion	156-172; deletion
HG13	E5	468-469-2 bp deletion	156; deletion
HG14	E5	488; TAC to TGC	163; Y to C
HG15	E5	488; TAC to TGC	163; Y to C
HG16	E5	517; GTG to ATG	173; V to M
HG17	E5	524; CGC to CAC	175; R to H
HG18	E5	524; CGC to CAC	175; R to H
HG19	E5	524; CGC to CAC	175; R to H
HG20	E5	524; CGC to CAC	175; R to H
HG21	E6	566-581-16 bp deletion	189-194; Deletion
HG22	E6	568; CGG to TGG	190; R to W
HG23	E6	568; CGG to TGG	190; R to W
HG24	E6	578; CAT to CGT	193; H to R
HG25	E6	581; CTT to CGT	194; L to R
HG26	E6	584; ATC to ACC	195; I to T
HG27	E6	596; AGG to ATG	199; R to M
HG28	E6	614; TAT to TGT	205; Y to C
HG29	E6	625-626-2 bp deletion	209; Deletion
HG30	E6	637; CGA to TGA	213; R to stop
HG31	E6	638; CGA to CTA	213; R to L
HG32	E6	641; CAT to CGT	214; H to R
HG33	E6	643; AGT to CGT	215 S to R
HG34	E6	647- 1 bp deletion	216; Deletion
HG35	E6	653; GTG to GAG	218; V to Q
HG36	E6	659; TAT to TGT	220; Y to C
HG37	E7	5′ Intron-2nd bp A to G	Splicing site
HG38	E7	686-687-2bp deletion	229; Deletion
HG39	E7	712; TGT to AGT	238; C to S
HG40	E7	715; AAC to TAC	239; N to Y
HG41	E7	723- TCC to TTC	239; S to F
HG42	E7	723-1 bp deletion	241; Deletion
HG43	E7	742; CGG to TGG	248; R to W
HG44	E7	742; CGG to TGG	248; R to W
HG45	E7	742; CGG to TGG	248; R to W
HG46	E7	742; CGG to TGG	248; R to W
HG47	E7	743; CGG to CAG	248; R to Q
HG48	E7	747; AGG to AGT	249; R to S
HG49	E7	772-782-11 bp deletion	258-261; Deletion
HG50	E7	777; GAT to GTT	259; D to V
HG51	E8	783-791-9 bp deletion	262-264; Deletion
HG52	E8	809; TTT to TGT	270; F to C
HG53	E8	818; CGT to CAT	272; R to H
HG54	E8	880; GAG to TAG	293; E to stop
HG55	E8	880; GAG to TAG	293; E to stop
HG56	E8	916; CGA to TGA	306; R to stop
HG57	E9	964-1 bp deletion	322; Deletion
HG58		WT	
HG59		WT	
HG60		WT	
HG61		WT	
HG62		WT	
HG63		WT	
HG64		WT	
HG65		WT	
HG66		WT	
HG67		WT	
HG68		WT	
HG69		WT	
HG70		WT	
HG71		WT	

The higher frequency of *TP53* mutations in high-grade serous carcinomas in this study compared to previous reports can be explained by the approaches that were used in this study, particularly the use of affinity-purified tumor cells. Contamination of DNA in tumor samples by stromal cells can significantly reduce the sensitivity of mutation detection. Furthermore, sequencing of DNA obtained from paraffin-embedded tissues is prone to sequencing artifacts. This study illustrates the importance of using enriched fresh tumor samples for molecular genetic analysis to accurately assess the frequency of genetic alterations. Approximately 20% of high-grade serous carcinomas

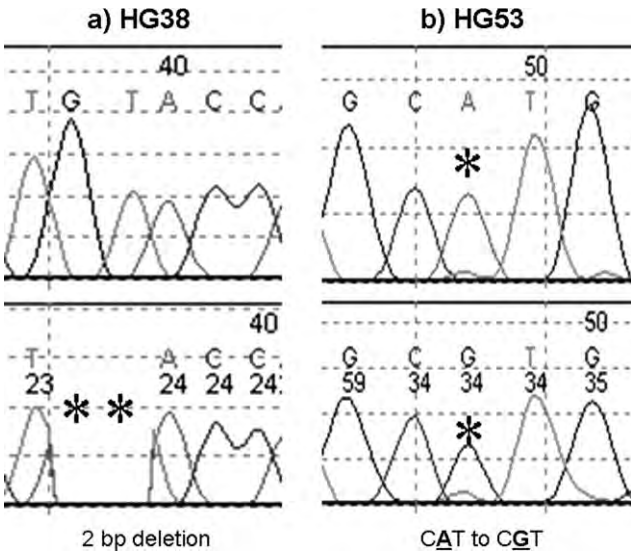

Figure 1. Examples of chromatograms of *TP53* mutations. a) 2 bp deletion at bp 686–687, b) point missense mutation at bp 818.

analyzed in this study did not harbor *TP53* mutations in exons 4–9. Although the vast majority of *TP53* mutations reside in those exons, it is likely that rare mutations may occur in other exons, and thus, the actual frequency of *TP53* mutations may be even higher than 80.3%. Likewise, molecular alterations in other genes in the p53 pathway could also occur in those samples without p53 mutations. For example, overexpression of HDM2, which promotes ubiqutin-dependent proteasomal p53 degradation, has been found in *TP53* wild-type bladder tumors[15]. Nevertheless, our findings suggest that aberration in the p53 pathway is probably the most prevalent molecular alteration in ovarian high-grade serous carcinomas.

Although a small study set, the lack of a statistically significant correlation between *TP53* mutation and *in vitro* drug resistance status suggests that *TP53* mutations are not involved in the development of drug resistance to carboplatin, cisplatin, paclitaxel, and docetaxel. This is not surprising, as *TP53* mutation appears to be an early event in tumor development of ovarian high-grade serous carcinomas.

In conclusion, the current study using affinity-purified tumor samples confirmed that *TP53* mutation occurs in approximately 80% of high-grade ovarian serous carcinomas. The study also showed that there is no significant correlation between *in vitro* drug resistance assays and *TP53* mutations. As most of the patients were treated within the last 3 years, it will be important in the future to correlate *TP53* mutation status with disease-free interval and overall survival.

Acknowledgments

This study was supported by a grant from the Ovarian Cancer Research Fund and Department of Defense Research Council Grant (OC0400600).

References

1 Fruehauf JP, Alberts DS. Assay-assisted treatment selection for women with breast or ovarian cancer. *Recent Results Cancer Res* 2003;**161:**126–45.
2 Horowitz J. Adenovirus-mediated p53 gene therapy: overview of preclinical studies and potential clinical applications. *Curr Opin Mol Ther* 1999;**1:**500–9.
3 Lavarino C, Pilotti S, Oggionni M *et al*. p53 gene status and response to platinum/paclitaxel-based chemotherapy in advanced ovarian carcinoma. *J Clin Oncol* 2000;**18:**3936–45.
4 Reles A, Wen WH, Schmider A *et al*. Correlation of p53 mutations with resistance to platinum-based chemotherapy and shortened survival in ovarian cancer. *Clin Cancer Res* 2001;**7:**2984–97.
5 Buttitta F, Marchetti A, Gadducci A *et al*. p53 alterations are predictive of chemoresistance and aggressiveness in ovarian carcinomas: a molecular and immunohistochemical study. *Br J Cancer* 1997;**75:**230–5.
6 Wen WH, Reles A, Runnebaum IB *et al*. p53 mutations and expression in ovarian cancers: correlation with overall survival. *Int J Gynecol Pathol* 1999;**18:**29–41.
7 Fallows S, Price J, Atkinson RJ, Johnston PG, Hickey I, Russell SE. p53 mutation does not affect prognosis in ovarian epithelial malignancies. *J Pathol* 2001;**194:**68–75.
8 Laframboise S, Chapman W, McLaughlin J, Andrulis IL. p53 mutations in epithelial ovarian cancers: possible role in predicting chemoresistance. *Cancer J* 2000;**6:**302–8.
9 Yakirevich E, Sabo E, Naroditsky I, Sova Y, Lavie O, Resnick MB. Multidrug resistance-related phenotype and apoptosis-related protein expression in ovarian serous carcinomas. *Gynecol Oncol* 2006; **100:**152–9.
10 Nakayama K, Nakayama N, Kurman RJ *et al*. Sequence mutations and amplification of PIK3CA and AKT2 genes in purified ovarian serous neoplasms. *Cancer Biol Ther* 2006;**5:**779–85.
11 Eltabbakh GH, Piver MS, Hempling RE *et al*. Correlation between extreme drug resistance assay and response to primary paclitaxel and cisplatin in patients with epithelial ovarian cancer. *Gynecol Oncol* 1998;**70:**392–7.
12 IARC TP53 Mutation Database [internet database]. International Agency for Research on Cancer. 2007. Available at: http://www-p53.iarc.fr/PolymorphismView.asp. Accessed June 3, 2007.
13 Singer G, Stohr R, Cope L *et al*. Patterns of p53 mutations separate ovarian serous borderline tumors and low- and high-grade carcinomas and provide support for a new model of ovarian carcinogenesis: a mutational analysis with immunohistochemical correlation. *Am J Surg Pathol* 2005;**29:**218–24.
14 Bell DA. Origins and molecular pathology of ovarian cancer. *Mod Pathol* 2005;**18**(Suppl. 2):S19–32.
15 Lopez-Knowles E, Hernandez S, Kogevinas M *et al*. The p53 pathway and outcome among patients with T1G3 bladder tumors. *Clin Cancer Res* 2006;**12:**6029–36.

Accepted for publication June 4, 2007

Research Article

The Roles of Human Sucrose Nonfermenting Protein 2 Homologue in the Tumor-Promoting Functions of Rsf-1

Jim Jinn-Chyuan Sheu,[1,2] Jung Hye Choi,[1] Isil Yildiz,[1] Fuu-Jen Tsai,[2] Yosef Shaul,[3] Tian-Li Wang,[1] and Ie-Ming Shih[1]

[1]Departments of Pathology, Oncology, and Gynecology and Obstetrics, Johns Hopkins Medical Institutions, Baltimore, Maryland; [2]Human Genetic Center, China Medical University Hospital and Graduate Institute of Chinese Medical Science, China Medical University, Taichung, Taiwan; and [3]Department of Molecular Genetics, Weizmann Institute of Science, Rehovot, Israel

Abstract

Rsf-1 interacts with human sucrose nonfermenting protein 2 homologue (hSNF2H) to form a chromatin remodeling complex that participates in several biological processes. We have previously shown that *Rsf-1* gene amplification was associated with the most aggressive type of ovarian cancer and cancer cells with Rsf-1 overexpression depended on Rsf-1 to survive. In this report, we determine if formation of the Rsf-1/hSNF2H complex could be one of the mechanisms contributing to tumor cell survival and growth in ovarian carcinomas. Based on immunohistochemistry, we found that Rsf-1 and hSNF2H were co-upregulated in ovarian cancer tissues. Ectopic expression of Rsf-1 in SKOV3 ovarian cancer cells with undetectable endogenous Rsf-1 expression enhanced hSNF2H protein levels and promoted SKOV3 tumor growth in a mouse xenograft model. Our studies also indicated that induction of Rsf-1 expression affected the molecular partnership of hSNF2H and translocated hSNF2H into nuclei where it colocalized with Rsf-1. Furthermore, analysis of Rsf-1 deletion mutants showed that the Rsf-D4 fragment contained the hSNF2H binding site based on coimmunoprecipitation and *in vitro* competition assays. As compared with other truncated mutants, expression of Rsf-D4 resulted in remarkable growth inhibition in ovarian cancer cells with *Rsf-1* gene amplification and overexpression, but not in those without detectable Rsf-1 expression. The above findings suggest that interaction between Rsf-1 and hSNF2H may define a survival signal in those tumors overexpressing Rsf-1. [Cancer Res 2008;68(11):4050–7]

Introduction

Gene amplification represents one of the molecular genetic hallmarks in human cancer. Elucidating the molecular mechanisms of how amplified genes maintain malignant phenotypes and propel tumor progression is fundamental in understanding the molecular etiology of human cancer and would have therapeutic implications. Previous genome-wide analysis using digital karyotyping (1) has identified a novel amplicon at chromosome 11q13.5 in high-grade serous carcinomas, the most common and malignant type of ovarian cancer (2). 11q13.5 amplification occurs in 13% to 15% of ovarian serous carcinoma based on fluorescence *in situ* hybridization analysis (2, 3) and the amplification is significantly associated with a shorter overall survival in patients with ovarian serous carcinoma (2). In addition to ovarian carcinoma, the 11q13.5 region is found to be amplified in other types of neoplastic diseases including breast, bladder, esophageal, and head and neck cancers (4).

Among the genes within the 11q13.5 amplicon, *Rsf-1* (also known as *HBXAPα*) was proposed as a candidate cancer-associated gene because it showed the highest correlation between DNA copy number and RNA copy number in ovarian cancer tissues. Rsf-1 protein partners with human sucrose nonfermenting protein 2 homologue (hSNF2H; also known as SMARCA5) to form the RSF complex, which belongs to the ISWI family of chromatin remodelers (5). In this complex, Rsf-1 functions as a histone chaperone to modulate DNA binding activity of RSF complex, whereas hSNF2H possesses nucleosome-dependent ATPase and helicase activities for DNA unwinding (5). In addition, Rsf-1 protein contains a novel PHD zinc finger domain, which has been shown to participate in protein-protein interaction and transcriptional regulation (6, 7). The Rsf-1/hSNF2H complex (RSF complex) mobilizes nucleosomes to remodel the chromatin structure in response to a variety of growth signals and environmental cues. It has been shown that such nucleosomal remodeling, as occurs in many ISWI and SWI/SNF complexes, is essential for transcriptional activation or repression (8–10), DNA replication (11), and cell cycle progression (12). Recently, a growing body of evidence has accumulated to support a novel role of chromatin remodeling in cancer (13–19). The change in the homeostasis of Rsf-1 and hSNF2H protein may be related to the aggressive behavior of tumors with *Rsf-1* gene amplification and overexpression.

Although alterations of chromatin structures have been linked to cancer development, the molecular mechanisms underlying how *Rsf-1* gene amplification and overexpression contribute to tumor progression are largely unknown. Our previous studies have shown that higher RNA or protein levels of Rsf-1 are associated with the most aggressive type of ovarian cancer (2, 20) and a shorter overall survival in cancer patients (2, 21). Furthermore, *Rsf-1* gene knockdown inhibited cell growth in ovarian cancer cells that harbor *Rsf-1* amplification, but not in cell lines without Rsf-1 overexpression, suggesting an important role of *Rsf-1* amplification in maintaining survival and growth in ovarian cancer. In this study, we address if interactions between Rsf-1 and hSNF2H proteins are required for survival and growth of cancer cells.

Materials and Methods

Tissue microarrays and immunohistochemistry. One hundred sixty-three paraffin-embedded high-grade ovarian serous carcinoma tissues were obtained from the Department of Pathology at the Johns Hopkins Hospital. Acquisition of tissue specimens was approved by the institutional review

Note: Supplementary data for this article are available at Cancer Research Online (http://cancerres.aacrjournals.org/).

Requests for reprints: Ie-Ming Shih, Department of Pathology, Johns Hopkins University, 1550 Orleans Street, Room 305, Baltimore, MD 21231. Phone: 410-502-7774; E-mail: ishih@jhmi.edu.

doi:10.1158/0008-5472.CAN-07-3240

board. Tissue microarrays (triplicate 1.5-mm cores from each specimen) were prepared to facilitate immunohistochemistry using an EnVision+ System peroxidase kit (DAKO) with an antibody dilution of 1:1,000 for the anti–Rsf-1 antibody (Upstate) and 1:1,000 for the anti-hSNF2H antibody (Upstate). Immunointensity was independently scored by two investigators based on nuclear immunoreactivity and labeled as negative (0), weakly positive (1+), moderately positive (2+), strongly positive (3+), and intensely positive (4+). For discordant cases, a third investigator scored the intensity and the final intensity score was determined by the majority scores.

Inducible constructs and Rsf-1–inducible cell clones. The full-length *Rsf-1* gene was tagged with a V5 epitope at the COOH terminus and was then cloned into Tet-off expression vectors, pBI or pTRE-hygro (Clontech). Parental RK3E and SKOV3 cells were transfected with a tetracycline-controlled transactivator (tTA) expression vector. The inducible Rsf-1 expression vectors were constructed and introduced into the RK3E-tTA and SKOV3-tTA cells, and the stable transfectants were selected. Transfection was done with Lipofectamine (Invitrogen) according to the manufacturer's protocol. To determine the efficiency of Rsf-1 induction in the Tet-off system, we carried out Western blots to analyze Rsf-1 protein expression at different time points after induction. The method of Western blot with the anti–Rsf-1 antibody has previously been described (2, 22).

Double immunofluorescence staining. Rsf-1–inducible RK3E cells were used to determine whether Rsf-1 and hSNF2H colocalized in the same cellular compartment. The inducible cells grown on chamber slides (Nunc) were transfected with an hSNF2H-expressing vector tagged with an Xpress epitope at the NH_2 terminus. Cells were washed with doxycycline-containing or doxycycline-free medium to turn off or turn on the *Rsf-1* gene, respectively. Forty-eight hours after transfection, cells were fixed and incubated with an anti-Xpress antibody (Invitrogen) to detect hSNF2H, followed by a FITC-conjugated goat anti-V5 antibody (QED Bioscience) to detect Rsf-1. The cells were then incubated with a rhodamine-conjugated antimouse antibody (Jackson ImmunoResearch Laboratories).

Coimmunoprecipitation. A series of Rsf-1 deletion mutants (Rsf-D1 to Rsf-D10) were cloned into pcDNA6/V5, which was used to transfect a stable HEK293 cell line constitutively expressing hSNF2H tagged with an Xpress epitope at the NH_2 terminus (Invitrogen). Forty-eight hours after transfection, cells were lysed and deletion mutant proteins were pulled down by anti-V5 agarose (Sigma) and immunoblotted with an anti-Xpress antibody to detect hSNF2H protein. For the competition assay, recombinant Rsf-1 deletion mutant protein, Rsf-D4, was expressed and purified by a PET27b *E. coli* purification system (Novagen). Rsf-D4 protein was added into cell lysate at different concentrations from 0 to 50 μg/mL during coimmunoprecipitation to compete with full-length Rsf-1 protein for hSNF2H binding. Coimmunoprecipitation was also done to assess the hSNF2H binding proteins. The anti-BAZ1A antibody (clone 1F6) was purchased from Abnova, and the anti-BAZ1B (W3614) was purchased from Sigma. The cell lysate was prepared from OVCAR3 cells treated with Rsf-1 shRNA or vector control. Cell lysate was also prepared from SKOV3 cells with *Rsf-1* gene turned on or turned off. The lysate was then equally aliquoted into three parts, and immunoprecipitation was done with anti–Rsf-1, anti-BAZ1A, and anti-BAZ1B antibodies. The immunoprecipitates were immunoblotted with an anti-hSNF2H antibody.

Quantitative real-time PCR. PCR reactions were done using an iCycler (Bio-Rad), and the threshold cycle numbers (C_t) were obtained using the iCycler Optical system interface software. Mean C_t of the gene of interest was calculated from duplicate measurements and normalized with the mean C_t of a control gene, β-amyloid precursor protein (*APP*), for which expression is relatively constant among the serial analysis of gene expression (SAGE) libraries analyzed (23). In cases where no gene expression was observed, a cutoff C_t value of 45 cycles was used. Data were expressed as fold increase or decrease as compared with the gene turned-off or vector control samples. We considered a change exceeding 2-fold ($\delta C_t > 1$) to be significant in this study.

Cell growth and apoptosis assays. OVCAR3 ovarian cancer cells transfected with Rsf-1 deletion mutants and empty vector were grown in 96-well plates at a density of 3,000 per well. To determine similar expression levels of deletion mutants, the deletion mutant constructs were cloned into the pBI vector, which coexpressed green fluorescent protein (GFP) in transfected cells. We also generated a new OVCAR3-tTA cell clone with a high transfection efficiency using the Amaxa transfection kit (T buffer with program T-16) and these OVCAR3-tTA cells were used for cell growth and apoptosis assays. We observed a similar percentage of transfected cells with equal green fluorescence signals in all transfection groups after the second day of transfection, suggesting a similar transfection efficiency for each construct. Cell number was measured 4 d after transfection based on the fluorescence intensity of SYBR Green I nucleic acid staining (Molecular Probes). Cell growth on Rsf-D4–transfected OC24 and RK3E cells was monitored daily for 4 consecutive days with SYBR Green I staining. Bromodeoxyuridine (BrdUrd) uptake and staining were done with a cell proliferation kit (Amersham) as previously described (2). For apoptosis assay, apoptotic cells were detected by staining with Annexin V-FITC (BioVision). The percentages of BrdUrd-positive and Annexin V–positive cells were determined by counting at least 400 cells from different fields for each experiment. The data were expressed as mean ± SD from triplicates.

Tumor xenograft in nude mice. Rsf-1–inducible SKOV3 cells were injected into the s.c. tissue of athymic *nu/nu* mice (5×10^6 cells per injection; five mice with 10 injection sites for each group). Doxycycline (125 μg/mouse) was i.p. injected everyday to suppress *Rsf-1* gene expression in the Rsf-1 turned-off control mice. For the Rsf-1 turned-on group, mice were treated with equal volume of PBS. Tumor volume was measured every 3 d and tumors were excised and weighed at day 51. Tumors from turned-on and turned-off groups were evaluated for Rsf-1 induction using anti-V5 antibody staining (Invitrogen) on paraffin-embedded tumor sections.

SAGE data analysis. Analysis of gene expression using the SAGE data has previously been described (24, 25). Briefly, ovarian SAGE libraries including the ovarian surface epithelial cells (OSE4) and ovarian cancer cell lines (MPSC1, ES2, A2780, and OVCAR3) were retrieved from the SAGE database[4] and previously established data (26, 27). The UniGene was searched for the protein of interest, and the appropriate match was chosen based on its specificity for the protein and number of sequences. The transcript expression levels were normalized as the number of tags per 100,000 tags in each library.

Results

Coexpression of Rsf-1 and hSNF2H. hSNF2H has been shown to directly interact with Rsf-1 to form a chromatin remodeling complex, RSF (5), but the evidence to support such interaction in cancer cells has not yet been shown. Here, we observed that both Rsf-1 and hSNF2H immunoreactivity were located in the nuclei of tumor cells (Fig. 1*A*) and showed a significant association (P = 0.048) with Rsf-1 and hNSF2H immunointensity on the same specimens based on χ^2 test (Table 1). Second, we carried out coimmunoprecipitation and showed that Rsf-1 protein interacted with hSNF2H protein in an ovarian cancer cell line, OVCAR3, which is known to contain *Rsf-1* amplification (Fig. 1*B*; ref. 2). Next, we asked whether induction of Rsf-1 expression enhanced the protein level of hSNF2H. An inducible (Tet-off) Rsf-1 expression system was generated in the SKOV3 cell line, which did not harbor *Rsf-1* amplification or express a detectable level of endogenous Rsf-1. After induction of Rsf-1, an increased amount of both Rsf-1 and hSNF2H protein levels was found in a time-dependent manner (Fig. 1*C*). In contrast to the significantly increased protein level, hSNF2H mRNA level, as measured at 6 hours after Rsf-1 induction, increased only by 1.04-fold. In addition, ectopic expression of

[4] http://www.hlm.nih.gov/SAGE/

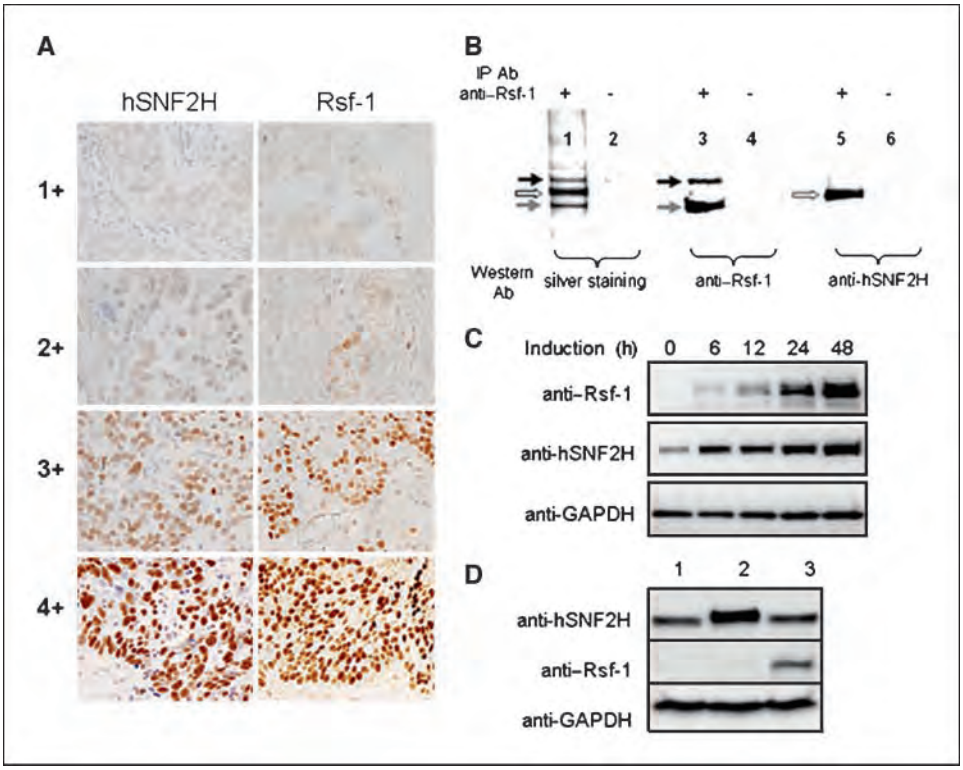

Figure 1. Co-upregulation of Rsf-1 and hSNF2H expression in ovarian carcinoma cells. *A,* immunohistochemistry with anti–Rsf-1 and anti-hSNF2H antibodies on ovarian serous carcinoma tissues. Representative tissue sections with different immunointensity (from 1+ to 4+) of Rsf-1 and hSNF2H. For each intensity group, both sections were obtained from similar areas of the same specimen. *B,* coimmunoprecipitation was done to assess if Rsf-1 protein forms a complex with hSNF2H protein in OVCAR3 cells. Protein lysate was pulled down with an anti–Rsf-1 antibody, separated by gel electrophoresis, and visualized by silver staining (*lane 1*). Western blotting was done to show that the major proteins in the pulled down fraction were Rsf-1 with a molecular weight of ~215 kDa (*black arrow*) and a degradation product of ~130 kDa (*gray arrow*, *lane 3*) and hSNF2H protein with a molecular weight of ~146 kDa (*open arrow*, *lane 5*). Protein G alone was used as the control in immunoprecipitation in lanes 2, 4, and 6. *C,* SKOV3 ovarian cancer line, which expresses an undetectable level of endogenous Rsf-1, was engineered to express Rsf-1 controlled by a Tet-off system. Rsf-1 induction increased the hSNF2H protein level in a time-dependent fashion based on Western blotting analysis. *D,* Western blot analysis showed no increase in Rsf-1 protein level in HEK293 cells, which were previously engineered to overexpress hSNF2H (*lane 2*) as compared with the parental cell control (*lane 1*). OVCAR3 cells served as the positive control for this assay (*lane 3*). Glyceraldehyde-3-phosphate dehydrogenase (GAPDH) was used as the loading control.

hSNF2H in HEK293 cells did not enhance Rsf-1 protein level (Fig. 1*D*). The above findings suggest that Rsf-1 proteins may function to stabilize hSNF2H protein level in cancer cells.

Induction of Rsf-1 expression promotes tumor growth in SKOV3 xenografts. As an attempt to determine whether Rsf-1 protein up-regulation contributes to tumor growth, we used the SKOV3 xenograft model in nude mice. Before s.c. injection, we analyzed Rsf-1 mRNA level in SKOV3-Rsf-1 Tet-off cells and found that its expression level gradually increased to a level that was comparable to that in *Rsf-1*–amplified ovarian carcinoma tissues (Fig. 2*A*). As compared with noninduced tumors, Rsf-1–induced tumors grew much faster and had an increased tumor weight ($P < 0.01$; Fig. 2*B–D*). Immunohistochemistry of the tumors excised at the time of sacrifice showed diffuse Rsf-1 nuclear staining in tumor cells in the Rsf-1–induced, but not the noninduced, group, indicating a sustained Rsf-1 expression in xenografts after Rsf-1

Table 1. hSNF2H and Rsf-1 immunointensity in high-grade ovarian serous carcinomas

Rsf-1 immunointensity	hSNF2H immunointensity					Total
	0	1+	2+	3+	4+	
0	0	1	3	0	0	4
1+	1	17	15	1	0	34
2+	1	17	35	6	2	61
3+	1	13	23	10	3	50
4+	0	1	6	4	3	14
Total	3	49	82	21	8	163

NOTE: $P = 0.048$.

induction. Consistent with increased tumor sizes in Rsf-1–induced tumors, the mitotic count (mitoses per 100 tumor cells) in the Rsf-1–induced tumors was 1.67 ± 0.34, which was significantly higher than 0.87 ± 0.27 in noninduced tumors ($P < 0.05$). We did not observe any significant difference between Rsf-1–induced tumors and noninduced controls in tumor cell morphology, blood vessel density, and invasiveness into surrounding soft tissues.

Rsf-1/hSNF2H complex is the predominant chromatin remodeling complex in Rsf-1–overexpressing cells. SNF2H-containing complexes (belonging to the ISWI subfamily) have been reported in mammalian cells and they included RSF, CHRAC, ACF/WCRF, NoRC, and WICH (28–32). Each complex contains subunits that may regulate the specificity or catalytic activity of SNF2H. For example, RSF contains Rsf-1 and SNF2H (5); ACF/WCRF contains BAZ1A (also known as ACF1 or WCRF180) and SNF2H (29); and WICH contains BAZ1B (also known as WSTF) and SNF2H (30). Because Rsf-1 is one of the binding partners for SNF2H, we assessed the cellular localization of both Rsf-1 and SNF2H in an Rsf-1–inducible cell line, RK3E. Immunofluorescence staining revealed that hSNF2H protein was diffusely distributed in both cytoplasm and nuclear compartments when Rsf-1 was turned off (Fig. 3*A*). On Rsf-1 induction, Rsf-1 protein, which contains several nucleus localization signal sites, was overexpressed in the nuclei. Interestingly, hSNF2H was translocated into nuclei and colocalized with Rsf-1 (Fig. 3*A*).

To determine the gene expression of the candidate binding partners of hSNF2H in ovarian cancer cells, we analyze the SAGE database. Among those binding partners, we found that Rsf-1, BAZ1A, BAZ1B, and BAZ2A were abundantly expressed in ovarian cancer cell lines including OVCAR3, A2780, ES2, and MPSC1, whereas their expression levels were relatively low in the OSE4 cell line, which was derived from normal ovarian surface epithelium (Supplementary Fig. S1). Of notice, Rsf-1 represented the major binding partner for hSNF2H expressed in OVCAR3 cells that amplified the *Rsf-1* locus.

Because Rsf-1 was found to be overexpressed in tumor cells, it is possible that in those cells, excessive Rsf-1 molecules compete with other SNF2H binding partners for SNF2H binding. To address this possibility, we carried out immunoprecipitation to determine the association of representative SNF2H binding partners, including BAZ1A, BAZ1B, and Rsf-1, with hSNF2H on Rsf-1 induction in SKOV3 cells and Rsf-1 knockdown in OVCAR3 cells. BAZ2A was not analyzed here because the antibody reacting to BAZ2A was not currently available. In SKOV3 cells with Rsf-1 induction, the protein level of hSNF2H that was coimmunoprecipitated with Rsf-1 was significantly increased whereas its level of coimmunoprecipitation with BAZ1A and BAZ1B was significantly reduced as compared with the SKOV3 cells without Rsf-1 induction (Fig. 3*B*). In the Rsf-1 shRNA approach, down-regulation of Rsf-1 significantly reduced the level of Rsf-1/hSNF2H complex and enhanced the formation of BAZ1A/hSNF2H and BAZ1B/hSNF2H complexes (Fig. 3*C*). The above results indicated that Rsf-1 overexpression, as occurred in Rsf-1–amplified tumors, "hijacked" hSNF2H from other partners to the Rsf-1 complex.

Mapping of hSNF2H binding domain on Rsf-1. We have previously shown that cell growth and survival depended on Rsf-1 expression in ovarian cancer cells with *Rsf-1* gene amplification and overexpression (2). To determine whether the formation of Rsf-1/hSNF2H complex is required for cell survival, we applied a dominant negative approach by generating an Rsf-1 deletion mutant that competed with wild-type (full-length) Rsf-1 for hSNF2H binding. First, we generated a series of Rsf-1 deletion mutants (from Rsf-D1 to Rsf-D10) that contained different protein motifs (PHD, DDT, Glu-rich, etc.; Fig. 4*A*). These fragments were cloned into expression vectors, which were used to transfect HEK293 cells to assess their ability to coimmunoprecipitate with hSNF2H (Fig. 4*B*). We found that among all deletion mutants, only the Rsf-D4 fragment (amino acids 1–973) could robustly coimmunoprecipitate with hSNF2H whereas others did not show

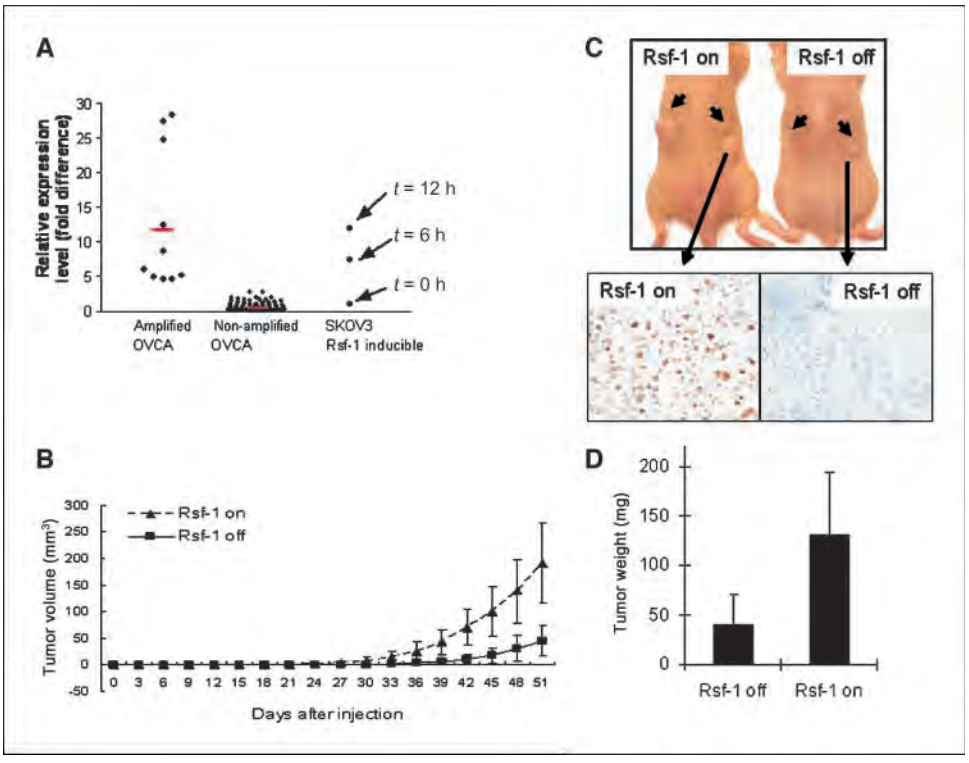

Figure 2. Rsf-1 expression increases tumor size in SKOV3 tumor xenografts. *A,* after Rsf-1 induction (6 and 12 h), the Rsf-1 mRNA levels in SKOV3 cells are comparable to those in ovarian carcinoma tissues (OVCA) with *Rsf-1* amplification and are significantly higher than in those without *Rsf-1* amplification. *B,* tumor xenograft experiment was done on athymic *nu/nu* mice by injecting Rsf-1–inducible SKOV3 cells s.c. Induction of Rsf-1 expression in SKOV3 tumors increased tumor volumes as compared with the noninduced group. *C,* representative photographs show larger tumors in Rsf-1–induced (*Rsf-1 on*) tumors than in noninduced (*Rsf-1 off*) tumors. The tumor sections were stained with an anti-V5 antibody to confirm the induction of Rsf-1 proteins. Diffuse nuclear staining of Rsf-1/V5 is observed in induced, but not in noninduced, tumor sections. *D,* tumors were excised and weighed at the end of experiment (day 51).

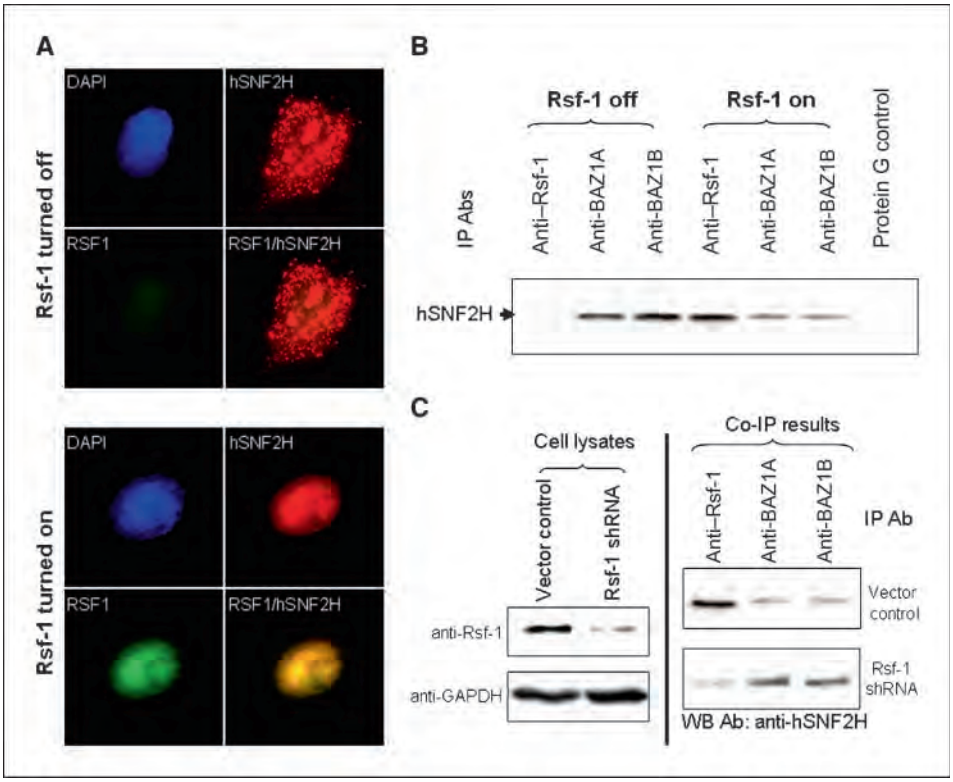

Figure 3. Analysis of interaction between hSNF2H and its binding partners. *A,* immunofluorescence staining of Rsf-1 and hSNF2H proteins shows that Rsf-1 colocalizes with hSNF2H in the nuclei. Rsf-1–inducible RK3E cells were transiently transfected with hSNF2H gene fused with an Xpress tag. Double immunofluorescence staining was done to detect Rsf-1 (*green fluorescence*; anti-V5) and hSNF2H (*red fluorescence*; anti-Xpress) proteins, respectively. *B,* immunoprecipitation was done in SKOV3 cells stably transfected with a Tet-off inducible Rsf-1 expression construct. The protein level of hSNF2H that was coimmunoprecipitated with Rsf-1 was increased in Rsf-1–induced (Rsf-1 on) cells but the level of hSNF2H that coimmunoprecipitated with BAZ1A and BAZ1B was significantly reduced as compared with control SKOV3 cells without Rsf-1 induction (Rsf-1 off). Equal protein amount was used in immunoprecipitation for each antibody. *C,* immunoprecipitation assays were done to compare the binding capability between hSNF2H and different binding partners. *Rsf-1* gene expression was knocked down by shRNA in *Rsf-1*–amplified OVCAR3 cells (*left*). The cell lysate of equal protein amounts from Rsf-1 shRNA– and control vector–transfected cells was then immunoprecipitated with anti–Rsf-1, anti-BAZ1A, and anti-BAZ1B antibodies (*Ab*), respectively (*right*). The immunoprecipitated complex was separated by SDS-PAGE and blotted with an anti-hSNF2H antibody to determine the amount of coimmunoprecipitated hSNF2H binding partners including Rsf-1, BAZ1A, and BAZ1B.

detectable coimmunoprecipitate (Fig. 4*C*). The Rsf-D4 contains DDT, Glu-rich, and PHD motifs but lacks the COOH-terminal Rsf-1 domain (Fig. 4*D*). By increasing the amount of recombinant Rsf-D4 protein during coimmunoprecipitation, we observed that the amount of hSNF2H immunoprecipitate decreased in a dose-dependent fashion, indicating that Rsf-D4 competed with the endogenous full-length Rsf-1 for interacting with hSNF2H (Fig. 5*A*).

Effects of Rsf-D4 expression on cell growth and apoptosis in ovarian cancer cells. To determine the biological effects of Rsf-D4 on ovarian cancer cells, we expressed deletion mutants from Rsf-D1 to Rsf-D10 individually in OVCAR3 cells that expressed the highest levels of Rsf-1 and hSNF2H proteins (ref. 2; Fig. 5*B*), and then the cell number was determined. As shown in Fig. 5*C*, the most significant decrease in cell number was observed in Rsf-D4–transfected cells and, to a lesser extent, in Rsf-D3-transfected cells (Fig. 5*C*). Furthermore, expression of Rsf-D4 suppressed cellular proliferation based on BrdUrd uptake (Fig. 5*D*) and increased the percentage of Annexin V–labeled cells (Fig. 5*E*). In contrast, Rsf-D4 expression did not lead to any significant decrease in cell number in OC24 and RK3E cells with undetectable Rsf-1 expression ($P > 0.05$; Supplementary Fig. S2).

Discussion

Our previous studies have shown the clinical significance of *Rsf-1* gene amplification and overexpression in ovarian carcinomas as its increased gene copy number and expression level are associated with the most aggressive type of ovarian cancer (2, 20, 21). Furthermore, we have shown that *Rsf-1*–amplified tumors depend on Rsf-1 proteins to survive. In this study, we provide new evidence that induction of Rsf-1 expression is associated with hSNF2H protein expression, and a higher copy number of Rsf-1/hSNF2H complexes increases tumor size in a tumor xenograft mouse model. We further show that expression of an Rsf-1 dominant negative protein that contains the hSNF2H binding motif is sufficient to suppress cell growth in cancer cells with Rsf-1 overexpression but not in cells with undetectable Rsf-1 expression levels. These findings provide new insights into the tumor-promoting functions of Rsf-1 and suggest that the formation of the RSF chromatin remodeling complex may be one of the mechanisms contributing to survival and growth in ovarian cancer cells.

Because Rsf-1 forms a chromatin remodeling complex with hSNF2H, it is likely that both proteins are coexpressed in tissues. Thus, we first asked if both Rsf-1 and hSNF2H proteins were co-upregulated. Based on immunostaining on ovarian serous carcinoma tissues, we were able to show that this was the case. To determine whether the co-upregulation is merely a coincident event or a result of Rsf-1 overexpression, we established an Rsf-1 inducible ovarian cancer cell line, SKOV3, which showed hSNF2H expression but with undetectable Rsf-1 expression. We observed that induction of Rsf-1 expression in SKOV3 increased the protein,

but not the mRNA, level of hSNF2H, suggesting that Rsf-1 stabilized the hSNF2H proteins probably through the complex formation that prevented its protein degradation. Therefore, it is likely that in *Rsf-1*–amplified or *Rsf-1*–overexpressing carcinomas, the amount of hSNF2H also increases as a result of Rsf-1 up-regulation to form the RSF chromatin remodeling complex. Besides, we compared the growth of SKOV3 xenografts in mice between Rsf-1 induction and control (noninduction) groups and found that the size of SKOV3 tumors in mice significantly increased on Rsf-1 induction as compared with those without induction. These data highly suggest that Rsf-1 overexpression promotes tumor growth.

Based on deletion mapping, coimmunoprecipitation study, and competition assay, we were able to define the hSNF2H binding domain (Rsf-D4) on the Rsf-1 molecule, which contains both DDT and PHD motifs at the NH_2-terminal region. It seems that both DDT and PHD domains are the required motifs for hSNF2H interaction because other deletion mutants containing only one of them did not show a robust coimmunoprecipitation with hSNF2H. Further structure biology studies should be helpful to disclose the precise physical interaction between DDT/PHD domains on Rsf-1 and hSNF2H proteins. The dominant negative effects of Rsf-D4 in ovarian cancer cells with *Rsf-1* gene amplification and overexpression but not in cells with low or undetectable Rsf-1 expression suggest that the complex formation of full-length Rsf-1 and hSNF2H is essential for tumor growth and survival for those tumor cells that are molecularly "addict" to *Rsf-1* gene amplification or up-regulation. Furthermore, the lack of growth-suppressive effects on cells with undetectable Rsf-1 expression indicates that the Rsf-D4 effects are not likely due to a nonspecific cytotoxic effect associated with the Rsf-D4 protein. Although the above represents our preferred view, alternative interpretations should be pointed out. For example, like other dominant negative approaches that are used to modulate the activity of an endogenous protein by interfering normal protein-protein interactions, the Rsf-D4 approach used in this study may not be entirely specific to interrupt the interaction between Rsf-1 and hSNF2H. It is possible that the Rsf-D4 may complex with other protein(s) besides hSNF2H and overexpression of Rsf-D4 can potentially interfere the binding of these protein(s) to full-length endogenous Rsf-1.

How does Rsf-1 overexpression, and thereby the increased Rsf-1/hSNF2H complex formation, contribute to tumor cell survival and growth? There are at least two possibilities based on the current study. First, it is plausible that an increased number of RSF complexes may facilitate remodeling of chromatin structures or modification of functions of oncogenes and tumor suppressors that interact with the complexes (32), thus promoting tumorigenesis. Second, overexpression of Rsf-1, as occurs in ovarian carcinoma

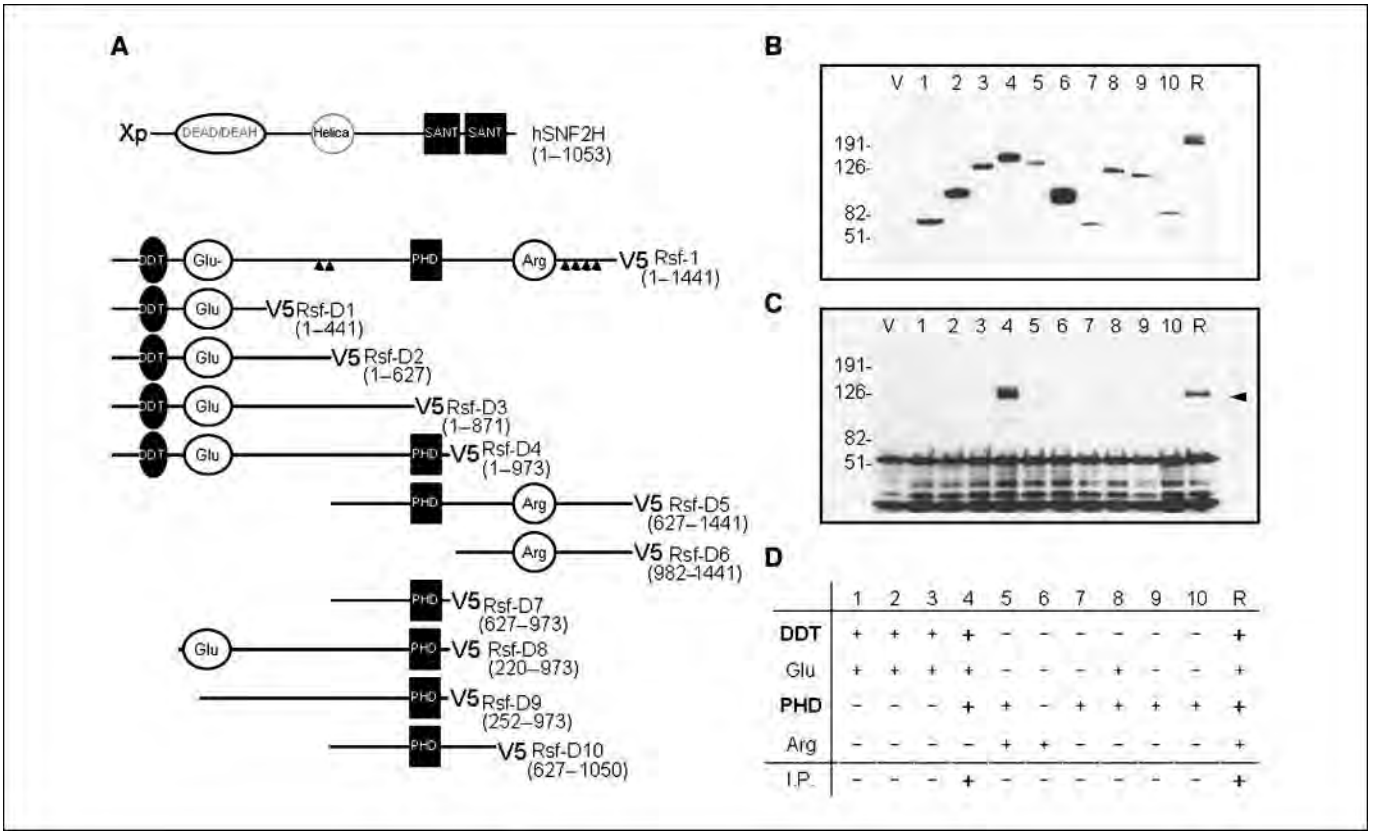

Figure 4. Mapping for the hSNF2H binding domain(s) on Rsf-1 protein. *A,* a series of Rsf-1 deletion mutants, Rsf-D1 to Rsf-D10, were generated and cloned into the pcDNA6/V5 vector. The locations of each mutant are shown in parentheses. ▲, the predicted nucleus localization signal site; *DEAD/DEAH box,* a conserved motif for ATP-dependent helicases. *Helica,* helicase catalytic domain. *SANT,* a conserved DNA-binding domain for SANT SWI3, ADA2, N-CoR, and TFIIIB proteins. *DDT,* a conserved domain of DNA-binding homeobox-containing proteins; *PHD,* plant homeodomain–type zinc finger domain; *Glu,* glutamine-rich region; *Arg,* arginine-rich region. *B,* deletion mutants, Rsf-D1 to Rsf-D10, and pcDNA6 (*V*) were transfected into hSNF2H-expressing HEK293 cells and their protein expression was confirmed by Western blot analysis with an anti-V5 antibody. *C,* coimmunoprecipitation was done to determine the minimal domain(s) of Rsf-1 protein that interacts with hSNF2H. The hSNF2H protein was tagged with Xpress and the Rsf-1 mutants were tagged with V5 to facilitate immunoprecipitation. The proteins pulled down with anti-V5 antibody were immunoblotted with an anti-Xpress antibody. In addition to the full-length Rsf-1 (*R*), Rsf-D4 is the only mutant that coimmunoprecipitated with hSNF2H (*arrowhead*). *D,* summary of different motifs on Rsf-1 deletion mutants and their hSNF2H binding capacity based on coimmunoprecipitation (*I.P.*).

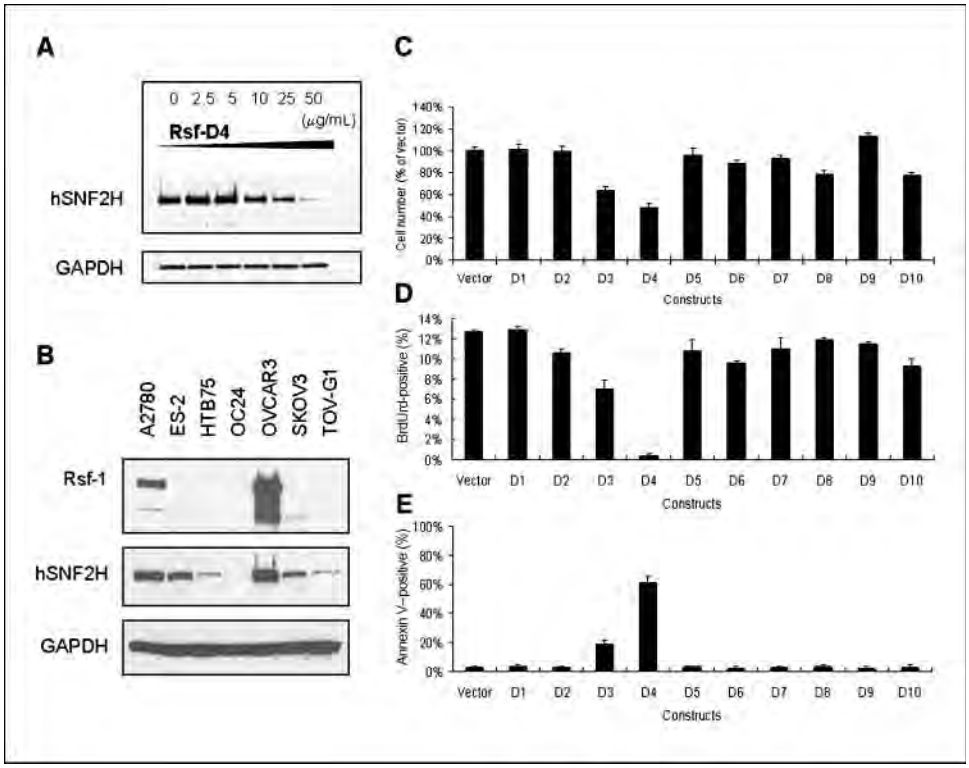

Figure 5. Effects of Rsf-D4 expression on OVCAR3 ovarian cancer cells. *A,* in a coimmunoprecipitation assay, recombinant Rsf-D4 proteins show a dose-dependent inhibition in the binding of Rsf-1 and hSNF2H. GAPDH was used as a loading control. *B,* Western blotting shows a robust Rsf-1 protein expression in the OVCAR3 cell line and a moderate expression in the A2780 cell line as compared with other ovarian carcinoma cell lines. *C,* the effects of deletion mutants were assessed by comparing the cell number of the OVCAR3 cells after transient transfection of Rsf-1 to Rsf-10 constructs. The cell number was measured at day 4 by SYBR Green I incorporation and the data were normalized to the empty vector control. *D,* the cellular proliferating activity in the transfected OVCAR3 cells was determined by the percentage of cells with positive BrdUrd staining. *E,* the percentage of apoptotic cells in each treatment was determined by Annexin V-FITC staining.

cells, can alter cellular distribution and the partnership of hSNF2H. hSNF2H is known to interact with several proteins other than Rsf-1, and the hSNF2H-containing ISWI complexes have diverse cellular functions. Thus, excessive Rsf-1 molecules may sequester hSNF2H, leading to a loss or a decrease in abundance of other hSNF2H-containing complexes such as hSNF2H/BAZ1A and hSNF2H/BAZ1B. Because several protein members in the SNF family have been reported as tumor suppressors and have been found to be down-regulated or inactivated in cancer tissues (16, 18), it is possible that reduction of these hSNF2H complexes with tumor suppressor potential by excessive Rsf-1 contributes to the observed growth-stimulating effects in cancer cells. However, our findings show that expressing a Rsf-D4 deletion mutant, which holds avid hSNF2H binding activity, can induce growth suppression in tumor cells. This observation suggests that sequestering hSNF2H from other complexes by Rsf-D4 mutant alone was not able to promote cell growth as seen in full-length Rsf-1. Therefore, the tumor-promoting phenotype mediated by full-length Rsf-1 is more likely due to an increase of RSF complex formation rather than a decrease of other hSNF2H-containing complexes. Further studies are needed to show the detailed mechanisms underlying how Rsf-1/hSNF2H complexes contribute to tumor development.

In conclusion, the current study attempts to explore the functional roles of a chromatin remodeling protein, Rsf-1, in promoting ovarian cancer. Our data provide evidence that the interaction of Rsf-1 and hSNF2H proteins to form the chromatin remodeling complex is essential for cell survival and growth in ovarian cancer. Our results should help understand the pathogenesis of ovarian cancer development and may have translational implications for new cancer therapy.

Acknowledgments

Received 8/21/2007; revised 1/24/2008; accepted 3/31/2008.

Grant support: NIH grant CA129080, Department of Defense grant OC0400600, the Johns Hopkins-Weizmann Institute of Science Research Collaboration Fund, and the Johns Hopkins-China Medical University Research Collaboration Fund grant CMU95-286.

The costs of publication of this article were defrayed in part by the payment of page charges. This article must therefore be hereby marked *advertisement* in accordance with 18 U.S.C. Section 1734 solely to indicate this fact.

We thank David Chu for technical assistance.

References

1. Wang TL, Maierhofer C, Speicher MR, et al. Digital karyotyping. Proc Natl Acad Sci U S A 2002;99:16156–61.
2. Shih IM, Sheu JJ, Santillan A, et al. Amplification of a chromatin remodeling gene, Rsf-1/HBXAP, in ovarian carcinoma. Proc Natl Acad Sci U S A 2005;102:14004–9.
3. Nakayama K, Nakayama N, Jinawath N, et al. Amplicon profiles in ovarian serous carcinomas. Int J Cancer 2007;120:2613–7.
4. Schwab M. Amplification of oncogenes in human cancer cells. Bioessays 1998;20:473–9.
5. Loyola A, Huang J-Y, LeRoy G, et al. Functional analysis of the subunits of the chromatin assembly factor RSF. Mol Cell Biol 2003;23:6759–68.
6. Shamay M, Barak O, Doitsh G, Ben-Dor I, Shaul Y. Hepatitis B virus pX interacts with HBXAP, a PHD finger protein to coactivate transcription. J Biol Chem 2002;277:9982–8.
7. Shamay M, Barak O, Shaul Y. HBXAP, a novel PHD-finger protein, possesses transcription repression activity. Genomics 2002;79:523–9.
8. Holstege FC, Jennings EG, Wyrick JJ, et al. Dissecting the regulatory circuitry of a eukaryotic genome. Cell 1998;95:717–28.
9. Vignali M, Hassan AH, Neely KE, Workman JL. ATP-dependent chromatin-remodeling complexes. Mol Cell Biol 2000;20:1899–910.
10. Huang JY, Shen BJ, Tsai WH, Lee SC. Functional interaction between nuclear matrix-associated HBXAP and NF-κB. Exp Cell Res 2004;298:133–43.
11. Flanagan JF, Peterson CL. A role for the yeast SWI/SNF complex in DNA replication. Nucleic Acids Res 1999;27:2022–8.
12. Cosma MP, Tanaka T, Nasmyth K. Ordered recruitment of transcription and chromatin remodeling factors to a cell cycle- and developmentally regulated promoter. Cell 1999;97:299–311.
13. Roberts CW, Orkin SH. The SWI/SNF complex—chromatin and cancer. Nat Rev Cancer 2004;4:133–42.

14. Mohrmann L, Verrijzer CP. Composition and functional specificity of SWI2/SNF2 class chromatin remodeling complexes. Biochim Biophys Acta 2005;1681:59–73.
15. Wolffe AP. Chromatin remodeling: why it is important in cancer. Oncogene 2001;20:2988–90.
16. Klochendler-Yeivin A, Muchardt C, Yaniv M. SWI/SNF chromatin remodeling and cancer. Curr Opin Genet Dev 2002;12:73–9.
17. Wong AK, Shanahan F, Chen Y, et al. BRG1, a component of the SWI-SNF complex, is mutated in multiple human tumor cell lines. Cancer Res 2000;60: 6171–7.
18. Klochendler-Yeivin A, Fiette L, Barra J, Muchardt C, Babinet C, Yaniv M. The murine SNF5/INI1 chromatin remodeling factor is essential for embryonic development and tumor suppression. EMBO Rep 2000;1:500–6.
19. Guidi CJ, Sands AT, Zambrowicz BP, et al. Disruption of Ini1 leads to peri-implantation lethality and tumorigenesis in mice. Mol Cell Biol 2001;21:3598–603.
20. Mao TT, Hsu C-Y, Yen MJ, et al. Expression of Rsf-1, a chromatin-remodeling gene, in ovarian and breast carcinoma. Hum Pathol 2006;37:1169–75.
21. Davidson B, Trope CG, Wang TL, Shih Ie M. Expression of the chromatin remodeling factor Rsf-1 is up-regulated in ovarian carcinoma effusions and predicts poor survival. Gynecol Oncol 2006;103:814–9.
22. Kobel M, Pohl G, Schmitt WD, Hauptmann S, Wang TL, Shih Ie M. Activation of mitogen-activated protein kinase is required for migration and invasion of placental site trophoblastic tumor. Am J Pathol 2005; 167:879–85.
23. Buckhaults P, Zhang Z, Chen YC, et al. Identifying tumor origin using a gene expression-based classification map. Cancer Res 2003;63:4144–9.
24. Yen MJ, Hsu CY, Mao TL, et al. Diffuse mesothelin expression correlates with prolonged patient survival in ovarian serous carcinoma. Clin Cancer Res 2006;12:827–31.
25. Nakayama K, Nakayama N, Davidson B, et al. A BTB/POZ protein, NAC-1, is related to tumor recurrence and is essential for tumor growth and survival. Proc Natl Acad Sci U S A 2006;103:18739–44.
26. Hough CD, Sherman-Baust CA, Pizer ES, et al. Large-scale serial analysis of gene expression reveals genes differentially expressed in ovarian cancer. Cancer Res 2000;60:6281–7.
27. Pohl G, Ho CL, Kurman RJ, Bristow R, Wang TL, Shih Ie M. Inactivation of the mitogen-activated protein kinase pathway as a potential target-based therapy in ovarian serous tumors with KRAS or BRAF mutations. Cancer Res 2005;65: 1994–2000.
28. Poot RA, Dellaire G, Hulsmann BB, et al. HuCHRAC, a human ISWI chromatin remodelling complex contains hACF1 and two novel histone-fold proteins. EMBO J 2000;19:3377–87.
29. Bochar DA, Savard J, Wang W, et al. A family of chromatin remodeling factors related to Williams syndrome transcription factor. Proc Natl Acad Sci U S A 2000;97:1038–43.
30. Bozhenok L, Wade PA, Varga-Weisz P. WSTF-ISWI chromatin remodeling complex targets heterochromatic replication foci. EMBO J 2002;21:2231–41.
31. Hakimi MA, Bochar DA, Schmiesing JA, et al. A chromatin remodelling complex that loads cohesin onto human chromosomes. Nature 2002;418:994–8.
32. Neely KE, Workman JL. The complexity of chromatin remodeling and its links to cancer. Biochim Biophys Acta 2002;1603:19–29.

Research Article

Jagged-1 and Notch3 Juxtacrine Loop Regulates Ovarian Tumor Growth and Adhesion

Jung-Hye Choi,[1,3] Joon T. Park,[1] Ben Davidson,[4] Patrice J. Morin,[2] Ie-Ming Shih,[1] and Tian-Li Wang[1]

Departments of [1]Pathology, Oncology, Gynecology and Obstetrics, Johns Hopkins Medical Institutions; [2]Laboratory of Cellular and Molecular Biology, National Institute on Aging, Baltimore, Maryland; [3]Department of Oriental Pharmacy, Kyung Hee University, Seoul, Korea; and [4]Department of Pathology, Radiumhospitalet-Rikshospitalet Medical Center, University of Oslo, Oslo, Norway

Abstract

Notch3 **gene amplification and pathway activation have been reported in ovarian serous carcinoma. However, the primary Notch3 ligand that initiates signal transduction in ovarian cancer remains unclear. In this report, we identify Jagged-1 as the highest expressed Notch ligand in ovarian tumor cells as well as in peritoneal mesothelial cells that are in direct contact with disseminated ovarian cancer cells. Cell-cell adhesion and cellular proliferation were reduced in Notch3-expressing ovarian cancer cells that were cocultured with Jagged-1 knockdown mesothelial and tumor feeder cells. Interaction of Notch3-expressing ovarian cancer cells with Jagged-1–expressing feeder cells activated the promoter activity of candidate Notch3 target genes, and this activity was attenuated by Notch3 siRNA. Constitutive expression of the Notch3 intracellular domain significantly suppressed the Jagged-1 shRNA–mediated growth inhibitory effect. In Notch3-expressing ovarian cancer cells, Jagged-1–stimulating peptides enhanced cellular proliferation, which was suppressed by γ-secretase inhibitor and Notch3 siRNA. Taken together, our results show that Jagged-1 is the primary Notch3 ligand in ovarian carcinoma and Jagged-1/Notch3 interaction constitutes a juxtacrine loop promoting proliferation and dissemination of ovarian cancer cells within the intraperitoneal cavity.** [Cancer Res 2008;68(14):5716–23]

Introduction

Ovarian serous carcinoma represents one of the most aggressive neoplastic diseases in women. Although the molecular etiology of ovarian serous carcinoma remains mostly unknown, the majority of high-grade serous carcinomas harbor *TP53* mutations. They also exhibit high levels of chromosomal instability as reflected by frequent changes in DNA copy number including allelic loss and gain involving almost all chromosomes (1, 2). Genome-wide analysis has shown amplification in genes with oncogenic potential at several loci. Based on digital karyotyping and single nucleotide polymorphism array analyses, our research group found that *cyclin E1, AKT2, Notch3, Rsf-1*, and *PIK3CA* loci were among the most frequently amplified genomic regions (2). One of the genes we have characterized is *Notch3* because of its well-established role in a variety of physiologic and pathologic processes including cancer development. Copy number gain in *Notch3* at chromosome 19p13.12 occurred in ~20% of high-grade serous carcinomas, and overexpression of Notch3 was observed in nearly 50% of the cases examined (3), suggesting that Notch3 signaling contributes to tumor progression in ovarian cancer.

The Notch signaling pathway is evolutionally conserved. Members of this pathway include Notch ligands (Delta and Jagged), Notch receptors, the nuclear transcription factors such as CSL (also known as RBP-J and CBF1) that bind to Notch intracellular fragment, as well as the target genes that are controlled by Notch3/CSL coactivators. The mammalian *Notch* family is composed of four Notch receptors encoded by *Notch1, 2, 3*, and *4*. Five Notch ligands including Jagged-1, Jagged-2, Delta-like-1 (DLL1), Delta-like-3 (DLL3), and Delta-like-4 (DLL4) have been reported in mammals. Notch signaling is initiated by receptor-ligand interaction, which leads to proteolytic cleavages that liberate the Notch intracellular cytoplasmic domain (NICD) from the membrane. NICD then translocates to the nucleus where it binds to the transcription factor CSL complex and converts CSL into a transcriptional activator that promotes the transcription of genes downstream in the Notch pathway (4). We have previously shown that inactivation of the Notch3 pathway by γ-secretase inhibitor (GSI), or by Notch3-specific siRNA, resulted in suppression of proliferation and induction of apoptosis in ovarian cancer cells, suggesting that targeting of Notch3 may offer a therapeutic intervention in ovarian cancer with Notch3 amplification and overexpression (3, 5).

As the first step in elucidating the molecular mechanisms underlying the role of the Notch signaling pathway in the progression of ovarian serous carcinomas, we analyzed all known Notch ligands for their expression levels in ovarian tumor cell lines and found that Jagged-1 was expressed at the highest level among all the ligands. In ovarian cancer tissues, expression of Jagged-1 and nuclear localization of Notch3 was highly correlated. This suggests that in ovarian carcinoma Jagged-1 interacts with Notch3 in juxtacrine fashion. We then characterized the functional role of Jagged-1 and Notch3 interaction in promoting cellular binding and proliferation. Because mesothelial cells constitute the tumor microenvironment in advanced stage ovarian cancer, we also analyzed the expression profile of Notch ligands in mesothelial cells. Our result showed that Jagged-1 was the predominant form of Notch ligand expressed by mesothelial cells. Its biological role in supporting adhesion and growth of ovarian cancer cells was further investigated in this study.

Materials and Methods

Tissue samples. A total of 77 high-grade serous carcinomas and 12 low-grade serous carcinomas of the ovary were retrieved from the Ovarian Cancer Tissue Bank in the Johns Hopkins Medical Institutions. In addition, mesothelial cells from benign ascites or primary cultures were harvested

Note: Supplementary data for this article are available at Cancer Research Online (http://cancerres.aacrjournals.org/).

Requests for reprints: Tian-Li Wang, Departments of Gynecology and Obstetrics and Oncology, Johns Hopkins Medical Institutions, CRB-II, Room 306, 1550 Orleans Street, Baltimore, MD 21231. Phone: 410-502-0863; Fax: 410-502-7943; E-mail: tlw@jhmi.edu.

doi:10.1158/0008-5472.CAN-08-0001

from fresh specimens. Acquisition of tissue specimens and clinical information was approved by an institutional review board.

Reagents and cell lines. Ovarian cancer cells including OVCAR3, A2780, ES2, SKOV3, and TOV21G cells were purchased from American Type Culture Collection. Immortalized ovarian surface epithelial cells (OSE) by SV40 large T antigen were used in this study (6). Parental L cell and J cells stably expressing the hemagglutinin (HA)-tagged Jagged-1 protein were generously provided by Dr. G. Weinmaster (University of California at Los Angeles, Los Angeles, CA). Type 1 GSI was purchased from Calbiochem and was dissolved in DMSO. Jagged-1 peptide (CDDYYYGFGCNKFCRPR) and scrambled peptide (RCGPDCFDNY GRYKYCF) were synthesized by GenScript Corporation. Disuccinimidyl glutarate (DSG), a crosslinking reagent, was purchased from Pierce.

Primary mesothelial cell culture. Mesothelial cells were derived from either benign peritoneal effusions or from primary tumor tissues containing benign mesothelium. The enrichment of mesothelial cells was performed by dissociating tissues with collagenase A followed by incubation with magnetic beads conjugated with Ber-EP4 (EpCAM) antibody to immunosort epithelial cells. The negative cellular fraction was short-term cultured to expand the number of mesothelial cells. The mesothelial cells used in this study were found to be positive for calretinin (a mesothelial cell marker) in >99% of cells and negative for Ber-EP4 and mucin 4 (carcinoma markers) as determined by immunocytochemistry. Representative stains for mucin 4 and calretinin in mesothelial cell and carcinoma cell cultures were shown in Supplementary Fig. S1. The procedure to isolate epithelial cells has been previously described (7) and the protocol is available upon request.

Real-time PCR. Relative mRNA expression was measured by quantitative real-time reverse transcription-PCR (RT-PCR) using an iCycler (Bio-Rad). Threshold cycle numbers (Ct) were obtained using the iCycler Optical system interface software. PCR primers were designed using the Primer 3 program, and the nucleotide sequences of the primers for determining transcript expression were listed in Supplementary Table S1. Mean Ct of the gene of interest was calculated from duplicate or triplicate measurements and normalized with the mean Ct of a control gene, β-amyloid precursor gene, for which mRNA expression is relatively constant among the SAGE libraries (8). Data were further normalized to the result obtained from OSE cell, OSE7.

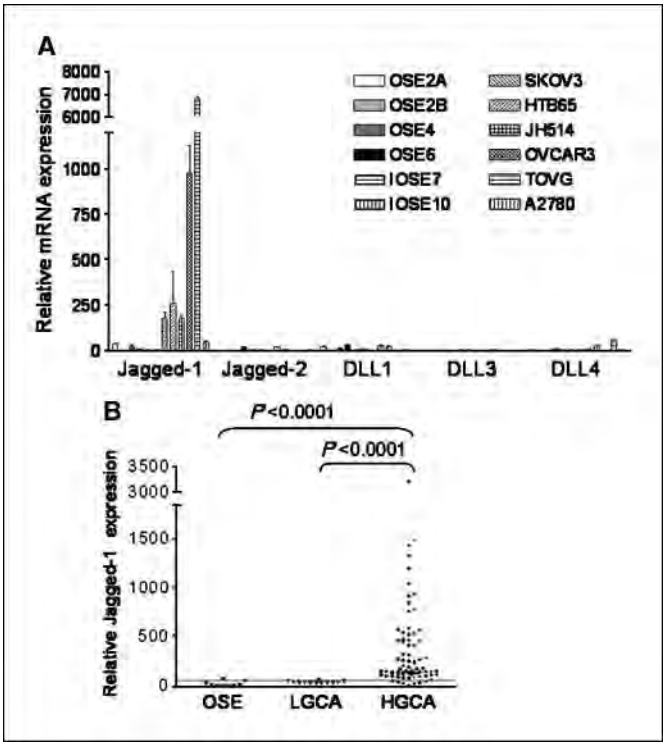

Figure 1. Expression of Notch ligands in ovarian cancer cells. *A,* mRNA expression levels of known Notch ligands including Jagged-1, Jagged-2, DLL1, DLL3, and DLL4 were measured by quantitative RT-PCR in six immortalized OSE cell lines and six ovarian cancer cell lines. *B,* mRNA expression levels of Jagged-1 in ovarian carcinoma tissues were measured by quantitative RT-PCR. Each symbol represents an individual specimen. *LGCA,* low-grade ovarian carcinoma; *HGCA,* high-grade ovarian carcinoma.

Gene knockdown using siRNA and small hairpin RNA. Jagged-1 small hairpin RNA (shRNA) vectors were purchased from Sigma-Aldrich. Jagged-1 shRNA sequence templates (CCGGCCGAATGGAGTACATCGTATACTCGAGTATACGATGTACTCCATTCGGTTTTTG) and (CCGGCCAGGATAACTGTGCGAACATCTCGAGATGTTCGCACAGTTATCCTGGTTTTTG) were inserted into lentiviral plasmids (pLKO.1-puro). Notch3-specific small interfering RNA (siRNA, GUCAAUGUUCACUUCGCAGUU) and (GCGUGGAUUCGGACCAGUCUGAGAGGG) and control siRNA that targets the *Luciferase* gene (GAUUAAAUCUUCUAGCGACUGCUUCGC) were synthesized by Integrated DNA Technologies. Cells were transfected with siRNA or shRNA at a final concentration of 200 nmol/L or 2 μg, respectively, using lipofectamine method (Invitrogen). Six hours after transfection, cells were replaced with fresh medium. On the following day, the treated cells were harvested and used for cell growth, binding and coculture assays.

Retrovirus transduction. The NICD3 retrovirus expressing the active intracellular domain of Notch3 was kindly provided by Dr. Michael Wang (University of Michigan, Ann Arbor, MI; ref. 9). Packaging cells (Phoenix cells) were transiently transfected with the NICD3 or empty vector using lipofectamine method (Invitrogen). On the following day, the supernatant was harvested and passed through a 0.45 μmol/L syringe filter. The filtered viral supernatant was resuspended in 4 μg/mL polybrene and added to cancer cell culture. Twenty-four hours after infection, cells were harvested and used for assays.

Immunohistochemistry. Anti-Notch3 rabbit polyclonal antibody and anti–Jagged-1 goat polyclonal antibody were purchased from Santa Cruz Biotechnology. An EnVision+System peroxidase kit (DAKO) was used for detection. Tissue microarrays (triplicate 1.5-mm cores from each specimen) including 60 high-grade serous carcinomas were used to facilitate immunohistochemistry. Immunointensity for Jagged-1 was scored as negative/low and high; nuclear staining for Notch3 was scored as negative (−) and positive (+) by two investigators.

Cell growth and colony formation assays. Cells were grown in 96-well plates at a density of 3,000 per well. Cell number was measured by the incorporation of SYBR green I nucleic acid gel stain (Molecular Probes) using a fluorescence microplate reader (Fluostar from BMG). Data were determined from five replicates and was expressed as the fold increase of control group. For colony formation assay, cells were seeded into 25-cm^2 flasks at a cell density of 1,500 or 4,500 cells per flask. After two weeks, the colonies were counted after staining with crystal violet dye (Sigma).

Cell-cell binding and coculture assay. For binding assay, the feeder cells were transfected with empty or Jagged-1 shRNA vector. One day after, the cells were seeded in 12-well plates at a density of 1.0×10^6 cells per well and were allowed to grow to confluence. A2780 cells (1.0×10^5) expressing green fluorescence protein (A2780-GFP) were laid on top of the feeder cells. Fifteen or forty-five minutes after coculture, A2780-GFP cells, which did not anchor to the bottom layer were harvested and classified as nonadherent cells. The A2780-GFP cells adhering to the bottom monolayer cells were dissociated by PBS containing 2 mmol/L EGTA and determined as adherent cells. For cell proliferation assay, 1.0×10^4 A2780-GFP cells were laid on top of the monolayer cells, which were previously irradiated after transfection with Jagged-1 shRNA. OVCAR3 cells were irradiated for 30 min with 68 cGy/min, whereas L cell, J cell, and mesothelial cells were irradiated at the same intensity for 8 min. The number of A2780-GFP cells was counted under a fluorescent microscope at day 2 of coculture.

Coimmunoprecipitation of Jagged-1 and Notch3. A2780 cells (1.0×10^7) were cocultured over the monolayer of J cells and incubated with a buffer containing 20 mmol/L HEPES (pH 7.5), 150 mmol/L NaCl, and 0.9 mmol/L $CaCl_2$ at room temperature for 45 min. DSG, a crosslinking reagent, was added to the culture at a final concentration of 20 μmol/L and incubated for 30 min. After crosslinking reaction, the cells were

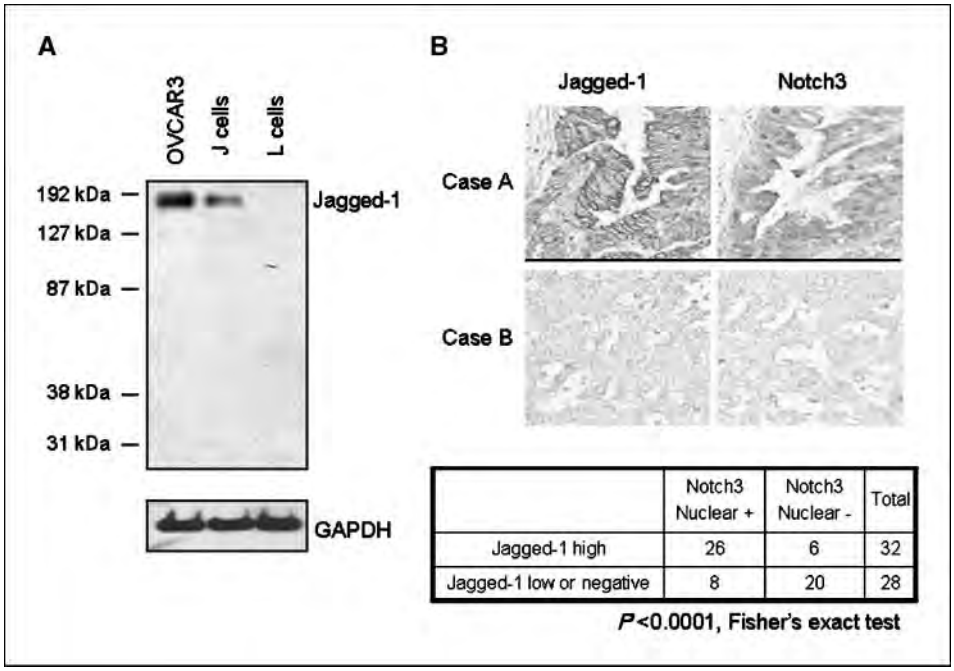

Figure 2. Correlation of Jagged-1 immunoreactivity with nuclear localization of Notch3 in ovarian carcinomas. *A,* Jagged-1 protein expression was determined by Western blot in OVCAR3, J, and L cells to validate the antibody specificity. J cell is an Ltk$^-$ mouse fibroblast cell line that was engineered to express the full-length Jagged-1. L cell is the parental Ltk$^-$ cell line. Jagged-1 protein bands (~175 kDa) were detected in both OVCAR3 and J cells but not in L cells. *B,* immunoreactivity of Jagged-1 and Notch3 in two representative ovarian high-grade carcinoma tissues (*top*). Case A shows intense Jagged-1 membrane staining and prominent Notch3 nuclear immunoreactivity. In contrast, case B shows very weak Jagged-1 and Notch3 staining. *Bottom,* summary table of Jagged-1 and Notch3 immunohistochemistry for 60 high-grade carcinomas. Jagged-1 protein expression and nuclear localization of Notch3 are significantly correlated ($P < 0.0001$, Fisher's exact test).

resuspended in TNE buffer [20 mmol/L Tris-Cl (pH 7.4),150 mmol/L NaCl,1% NP40, 5 g/mL aprotinin, and 1 mmol/L EDTA; ref. 10], and the lysate was immunoprecipitated with a Notch3 antibody or a control rabbit serum. To reverse the crosslink, a portion of the pull-down immunocomplex was treated with 50 mmol/L DTT and boiled for 10 min before electrophoresis.

Promoter activity assay. Hes1-luc and Hes5-luc reporter constructs were gifts from Dr. R Kageyama (Kyoto University, Japan). Pbx1-luc containing the 3Kb region of Pbx1 promoter was gift by Dr. S Higashiyama (Ehime University, Japan). Promoter reporter constructs and pRL-Renilla control plasmid (Promega) were transiently transfected into OVCAR3 cells by lipofectamine (Invitrogen). Twenty-four hours after transfection, the cells were seeded onto 48-well plates prelayered with J cells or L cells. Luciferase activity was determined by the Dual-Glo luciferase reagent (Promega). The reporter luciferase was normalized to Renilla luciferase and the ratio of luminescence from the experimental reporter to luminescence from the control reporter was calculated.

Results

Jagged-1 is the primary Notch ligand expressed in ovarian cancer cells. Gene expression levels among the known Notch ligands (Jagged-1, Jagged-2, DLL1, DLL3, and DLL4) were analyzed in a panel of OSEs and ovarian cancer cell lines by quantitative RT-PCR (Fig. 1*A*). Jagged-1 was found to be highly expressed in ovarian cancer cell lines but not in OSE. Because the expression level of other Notch ligands was relatively low in ovarian cancer cells, a different scale was used to present the relative expression levels among cell lines (Supplementary Fig. S2). To extrapolate the findings from ovarian cell lines to ovarian cancer tissues, we performed two additional experiments. First, quantitative RT-PCR was conducted to determine if Jagged-1 was overexpressed in ovarian carcinoma tissues. The data showed that Jagged-1 was highly expressed in ovarian carcinoma tissues compared with either low-grade ovarian carcinomas or OSE cells ($P < 0.0001$, Mann-Whitney test; Fig. 1*B*). Second, immunohistochemistry was performed on a larger panel of ovarian high-grade carcinomas ($n = 60$) to assess the expression of Jagged-1 and Notch3. The specificity of the Jagged-1 antibody was shown by Western blot analysis. A single protein band corresponding to Jagged-1 protein was observed in OVCAR3, an ovarian cancer cell line showing high Jagged-1 mRNA expression, and in J cells, a mouse fibroblast cell line engineered to express full-length Jagged-1, but not in nontransfected parental L cells (Fig. 2*A*). The Notch3 antibody used for immunohistochemistry has been previously reported (3), and its specificity was further validated by Western blot. In this analysis, HeLa cells were transduced with retrovirus expressing NICD and a single band corresponding to the molecular weight of NICD was detected (Supplementary Fig. S3). In addition, this band was absent in either nontransduced or empty vector–transduced group. We used prominent nuclear Notch3 immunoreactivity as a surrogate marker for Notch3 signaling activation in immunohistochemistry. By parallel comparison of Jagged-1 and Notch3 immunoreactivity in the same tissue samples, the data showed a significant correlation between intense Jagged-1 immunoreactivity and Notch3 nuclear immunoreactivity (Fig. 2*B*; $P < 0.0001$, Fisher's exact test).

Biological effects of Jagged-1 expression on cell adhesion and proliferation. The finding that Jagged-1 and Notch3 were coexpressed in ovarian carcinoma tissues and cell lines suggested that this ligand-receptor interaction could play an important functional role in ovarian cancer development. In this regard, we performed a cocultivation experiment to determine the ability of Jagged-1–expressing cells to enhance cell-cell adhesion and to stimulate cell growth of Notch-expressing tumor cells. OVCAR3, which expresses abundant Jagged-1, was selected to represent Jagged-1–expressing cells. Aliquots of OVCAR3 cells were transfected with Jagged-1 shRNAs to knock down Jagged-1 protein expression (Fig. 3*A, left*). Notch3 receptor–expressing cells, A2780, were pre-engineered to stably express GFP to facilitate quantification of cell numbers (designated as A2780-GFP). The A2780-GFP cells were overlaid onto a sublethally irradiated OVCAR3 monolayer and at indicated time points, the number of adherent and nonadherent A2780-GFP cells was counted. Our results showed

that a significant fraction of the overlaid A2780-GFP cells bound to the vector control–transfected OVCAR3 cells at both 15 and 45 minutes of coculture (Fig. 3*A, middle*). In contrast, knockdown of Jagged-1 by either shRNA1 or shRNA2 significantly reduced the number of A2780 cells that adhered to the OVCAR3 monolayer at 45 minutes. The binding of A2780-GFP to the OVCAR3 monolayer increased gradually, and the vast majority of cells bound to the OVCAR3 monolayer (with or without Jagged-1 shRNA treatment) after 2 hours of coculture.

Cell growth assay was performed by seeding the same number of A2780-GFP cells and measuring A2780-GFP cell numbers at 48 hours after coculture. The data showed that Jagged-1 knockdown in OVCAR3 cells reduced the ability of OVCAR3 cells to stimulate the growth of A2780-GFP cells (Fig. 3*A, right*).

To further show that biological effects of cell-cell adhesion and cell growth were due to interactions between Jagged-1 and Notch3, we performed an additional coculture assay using the J cell, which is an Ltk$^-$mouse fibroblast cell line engineered to express Jagged-1 (11), as the feeder monolayer. The parental Ltk$^-$ cell (L cell) was used as a control. Similarly, in the cell-binding assay, the A2780-GFP cells were overlaid on top of sublethally irradiated J cells or L cells and the number of adherent A2780-GFP cells was counted. The data showed that a higher number of A2780-GFP cells adhered to J-cell monolayer than to L-cell monolayer at 15 and 45 minutes after coculture (Fig. 3*B, top*). The number of A2780-GFP cells that adhered to J cells and L cells gradually increased, and almost all A2780 cells bound to J cells and L cells after 2 hours after coculture. In the cell growth assay, same number of A2780-GFP cells was laid on top of irradiated J cells or L cells and total number of A2780-GFP cells was determined 48 hours after coculture. The results showed a higher A2780-GFP cell number when cocultured with J cells compared with L cells (Fig. 3*B, bottom*). The above results imply that the presence of Jagged-1 in feeder cells is important in mediating cell binding and growth.

To determine if Jagged-1 directly bound to Notch3, a coimmunoprecipitation experiment was performed using a Notch3 antibody to pull down the receptor/ligand complex from a coculture of J cells and A2780-GFP cells (Fig. 3*C*). The coculture was first treated with a crosslinking reagent, DSG, before immunoprecipitation. Western blot was then performed in the presence or absence of DTT (to reverse crosslink). Our results showed that in the absence of DTT, high molecular weight immunoprecipitate was detected by both HA antibody (to detect Jagged-1-HA fusion protein expressed in J cells, *lane 6*) and Notch3 antibody (*lane 8*). When the same cell lysates were treated with DTT, the higher molecular weight band disappeared and lower molecular weight bands corresponding to monovalent Jagged-1 (*lane 4*) and Notch3 (*lane 9*) were detected. The Notch3-Jagged-1

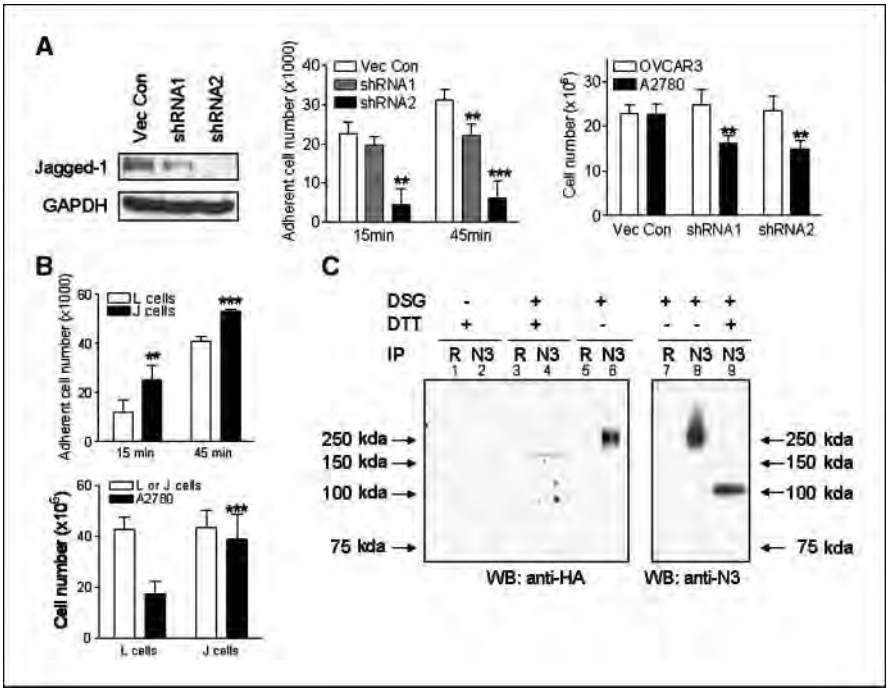

Figure 3. Coculture experiments show Jagged-1 in feeder cells is essential in promoting cell adhesion and growth of Notch3-expressing cancer cells. *A,* Western blot (*WB*) analysis shows that both Jagged-1 shRNAs, shRNA1 and shRNA2, significantly reduce Jagged-1 protein expression in OVCAR3 cells compared with the empty vector control (*left*). When compared with shRNA1, shRNA2 shows a more potent inhibitory effect. *Middle,* binding of A2780-GFP cells to Jagged-1 shRNA–transfected OVCAR3 cells was examined in a cell-cell association assay. The cell number of Notch3 expressing A2780-GFP cells that adhered to Jagged-1 shRNA–transfected OVCAR3 cells (feeder monolayer) was reduced when compared with the vector-transfected cells at both 15 and 45 min of cocultivation. *Right,* the growth of A2780-GFP cells is significantly reduced when cocultured with Jagged-1 shRNA–transfected feeder cells (OVCAR3) compared with vector control–transfected cells. Data were measured on the 2nd day of coculture. Data also shows similar number of feeder cells (OVCAR3) was present in each experimental group. **, $P < 0.01$; ***, $P < 0.001$, Student's *t* test. *B,* coculture of A2780-GFP cells and J- or L-feeder monolayer (*top*). The cell number of A2780-GFP bound to L cells (without Jagged-1 expression) was lower than that of J cells (with Jagged-1 expression) at both 15 and 45 min coculture incubation. *Bottom,* the growth of A2780-GFP cells is promoted when cocultured with J cells comparing to L cells. Similar number of L and J feeder cells was present in each experiment. **, $P < 0.01$; ***, $P < 0.001$, Student's *t* test. *C,* binding of Jagged-1 to Notch3 was verified by immunoprecipitation/Western experiment. The J cell and A2780-GFP cell coculture lysates were immunoprecipitated with an anti-Notch3 rabbit polyclonal antibody (N3) and were blotted with an HA antibody or a Notch3 antibody. HA antibody was used to detect expression of Jagged-1 in J cells because the expression construct contained an HA epitope tag. Rabbit antiserum (*R*) was used as the control in immunoprecipitation.

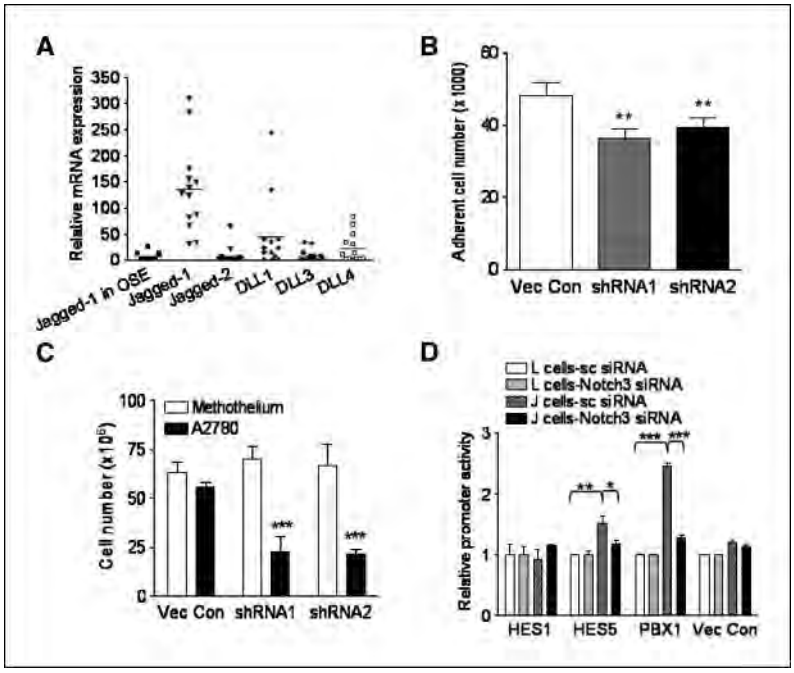

Figure 4. Expression of Jagged-1 in human peritoneal mesothelial cells is important in supporting adhesion and growth of ovarian tumor cells. *A,* quantitative RT-PCR measured Notch ligand expression levels in peritoneal mesothelial cells. *B* to *C,* coculture experiments. Human mesothelial cells expressing Jagged-1 were transfected with Jagged-1 shRNA and served as feeder monolayer. They were cocultured with Notch3-expressing A2780-GFP cells. *B,* compared with vector-transfected control (*vec con*), Jagged-1 shRNA treatment in mesothelial cells significantly reduced the binding capability of A2780-GFP cells. *C,* mesothelial cells pretreated with Jagged-1 shRNA significantly lose the ability to support growth of A2780-GFP cells. Similar number of mesothelial feeder cells was present in each experiment. Data were measured at 48 h after coculture. *D,* coculture of J cells with ovarian cancer cells stimulates the promoter activity of candidate Notch3 target genes. Promoter reporter constructs for Notch3 candidate target genes including Hes1, Hes5, and Pbx1 were transfected into Notch3-expressing OVCAR3 cells. The transfected cells were then cocultivated with J cells or L cells. High luciferase activity was detected in Pbx1 and Hes5 promoter construct–transfected groups when cocultured with J cell. This luciferase activity could be potently suppressed by Notch3-specific siRNA. *, $P < 0.02$; **, $P < 0.01$; ***, $P < 0.001$, Student's t test.

immunocomplex was not detectable in the control experiment using rabbit control serum in the immunoprecipitation step. The Notch3 protein under the crosslink/DTT denaturing condition migrated at a molecular weight higher than native NICD (~86 kDa), probably because it contained the NH_2-terminal transmembrane domain, a subunit that was not yet cleaved by secretases.

Interaction of Notch3-expressing tumor cells and Jagged-1–expressing mesothelial cells. Mesothelial cells are the main cell type in direct contact with ovarian cancer cells in the peritoneal cavity. It is possible that expression of Notch ligands in mesothelial cells creates a microenvironment suitable for ovarian cancer cells to survive and disseminate. Therefore, expression of Notch ligands in mesothelial cells derived from benign effusions or purified from tumor tissues was analyzed. The results showed that Jagged-1 was expressed in the majority of mesothelial cell samples and was the primary Notch ligand expressed by mesothelial cells ($P < 0.01$, Mann-Whitney test; Fig. 4*A*). To determine if mesothelial cells would support tumor adhesion and growth, we performed coculture experiments using mesothelial cells as the feeder layer. Primary mesothelial cell cultures were treated with Jagged-1 shRNA to reduce Jagged-1 expression. Although expression of Jagged-1 was significantly reduced, growth of mesothelial cells was not significantly affected (Supplementary Fig. S4). However, the cell-cell binding activity measured at 45 minutes was significantly reduced in A2780-GFP cells cocultured with mesothelial cells pretreated with Jagged-1 shRNA compared with those cocultured with control shRNA–treated mesothelial cells (Fig. 4*B*). Similar to previous coculture systems, almost all A2780-GFP eventually adhered to mesothelial feeder cells 2 hours after coculture. In cell growth assay, knockdown of Jagged-1 expression in mesothelial feeder cells significantly suppressed cell growth (Fig. 4*C*). The data indicated that the Jagged-1 expression in mesothelial cells is important for binding and growth of adjacent tumor cells.

To further determine if Jagged-1 expressed by the feeder cells could stimulate Notch3 signaling in tumor cells, we performed promoter reporter assays in which A2780 cell was transiently transfected with reporter plasmids containing promoter regions of candidate Notch3 downstream target genes including Hes1, Hes5 (12), and Pbx1,[5] and the transfected cells were cocultured with J cells or L cells. The data showed that Hes5 and Pbx1 promoter activities in A2780 cell were significantly induced by coculturing with J cells but not with L cells. Furthermore, these promoter activities were significantly suppressed by Notch3-siRNA (Fig. 4*D*) or GSI (data not shown). In contrast, we did not detect luciferase activity from Hes1 promoter reporter or vector control plasmid in any of the experimental conditions.

Jagged-1 gene knockdown reduces cellular proliferation in ovarian cancer cells overexpressing Jagged-1. To determine if Jagged-1 expression in cancer cells was essential for tumor cell growth, we knocked down Jagged-1 in TOV21G and OVCAR3 ovarian cancer cell lines, both expressing relatively high levels of Jagged-1 (Fig. 5*A*). In addition, two immortalized OSE cell lines (IOSE7 and IOSE10), neither of which expressed robust level of Jagged-1, were used as negative controls. The results showed that both of the Jagged-1–negative cell lines continued proliferating after shRNA transfection (Fig. 5*B*). There was no statistically significant difference between Jagged-1 shRNA-treated versus vector control-treated groups (Student's t test). In contrast, both Jagged-1–high cell lines showed a significant growth inhibitory effect after transfection with Jagged-1 shRNA as revealed by growth curves (Fig. 5*C*) and colony formation assay (Fig. 5*D*).

The effects of Jagged-1 are mediated by the Notch3 signaling pathway. To determine if the observed biological effects of Jagged-1 involved the Notch3 signaling pathway, we applied two independent but complementary approaches. First, we asked if constitutive expression of the NICD could reverse the growth inhibitory effect of Jagged-1 shRNA. As shown in Fig. 6*A*, ectopic expression of NICD had minor effect on cell growth; however, it

[5] J.T. Park et al., unpublished observation.

significantly abrogated the growth inhibitory effect of Jagged-1 shRNA. Second, a Jagged-1 peptide known to activate Notch signaling comparably to full-length Jagged-1 was used. When cultured in medium containing Jagged-1 peptide, the number of ovarian cancer cell OVCAR3 was significantly increased compared with the number of cells cultured in medium containing control peptide (Fig. 6*B*). The increase in cell number was likely due to increased proliferation activity because BrdUrd incorporation was enhanced in OVCAR3 cells incubated with Jagged-1 peptides (Supplementary Fig. S5). This proliferation-stimulating effect of Jagged-1 peptide could be inhibited by inactivating Notch3 signaling using either GSI (Fig. 6*C*) or Notch3-specific siRNA (Fig. 6*D*).

To determine if Notch3 could regulate Jagged-1 expression and thus initiate a positive-feedback loop in Notch signaling, we applied Notch3-siRNA in A2780, TOV21G, and OVCAR3 and measured the amount of Jagged-1 mRNA using quantitative real-time PCR. As shown in Supplementary Fig. S6, the results showed that Notch3 siRNA did not significantly affect Jagged-1 mRNA expression, suggesting a lack of such feedback loop in ovarian cancer cells. Taken together, the above data indicated that the biological effects of Jagged-1 observed in this study were mediated at least in part through Notch3 signaling.

Discussion

Growth and survival of tumor cells, as well as their ability to metastasize, depend on intricate interactions with their microenvironment. Despite accumulation of a variety of genetic lesions, human ovarian cancer cells remain dependent on their microenvironment during the progression of the disease. Our previous studies have shown *Notch3* gene amplification and overexpression in a significant fraction of ovarian carcinomas (2, 3). In the current study, we provided evidence that Jagged-1 expressed by mesothelial and ovarian cancer cells formed a juxtacrine loop with Notch receptor expressed on the surface of ovarian cancer cells. This promotes adhesion and proliferation of cancer cells within the peritoneal cavity.

Although Jagged-1 has been shown to be one of the Notch ligands, its role in initiating Notch signaling has not been well-established in ovarian cancer. In this study, we have shown the following pieces of evidence to suggest an important role of the Notch3/Jagged1 axis in promoting adhesion and growth in ovarian cancer cells. First, Jagged-1 was coexpressed with Notch3 in a significant number of ovarian cancers. Second, Jagged-1 expression in feeder cells is responsible for the binding and growth of cocultured ovarian cancer cells. Third, stimulatory Jagged-1 peptide increased cell number in Notch3-expressing ovarian cancer cell line, in which the effect could be reduced by GSI or by Notch3-specific siRNA. Forth, the growth suppression effect of Jagged-1 shRNA in ovarian cancer cells can be rescued by ectopic expression of NICD. Finally, in the coculture system, Jagged-1 expressed by the feeder cells induced promoter activation of candidate Notch3 target genes, *Hes5* and *Pbx1*. In aggregate, these findings suggest that Jagged-1 and Notch3 form a functional signaling network. Our results are consistent with a previous report showing that expression of Notch1 and its ligands, Jagged-1 and DLL1, is critical for cell survival and proliferation in glioma (13).

Expression of Jagged-1 in ovarian cancer cells and peritoneal mesothelial cells has significant biological implications. First, in primary ovarian tumors, reciprocal binding of Jagged-1 to Notch3 between adjacent tumor cells acts as a juxtacrine mediator that initiates and sustains Notch3 pathway activation, which is responsible for ovarian tumor development (Supplementary Fig. S7). Second, during tumor cell dissemination in the peritoneal cavity, Jagged-1 expressed by mesothelial cells may enhance tumor cell binding to and growth on the peritoneal surface, thus facilitating i.p. tumor dissemination, a cardinal feature in ovarian serous carcinoma (Supplementary Fig. S7). Ovarian serous carcinoma is associated with a devastating clinical outcome because most patients present at advanced stages when the tumor has widely spread in the peritoneal cavity (14). This "transcoelomic" dissemination involves multiple processes including tumor cell detachment, migration, and implantation on mesothelial cells carpeting the peritoneal cavity and the surface of abdominal

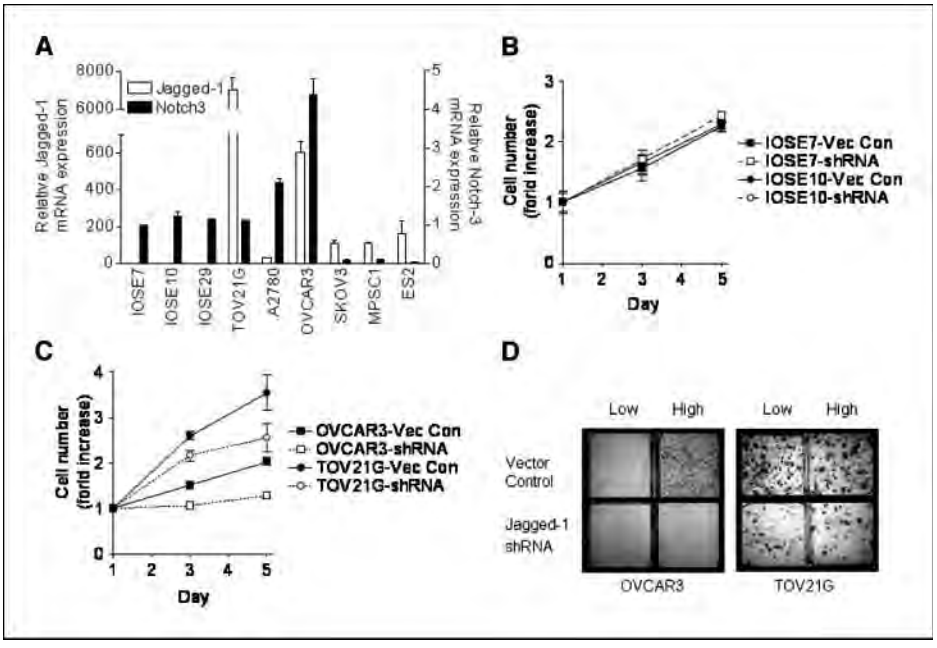

Figure 5. Effect of Jagged-1 knockdown on cell proliferation in ovarian cancer cells. *A,* expression of Jagged-1 and Notch3 mRNA in IOSE cells (IOSE7, IOSE10, and IOSE29) and ovarian cancer cell lines (TOV21G, A2780, OVCAR3, SKOV3, MPSC1, and ES2) was measured by quantitative RT-PCR. TOV21G and OVCAR3 showed the highest levels of Jagged-1 expression. *B,* Jagged-1 shRNA does not have a significant effect on cell growth at both day 3 and day 5 in IOSE 7 and IOSE10 cells. *C,* Jagged-1 shRNA significantly inhibits cell growth in ovarian cancer cell lines, which overexpress Jagged-1. $P < 0.01$ (day 3); $P < 0.001$ (day 5), Student's *t* test. *D,* colony formation is significantly reduced in both OVCAR3 and TOV21G cells transfection with Jagged-1 shRNA, comparing to vector-transfected group ($P < 0.01$, Student's *t* test). Cells were seeded at both low and high density and cell colonies were counted 2 wk after plating.

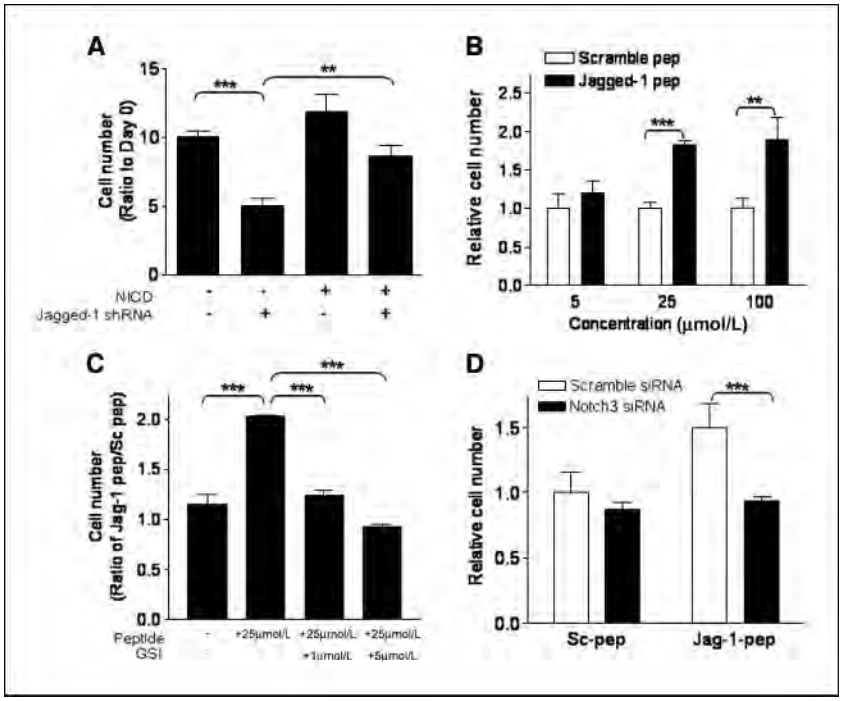

Figure 6. Involvement of Notch3 in Jagged-1–induced cell growth in ovarian cancer cells. *A,* OVCAR3 cells were transduced with retrovirus expressing active form of Notch3 (NICD) or with retrovirus prepared from empty vector. Jagged-1 shRNA inhibited cell proliferation in OVCAR3 cells and this growth inhibitory effect can be rescued by ectopic NICD expression. *B,* incubation of stimulatory Jagged-1 peptide in A2780 cells significantly increases cell number in a dose-dependent manner. Conversely, scramble peptide does not show growth stimulatory effect. *C,* the growth stimulatory effect of Jagged-1 peptide is blocked in a dose-dependent manner by treatment of GSI. *D,* similar to GSI, attenuation of Notch3 pathway using Notch3-specific siRNA suppressed Jagged-1 peptide-induced cell growth. **, $P < 0.01$; ***, $P < 0.001$, Student's *t* test.

organs. Transcoelomic dissemination is a major factor contributing to morbidity and mortality in women with ovarian carcinomas. It is plausible that ovarian cancer cells detached from the primary site directly contact with peritoneal mesothelial cells, which provide abundant Jagged-1 to facilitate the attachment of cancer cells to mesothelial cells and to enhanced proliferation of ovarian cancer cells. This process would contribute establishment of cancer cell colonies on the peritoneal surface, where the tumor cells might invade the underlying stromal tissue and establish implanted tumors.

Although the above represents our preferred view how Jagged-1 contributes to tumor progression in ovarian cancer, it should be noted that other mechanisms may exist. For example, Jagged-1 may have its own signaling function that is independent of the canonical Notch pathway. It has been shown that Jagged-1 and Delta-like-1, upon binding to Notch receptors, are sequentially processed by α- and γ-secretase, which lead to the release of nuclear signaling fragments (15, 16). The soluble Jagged-1 intracellular fragment translocates into the nucleus and activates gene expression via the transcription factor AP1 (15). Furthermore, ectopic expression of Jagged-1 was found to transform kidney epithelial cells, and this ability depends on the PDZ ligand domain at the C terminus of Jagged-1 (17). Therefore, in ovarian cancer cells that coexpress Notch3 and Jagged-1, Jagged-1 may play two functional roles. First, Jagged-1 serves as a membrane ligand to stimulate adjacent tumor cells in a juxtacrine manner through Notch3 receptor. Second, the intracellular domain of Jagged-1 may trigger signaling pathway distinct from Notch3 and promote tumor cell growth. Although the biological effects of Notch activation are well-known in human cells, it would be of interest to determine the Notch-independent role of Jagged-1 in human neoplasms.

In summary, we provided new evidence that Jagged-1 is the primary Notch3 ligand expressed by ovarian cancer cells and mesothelial cells. Interaction of Jagged-1 and Notch3 that activates intracellular Notch3 signaling may provide growth advantage of ovarian cancer cells in the peritoneal microenvironment. The above results show the dependence of ovarian cancer cells on a single Notch ligand and suggest that antagonizing Jagged-1 or disrupting the interaction between Jagged-1 and Notch3 can be potential therapeutic strategies for ovarian cancer.

Disclosure of Potential Conflicts of Interest

No potential conflicts of interest were disclosed.

Acknowledgments

Received 1/1/2008; revised 4/9/2008; accepted 5/4/2008.

Grant support: Individual Investigator Grant, Ovarian Cancer Research Fund (T.L. Wang); Institutional Research Grant, American Cancer Society (T.L. Wang); Department of Defense Ovarian Cancer Research Program OC040060 (T.L. Wang); and National Cancer Institute RO1 CA103937 and RO1 CA129080 (I.M. Shih).

The costs of publication of this article were defrayed in part by the payment of page charges. This article must therefore be hereby marked *advertisement* in accordance with 18 U.S.C. Section 1734 solely to indicate this fact.

We thank Kevin Lee for the help with the manuscript preparation.

References

1. Kohler MF, Marks JR, Wiseman RW, et al. Spectrum of mutation and frequency of allelic deletion of the p53 gene in ovarian cancer. J Natl Cancer Inst 1993;85:1513–9.
2. Nakayama K, Nakayama N, Jinawath N, et al. Amplicon profiles in ovarian serous carcinomas. Int J Cancer 2007; 120:2613–7.
3. Park JT, Li M, Nakayama N, et al. Notch-3 gene amplification in ovarian cancer. Cancer Res 2006;66:6312–8.
4. Weng AP, Aster JC. Multiple niches for Notch in cancer: context is everything. Curr Opin Genet Dev 2004;14:48–54.
5. Shih Ie M, Wang TL. Notch signaling, γ-secretase inhibitors, and cancer therapy. Cancer Res 2007;67: 1879–82.
6. Nitta M, Katabuchi H, Ohtake H, Tashiro H, Yamaizumi M,Okamura H. Characterization and tumorigenicity of human ovarian surface epithelial cells

immortalized by SV40 large T antigen. Gynecol Oncol 2001;81:10–7.
7. Nakayama K, Nakayama N, Kurman RJ, et al. Sequence mutations and amplification of PIK3CA and AKT2 genes in purified ovarian serous neoplasms. Cancer Biol Ther 2006;5:779–85.
8. Buckhaults P, Zhang Z, Chen YC, et al. Identifying tumor origin using a gene expression-based classification map. Cancer Res 2003;63:4144–9.
9. Dang L, Yoon K, Wang M, Gaiano N. Notch3 signaling promotes radial glial/progenitor character in the mammalian telencephalon. Dev Neurosci 2006;28: 58–69.
10. Shimizu K, Chiba S, Hosoya N, et al. Binding of Delta1, Jagged1, and Jagged2 to Notch2 rapidly induces cleavage, nuclear translocation, and hyperphosphorylation of Notch2. Mol Cell Biol 2000;20:6913–22.
11. Lindsell CE, Shawber CJ, Boulter J, Weinmaster G. Jagged: a mammalian ligand that activates Notch1. Cell 1995;80:909–17.
12. Ohtsuka T, Ishibashi M, Gradwohl G, Nakanishi S, Guillemot F, Kageyama R. Hes1 and Hes5 as notch effectors in mammalian neuronal differentiation. EMBO J 1999;18:2196–207.
13. Purow BW, Haque RM, Noel MW, et al. Expression of Notch-1 and its ligands, Delta-like-1 and Jagged-1, is critical for glioma cell survival and proliferation. Cancer Res 2005;65:2353–63.
14. Tan DS, Agarwal R, Kaye SB. Mechanisms of transcoelomic metastasis in ovarian cancer. Lancet Oncol 2006;7:925–34.
15. LaVoie MJ, Selkoe DJ. The Notch ligands, Jagged and Delta, are sequentially processed by α-secretase and presenilin/γ-secretase and release signaling fragments. J Biol Chem 2003;278:34427–37.
16. Bland CE, Kimberly P, Rand MD. Notch-induced proteolysis and nuclear localization of the Delta ligand. J Biol Chem 2003;278:13607–10.
17. Ascano JM, Beverly LJ, Capobianco AJ. The C-terminal PDZ-ligand of JAGGED1 is essential for cellular transformation. J Biol Chem 2003;278: 8771–9.

Research Article

Identification of *Pbx1*, a Potential Oncogene, as a Notch3 Target Gene in Ovarian Cancer

Joon T. Park,[1,3] Ie-Ming Shih,[1,2,3] and Tian-Li Wang[2]

[1]Department of Pathology, [2]Departments of Oncology, Gynecology and Obstetrics, and [3]Pathobiology Graduate Program, Johns Hopkins Medical Institutions, Baltimore, Maryland

Abstract

Notch3 gene amplification has recently been identified in ovarian cancer but the Notch3 effectors that are involved in the development of ovarian cancer remain elusive. In this study, we have identified *Pbx1*, a proto-oncogene in hematopoietic malignancy, as a Notch3 target gene. Pbx1 expression is transcriptionally regulated by Notch3 activation, and Notch3/CSL protein complex directly binds to the Pbx1 promoter segment harboring the CSL-binding sequence. The growth-inhibitory effect of γ-secretase inhibitor could be partially reversed by ectopic Pbx1 expression. Furthermore, functional studies by *Pbx1* short hairpin RNA knockdown show that Pbx1 is essential for cell proliferation and tumorigenicity. Taken together, the above findings indicate that *Pbx1* is a direct Notch3-regulated gene that mediates the survival signal of Notch3 in ovarian cancer. [Cancer Res 2008;68(21):8852–60]

Introduction

Cancer development has been known to share many molecular frameworks with embryonic development, tissue renewal, and differentiation (1). For example, in normal tissues, the Notch signaling pathway is activated under strict temporal and spatial control during tissue regeneration and cell fate determination. In contrast, during tumor development, Notch is constitutively activated and its sustained activation could be a result of genetic or epigenetic alterations. In human cancer, activation of the Notch receptor due to point mutations and gene translocations has been found in T-cell leukemia/lymphoma, non–small cell lung cancer, and breast carcinoma (2–5). Based on a genome-wide analysis of DNA copy number changes using both digital karyotyping (6) and single nucleotide polymorphism array analysis (7), we have identified Notch3 gene amplification in high-grade ovarian serous carcinomas (8). Notch3 gene amplification correlated with gene overexpression and pathway activation in ovarian serous carcinoma tissues. Functional inactivation of Notch3 either by γ-secretase inhibitor (GSI) or by Notch3-specific small interfering RNA (siRNA) resulted in suppression of cell proliferation and induction of apoptosis, suggesting that Notch3 activation is an important survival signal in ovarian cancer cells.

The Notch signaling pathway is evolutionally conserved. The primary members of this signaling pathway include Notch ligands (Delta and Jagged), Notch receptors (Notch1, Notch2, Notch3, and Notch4), the nuclear transcription factors such as CSL (also known as RBP-J and CBF1) that bind to Notch intracellular fragment, and the target genes that are controlled by Notch3/CSL coactivator. Activation of Notch signaling is initiated by receptor-ligand interaction, which leads to proteolytic cleavages that liberate the Notch intracellular cytoplasmic domain (NICD) from the plasma membrane. NICD translocates to the nucleus and binds to transcription complexes that contain CSL. NICD binding converts the CSL complex from a transcription repressor to a transcription activator, thereby initiating transcription of downstream effectors. The diverse biological activities of Notch signaling are thought to be mediated by the context-dependent expression of a heterogeneous group of downstream effectors.

Although several downstream genes in the Notch pathway have been reported (9–12), it is not known which of them are regulated by Notch3 in ovarian cancer cells. We have analyzed the known Notch target genes represented in the serial analysis of gene expression database in ovarian tissues. We found that the expression level of most of the known target genes, such as the Hes gene family, was extremely low and did not correlate with the expression level of Notch3 in ovarian cancer tissues. This suggested that the Notch3 targets in ovarian cancer were distinct from other known Notch targets. To identify candidate Notch3 targets, we analyzed the genes that were down-regulated following functional inactivation of Notch3 by treatment of ovarian cancer cells with GSI in this study. We selected one of the most promising candidate genes, *Pbx1*, for further characterization.

Materials and Methods

Affymetrix GeneChip analysis. Cancer cell lines, including OVCAR3, A2780, and MCF7, were cultured in the presence of 1 μmol/L GSI (EMD Chemicals) for 48 h. Control cells were cultured in the presence of DMSO under the same experimental condition. Total RNA was purified using a RNA purification kit (Qiagen) and RNA samples were hybridized onto the GeneChip arrays, HG-U133 Plus 2.0 (Affymetrix), which were spotted with over 47,000 human transcripts. The dChip software package[4] was used for data analysis. By comparing global gene expression profiles between GSI-treated and mock-treated cells, we selected the differentially expressed genes with levels >2-fold in all three tested cell lines. The differentially expressed genes were presented as individual boxes with pseudocolor to indicate gene expression levels.

Quantitative real-time PCR. Relative transcript expression levels were measured by quantitative real-time PCR using method previously described (13). The primer sequences were shown in Supplementary Table S1. PCRs were performed in triplicates using an iCycler (Bio-Rad). The amplified products were quantified by fluorescence intensity of SYBR Green I (Molecular Probes). Average fold changes were calculated by differences in threshold cycles (C_t) between pairs of samples to be compared. β-Amyloid

Note: Supplementary data for this article are available at Cancer Research Online (http://cancerres.aacrjournals.org/).

Requests for reprints: Tian-Li Wang, Johns Hopkins Medical Institutions, Cancer Research Building II, Room 306, 1550 Orleans Street, Baltimore, MD 21231. Phone: 410-502-0863; Fax: 410-502-7943; E-mail: tlw@jhmi.edu.

doi:10.1158/0008-5472.CAN-08-0517

[4] http://biosun1.harvard.edu/complab/dchip/

precursor gene was used for normalizing the cDNA concentration of each sample.

Western blot analysis. Protein lysates were prepared by resuspending cell pellets in Laemmli sample buffer containing 5% β-mercaptoethanol. Protein lysates were separated by 4% to 12% Tris-glycine gel electrophoresis and transferred onto polyvinylidene difluoride membrane using semidry apparatus (Bio-Rad). The membrane was blocked with 5% nonfat dry milk in TBST (20 mmol/L Tris-HCl, 0.5 mol/L NaCl, 0.1% Tween 20) and incubated with primary antibody at room temperature for 3 h followed by washing with TBST. Subsequently, the membrane was incubated with horseradish peroxidase (HRP)-conjugated secondary antibody and detected with enhanced chemiluminescence solution (Thermo Scientific). Antibodies used in this study include anti-NICD3 (Santa Cruz Biotechnology), anti-NH_2-terminal extracellular subunit of Notch3 (Abnova), anti-Pbx1 (Santa Cruz Biotechnology), and anti-Pbx1b (gift from Dr. Michael Cleary, Stanford University, Stanford, CA).

Chromatin immunoprecipitation assay. Chromatin immunoprecipitation (ChIP) was performed using the ChIP-IT enzymatic kit (Active Motif). HEK293 cells were infected with control pBabe-puro retrovirus and pBabe-CSL/V5 retrovirus for 24 h before fixation with 1% paraformaldehyde. The lysates of fixed cells were treated with an enzymatic shearing cocktail (Active Motif), and the soluble fraction was incubated with 4 μL of anti-V5 antibody or normal mouse IgG and precipitated with protein G magnetic beads at 4°C for overnight. The cross-links of the DNA eluate were reversed by heating at 65°C for 6 h, and the samples were treated with proteinase K (10 μg/mL) at 37°C for 1 h. Quantitative PCR was performed using SYBR Green I–based detection system as described above with the PCR primers that amplified different Pbx1 promoter regions (primer sequences shown in Supplementary Table S1). The input DNA was defined as an aliquot of sheared chromatin before immunoprecipitation and was used to normalize the amount of chromatin used in each experiment as previously described (14).

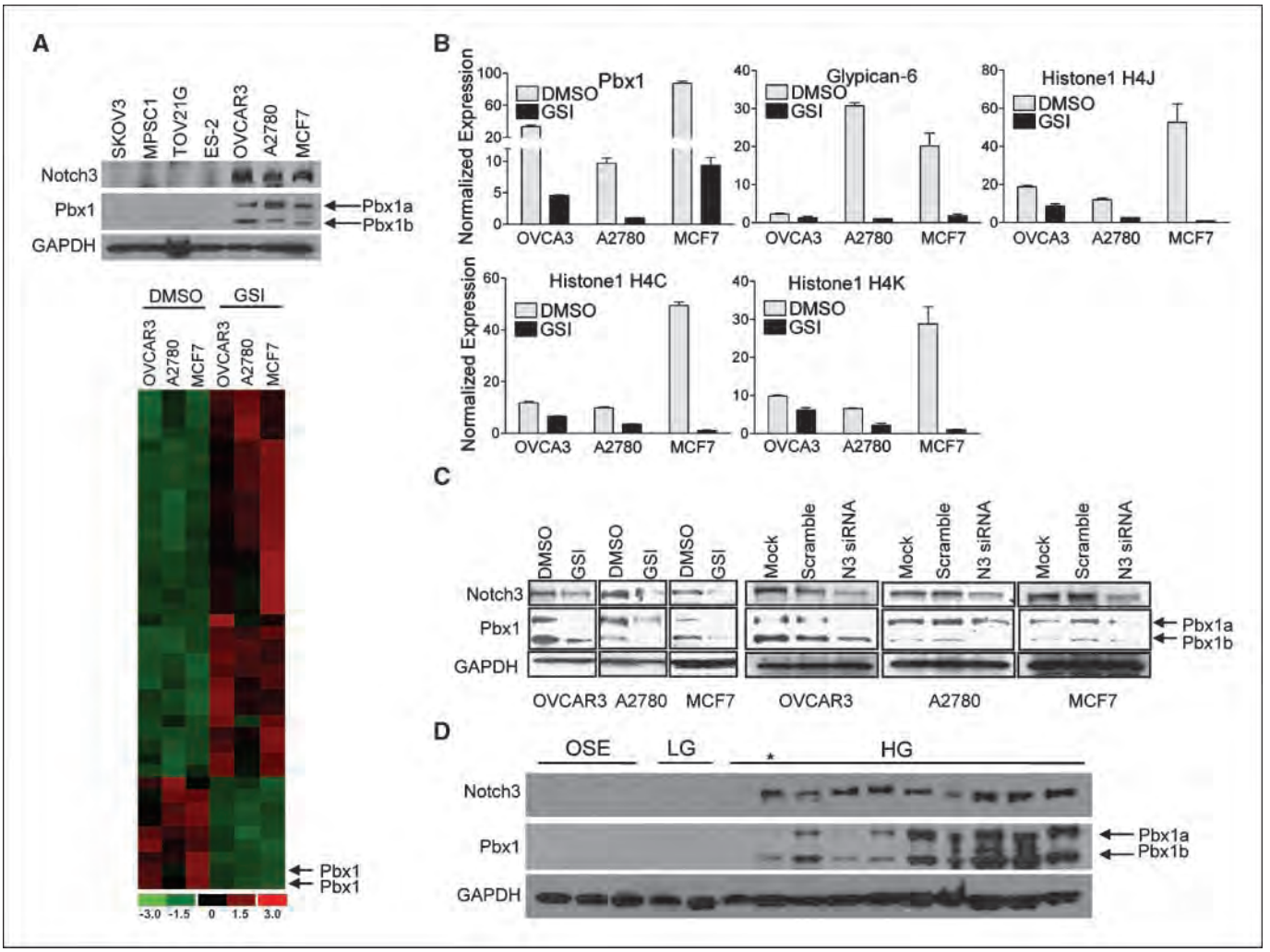

Figure 1. Identification of *Pbx1* as a putative Notch3 target gene. *A, top,* Western blot was performed to assess Notch3 protein expression in a panel of cancer cell lines. OVCAR3, A2780, and MCF7, which express abundant Notch3 proteins, were selected for microarray analysis. Glyceraldehyde-3-phosphate dehydrogenase (*GAPDH*) protein expression was used as loading control. Of note, the three cell lines with Notch3 overexpression also show Pbx1 overexpression. *Bottom,* Affymetrix GeneChip analysis was performed to identify genes differentially expressed between GSI-treated (1 μmol/L) versus DMSO-treated cancer cells. dChip software was used to analyze the data. A cutoff ratio of 2 was used to select the GSI-sensitive genes. Columns represent experimental samples (cell lines), whereas rows represent genes. The expression level of each gene in an individual specimen is shown as a pseudocolor gradient based on the relative expression level normalized for each gene, where red indicates high expression and green indicates low expression. *B,* quantitative real-time PCR was performed to confirm the candidate GSI-sensitive genes identified by GeneChip analysis. The genes that can be confirmed by quantitative PCR include *Pbx1, glypican-6, histone 4C, histone 4K*, and *histone 4J. C,* Western blot analysis shows that Pbx1 protein is down-regulated by either GSI or Notch3 siRNA. In contrast, mock (no transfection) and scramble siRNA do not have significant effects on Pbx1 protein expression. Cells were incubated with GSI or Notch siRNA for 48 h before assay. *D,* Western blot analysis of Pbx1 expression in a panel of ovarian tissues. *LG,* low-grade ovarian serous carcinoma; *HG,* high-grade ovarian serous carcinoma. *, samples with protein degradation. Pbx1a was found to be more susceptible to protein degradation.

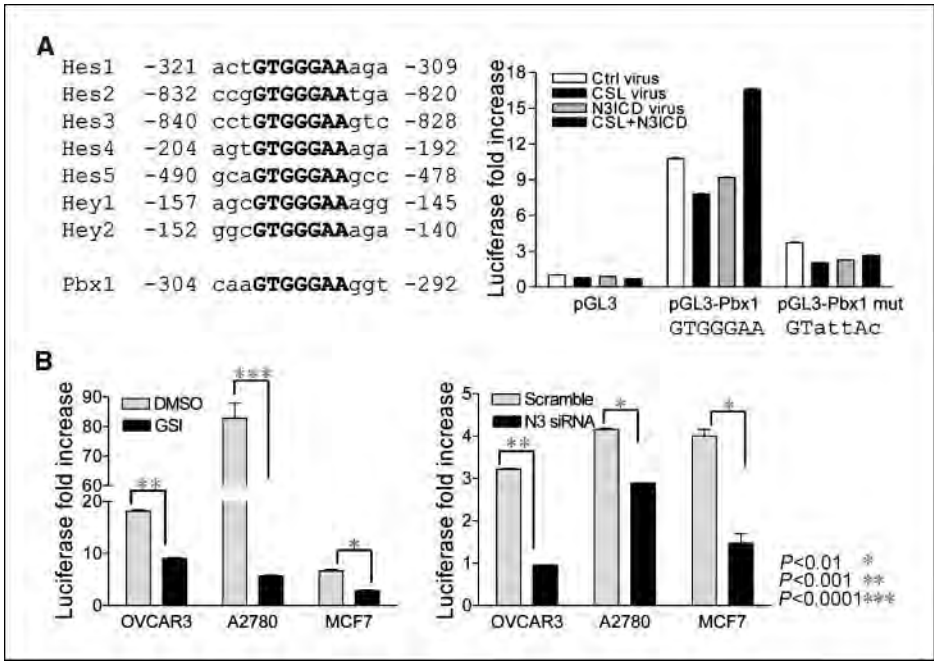

Figure 2. Notch3 induces Pbx1 expression through promoter activation. *A, left,* examples of the conserved CSL-binding site in Notch-regulated genes in human. Consensus CSL-binding sequence is bolded. The consensus CSL-binding site is located at −304 to −292 at Pbx1 promoter. *Right,* Pbx1 promoter assay shows increased reporter activity in cells transfected with the wild-type Pbx1 promoter construct (*pGL3-Pbx1*) compared with cells transfected with vector only control (*pGL3*). In pGL3-Pbx1–transfected groups, cells cotransduced with both CSL and NICD3 retroviruses show the highest promoter activity. Cells transduced with vector only virus and pGL3-Pbx1 also showed above background luciferase activity, likely due to the endogenous background expression of CSL and Notch in OSE. In contrast, cells transfected with the mutant Pbx1 promoter construct (*pGL3-Pbx1 mut*) containing the mutant CSL-binding site show a significantly lower luciferase activity compared with that of wild-type Pbx1 promoter. *B,* the pGL3-Pbx1 promoter construct was transfected into three cancer cell lines overexpressing Notch3. Pbx1 promoter activity was high in each of these transfected lines but was significantly reduced by either GSI or Notch3 siRNA.

Electrophoretic mobility shift assays. Nuclear extracts were prepared using the NE-PER nuclear and cytoplasmic extraction reagents (Pierce Biotechnology). Electrophoretic mobility shift assay (EMSA) was performed using the LightShift Chemiluminescent EMSA kit (Pierce Biotechnology) according to the manufacturer's protocol. DNA fragments for two Pbx1 promoter regions (−254 to −111 bp and −354 to −254 bp) were PCR amplified using biotinylated PCR primers. The biotin-labeled DNA fragments were incubated with nuclear lysate from 293 cell transfected with SG5-flag-CSL and/or infected with NICD3 retrovirus. Nuclear protein (5 μg) was incubated with 20 fmol of biotin-labeled DNA probe for 20 min at room temperature. DNA probe/protein complexes were separated by electrophoresis, transferred to a nylon membrane, incubated with streptavidin-HRP, and visualized by chemiluminescence.

Immunohistochemistry. A rabbit polyclonal anti-NICD3 antibody and a mouse anti-Pbx1b primary antibody against Pbx1b (15) were used in immunohistochemistry. Tissue microarrays containing 81 high-grade ovarian serous carcinoma tissues per slide were deparaffinized and antigen retrieved in a citrate buffer (pH 6.0) for 10 min. Immunostaining was performed using an EnVision+ System Peroxidase kit (DAKO). Immunointensity was independently scored by two investigators based on nuclear immunoreactivity. For discordant cases, a third investigator scored and the final intensity score was determined by the majority votes.

Production of Pbx1 and CSL retroviruses and rescue assay. The PCR products of Pbx1a, Pbx1b, and CSL were cloned into an expression vector, pCDNA6 with a V5 tag. The coding sequence of Pbx1a-V5, Pbx1b-V5, and CSL-V5 was subcloned into the pBabe-puro retroviral vector and high-titer retroviral stocks were generated using Phoenix ecotropic packaging cell line. Retroviral gene transfer was performed as previously described (16). For rescue assay, cells were infected with Pbx1a retrovirus and the empty pBabe-puro retrovirus. Cells were cultured in the presence of 0.7, 1.0, 1.5, and 2.0 μmol/L of GSI for 24 h. Mock-treated cells were cultured in the presence of DMSO vehicle control. Average cell counts and SDs were derived from five replicates. Student's *t* test was used to determine statistical significance.

Luciferase reporter assay. Immortalized ovarian surface epithelial (OSE) cells (OSE10) were transfected with pGL3 plasmid (Promega) or pGL3-Pbx1, which contains 3.0-kb Pbx1 promoter (gift from Dr. S. Higashiyama, Ehime University, Ehime, Japan; ref. 17). pRL-*Renilla* reporter plasmid (Promega), which serves to monitor the transfection efficiency, was cotransfected with the pGL3 plasmid. Transfection was carried out by Lipofectamine 2000 (Invitrogen) and luciferase expression was determined by Dual-Glo luciferase reagent (Promega). The firefly luciferase activity was normalized to luminescence from *Renilla* luciferase, and the ratio of luminescence from the experimental reporter to luminescence from the control reporter was calculated.

Transfection and cell growth assay. The sequences of Notch3-specific siRNAs and transfection method have been previously described (8). Pbx1 short hairpin RNA (shRNA) plasmid that targeted Pbx1 coding sequence 5′-GCAAGCGACAGAAATCCTGAA-3′ was purchased from the Mission shRNA collection at Sigma-Aldrich. The shRNA sequence was subcloned into a pLKO.1-puro vector. For cell proliferation assays, cells were seeded in 24-well culture plate and transfected with 1 μg Pbx1 shRNA plasmid using Lipofectamine 2000. One day after transfection, cells were plated into 96-well plates at a density of 3,000 per well and cell number was measured at different time points by the incorporation of SYBR Green I using a fluorescence microplate reader (FLUOstar, BMG). To determine if Pbx1 expression is essential for tumor cell survival *in vivo*, we transfected A2780 ovarian cancer cells with Pbx1 shRNA. Two millions of transfected cells were injected into the s.c. tissue of nude mice. Tumor volume was measured every other day for 18 d.

Results

Identification and validation of Notch3-regulated genes in cancer cells. To elucidate the mechanisms by which Notch3 signaling promotes tumor growth and survival, we first sought to identify Notch3-regulated genes by comparing gene expression between cancer cells treated either with GSI or with DMSO vehicle control. The release of NICD, which is required for Notch signaling, is mediated by γ-secretase. GSI has been shown to potently inhibit γ-secretase, thereby inactivating Notch signaling (18, 19). Ovarian cancer cell lines, including OVCAR3 and A2780, and a breast cancer cell line, MCF7, overexpressing Notch3 were selected for Affymetrix GeneChip analysis (Fig. 1*A, top*). Genes that showed 2-fold differential expression from all three cell lines were identified using the dChip software (Fig. 1*A, bottom*). We specifically focused on genes that were suppressed by GSI because those genes were potentially up-regulated by Notch3. Among those genes were *Pbx1, glypican-6, histone 1 H4C, 4K*, and *4J*, and *H2A member V* and a gene

containing the RERE repeats. Using quantitative real-time PCR, we were able to confirm five of them (Fig. 1*B*). *Pbx1* (pre-B-cell leukemia transcription factor 1) was selected for further characterization for several reasons. First, by GeneChip analysis, *Pbx1* showed the most dramatic and consistent down-regulation by GSI in all three cell lines tested. Second, Pbx1 protein expression correlated with Notch3 expression in cell lines based on Western blot analysis (Fig. 1*A, top*). Third, Pbx1 fusion protein, E2A-Pbx1, is known as a proto-oncogene in leukemia (20, 21). Lastly, the Pbx1 promoter contained a consensus sequence for CSL/NICD binding.

Two alternatively spliced variants of Pbx1, Pbx1a and Pbx1b, have been previously reported and both shares same sequences, except an additional exon in Pbx1a. Pbx1a encodes 430 amino acids, whereas Pbx1b encodes 347 amino acids. Pbx1b shares the same amino acid sequences as Pbx1a from 1 to 333 amino acids but differs in its last 14 amino acids. Using Western blot and reverse transcription-PCR (RT-PCR) analyses, we found that both splicing variants were present in ovarian cancers, with Pbx1a appearing as the predominant form (Fig. 1*A*; Supplementary Fig. S1).

The results of GeneChip analysis (based on 2-fold differential expression) did not identify the Notch downstream target genes previously reported in other organ systems. However, when the selection criteria were relaxed, we found that several of the known Notch target genes were moderately down-regulated by GSI (Supplementary Fig. S2*A*). Quantitative real-time PCR was performed on eight of the previously known target genes, including *HeyL, Hey2, TLE2, TLE4*, and *c-Myc*, in the same three cell lines selected for GeneChip analysis. The real-time PCR results showed that a consistent down-regulation of gene expression on GSI treatment could be observed in TLE2 and TLE4 (Supplementary Fig. S2*B*). In addition, c-Myc and cyclin A2 were significantly decreased by GSI in two of the three cell lines. These results suggested that these four genes may also have a role in mediating the function of Notch3 in some ovarian cancer cells.

Notch3-dependent Pbx1 expression. To determine whether Pbx1 expression is associated with Notch3 expression, we used the following approaches. First, we inhibited NICD3 expression using GSI and Notch3-specific siRNA in the Notch3-expressing cell lines OVCAR3, A2780, and MCF7. As shown in Fig. 1*C*, both Notch3 and Pbx1 protein levels (both splicing isoforms) were significantly reduced by either GSI or Notch3 siRNA treatment. We found that GSI inhibited the expression of NICD3 in a time-dependent fashion (Supplementary Fig. S3*A*). Similar findings were previously reported (22–24).

To determine whether Pbx1 protein expression correlates with Notch3 protein expression in ovarian cancer tissues, Western blot was performed in a panel of protein lysates prepared from immortalized OSEs, low-grade serous carcinoma tumor tissues, and high-grade serous carcinoma tumor tissues. The result showed that OSEs and low-grade tumors expressed low abundance of Pbx1

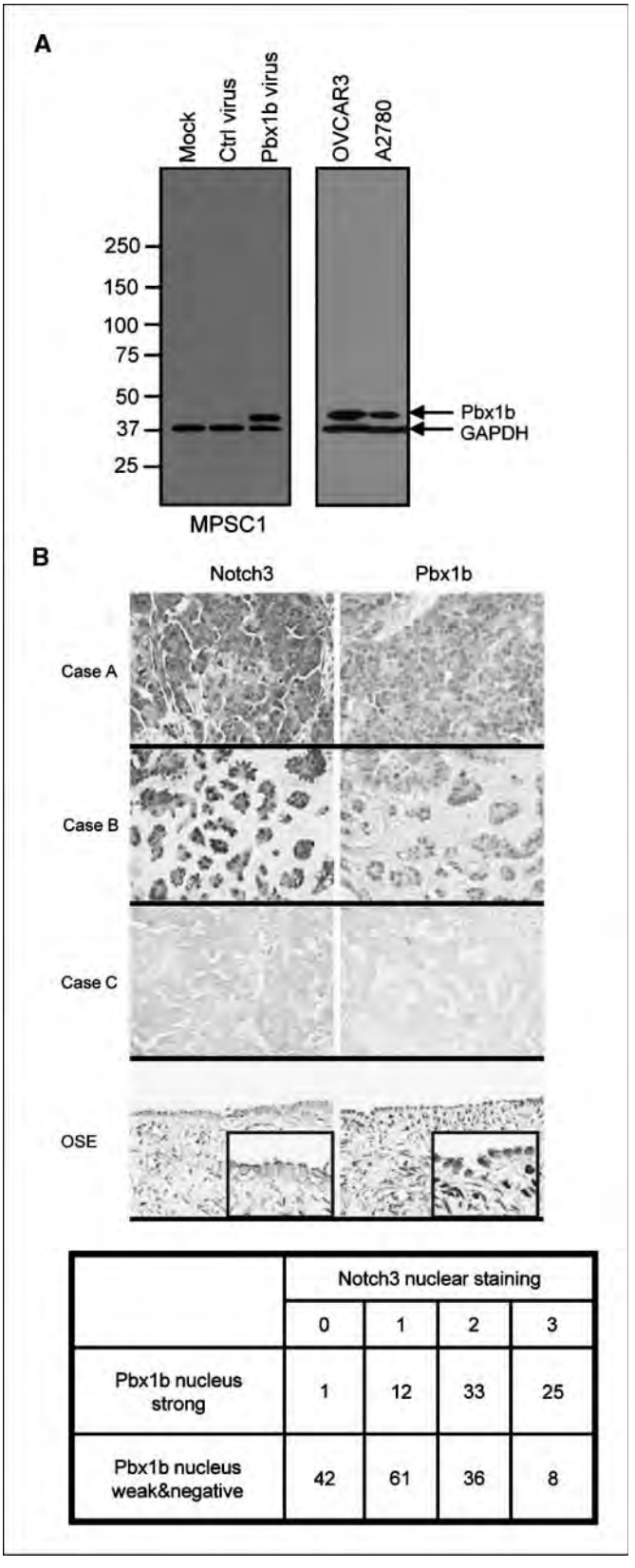

	Notch3 nuclear staining			
	0	1	2	3
Pbx1b nucleus strong	1	12	33	25
Pbx1b nucleus weak&negative	42	61	36	8

Figure 3. Pbx1b is overexpressed in high-grade ovarian serous tumors and its nuclear expression level is positively correlated with Notch3 activation. *A,* Western blot was performed to determine the specificity of the used anti-Pbx1b antibody. A predominant protein band corresponding to Pbx1b (~38.4 kDa) is detected in MPSC1 transduced with Pbx1b retrovirus but not in MPSC1 transduced with control virus or in nontransduced MPSC1 cells. A single band corresponding to Pbx1b protein can also be detected in ovarian cancer cell lines, including OVCAR3 and A2780. Glyceraldehyde-3-phosphate dehydrogenase was used as the loading control. *B,* immunohistochemistry of Notch3 and Pbx1b in ovarian high-grade serous carcinoma tissues and in normal ovaries. *Top,* immunostaining of Notch3 and Pbx1b was performed on the same set of high-grade serous ovarian tumors. Three representative specimens with high Notch3 and Pbx1b expression (*Case A*), medium Notch3 and Pbx1b expression (*Case B*), and undetectable Notch3 and Pbx1b expression (*Case C*) are shown. Normal OSE does not show nuclear Notch3 or Pbx1b immunoreactivity. *Bottom,* summary of immunohistochemical result. Data show a significant trend of Notch3 and Pbx1b coexpression in nucleus ($P < 0.0001$, Cochran-Armitage trend test).

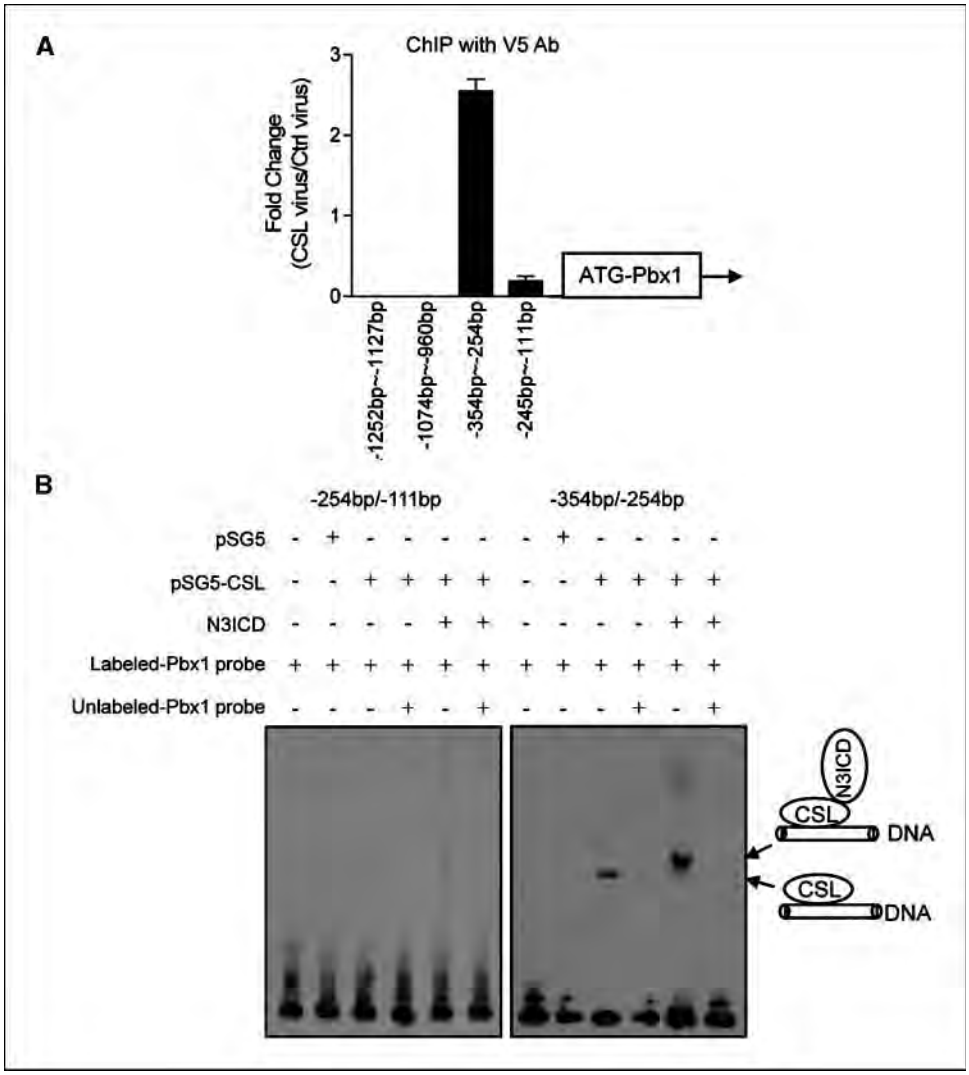

Figure 4. ChIP and EMSA of Pbx1 promoter region. *A,* ChIP assay was performed to determine the CSL-binding region at the Pbx1 promoter. Real-time PCR was performed on fragmented chromatin precipitated by an anti-V5 antibody (*Ab*) from 293T cells previously infected with CSL-V5 virus or control virus. PCR primers were designed to amplify four different regions at the Pbx1 promoter (−254/−111 bp, −354/−254 bp, −1,074/−960 bp, and −1,252/−1,127 bp). Results were normalized to the total input of chromatin DNA and were presented as the fold change of CSL-V5–infected cells relative to control virus–infected cells. *Columns,* mean of triplicate experiments; *bars,* SD. *B,* EMSA was performed on two adjacent regions at the Pbx1 promoter, −254/−111 bp and −354/−254 bp. The −354/−254 bp region contains the CSL consensus binding sequence. Biotin-labeled DNA probe for each promoter region was incubated with nuclear lysates from HEK293 cells transfected with CSL and/or transduced with NICD3 virus. The specificity of CSL binding was determined in a competition reaction in which a 100-fold molar excess of unlabeled DNA probe was added to the binding reaction. The binding complex was resolved by electrophoresis on a 4% to 12% Tris-borate EDTA gel. The position of biotin-labeled probe was detected with avidin-HRP followed by chemiluminescence.

or Notch3. In comparison, most high-grade tumors expressed high levels of Notch3 and Pbx1 (Fig. 1*D*).

To determine if protein synthesis was required for suppression of Pbx1 transcription by GSI, cycloheximide was added to the cell culture system to block protein synthesis. Cells overexpressing Notch3 were treated with 1 μmol/L GSI for 6 hours to down-regulate Pbx1 expression. Cells were then washed and incubated with medium with (mock washout) or without GSI. As shown in Supplementary Fig. S4, in the absence of GSI, a rapid up-regulation of Pbx1 transcripts was detected even in the presence of cycloheximide. In contrast, continuous presence of GSI suppressed the Pbx1 transcription. These results indicated that Pbx1 transcription regulation by Notch3 did not require *de novo* protein synthesis.

Next, we asked if Notch3 was directly involved in transcriptional regulation of Pbx1. Using a Pbx1 promoter-luciferase reporter construct (17), we measured *Pbx1* promoter activity in OSE cells derived from normal OSE. This promoter construct, pGL3-Pbx1, includes a 3.0-kb Pbx1 promoter region containing one CSL consensus binding site located at −304 to −292 bp upstream of the translation initiation codon (Fig. 2*A, left*). pGL3-Pbx1 was transfected into OSE cells, which were previously engineered to express CSL, NICD3, or both. As shown in Fig. 2*A* (*right*), luciferase activity was significantly higher in pGL3-Pbx1–transfected groups compared with pGL3-transfected groups. A low level of luciferase activity was detected in pGL3-Pbx1–transfected cells even in the absence of CSL or NICD3 virus transduction, likely due to endogenous CSL and NICD3 in OSE cells. Luciferase activity was further enhanced in cells cotransduced with CSL and NICD3. To test the specificity of the promoter activity, we created a promoter construct that carried mutated CSL-binding site (GTAATAC). When assayed in OSE cells, luciferase activity driven by the pGL3-Pbx1 mutant reporter was significantly reduced under all experimental conditions, indicating that a functional CSL site was required for promoter activity.

Pbx1 promoter reporter construct was also used to test promoter activity in cell lines (OVCAR3, A2780, and MCF7) that expressed both Notch3 and Pbx1. In these experiments, we determined if inactivating Notch3 using GSI or Notch3 siRNA would lead to inhibition of luciferase reporter activity. Indeed, in all Notch3-expressing cell lines examined, GSI and Notch3 siRNA treatment led to a significant suppression in Pbx1 promoter reporter activity (Fig. 2*B*).

Correlation of Pbx1b expression and NICD3 immunoreactivity in tumor samples. The above results showed that Pbx1 expression was transcriptionally regulated by Notch3 pathway

activation. To determine if this association also occurred *in vivo*, we performed immunohistochemistry to assess Notch3 and Pbx1 expression levels in a series of ovarian serous carcinoma tissues. After an extensive search for Pbx1 antibodies that worked in formalin-fixed, paraffin-embedded tissues, we only identified an antibody against the COOH terminus of Pbx1b that recognized the antigen in paraffin sections. The specificity of this antibody was confirmed by showing that a single protein band, corresponding to the molecular mass of Pbx1b protein, was detected in Pbx1b gene-transduced MPSC1 cells but not in vector-transduced or in parental MPSC1 cells (Fig. 3*A*). Because Western blot and RT-PCR both showed coexpression of Pbx1a and Pbx1b in ovarian tissues, Pbx1b immunoreactivity was used as the surrogate marker for Pbx1 expression. The specificity of the Notch3 antibody and its application in immunohistochemistry has been shown in previous reports (8, 16). Because nuclear localization of Notch is an indication of pathway activation and Pbx1b is a nuclear transcription factor, we focused on evaluating nuclear immunoreactivity of both proteins. Pbx1b nuclear immunoreactivity was always either intense or very weak/undetectable, whereas Notch3 nuclear immunoreactivity showed a range of intensity (0, 1+, 2+, and 3+). Representative immunostaining results on tissue sections are shown in Fig. 3*B*. Using the Cochran-Armitage trend test, we found that there was a significant trend between Pbx1b and Notch3 nuclear co-overexpression in ovarian serous carcinoma tissues ($P < 0.0001$; Fig. 3*B*).

To further determine the Pbx1 expression pattern in OSE, low-grade, and high-grade serous carcinoma tissues, we performed quantitative RT-PCR using PCR primers that amplified both Pbx1a and Pbx1b. The data showed significantly higher Pbx1 mRNA levels in high-grade serous carcinoma tissues than in normal OSE cells or low-grade serous carcinomas (Supplementary Fig. S5), a finding supporting the results using Western blot analysis shown in Fig. 1*D*.

Direct interaction between CSL/NICD3 protein complex and the *Pbx1* promoter region. The above findings indicated transcriptional regulation of Pbx1 by Notch3 and were suggestive of direct interaction of Notch3/CSL complex with the Pbx1 promoter. To determine if this is the case, we performed ChIP and EMSA. ChIP using an anti-V5 tag antibody in CSL-V5–transduced HEK293 cells compared with vector-transduced HEK293 cells showed that among different Pbx1 promoter segments, a fragment spanning nucleotides −354 to −254 bp (−354/−254) containing the canonical consensus CSL-binding sequence bound most robustly to the CSL protein (Fig. 4*A*). Immunoprecipitation of the CSL-containing DNA segment seemed to be specific, as ChIP using control mouse IgG instead of anti-V5 antibody did not bring down this fragment (data not shown).

EMSA was performed to determine if the NICD3/CSL protein complex directly bound to the *Pbx1* promoter region containing the CSL-binding sequence. For this purpose, a DNA probe spanning the −354/−254 region at the *Pbx1* promoter containing the canonical CSL consensus site was generated. An adjacent DNA segment (−254/−111) was used as a control. As shown in Fig. 4*B*, a band shift can be detected in the CSL-expressing group only when the −354/−254 probe was used in the assay. Binding of the CSL complex to the labeled probe could be competitively inhibited by 100-fold molar excess of unlabeled probes (Fig. 4*B*). Furthermore, when NICD3 was coexpressed with CSL in the same cells, the band shifted to a higher molecular weight, corresponding to the NICD3/CSL complex. This higher molecular weight band is more intense than the band formed in the absence of Notch3, suggesting that the NICD3/CSL complex forms a more stable complex with the Pbx1 promoter. A similar effect in the molecular weight shift has been reported in the Notch1/CSL complex (9).

Functional roles of Pbx1 in Notch3 signaling. To determine the biological effects of Pbx1 in mediating Notch3 signaling, we examined if ectopic expression of Pbx1 (Fig. 5*A*) could reverse GSI-mediated growth inhibition in A2780, OVCAR3, and MCF7 cells. We found that compared with control virus expression, constitutive expression of ectopic Pbx1 could significantly protect the cells from the growth-inhibitory effect of GSI at 1 to 2 μmol/L concentration (Fig. 5*B*). However, ectopic expression of Pbx1 did not increase cell number in the same cell lines (data not shown), suggesting that Pbx1 alone is not sufficient to promote cell growth.

To assess if Pbx1 was essential for ovarian cancer cell growth, we examined the effect of Pbx1 shRNA on cell proliferation. Pbx1 shRNA was transfected into A2780, OVCAR3, and MCF7 cells, all of which expressed both Notch3 and Pbx1. The efficiency of Pbx1

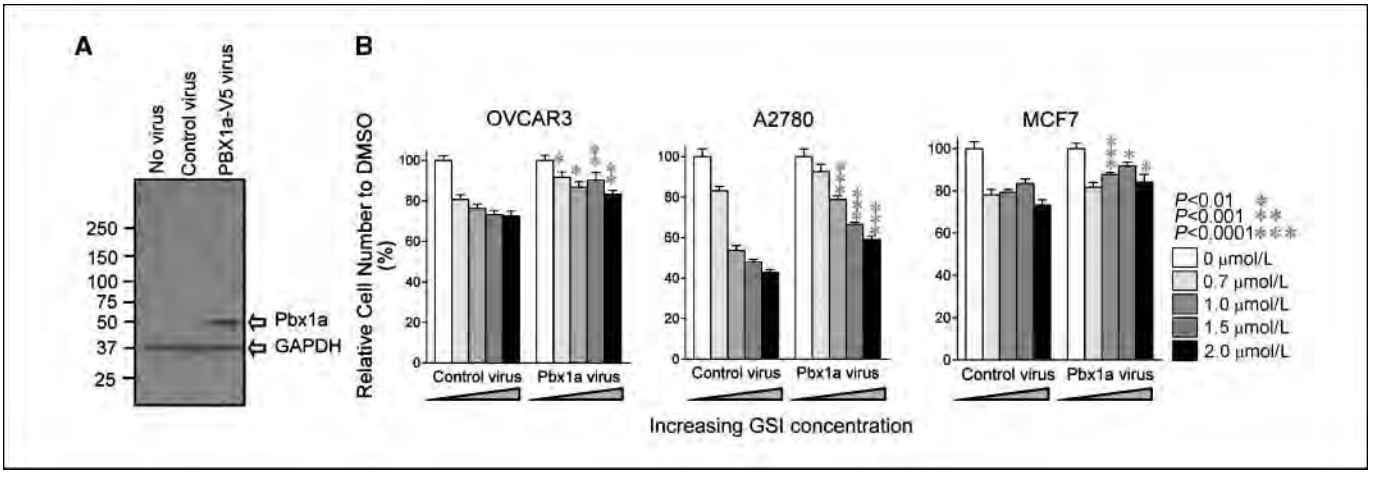

Figure 5. Constitutive Pbx1a expression rescues cancer cells from GSI-induced growth inhibition. *A,* Pbx1a cDNA tagged with a V5 epitope was cloned into the pBabe retroviral vector (controlled by a cytomegalovirus promoter). Cells were transduced with the resulting Pbx1a retrovirus and analyzed by Western blot. Pbx1a protein was detected using an anti-V5 antibody. *B,* Notch3-expressing cancer cell lines (including OVCAR3, A2780, and MCF7) transduced with Pbx1a or control retrovirus were treated with various concentrations of GSI. The results show that ectopic Pbx1a expression reduces sensitivity to growth inhibition at 1 to 2 μmol/L of GSI.

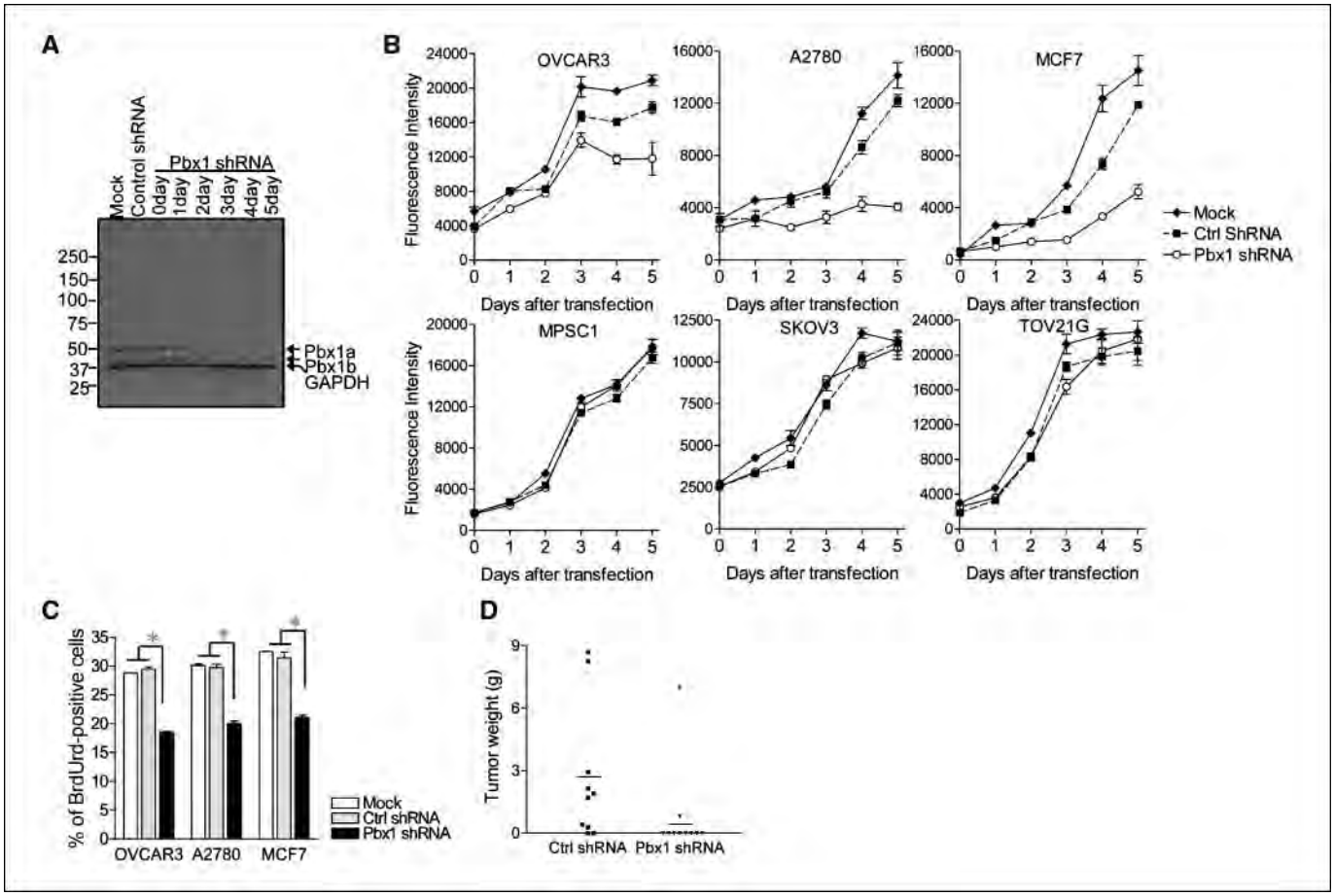

Figure 6. Pbx1 knockdown by shRNA inhibits cell proliferation. *A,* Pbx1 shRNA was found to specifically suppress Pbx1 protein expression during the course of the experiment (2–5 d after transfection). Control shRNA or mock transfection did not have such effect. *B,* Pbx1 shRNA suppresses the growth of tumor cell lines, including OVCAR3, A2780, and MCF7, which express both Notch3 and Pbx1 *in vitro*. In contrast, Pbx1 shRNA does not show significant growth-inhibitory effects on MPSC1, SKOV3, and TOV21G ovarian cancer cells that do not express detectable levels of Pbx1. *C,* BrdUrd uptake assay showed a reduction in DNA synthesis in cancer cells treated with Pbx1 shRNA compared with control shRNA–transfected and mock-transfected groups. *, $P < 0.001$. *D,* Pbx1 gene knockdown reduces tumorigenicity of A2780 tumors in nude mice. *Bars,* average of tumor weight.

shRNA in suppressing Pbx1 protein expression was shown by Western blot analysis (Fig. 6*A*). Among all three cell lines, compared with cells with mock transfection or control shRNA transfection, Pbx1 shRNA–transfected cells showed a significant reduction in cell number (Fig. 6*B*). The decrease in cell number in Pbx1 shRNA–treated cells was due to suppression of DNA synthesis as evidenced by reduced bromodeoxyuridine (BrdUrd) uptake (Fig. 6*C*). Increased apoptosis did not seem to be a factor because the percentage of apoptotic cells was similar between Pbx1 shRNA–treated and control shRNA–treated cells (data not shown). In ovarian cancer cells, including MPSC1, SKOV3, and TOV21G, which did not express detectable levels of Pbx1 or Notch3, Pbx1 shRNA did not have significant effects on cell growth (Fig. 6*B*).

To determine the role of Pbx1 on tumor development, we used shRNA to knock down Pbx1 expression in A2780 cells and measured their ability to form s.c. tumors in athymic *nu/nu* mice. We observed a difference in forming s.c. tumors between Pbx shRNA–treated versus control shRNA–treated groups (Fig. 6*D*). Eight of 10 mice in the control shRNA–treated group grew tumors, whereas only 2 of 10 mice in the Pbx1 shRNA–treated group grew tumor ($P < 0.05$, Fisher's exact test). The two tumors that grew in the Pbx1 shRNA–transfected group were examined for Pbx1 expression by immunohistochemistry and quantitative RT-PCR and were found to harbor significant Pbx1 expression. This result suggests that tumor cell formation in these animals was likely the result of clonal selection in favor of Pbx1-expressing cells. However, there is no significant difference in tumor volume between Pbx1 shRNA–treated versus control shRNA–treated group possibly due to high variance of tumor size.

Discussion

Notch signaling is involved in diverse cellular functions, including cell fate determination, morphogenesis, and oncogenesis, which are mediated by unique Notch downstream effectors. Expression of specific Notch downstream genes is tissue and context dependent. Although a repertoire of Notch-controlled genes has been identified, the Notch effectors that are involved in the development of human cancer remain elusive. In this study, we report a novel Notch3-regulated gene, *Pbx1*, in ovarian cancer cells and show that transcriptional regulation of Pbx1 is a direct consequence of Notch3 activation. Our functional studies provide evidence that Pbx1 mediates, at least in part, the effect of Notch activation in the development of ovarian cancer.

Several approaches were used in this study to show that *Pbx1* was the direct downstream target gene of the Notch3 signaling

pathway. First, Pbx1 promoter activity increased on ectopic expression of CSL and NICD3 and decreased after treating cells with either GSI or Notch3-specific siRNA. Furthermore, mutating CSL consensus binding site at Pbx1 promoter leads to an abolishment of Pbx1 promoter activity. Therefore, our data showed a significant association between Notch3 pathway activation and Pbx1 transcription activity. Second, ChIP and gel shift assays showed that there was a direct interaction between the NICD3/CSL complex and the Pbx1 promoter sequence containing the consensus CSL-binding site. Third, constitutive expression of Pbx1 could rescue cells, at least partially, from the growth-suppressive effects of GSI. Furthermore, our recent study using a coculture system also showed that Pbx1 promoter activity was stimulated on Notch3 and Jagged-1 binding, and this activity was attenuated by Notch3 siRNA (25).

In this study, GSI treatment in Notch3-expressing cell lines was associated with a time-dependent decrease of NICD3 protein. This observation is similar to those previously reported (22–24). Furthermore, we also found that the expression of full-length Notch3 as well as NH_2-terminal extracellular subunit of Notch3 was also down-regulated by GSI (Supplementary Fig. S3*B*). This could be due to Notch3 transcription, which is regulated by NICD3 through a positive feedback loop. Accordingly, when NICD3 generation was inhibited by GSI, it also affected the transcription of Notch3, leading to further reduction of the Notch3 protein expression. Indeed, several studies have shown the positive feedback regulation of Notch expression by its own signaling in a variety of organisms, including *Caenorhabditis elegans* (26), *Drosophila* (27), and mouse (28). Although the above is our preferred explanation, it remains possible that GSI can directly affect transcription of certain genes in addition to its effect in inhibiting γ-secretase.

In this study, Pbx1 shRNA was found to inhibit proliferation but did not have a significant effect on apoptosis. Our earlier study, however, showed that inhibiting Notch3 signaling affected both proliferation and apoptosis (8). These results suggest that Pbx1 mediates part, but not all, of the effects of the Notch3 pathway activation. Toward this end, we have identified other candidate Notch3-regulated genes in ovarian carcinoma through microarray analysis. Although confirmation is required, it is possible that some of these genes work in concert with Pbx1 to mediate the tumor survival of Notch3 activation.

Pbx1 is a member of the three–amino acid loop extension class of homeodomain transcription factors and can form multimeric transcriptional complexes with other homeodomain proteins, such as Hox (29) and MyoD (30), and can participate in a variety of transcriptional regulatory processes. Deletion of *Pbx1* resulted in organ hypoplasia and defects in B-cell differentiation, indicating that Pbx1 expression is essential for organ development (31–35). *Pbx1* was initially identified as a proto-oncogene in human leukemia cells harboring the translocation t(1;19)(q23;p13.3) that produced an oncogenic E2A-Pbx1 fusion protein (20, 36). The fusion of the potent transcriptional activation domain of E2A in chromosome 19 onto the DNA-binding domain of Pbx1 in chromosome 1 contributes to the acute lymphoblastic phenotype by modifying expression of genes normally responsive to Pbx1. In addition to leukemia, Pbx1 is highly expressed in melanoma cells and Pbx1 gene knockdown leads to growth suppression in melanoma cells (17). Consistent with this result, we showed in this report that knockdown of Pbx1 significantly reduced cellular proliferation and tumorigenicity in cancer cells over-expressing both Pbx1 and Notch3, suggesting that Pbx1 expression provides a survival signal in cancer cells that are dependent on Pbx1 pathway.

Identification of *Pbx1* as a Notch3-regulated gene in cancer cells has the following biological and clinical implications. First, our results further support the view that Notch3 signaling is mediated by different downstream targets in different pathophysiologic settings. In ovarian cancer, Pbx1 seems to be one of the downstream targets that mediate Notch3 function. Second, Pbx1 may function as a molecular hub for different pathways, including Notch and Hox. It has been shown that Pbx1 can directly interact with Hox (37) and other homeodomain proteins, including Meis (38). The Pbx1-Meis complex functions as a cofactor with Hox to further enhance DNA-binding activity (15). The critical role of Hox has been well documented in a variety of human neoplastic diseases, including leukemia (39, 40) and ovarian cancer (41–43). Our findings suggest that Notch3 activation potentially modulates the function of Hox protein through transcriptional up-regulation of Pbx1. Further experiments are needed to more fully establish the putative link between Notch3 and Hox in the tumorigenesis of ovarian cancer. Third, the findings that Pbx1 is essential for ovarian cancer cell survival and proliferation suggest that Pbx1 might be a potential target for therapeutics in ovarian cancer in which Notch3 is activated. These tumors may have developed Notch3-Pbx1 pathway-dependent cellular machinery for growth and survival. If so, withdrawal or inhibition of Pbx1 expression may have a potent growth-inhibitory effect. The cytotoxicity associated with GSI, especially on the gastrointestinal tract, is a major obstacle of its application to cancer patients (19, 44). Alternative strategies to specifically block Notch downstream targets, such as Pbx1, are warrant to be developed.

Disclosure of Potential Conflicts of Interest

No potential conflicts of interest were disclosed.

Acknowledgments

Received 2/11/2008; revised 7/2/2008; accepted 8/6/2008.

Grant support: American Cancer Society Research Scholar Grant (T-L. Wang), Ovarian Cancer Research Foundation Individual Investigator Grant (T-L. Wang), Department of Defense New Investigator Research Grant W81XWH (T-L. Wang), NIH career development award P50CA098252 (T-L. Wang), American Cancer Society Institutional Research Grant (T-L. Wang), and NIH grants CA129080 and CA103937 (I-M. Shih).

The costs of publication of this article were defrayed in part by the payment of page charges. This article must therefore be hereby marked *advertisement* in accordance with 18 U.S.C. Section 1734 solely to indicate this fact.

We thank Dr. Michael Cleary for the anti-Pbx1 antibody, Dr. S. Higashiyama for the pGL3-Pbx1 promoter construct, Dr. Diane Hayward (Johns Hopkins University) for the SG5-flag-CSL plasmid, and Drs. Ching-Hung Lin and Kuan-Ting Kuo for help in statistical analyses.

References

1. Beachy PA, Karhadkar SS, Berman DM. Tissue repair and stem cell renewal in carcinogenesis. Nature 2004; 432:324–31.
2. Weng AP, Ferrando AA, Lee W, et al. Activating mutations of NOTCH1 in human T cell acute lymphoblastic leukemia. Science 2004;306:269–71.
3. Ellisen LW, Bird J, West DC, et al. TAN-1, the human homolog of the *Drosophila* notch gene, is broken by chromosomal translocations in T lymphoblastic neoplasms. Cell 1991;66:649–61.
4. Dang TP, Gazdar AF, Virmani AK, et al. Chromosome 19 translocation, overexpression of Notch3, and human lung cancer. J Natl Cancer Inst 2000;92:1355–7.

5. Wood LD, Parsons DW, Jones S, et al. The genomic landscapes of human breast and colorectal cancers. Science 2007;318:1108–13.
6. Wang TL, Maierhofer C, Speicher MR, et al. Digital karyotyping. Proc Natl Acad Sci U S A 2002;99:16156–61.
7. Matsuzaki H, Dong S, Loi H, et al. Genotyping over 100,000 SNPs on a pair of oligonucleotide arrays. Nat Methods 2004;1:109–11.
8. Park JT, Li M, Nakayama N, et al. Notch-3 gene amplification in ovarian cancer. Cancer Res 2006;66:6312–8.
9. Weng AP, Millholland JM, Yashiro-Ohtani Y, et al. c-Myc is an important direct target of Notch1 in T-cell acute lymphoblastic leukemia/lymphoma. Genes Dev 2006;20:2096–109.
10. Talora C, Cialfi S, Oliviero C, et al. Cross talk among Notch3, pre-TCR, and Tal1 in T-cell development and leukemogenesis. Blood 2006;107:3313–20.
11. Jarriault S, Brou C, Logeat F, Schroeter EH, Kopan R, Israel A. Signalling downstream of activated mammalian Notch. Nature 1995;377:355–8.
12. Ronchini C, Capobianco AJ. Induction of cyclin D1 transcription and CDK2 activity by Notch(ic): implication for cell cycle disruption in transformation by Notch(ic). Mol Cell Biol 2001;21:5925–34.
13. Buckhaults P, Zhang Z, Chen YC, et al. Identifying tumor origin using a gene expression-based classification map. Cancer Res 2003;63:4144–9.
14. Wysocka J, Swigut T, Xiao H, et al. A PHD finger of NURF couples histone H3 lysine 4 trimethylation with chromatin remodelling. Nature 2006;442:86–90.
15. Jacobs Y, Schnabel CA, Cleary ML. Trimeric association of Hox and TALE homeodomain proteins mediates Hoxb2 hindbrain enhancer activity. Mol Cell Biol 1999;19:5134–42.
16. Dang L, Fan X, Chaudhry A, Wang M, Gaiano N, Eberhart CG. Notch3 signaling initiates choroid plexus tumor formation. Oncogene 2006;25:487–91.
17. Shiraishi K, Yamasaki K, Nanba D, et al. Pre-B-cell leukemia transcription factor 1 is a major target of promyelocytic leukemia zinc-finger-mediated melanoma cell growth suppression. Oncogene 2007;26:339–48.
18. Geling A, Steiner H, Willem M, Bally-Cuif L, Haass C. A γ-secretase inhibitor blocks Notch signaling *in vivo* and causes a severe neurogenic phenotype in zebrafish. EMBO Rep 2002;3:688–94.
19. Shih IM, Wang TL. Notch signaling, γ-secretase inhibitors, and cancer therapy. Cancer Res 2007;67:1879–82.
20. Nourse J, Mellentin JD, Galili N, et al. Chromosomal translocation t(1;19) results in synthesis of a homeobox fusion mRNA that codes for a potential chimeric transcription factor. Cell 1990;60:535–45.
21. Kamps MP, Murre C, Sun XH, Baltimore D. A new homeobox gene contributes the DNA binding domain of the t(1;19) translocation protein in pre-B ALL. Cell 1990;60:547–55.
22. Minter LM, Turley DM, Das P, et al. Inhibitors of γ-secretase block *in vivo* and *in vitro* T helper type 1 polarization by preventing Notch upregulation of Tbx21. Nat Immunol 2005;6:680–8.
23. O'Neil J, Grim J, Strack P, et al. FBW7 mutations in leukemic cells mediate NOTCH pathway activation and resistance to γ-secretase inhibitors. J Exp Med 2007;204:1813–24.
24. Lewis HD, Leveridge M, Strack PR, et al. Apoptosis in T cell acute lymphoblastic leukemia cells after cell cycle arrest induced by pharmacological inhibition of notch signaling. Chem Biol 2007;14:209–19.
25. Choi JH, Park JT, Davidson B, Morin PJ, Shih IM, Wang TL. Jagged-1 and Notch3 juxtacrine loop regulates ovarian tumor growth and adhesion. Cancer Res 2008;68:5716–23.
26. Wilkinson HA, Fitzgerald K, Greenwald I. Reciprocal changes in expression of the receptor lin-12 and its ligand lag-2 prior to commitment in a *C. elegans* cell fate decision. Cell 1994;79:1187–98.
27. Carmena A, Buff E, Halfon MS, et al. Reciprocal regulatory interactions between the Notch and Ras signaling pathways in the *Drosophila* embryonic mesoderm. Dev Biol 2002;244:226–42.
28. Robey E, Chang D, Itano A, et al. An activated form of Notch influences the choice between CD4 and CD8 T cell lineages. Cell 1996;87:483–92.
29. Mann RS, Chan S-K. Extra specificity from extradenticle: the partnership between HOX and PBX/EXD homeodomain proteins. Trends Genet 1996;12:258.
30. Berkes CA, Bergstrom DA, Penn BH, Seaver KJ, Knoepfler PS, Tapscott SJ. Pbx marks genes for activation by MyoD indicating a role for a homeodomain protein in establishing myogenic potential. Mol Cell 2004;14:465.
31. Selleri L, Depew MJ, Jacobs Y, et al. Requirement for Pbx1 in skeletal patterning and programming chondrocyte proliferation and differentiation. Development 2001;128:3543–57.
32. DiMartino JF, Selleri L, Traver D, et al. The Hox cofactor and proto-oncogene Pbx1 is required for maintenance of definitive hematopoiesis in the fetal liver. Blood 2001;98:618–26.
33. Kim SK, Selleri L, Lee JS, et al. Pbx1 inactivation disrupts pancreas development and in Ipf1-deficient mice promotes diabetes mellitus. Nat Genet 2002;30:430.
34. Schnabel CA, Godin RE, Cleary ML. Pbx1 regulates nephrogenesis and ureteric branching in the developing kidney. Dev Biol 2003;254:262.
35. Sanyal M, Tung JW, Karsunky H, et al. B-cell development fails in the absence of the Pbx1 proto-oncogene. Blood 2007;109:4191–9.
36. Kamps MP, Look AT, Baltimore D. The human t(1;19) translocation in pre-B ALL produces multiple nuclear E2A-Pbx1 fusion proteins with differing transforming potentials. Genes Dev 1991;5:358–68.
37. LaRonde-LeBlanc NA, Wolberger C. Structure of HoxA9 and Pbx1 bound to DNA: Hox hexapeptide and DNA recognition anterior to posterior. Genes Dev 2003;17:2060–72.
38. Schnabel CA, Jacobs Y, Cleary ML. HoxA9-mediated immortalization of myeloid progenitors requires functional interactions with TALE cofactors Pbx and Meis. Oncogene 2000;19:608–16.
39. Argiropoulos B, Yung E, Humphries RK. Unraveling the crucial roles of Meis1 in leukemogenesis and normal hematopoiesis. Genes Dev 2007;21:2845–9.
40. Wong P, Iwasaki M, Somervaille TC, So CW, Cleary ML. Meis1 is an essential and rate-limiting regulator of MLL leukemia stem cell potential. Genes Dev 2007;21:2762–74.
41. Naora H, Montz FJ, Chai CY, Roden RB. Aberrant expression of homeobox gene HOXA7 is associated with mullerian-like differentiation of epithelial ovarian tumors and the generation of a specific autologous antibody response. Proc Natl Acad Sci U S A 2001;98:15209–14.
42. Cheng W, Liu J, Yoshida H, Rosen D, Naora H. Lineage infidelity of epithelial ovarian cancers is controlled by HOX genes that specify regional identity in the reproductive tract. Nat Med 2005;11:531–7.
43. Miao J, Wang Z, Provencher H, et al. HOXB13 promotes ovarian cancer progression. Proc Natl Acad Sci U S A 2007;104:17093–8.
44. van Es JH, van Gijn ME, Riccio O, et al. Notch/γ-secretase inhibition turns proliferative cells in intestinal crypts and adenomas into goblet cells. Nature 2005;435:959–63.

Research Article

Functional Analysis of 11q13.5 Amplicon Identifies *Rsf-1* (*HBXAP*) as a Gene Involved in Paclitaxel Resistance in Ovarian Cancer

Jung Hye Choi,[1,2] Jim Jinn-Chyuan Sheu,[3] Bin Guan,[1] Natini Jinawath,[1] Paul Markowski,[1] Tian-Li Wang,[1] and Ie-Ming Shih[1]

[1]Departments of Pathology, Oncology, and Gynecology and Obstetrics, Johns Hopkins Medical Institutions, Baltimore, Maryland; [2]Department of Oriental Pharmacy, Kyung Hee University, Seoul, Korea; and [3]Human Genetic Center, China Medical University Hospital and Graduate Institute of Chinese Medical Science, China Medical University, Taichung City, Taiwan

Abstract

The chromosome 11q13.5 locus is frequently amplified in several types of human cancer. We have previously shown that 11q13.5 amplification was associated with significantly shorter overall survival in ovarian cancer patients, but the molecular mechanisms of how amplification of this locus contributes to disease aggressiveness remain unclear. Because ovarian cancer mortality is primarily related to resistance of chemotherapeutic agents, we screened the top six candidate genes within this amplicon for their contribution to drug resistance. *Rsf-1* (also known as *HBXAP*) was found to be the only gene in which gene knockdown sensitized tumor cells to paclitaxel. Rsf-1 has been known to interact with hSNF2H to form an ISWI chromatin remodeling complex. We found that Rsf-1 was up-regulated in paclitaxel-resistant ovarian cancer cell lines, and Rsf-1 immunoreactivity in primary ovarian carcinoma tissues correlated with *in vitro* paclitaxel resistance. Ectopic expression of Rsf-1 significantly enhanced paclitaxel resistance in ovarian cancer cells. Down-regulation of hSNF2H or disruption of hSNF2H and Rsf-1 interaction enhanced paclitaxel sensitivity in tumor cells with Rsf-1 up-regulation. Rsf-1 expression altered expression in several genes and activated certain signaling pathways that may contribute to drug resistance. In conclusion, our results suggest that *Rsf-1* is the major gene within the 11q13.5 amplicon that contributes to paclitaxel resistance, and the formation of the Rsf-1/hSNF2H complex is required for inducing this phenotype. [Cancer Res 2009;69(4):OF1–9]

Introduction

Gene amplification is a common mechanism underlying oncogenic activation in human cancer (1, 2). Amplification of *MYC* family genes, *EGFR, ERBB2* (*Her2/neu*), *CCND1* (*cyclin D1*), *CCNE* (*cyclin E*), and *FGFR*, has been reported in a variety of human neoplastic diseases. Amplifications in several of the oncogenes are associated with worse clinical outcome and are amenable to specific targeted therapy (3). In an effort to identify amplified chromosomal regions that may harbor novel cancer-associated genes, we have applied both digital karyotyping (4) and single nucleotide polymorphism arrays (5) to analyze DNA copy number alterations in purified high-grade ovarian serous carcinoma, one of the most aggressive type of neoplastic diseases in women. Based on previous studies (6, 7), we found that the most common amplicons in high-grade ovarian serous carcinomas were those harboring *CCNE* (*cyclin E1*), *Notch3, AKT2*, and a discrete chromosomal region at 11q13.5 that contained several cancer-associated genes including *p21/cdc42/Rad-activated kinase* (*PAK1*; refs. 8, 9), *Gab2* (10), and *Rsf-1* (*HBXAP*; ref. 6). Fluorescence *in situ* hybridization analysis showed 11q13.5 amplification in 13% to 15% of high-grade ovarian serous carcinomas (6, 7). 11q13.5 amplification was significantly associated with worse clinical outcome in patients with high-grade serous carcinomas in independent retrospective cohorts (6, 11). Besides ovarian cancer, this amplicon is frequently detected in several human malignancies including breast, oral, esophageal, and head and neck carcinomas (12). These findings suggest that gene(s) within this amplicon may contribute to clinical aggressiveness in the neoplasms with 11q13.5 amplification.

The clinical outcome in ovarian cancer patients depends on several factors, and the development of drug resistance is one of the main causes that account for the poor prognosis in patients who suffer from this disease. To identify the potential gene(s) within the 11q13.5 amplicon that may play a mechanistic role in developing drug resistance in high-grade ovarian serous carcinomas, we first selected the top six genes within this amplicon that showed the most significant correlation between DNA and RNA copy number from a total of 14 genes within the amplicon. After knockdown of each gene using RNA interference, we determined their sensitivity to paclitaxel and carboplatin, which are routinely used in treating ovarian cancer patients after cytoreduction surgery. We found that Rsf-1 knockdown significantly decreased the IC_{50} of paclitaxel in ovarian cancer cells. In this study, we further characterized the molecular mechanism of how Rsf-1 expression contributed to the development of drug resistance.

Materials and Methods

Cell lines and culture conditions. Ovarian cancer cells including OVCAR3, SKOV3, and A2780 cells were purchased from American Type Culture Collection, and MPSC1 was previously established by us (13). Paclitaxel- and carboplatin-resistant cell lines were generated by selecting the viable MPSC1, A2780, OVCAR3, and SKOV3 cells 3 mo after exposure to paclitaxel (0.25–0.5 μmol/L) or carboplatin (0.5–2.0 μg/mL). The resistant cell clones from each cell line were maintained in culture medium containing paclitaxel (0.25 μmol/L for SKOV3 and 0.5 μmol/L for A2780, OVCAR3, and MPSC-1) or carboplatin (2.0 μg/mL for SKOV3 and MPSC1, 1.0 μg/mL for A2780, and 0.5 μg/mL for OVCAR3). All the cell lines used in this study were cultured in RPMI 1640 containing 5% fetal bovine serum.

Selection of genes within the 11q13.5 amplicon for functional studies. As reported in our previous study (6), 10 high-grade ovarian serous carcinomas with 11q13.5 amplification and 53 control specimens without such amplification were analyzed to assess mRNA levels in all the genes within the minimal amplicon using quantitative real-time PCR. The control

Requests for reprints: Ie-Ming Shih, Department of Pathology, Johns Hopkins Medical Institutions, CRB-II, Room 305, 1550 Orleans Street, Baltimore, MD 21231. Phone: 410-502-7774; Fax: 410-502-7943; E-mail: shihie@yahoo.com.

doi:10.1158/0008-5472.CAN-08-3602

group included 1 freshly brushed ovarian surface epithelium (kind gift from Dr. M. Birrer), 6 benign cystadenomas, 10 serous borderline tumors, and 36 high-grade serous carcinomas that did not harbor 11q13.5 amplification. In our previous report (6), we performed quantitative real-time PCR for all the genes except *NARS2* because this gene has only recently been updated to the genome assembly database. Thus, the NARS2 expression level was analyzed in this study using the same method as used for other genes (6). The Mann-Whitney (rank sum) test was used to determine the significance in individual gene expression between 11q13.5-amplified and nonamplified specimens.

Rsf-1 inducible cell clones. The full-length Rsf-1 gene tagged with a V5 epitope tag at the COOH-terminal was cloned into the Tet-off expression vector, pTRE-hygro (Clontech). Parental SKOV3 cells were first transfected with a tetracycline-controlled transactivator (tTA) expression vector, and the tTA stable clones were selected by G418 (300 μg/mL). The inducible Rsf-1 vector was then introduced into the SKOV3-tTA cells, and the stable transfectants were selected by 150 μg/mL hygromycin and maintained in the culture medium containing 300 μg/mL G418, 150 μg/mL hygromycin, and 2 μg/mL doxycycline. In this study, we selected two clones of Rsf-1 inducible cells and the pooled control cells with the tTA-vector only construct. To determine the efficiency of Rsf-1 induction in the Tet-off system, we performed Western blots to analyze Rsf-1 protein expression at different time points after the gene was turned on using doxycycline-free medium.

Immunohistochemistry. A mouse monoclonal anti–Rsf-1 antibody (clone 5H2/E4) was purchased from Upstate and was used in immunohistochemistry at a dilution of 1:2,000. The specificity of the antibody has been validated in previous reports (6, 14). An EnVision+ System peroxidase kit (DAKO) was used for staining following the manufacturer's instruction. Immunohistochemical staining was carried out on tissue microarrays containing 99 high-grade ovarian serous carcinoma tissues for which their *in vitro* drug resistance status was available. Immunointensity for Rsf-1 was scored as low (≤2) or high (>2). This criterion was used because of a significant correlation between immunointensity (score >2) and *Rsf-1* amplification (6).

Real-time reverse transcription-PCR. Relative gene expression was measured by quantitative real-time PCR using an iCycler (Bio-Rad), and threshold cycle numbers (C_t) were obtained using the iCycler Optical system interface software. PCR primers were designed using the Primer 3 program. The primers for NARS2 real-time PCR were 5′-GACTCTGAGGGAGCTG GAGAAC-3′ (forward) and 5′-AAGGTCGGACCAAAGGTAAACA-3′ (reverse). The primers for cysteine-rich protein 61 (*CYR61*) were 5′-CTCCCTGTTTTTGGAATGGA-3′ (forward) and 5′-TGGTCTTGCTGCATTTCTTG-3′ (reverse). The primers for osteopontin were 5′-TGAAATTCATGGCTGTGGAA-3′ (forward) and 5′-ATG GTGCATACAAGGCCATC-3′ (reverse). The primers for *CTGF* were 5′-CCTGGTCCAGACCA CAGAGT-3′ (forward) and 5′-TGGAGATTTTGGGAGTACGG-3′ (reverse). The other primers including those for *Rsf-1, hSNF2H*, and β-amyloid precursor protein (*APP*) genes were shown in previous reports (6, 15). The mean C_t of the gene of interest was calculated from replicate measurements and normalized with the mean C_t of a control gene, *APP*, for which expression is relatively constant among the SAGE libraries analyzed (16).

Gene knockdown using small interfering RNA and small hairpin RNA. For functional screening of the top six genes, we purchased two small hairpin RNAs (shRNA) for each gene from Sigma. hSNF2H-specific small interfering RNAs (siRNA; UUCAAAUCGAGUGCAAACA and UUAAUAUCCGAGUAUACCA) and control siRNA that targeted the *Luciferase* gene (GAUUAAAUCUUCUAGCGACUGCUUCGC) were synthesized by the Integrated DNA Technologies. Cells were transfected with shRNA or siRNA at a final concentration of 2 μg or 200 nmol/L, respectively, using Lipofectamine (Invitrogen). Six hours after transfection, the cells were washed and harvested the next day for cell growth and drug resistance assays. To enhance the silencing effect of Rsf-1 transcripts in the follow-up experiments, we used lentivirus carrying the Rsf-1 shRNA sequence templates (CCGGCCAGTTCTGAAC TTTGAAGATCTCGAGATCTTCAAAGTTCAGAACT) and (CCGGCTTCTGAGA CAAAGGGTTCTACTCGAGTAGAACCCTTTGTCTCAGA), which were inserted into the lentiviral plasmid (pLKO.1-puro).

Cell growth and drug resistance assay. Cells were grown in 96-well plates at a density of 3,000 per well. Cell number was measured by the incorporation of SYBR green I nucleic acid gel stain (Molecular Probes) using a fluorescence microplate reader (Fluostar from BMG). Data were determined from four replicates and were expressed as the fold increase to the control group. For drug resistance assay, cells were seeded in 384-well plates at a density of 600 per well. After overnight culture, the cells were treated with a series of concentrations of paclitaxel or carboplatin. Four days after transfection (i.e., 3 d after drug treatment), 8 μL of CellTiter-Blue (Promega) were added and the plates were incubated for 5 h. The absorbance was determined using a fluorescence microplate reader. The signal produced by conversion of resazurin to resorufin is directly proportional to viable cell number. Data were determined from four replicates and were expressed as the fold increase of the control group. IC_{50} was defined as the concentration that results in a 50% decreased in the number of cells as compared with that of the control cultures in the absence of the drug.

GeneChip analysis for transcript expression. RNA was prepared using a Qiagen RNAeasy kit from Rsf-1 inducible SKOV3 cells (15) in different experimental conditions. Affymetrix U133 Plus 2 arrays were used to analyze gene expression from Rsf-1–induced SKOV3 cells (48 h after induction), mock-induced SKOV3 cells (48 h after mock induction), and vector-only control SKOV3 cells. Probe labeling, hybridization, and scanning for the arrays were done using the standard protocols at the Johns Hopkins Microarray Core. The dCHIP program was used to analyze the array data to select the differentially expressed genes that were overexpressed in the Rsf-1–induced group as compared with the mean of control groups including mock-induced and vector-only control SKOV3 cells. The top up-regulated and down-regulated genes with corresponding expression values that were >2.5-fold of increase or decrease as compared with the control were input into the Ingenuity Pathways Analysis System.[4] These genes, called focus genes, were overlaid onto a global molecular network developed from information updated in the Ingenuity Pathways Knowledge Base. Networks of these focus genes were then algorithmically generated based on their connectivity. FN1

Drug resistance clinical assay. The assay was done in Oncotech, Inc., using published protocol.[5] Briefly, a small piece of fresh tumor tissue was cultured in agar-based cell culture system, and radioactive thymidine incorporation was used for measuring cell growth in the presence of different chemotherapeutic drugs. The level of drug resistance was quantified and was classified into three groups: (*a*) low if tumor cells were inhibited by the tested agent and showed less than median growth; (*b*) intermediate if there was moderate tumor growth; and (*c*) extreme if tumor cell growth was virtually unaffected by the chemotherapeutic agent. As defined in previous reports, extreme drug resistance was interpreted as drug resistant and intermediate and low drug resistance were interpreted as drug sensitive (1, 11). FN2

Results

Selection of genes within the 11q13.5 amplicon for functional characterization. Using digital karyotyping to detect genome-wide DNA copy number alterations in high-grade ovarian serous carcinomas, we identified a minimal amplicon in the 11q13.5 chromosomal region (6). According to the UCSC Human Genome Browser Gateway in March 2006,[6] there were a total of 14 genes in which their complete coding sequences were located within this minimal amplicon. To identify the candidate cancer-driving genes from the 14 genes, we applied an approach based on the rationale that a tumor-driving gene, if amplified, is almost FN3

[4] http://www.ingenuity.com
[5] http://www.oncotech.com/pdfs/edr_4_pager.pdf
[6] http://genome.ucsc.edu/cgi-bin/hgGateway

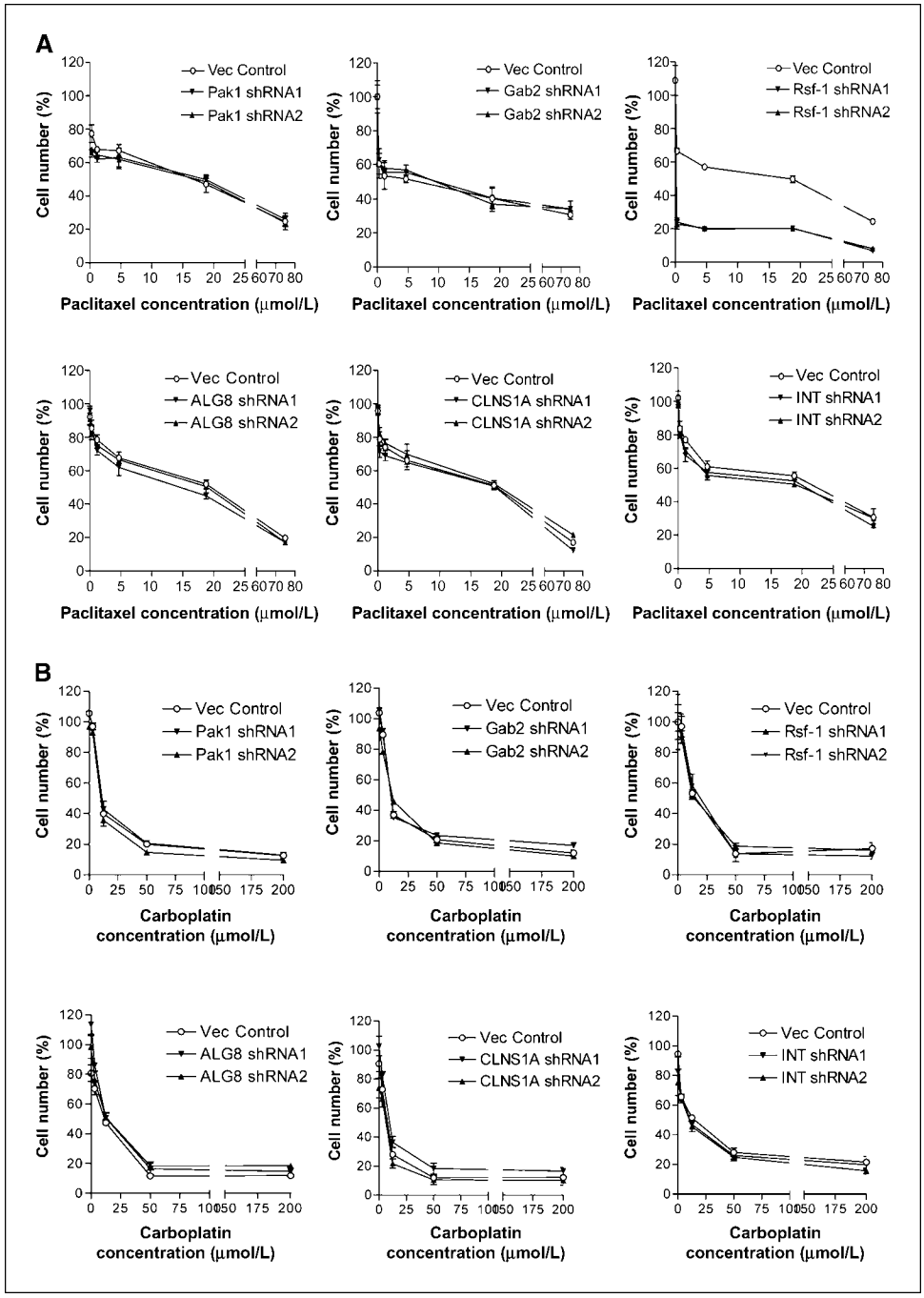

Figure 1. Effect of knockdown of the six genes within the ch11q13.5 on IC_{50} of paclitaxel (*A*) and carboplatin (*B*) in OVCAR3 cells. Two shRNAs (shRNA1 and shRNA2) to target each gene were used to knock down *PAK-1, Gab2, Rsf-1, ALG8, CLNS1A*, and *INTS4* in OVCAR3 cells with ch11q13.5 amplification. Vector only was used as the negative control. Rsf-1 is the only gene in which shRNAs significantly reduce IC_{50} of paclitaxel.

always overexpressed whereas the coamplified "passenger" genes that are not involved in tumor development may or may not be so (17). Based on the Mann-Whitney (rank sum) test, we selected six genes showing the highest correlation between DNA and transcript copy number ($P < 0.001$). They included *Rsf-1* (*HBXAP*; $P < 0.0001$), *INTS4* ($P = 0.0001$), *CLNS1A* ($P = 0.0001$), *ALG8* ($P = 0.0001$), *GAB2* ($P = 0.0001$), and *PAK1* ($P = 0.0002$). The *P* values for *NDUFC2, C11orf67*, and *USP35* were 0.0015, 0.012, and 0.022, respectively. There was no statistical significance for the remaining genes including *GFPD4, AQP11, KCTD14, THRSP*, and *NARS2*. Therefore, we selected *Rsf-1* (*HBXAP*), *INTS4, CLNS1A, ALG8, GAB2*, and *PAK1* for functional characterization.

Biological effects of gene knockdown of the six candidate genes. To determine the biological roles of those six genes in sustaining cell growth and in conferring drug resistance, we transfected OVCAR3 ovarian cancer cells, known to harbor a high level of 11q13.5 amplification, with shRNAs to knockdown each of the six genes. Two independent shRNAs with satisfied knockdown efficiency were used for each gene. Cell number of OVCAR3 cells was determined 1 day and 4 days after shRNA transfection. Supplementary Fig. S1 showed that cell number was most remarkably reduced in the cells transfected with Rsf-1 shRNAs as compared with PAK1, Gab2, ALG8, INTS4, and CLNS1A shRNAs. To determine if these six genes are potentially involved

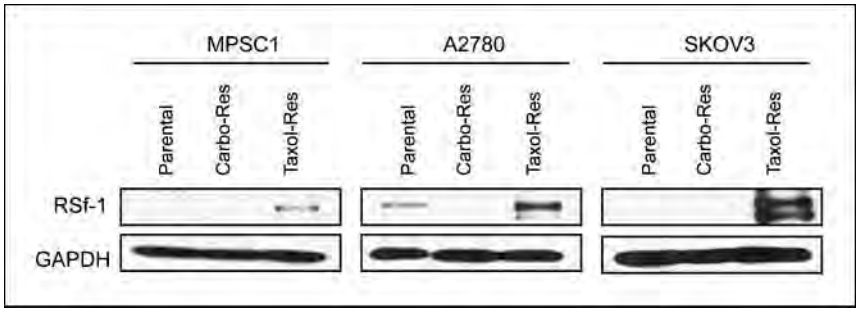

Figure 2. Enhanced expression of Rsf-1 protein in paclitaxel-resistant ovarian cancer cells. Western blot analysis shows that Rsf-1 protein levels are significantly higher in the paclitaxel-resistant ovarian cancer cell lines as compared with the parental and carboplatin-resistant cells. Glyceraldehyde-3-phosphate dehydrogenase (*GAPDH*) was used as a loading control.

in drug resistance, we measured the IC_{50} of paclitaxel and carboplatin in OVCAR3 cells after shRNA transfection. Of note, the cell numbers in drug sensitivity assays were normalized to those in shRNA-treated SKOV3 cells without gene knockdown. For paclitaxel, we found that a significant decrease in the IC_{50} occurred only in Rsf-1 gene knockdown but not in other genes (Fig. 1*A*). For carboplatin, none of the shRNAs that target these six genes affected the IC_{50} (Fig. 1*B*). Therefore, we selected Rsf-1 to further study its role in enhancing paclitaxel resistance in ovarian cancer cells.

Correlation of Rsf-1 protein expression and drug resistance *in vitro* and *in vivo*. To determine whether Rsf-1 gene up-regulation was correlated with paclitaxel resistance, we performed Western blot on the ovarian cancer cell lines including MPSC1, A2780, and SKOV3, and performed immunohistochemistry on clinical tumor specimens. First, we established three paclitaxel-resistant ovarian cancer cell lines, $SKOV3^{TR}$, $A2780^{TR}$, and $MPSC1^{TR}$, and three carboplatin-resistant ovarian cancer cell lines, $SKOV3^{CR}$, $A2780^{CR}$, and $MPSC1^{CR}$, by treating the parental cells with increasing concentrations of paclitaxel and carboplatin. We then compared Rsf-1 expression between drug-resistant and parental cells. As shown in Fig. 2, Rsf-1 protein levels were significantly higher in paclitaxel-resistant cells than their parental controls in all three cell lines. Like in OVCAR3 cells, the cell number was decreased in $SKOV3^{TR}$ cells after treatment with Rsf-1 shRNAs ($P < 0.01$; Supplementary Fig. S2). Next, we determined whether Rsf-1 expression correlated with paclitaxel resistance in ovarian cancer cells isolated from the primary tumors in patients with stage III or IV ovarian cancer. Based on immunohistochemistry, we were able to show that Rsf-1 immunointensity was significantly associated with increased paclitaxel resistance (Table 1). In contrast, there was no statistically significant correlation between Rsf-1 expression level and resistance to carboplatin. Rsf-1 immunoreactivity in representative specimens was shown in Supplementary Fig. S3.

Rsf-1 expression enhances paclitaxel resistance in ovarian cancer cells. To show the causal role of Rsf-1 in developing drug resistance, we used Tet-off Rsf-1 inducible SKOV3 ovarian cancer cells, which expressed a very low level of Rsf-1 in the parental and noninduced cells (15). Western blot analysis showed that Rsf-1 protein was detected 6 and 12 hours after induction in two independent clones (Fig. 3*A*). Rsf-1 expression did not have a significant effect on cellular proliferation (Supplementary Fig. S4); however, both clone 1 and clone 2 after Rsf-1 induction became more resistant to paclitaxel than the control clones without Rsf-1 induction (Fig. 3*B*). The IC_{50} of paclitaxel in noninduced (doxycycline on) clone 1 and clone 2 cells were 0.15 and 0.11 μmol/L, respectively, whereas the IC_{50} of paclitaxel in clone 1 and clone 2 after Rsf-1 induction (doxycycline off) were 2.8 and 7.2μmol/L, respectively. In contrast, the control cells had a similar IC_{50} in both doxycycline-on and doxycycline-off conditions. Rsf-1 induction did not confer carboplatin resistance as reflected by similar IC_{50} curves between Rsf-1–induced and noninduced cells (Fig. 3*C*).

The role of hSNF2H in Rsf-1–dependent paclitaxel resistance. It has been known that Rsf-1 interacts with hSNF2H to form an ISWI chromatin remodeling complex in which Rsf-1 serves as a histone chaperone and hSNF2H as an ATPase (18–21). Here, we determined if hSNF2H was required for Rsf-1 to confer paclitaxel resistance. As shown in Fig. 4*A*, gene knockdown of hSNF2H reduced its expression at both mRNA and protein levels in SKOV3 cells. Reducing hSNF2H expression had only a minimal effect on cell proliferation in the control SKOV3 cell line (Supplementary Fig. S5). Next, we measured the IC_{50} of paclitaxel in Rsf-1 inducible SKOV3 cells after transfection with hSNF2H or control siRNA in both Rsf-1–induced and noninduced conditions. We found that hSNF2H siRNA significantly decreased the IC_{50} of paclitaxel in Rsf-1–expressing SKOV3 cells. In contrast, hSNF2H siRNA had only a modest effect on the IC_{50} in cells without Rsf-1 induction (Fig. 4*B*). Next, we further tested if hSNF2H knockdown or expression of an Rsf-1 dominant

Table 1. Correlation between *in vitro* drug resistance and *Rsf-1* expression

	Staining score ≤2	Staining score >2	χ^2 test
Carboplatin sensitive	31	15	$P = 0.8305$
Carboplatin resistant	32	18	
Paclitaxel sensitive	43	7	$P < 0.0001$*
Paclitaxel resistant	20	26	

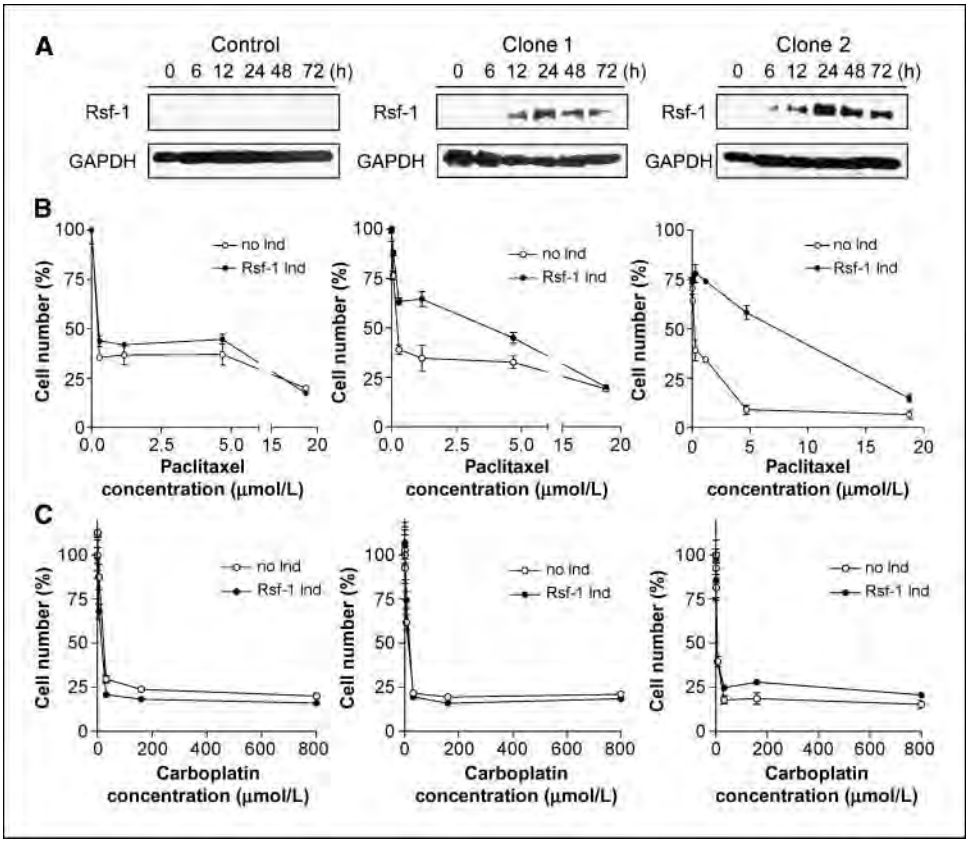

Figure 3. Rsf-1 induction in SKOV3 cells increases paclitaxel resistance. *A,* Western blot analyses show that Rsf-1 protein expression is detectable as early as 6 h after removal of doxycycline in two randomly selected clones (clone 1 and clone 2). *B* and *C,* drug resistance assay shows that Rsf-1 expression confers resistance to paclitaxel (*B*) but not to carboplatin (*C*) in both Rsf-1 inducible SKOV3 clones.

negative protein, Rsf-D4 (15), could sensitize OVCAR3 cells with abundant endogenous Rsf-1 expression to paclitaxel. We found that either hSNF2H siRNA or Rsf-D4 reduced the cell proliferation to 81% and 70% of the controls, respectively. Interestingly, both approaches also enhanced the paclitaxel sensitivity in OVCAR3 cells (Fig. 4*C*). The above results indicated an important role of hSNF2H in Rsf-1–mediated paclitaxel resistance.

Genes regulated by Rsf-1 expression. To further identify the Rsf-1–regulated genes and pathways that were potentially involved in drug resistance, we performed global transcript profiling to compare gene expression in Rsf-1–induced and control SKOV3 cells (mock induced and vector only controls) using the Affymetrix U133-Plus 2 microarrays. As compared with the Rsf-1 turn-off (mock induced) group and the vector-only control, Rsf-1–induced cells showed up-regulation and down-regulation in 62 genes with at least 2.5-fold increase or decrease as compared with the controls (Supplementary Table S1). To identify the hidden connections among the regulated genes, we performed a network analysis of the top 25 up-regulated and 37 down-regulated genes using the Ingenuity Pathways Analysis Systems. Applying this Ingenuity Network filter, four functional networks could be constituted with significant Ingenuity scores. The network with the highest score was related to the Tissue Morphology, Cellular Assembly and Organization System (Fig. 5*A*). Several molecular hubs including nuclear factor κB (NFκB), extracellular signal–regulated kinase (ERK), Akt, and EGR1 to which many pathways converge were identified in the network. Among the candidate genes, three representative genes including osteopontin, cysteine-rich protein 61 (*CYR61*), and connective tissue growth factor (*CTGF*) were selected for validation by quantitative real-time PCR because these three genes have been implied in the pathogenesis of in human cancer (22–24). As shown in Fig. 5*B* and *C*, all three genes showed statistically significant up-regulation in SKOV3 cells after Rsf-1 induction and showed down-regulation in OVCAR3 cells after Rsf-1 shRNA transfection, indicating that Rsf-1 proteins were required and sufficient to up-regulate the expression of CYR61, CTGF, and osteopontin.

F5

Discussion

Chromosome 11q13.5 amplification has been detected in several types of human cancer, and the presence of the amplicon is associated with a worse clinical outcome. For example, our previous reports (6, 11) showed that 11q13.5 amplification in ovarian serous carcinomas was significantly associated with shorter overall survival. However, the mechanisms accounting for the dismal clinical outcome are not clear. In the current study, we performed a functional genomic screening on genes located in the 11q13.5 amplicon for their roles in developing drug resistance to paclitaxel and carboplatin, which are routinely used in treating patients at advanced stages of ovarian cancer. Our result showed that *Rsf-1* (*HBXAP*) played an important role in conferring paclitaxel resistance in ovarian cancer cells.

Rsf-1/HBXAP encodes a nuclear protein containing several distinct structure motifs including a PHD domain (25). This protein was first identified as a novel cellular protein that bound to the pX nuclear protein of hepatitis B virus (26). HBXAP expression increases HBV transcription in a pX-dependent manner, suggesting its role in regulating the virus life cycle. Further studies showed that the interaction between HBXAP and pX proteins regulated

NF-κB activation (26). Soon after HBXAP was identified, an independent research group reported the full-length HBXAP (Rsf-1) protein as a subunit in a chromatin assembly factor, called ISWI-containing *r*emodeling and *s*pacing *f*actor (RSF; ref. 18). The human RSF complex is composed of two subunits: the nucleosome-dependent ATPase, hSNF2H, and the histone chaperon, Rsf-1 (18, 20, 27). The Rsf-1/hSNF2H (or RSF) complex mediates nucleosome deposition and assembly and participates in chromatin remodeling by mobilizing nucleosomes in response to a variety of growth-modifying signals and environmental cues (18–21). Such nucleosome remodeling is essential for transcriptional regulation (25, 26, 28), DNA replication (29), and cell cycle progression (30). We have previously shown that Rsf-1 and hSNF2H were co-upregulated in ovarian cancer tissues and that expression of Rsf-1 may likely prevent hSNF2H from protein degradation (15). Ectopic expression of Rsf-1 in SKOV3 ovarian cancer cells with a very low level of endogenous Rsf-1 expression increased hSNF2H protein levels and promoted SKOV3 tumor growth in a mouse tumor xenograft model (15).

Our findings from this study could have several biological and clinical implications. First, the current results provide a possible explanation for how 11q13.5 amplification in ovarian serous carcinomas contributes to shorter overall survival as compared with those without 11q13.5 amplification (6, 11). It is likely that tumors with increased DNA copy number of *Rsf-1* overexpress Rsf-1 protein, which renders the *de novo* paclitaxel resistance. The Rsf-1–expressing residual tumors after tumor cytoreduction surgery may survive better during chemotherapy and tend to recur earlier, and thus they are likely related to poor clinical outcome in ovarian cancer patients. Second, hSNF2H knockdown or expression of an Rsf-1 dominant negative protein containing the hSNF2H binding motif sensitized cancer cells with Rsf-1 overexpression to paclitaxel. These observations suggest that paclitaxel resistance in Rsf-1 up-regulated cells is mediated by the chromatin remodeling activity from the Rsf-1/hSNF2H complex. This finding may have translational implications for new cancer therapy because enhancing the sensitivity of chemotherapy can be achieved by inactivating the Rsf-1/hSNF2H or by interrupting the complex formation in cancer cells. Third, our previous result showed that hSNF2H was required for cell proliferation and survival in Rsf-1–expressing OVCAR3 cells but not in SKOV3 cells with or without Rsf-1 induction. This finding is probably because OVCAR3 cells with Rsf-1 gene amplification and constitutive up-regulation have become molecularly "addicted" to Rsf-1/hSNF2H expression, whereas SKOV3 cells that have a very low level of endogenous Rsf-1 expression (15) are less sensitive to hSNF2H

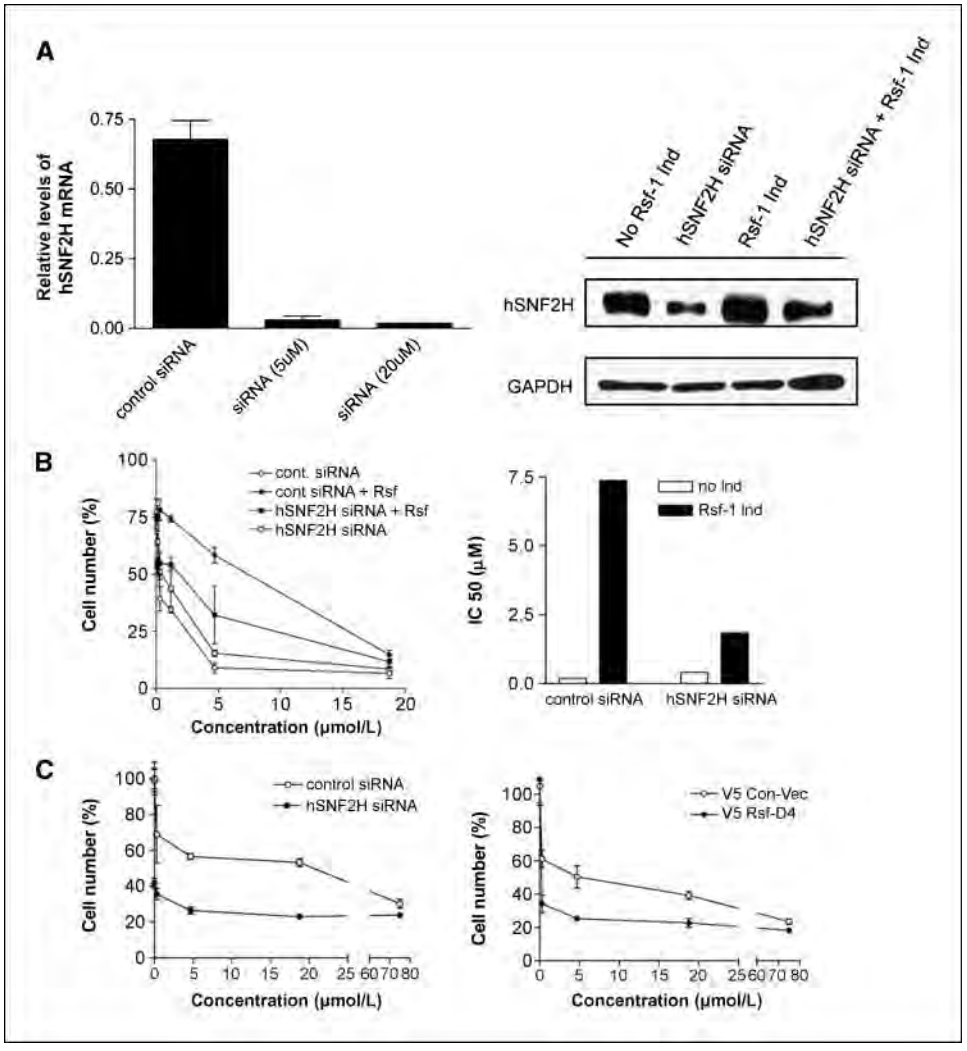

Figure 4. The role of hSNF2H in paclitaxel sensitivity. *A,* quantitative reverse transcription-PCR shows mRNA expression levels of hSNF2H are greatly reduced by hSNF2H siRNA in OVCAR3 cells with high level expression of endogenous hSNF2H (*left*). Similarly, Western blot analysis shows reduction of hSNF2H expression by hSNF2H siRNA 24 h after siRNA transfection in the Rsf-1 inducible SKOV3 cells (*right*). siRNA against luciferase was used as the control. *B,* Rsf-1 inducible cells transfected with control or hSNF2H siRNAs were treated with various concentrations of paclitaxel under Rsf-1 turned-on or turned-off condition. Relative cell number in different treatment group was determined and presented as percentage of the control group at day 3 (*left*). IC_{50} of paclitaxel in Rsf-1 inducible SKOV3 cells transfected with control or hSNF2H siRNAs were determined under Rsf-1 turned-on or turned-off condition (*right*). hSNF2H siRNAs significantly decreases the IC_{50} of paclitaxel in Rsf-1–expressing SKOV3 cells. *C,* effect of hSNF2H siRNA and Rsf-D4 expression on sensitivity of OVCAR3 cells to paclitaxel. In contrast to SKOV3 cells, OVCAR3 cells constitutively express Rsf-1 due to a high level of 11q13.5 amplification. Both hSNF2H siRNA (*left*) and Rsf-D4 (*right*) significantly sensitize OVCAR3 cells to paclitaxel treatment. The cell number at each concentration points was normalized to hSNF2H siRNA– and Rsf-D4–treated cells without paclitaxel treatment.

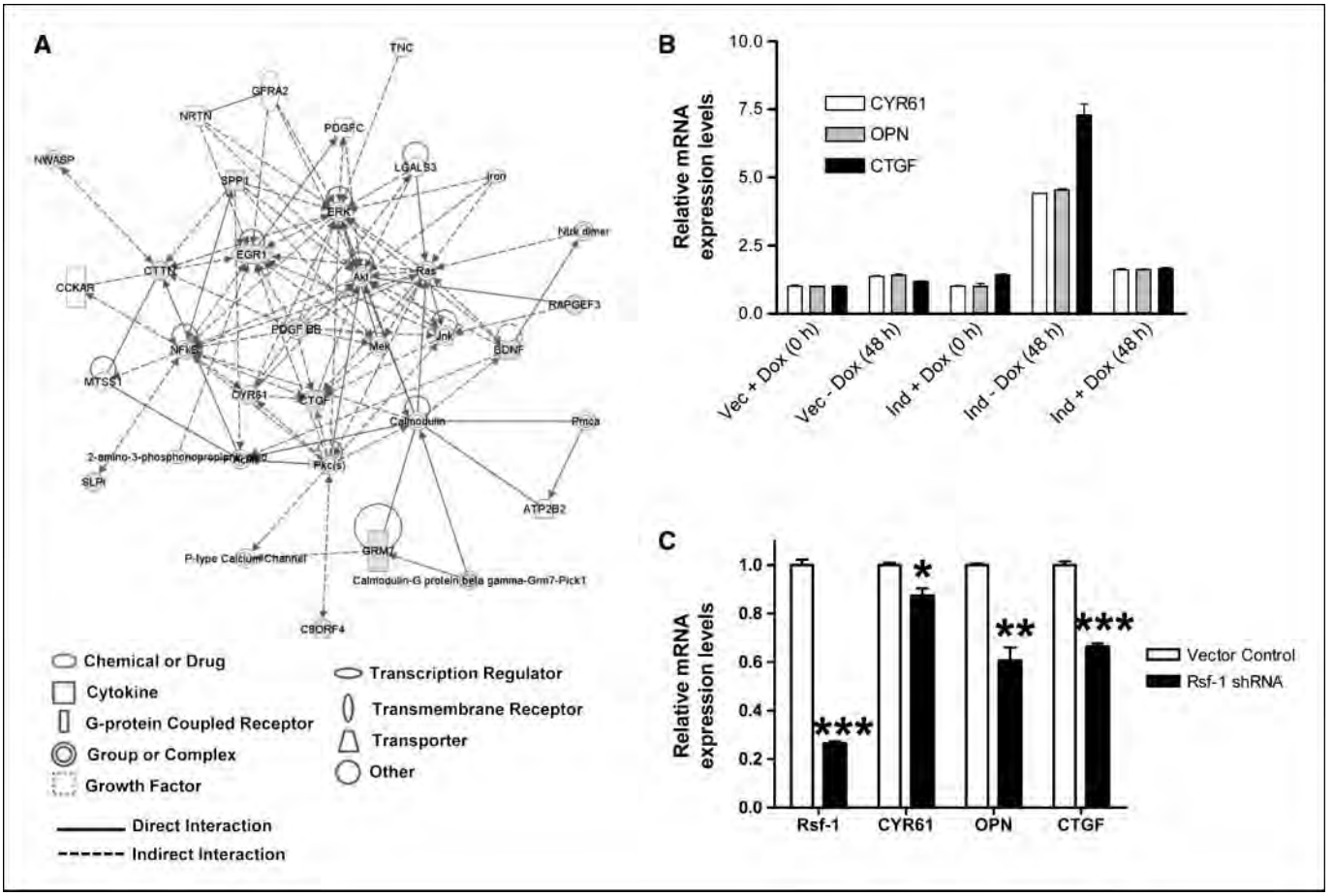

Figure 5. Candidate genes regulated by Rsf-1 and their interaction network. SKOV3-Rsf-1-TRE (Rsf-1 inducible) cells and SKOV3-TRE (vector control) cells were incubated in culture medium with or without doxycycline and cells were harvested for mRNA extraction and Affymetrix array hybridization. *A,* the Ingenuity pathways analysis of Rsf-1–regulated genes listed in Supplementary Table S1. A total of 25 up-regulated and 37 down-regulated genes with fold increase or decrease by at least 2.5-fold were input to the Ingenuity Pathways Analysis System. This system facilitates the identification of functional connections among Rsf-1–regulated genes with known relevance to the Tissue Morphology, Cellular Assembly and Organization System. Only the top network with a score of 34 is shown. *Red shapes,* up-regulated genes; *green shapes,* down-regulated genes; *white shapes,* molecules added from the Ingenuity knowledge base. *B,* quantitative real-time PCR shows the pattern of gene expression in three selected genes including osteopontin (*OPN*), *CYR61*, and *CTGF* in Rsf-1 inducible (*ind*) and tTA-vector only (*vec*) SKOV3 cells in the presence (*+Dox*) or absence (*−Dox*) of doxycyline. *C,* the expression of *OPN, CYR61*, and *CTGF* and Rsf-1 decrease after transfection of Rsf-1 shRNAs into the OVCAR3 cells with a high-level expression of endogenous Rsf-1. *, $P = 0.018$; **, $P = 0.002$; ***, $P < 0.001$.

knockdown even after an acute induction of Rsf-1. However, reducing hSNF2H expression sensitized both OVCAR3 cells and Rsf-1–expressing SKOV3 cells to paclitaxel, suggesting that different mechanisms are involved in promoting cell growth and drug resistance. Fourth, Rsf-1 expression in tumor specimens can be used as a surrogate marker alone or in combination with other markers to predict treatment response to paclitaxel. To this end, future multi-institutional cohort studies are required to validate the usefulness of Rsf-1 immunoreactivity as a potential diagnostic test for ovarian cancer or other cancer types with Rsf-1 amplification and overexpression.

There are at least two possible mechanisms that could explain how Rsf-1 overexpression contributes to tumor cell survival and growth in the presence of paclitaxel. First, an increased number of RSF complexes may concentrate on specific promoter and/or enhancer regions to modulate transcription activity of a set of genes which participate in drug resistance. In fact, based on comparison of gene profiles between Rsf-1–induced and non-induced SKOV3 ovarian cancer cells, we found that Rsf-1 expression was associated with changes in the expression of several genes. Among them, up-regulation of CYR61 and osteopontin is of interest because both gene products were previously reported to be involved in developing drug resistance (22, 23). Furthermore, using interaction network analysis, it seems that several major molecular hubs were identified in this network and they included NF-κB, ERK, Akt, and EGR1. Among them, NF-κB, ERK, and Akt have been suggested to participate in developing chemoresistance in cancer cells (30–37). For example, the Akt pathway has been shown to play a causal role in the development of docetaxel and paclitaxel resistance in cancer cell lines including those derived from ovarian cancer (31–33). It is of great interest that Rsf-1 has been shown to interact with NF-κB (34). Further studies are required to show the detailed mechanisms of how the Rsf-1/hSNF2H complex contributes to tumor development through their downstream mediators. Second, Rsf-1 overexpression may alter the dynamics of partnership between hSNF2H and hSNF2H binding proteins. Besides Rsf-1, hSNF2H is known to interact with several cellular proteins to form different hSNF2H-containing protein complexes that have diverse cellular functions. In our previous study, we showed that excessive Rsf-1 molecules

sequestered hSNF2H, leading to a loss or a decrease in the abundance of other hSNF2H-binding complexes such as hSNF2H/BAZ1A and hSNF2H/BAZ1B (15). Because several members in the SNF family have been suggested as tumor suppressors and are found to be down-regulated or inactivated in cancer tissues (35, 36), it is plausible that reduction of these hSNF2H complexes with tumor suppressor potential by excessive Rsf-1 contributes to the observed drug-resistant phenotype in cancer cells. However, in this study, we found that expressing the Rsf-D4 deletion mutant, which has the hSNF2H binding activity, enhanced the growth inhibitory effect of paclitaxel in tumor cells. This observation suggests that sequestering hSNF2H from other protein complexes by the Rsf-D4 mutant alone is not able to confer paclitaxel resistance as seen in the full-length Rsf-1. Therefore, the paclitaxel-resistant phenotype mediated by the full-length Rsf-1 is more likely due to an increase in RSF complex formation rather than a decrease in other hSNF2H-containing complexes.

Although the above represents our preferred views, alternative interpretations should be indicated. First, the shRNA screening approach used in this study suggests that *Rsf-1* is the main gene within the 11q13.5 amplicon responsible for paclitaxel resistance. However, other gene(s) within the 11q13.5 amplicon might also be involved in the aggressive behavior of 11q13.5-amplified carcinomas. For example, *PAK1*, a member of serine/threonine kinase family, plays a critical role in controlling anchorage-independent growth and invasiveness in breast cancer cells (37) and in promoting mammalian tumorigenesis (38) and angiogenesis (39). Thus, PAK1 expression may lead to a more aggressive clinical course in ovarian cancer. It is thus plausible that *Rsf-1* collaborates with *PAK1* and other genes to propel tumor progression. Second, similar to other dominant negative approaches that are applied to modulate activity of endogenous proteins, the Rsf-D4 approach reported in this study may not be specific to interrupt the interaction between Rsf-1 and hSNF2H. It is possible that the Rsf-D4 mutant may complex with other protein(s) besides hSNF2H and that overexpression of Rsf-D4 can potentially interfere with the binding of these protein(s) to the endogenous full-length Rsf-1. Finally, Although the correlation is statistically significant, seven tissues with high Rsf-1 did not show significant drug resistance. This finding suggests that other factors may also play a role in conferring a Taxol resistance phenotype that is independent of Rsf-1.

In summary, we showed in this report that development of paclitaxel resistance in ovarian cancer cells was attributed, at least in part, to *Rsf-1*, which is frequently amplified in several types of human cancer. We further showed that the formation of Rsf-1 and hSNF2H chromatin remodeling complexes was essential for developing this resistance phenotype. Our results suggest that Rsf-1 can be used as a biomarker for paclitaxel resistance and can be exploited as a potential target for chemosensitization in carcinomas with Rsf-1 amplification or overexpression.

Disclosure of Potential Conflicts of Interest

No potential conflicts of interest were disclosed. Q5

Acknowledgments

Received 9/17/2008; revised 11/12/2008; accepted 11/14/2008.

Grant support: National Cancer Institute/NIH grants RO1 CA129080 and RO1 CA103937 (I-M. Shih), American Cancer Society grant RSG-08-174-01-GMC (T-L. Wang), and Department of Defense Research Council grant OC0400600 (T-L. Wang).

The costs of publication of this article were defrayed in part by the payment of page charges. This article must therefore be hereby marked *advertisement* in accordance with 18 U.S.C. Section 1734 solely to indicate this fact.

We thank the laboratory members for their valuable comments.

References

1. Kinzler KW, Vogelstein B. The genetic basis of human cancer. 2nd ed. Toronto: McGraw-Hill; 2002.
2. Meltzer PS, Kallioniemi A, Trent JM. Chromosome alterations in human solid tumors. In: Vogelstein B, Kinzler KW, editors. The genetic basis of human cancer. New York: McGraw-Hill; 2002. p. 93–113.
3. Croce CM. Oncogenes and cancer. N Engl J Med 2008; 358:502–11.
4. Wang TL, Maierhofer C, Speicher MR, et al. Digital karyotyping. Proc Natl Acad Sci U S A 2002;99:16156–61.
5. Bignell GR, Huang J, Greshock J, et al. High-resolution analysis of DNA copy number using oligonucleotide microarrays. Genome Res 2004;14:287–95.
6. Shih Ie M, Sheu JJ, Santillan A, et al. Amplification of a chromatin remodeling gene, Rsf-1/HBXAP, in ovarian carcinoma. Proc Natl Acad Sci U S A 2005;102:14004–9.
7. Nakayama K, Nakayama N, Jinawath N, et al. Amplicon profiles in ovarian serous carcinomas. Int J Cancer 2007; 120:2613–7.
8. Bekri S, Adelaide J, Merscher S, et al. Detailed map of a region commonly amplified at 11q13→q14 in human breast carcinoma. Cytogenet Cell Genet 1997;79:125–31.
9. SchramL P, Schwerdtfeger G, Burkhalter F, et al. Combined array comparative genomic hybridization and tissue microarray analysis suggest PAK1 at 11q13.5-q14 as a critical oncogene target in ovarian carcinoma. Am J Pathol 2003;163:985–92.
10. Bentires-Alj M, Gil SG, Chan R, et al. A role for the scaffolding adapter GAB2 in breast cancer. Nat Med 2006;12:114–21.
11. Brown LA, Kalloger SE, Miller MA, et al. Amplification of 11q13 in ovarian carcinoma. Genes Chromosomes Cancer 2008;47:481–9.
12. Schwab M. Amplification of oncogenes in human cancer cells. Bioessays 1998;20:473–9.
13. Pohl G, Ho CL, Kurman RJ, Bristow R, Wang TL Shih Ie M. Inactivation of the mitogen-activated protein kinase pathway as a potential target-based therapy in ovarian serous tumors with KRAS or BRAF mutations. Cancer Res 2005;65:1994–2000.
14. Mao TL, Hsu CY, Yen MJ, et al. Expression of Rsf-1, a chromatin-remodeling gene, in ovarian and breast carcinoma. Hum Pathol 2006;37:1169–75.
15. Sheu JJ, Choi JH, Yildiz I, et al. The roles of human sucrose nonfermenting protein 2 homologue in the tumor-promoting functions of Rsf-1. Cancer Res 2008; 68:4050–7.
16. Buckhaults P, Zhang Z, Chen YC, et al. Identifying tumor origin using a gene expression-based classification map. Cancer Res 2003;63:4144–9.
17. Hogarty MD, Brodeur GM. Gene amplification in human cancers: biological and clinical significance. In: Vogelstein B, Kinzler Kw, editors. The genetic basis of human cancer. 2nd ed. New York: McGraw-Hill; 2002. p. 115–28.
18. Loyola A, Huang J-Y, LeRoy G, et al. Functional analysis of the subunits of the chromatin assembly factor RSF. Mol Cell Biol 2003;23:6759–68.
19. Loyola A, LeRoy G, Wang YH, Reinberg D. Reconstitution of recombinant chromatin establishes a requirement for histone-tail modifications during chromatin assembly and transcription. Genes Dev 2001;15:2837–51.
20. LeRoy G, Loyola A, Lane WS, Reinberg D. Purification and characterization of a human factor that assembles and remodels chromatin. J Biol Chem 2000; 275:14787–90.
21. LeRoy G, Orphanides G, Lane WS, Reinberg D. Requirement of RSF and FACT for transcription of chromatin templates *in vitro*. Science 1998;282: 1900–4.
22. Menendez JA, Vellon L, Mehmi I, Teng PK, Griggs DW, Lupu R. A novel CYR61-triggered "CYR61-3 integrin loop" regulates breast cancer cell survival and chemosensitivity through activation of ERK1/ERK2 MAPK signaling pathway. Oncogene 2005;24:761–79.
23. Graessmann M, Berg B, Fuchs B, Klein A, Graessmann A. Chemotherapy resistance of mouse WAP-SVT/t breast cancer cells is mediated by osteopontin, inhibiting apoptosis downstream of caspase-3. Oncogene 2007;26: 2840–50.
24. Chu CY, Chang CC, Prakash E, Kuo ML. Connective tissue growth factor (CTGF) and cancer progression. J Biomed Sci 2008;15:675–85. Q6
25. Shamay M, Barak O, Shaul Y. HBXAP, a novel PHD-finger protein, possesses transcription repression activity. Genomics 2002;79:523–9.
26. Shamay M, Barak O, Doitsh G, Ben-Dor I, Shaul Y. Hepatitis B virus pX interacts with HBXAP, a PHD finger protein to coactivate transcription. J Biol Chem 2002; 277:9982–8.
27. Aihara T, Miyoshi Y, Koyama K, et al. Cloning and mapping of SMARCA5 encoding hSNF2H, a novel human homologue of *Drosophila* ISWI. Cytogenet Cell Genet 1998;81:191–3.
28. Vignali M, Hassan AH, Neely KE, Workman JL. ATP-dependent chromatin-remodeling complexes. Mol Cell Biol 2000;20:1899–910.
29. Flanagan JF, Peterson CL. A role for the yeast SWI/SNF complex in DNA replication. Nucleic Acids Res 1999;27:2022–8.
30. Cosma MP, Tanaka T, Nasmyth K. Ordered recruitment of transcription and chromatin remodeling factors

to a cell cycle- and developmentally regulated promoter. Cell 1999;97:299–311.

31. Riedel RF, Porrello A, Pontzer E, et al. A genomic approach to identify molecular pathways associated with chemotherapy resistance. Mol Cancer Ther 2008;7:3141–9.

32. Weng D, Song X, Xing H, et al. Implication of the Akt2/sruvivin pathway as a critical target in paclitaxel treatment in human ovarian cancer cells. Cancer Lett 2009;273:257–65.

33. Kim SH, Juhnn YS Song YS. Akt involvement in paclitaxel chemoresistance of human ovarian cancer cells. Ann N Y Acad Sci 2007;1095:82–9.

34. Huang JY, Shen BJ, Tsai WH, Lee SC. Functional interaction between nuclear matrix-associated HBXAP and NF-κB. Exp Cell Res 2004;298:133–43.

35. Klochendler-Yeivin A, Muchardt C, Yaniv M. SWI/SNF chromatin remodeling and cancer. Curr Opin Genet Dev 2002;12:73–9.

36. Klochendler-Yeivin A, Fiette L, Barra J, Muchardt C, Babinet C, Yaniv M. The murine SNF5/INI1 chromatin remodeling factor is essential for embryonic development and tumor suppression. EMBO Rep 2000;1:500–6.

37. Vadlamudi RK, Adam L, Wang RA, et al. Regulatable expression of p21-activated kinase-1 promotes anchorage-independent growth and abnormal organization of mitotic spindles in human epithelial breast cancer cells. J Biol Chem 2000;275:36238–44.

38. Wang RA, Mazumdar A, Vadlamudi RK, Kumar R. P21-activated kinase-1 phosphorylates and transactivates estrogen receptor-α and promotes hyperplasia in mammary epithelium. EMBO J 2002;21:5437–47.

39. Bagheri-Yarmand R, Vadlamudi RK, Wang RA, Mendelsohn J, Kumar R. Vascular endothelial growth factor up-regulation via p21-activated kinase-1 signaling regulates heregulin-β1-mediated angiogenesis. J Biol Chem 2000;275:39451–7.

Frequent activating mutations of *PIK3CA* in ovarian clear cell carcinoma

Kuan-Ting Kuo[13*], Tsui-Lien Mao[3*], Siân Jones[2], Emanuela Veras[1], Ayse Ayhan[4], Tian-Li Wang[1], Ruth Glas[5], Joan Brugge[6], Dennis Slamon[5], Victor E. Velculescu[2], Robert J. Kurman[1], Ie-Ming Shih[1]

Affiliations of authors: [1]Departments of Pathology, Gynecology and Obstetrics, and Kimmel Cancer Center, [2]The Ludwig Center and the Howard Hughes Medical Institute at the Kimmel Cancer Center, Johns Hopkins Medical Institutions, Baltimore, MD; [3]Department of Pathology, National Taiwan University Hospital, Taipei, Taiwan; [4]Department of Pathology, Seirei Mikatahara Hospital, Hamamatsu, Japan; [5]Division of Hematology/Oncology, David Geffen School of Medicine at UCLA; [6]Department of Cell Biology, Harvard Medical School

*Both authors contribute equally.

Corresponding to:

Ie-Ming Shih

Johns Hopkins University School of Medicine, 1550 Orleans Street, Room 305

Baltimore, MD 21231. Phone: 410-502-7774; Fax: 410-502-7943; E-mail:

shihie@yahoo.com

Number of text page: 18

Short Title: PIK3CA mutation in ovarian clear cell carcinoma

Acknowledgements: This study was supported by US Department of Defense grant OC0400600 (TLW), Richard TeLinde Endowed Fund (IMS), Dr. Miriam and Sheldon G. Adelson Medical Research Foundation (VEV), and NIH grant CA121113 (VEV) and CA116184 (RJK).

Abstract

Ovarian clear cell carcinoma (CCC) is one of the most highly malignant types of ovarian carcinomas, particularly at advanced stage. Unlike the more common type of ovarian cancer, high-grade serous carcinoma, ovarian CCC tends to be resistant to platinum-based chemotherapy and therefore effective treatment for this tumor type at advanced stage is urgently needed. In this study, we analyzed 97 ovarian CCCs for sequence mutations in *KRAS*, *BRAF*, *PIK3CA*, *TP53*, *PTEN* and *CTNNB1* as these mutations frequently occur in the other major types of ovarian carcinomas. The samples included 18 CCCs for which affinity-purified tumor cells from fresh specimens were available, 69 micro-dissected tumors from paraffin tissues, and 10 tumor cell lines. Sequence mutations of *PIK3CA*, *TP53*, *KRAS*, *PTEN, CTNNB1* and *BRAF*, occurred in 33%, 16%, 7%, 5%, 3% and 1% of CCC cases, respectively. Sequence analysis of *PIK3CA* in 28 affinity-purified CCCs and 10 CCC cell lines showed a mutation frequency of *PIK3CA* of 46%, suggesting that paraffin embedded samples likely underestimate the mutation frequency of this gene. Samples with *PIK3CA* mutations showed intense phosphorylated AKT immunoreactivity. These findings demonstrate that ovarian CCCs have a high frequency of activating *PIK3CA* mutations, and suggest that PIK3CA targeting drugs may be a more effective therapy than current chemotherapeutic agents for patients with advanced stage and recurrent disease.

Introduction

Ovarian carcinomas are a heterogeneous group of neoplasms that can be classified according to the type and degree of differentiation. Despite the fact that clinical management of ovarian cancer at the present time largely fails to take this heterogeneity into account, it has becoming clear that each major histological type has unique molecular genetic defects that deregulate specific signaling pathways in the cancer cells [1]. Ovarian clear cell carcinoma (CCC) is one of the most lethal types of ovarian cancer with a 5-year survival rate (all stages) of less than 35% [2]. Unlike the more common type of ovarian carcinoma, high-grade serous carcinoma, CCC is often resistant to platinum-based chemotherapy [3-8]. Several studies have attempted to elucidate the molecular pathogenesis of ovarian CCC with the goal of identifying molecular targets that are altered in this tumor type [1], but these reports have been of limited value because of insufficient sample size.

In this study, we analyzed 97 ovarian CCCs for sequence alterations in genes that participate in several major cancer-associated pathways including *TP53, KRAS*, *BRAF, PIK3CA, PTEN* and *CTNNB1*. We demonstrated frequent *PIK3CA* mutations in CCCs, especially those from purified tumors and cell lines. Our findings suggest that PIK3CA targeting drugs may be a more effective therapy than current chemotherapeutic agents for patients with advanced stage and recurrent disease.

Materials and Methods

Tissue specimens

The tumors included 10 cases from the Johns Hopkins Hospital, USA, 52 cases from National Taiwan University Hospital, and 25 cases from the Seirei Mikatahara Hospital, Japan. Hematoxylin and eosin stained sections from tissue specimens were reviewed and the diagnosis of ovarian CCCs confirmed by an expert gynecologic pathologist (RJK). All the specimens were anonymized and tissues collected in compliance with institutional review board regulations. In addition, we also analyzed 10 established ovarian CCC cell lines. As the sensitivity of mutation detection in primary tumors is dramatically affected by the purity of the tumor DNA samples analyzed, we affinity purified tumor cells using Epi-CAM antibody magnetic beads from all 18 freshly collected samples [9]. We also micro-dissected tumor cells from 69 paraffin-embedded tumors.

Mutational analysis

The relevant exons of the genes indicated in the supplementary Table 1 in each tumor sample were PCR amplified, sequenced and assessed for potential sequence alterations using approaches previously described [9,10]. The nucleotide sequences were then analyzed using the Mutation Surveyor program (Soft Genetics LLC, State College, PA) and the sequencing data were analyzed by two investigators independently.

Immunohistochemistry

We assessed AKT phosphorylation in 41 CCCs including those with and without *PIK3CA* mutations using an anti-pAkt (Ser473) monoclonal antibody (Cell Signaling).

Immunohistochemistry was performed on deparaffinized sections using the antibody at a dilution of 1:50 and an EnVision+System peroxidase kit (DAKO, Carpinteria, CA). Immunoreactivity was scored by two investigators as follows: 0: undetectable, 1+: weakly positive, 2+: moderately positive and 3+: intensely positive.

SNP array analysis

SNPs were genotyped using the 250K StyI arrays (Affymetrix, Santa Clara, CA) in the Microarray Core Facility at the Dana-Farber Cancer Institute, Boston, MA (http://chip.dfci.harvard.edu/lab/ services.php). The dChip 2006 program was used to analyze SNP array data [11,12]. Data was normalized to a baseline array with median signal intensity at the probe intensity level using the invariant set normalization method. Signal values for each SNP were compared with the average intensities from 15 normal samples. To infer the DNA copy number from the raw signal data, we used the Hidden Markov Model [11], based on the assumption of diploid for normal samples. Mapping information of SNP locations and cytogenetic bands were based on curation of Affymetrix and University of California Santa Cruz hg17. In this study, we used an arbitrary cutoff of >3 copies in more than 6 consecutive SNPs to define an amplification.

Quantitative real-time PCR

DNA copy number of the PIK3CA locus in 10 CCC cell lines was assessed by quantitative real-time PCR using an iCycler (Bio-Rad, Hercules, CA) with SYBR green dye (Molecular Probes, Eugene, OR). The primer sequences that amplified the first exon are: CCCCTCCATCAACTTCTTCAA (forward) and ATTGTATCATACCAATTTCTCGATTG (reverse).

Averages in the threshold cycle number (Ct) of triplicate measurements were obtained.

The results were expressed as the difference between the Ct of the gene of interest and the Ct of a *Line-1* gene for which expression is relatively constant among tumor tissues.

Results and Discussion

The mutation profile of all the specimens is summarized in Table 1 and the detailed mutations in each sample were listed in supplementary Table 2. Sequence mutations of *PIK3CA*, *TP53*, *KRAS*, *PTEN, CTNNB1* and *BRAF*, were detected in 33%, 16%, 7%, 5%, 3% and 1%, of informative CCC cases, respectively. Among the genes analyzed, *PIK3CA* was the most frequently mutated and was therefore selected for further characterization. We found that the percentage of *PIK3CA* mutations was even higher (46%) in the 28 cases of affinity purified CCCs and CCC cell lines, suggesting that the percentage of *PIK3CA* mutations in paraffin tissues was likely underestimated due to contamination by stromal cells and the relatively poor DNA quality of formalin-fixed and paraffin-embedded tissue. Most of the *PIK3CA* mutations were mapped to exon 9 and exon 20 resulting in kinase activation of p110α which has been shown to result in increased cellular survival and invasion. Because AKT activation by phosphorylation can occur as a result of constitutive activating mutations in *PIK3CA*, we assessed AKT phosphorylation in 41 tumors including those with and without *PIK3CA* mutations. We found that all 10 specimens with *PIK3CA* mutations showed intense phosphorylated AKT immunoreactivity. These results indicate that *PIK3CA* mutations directly activate AKT in CCCs, and suggest that the PI3K pathway is activated in an even higher fraction of these tumors.

In an effort to determine if the *PIK3CA* locus was genomically amplified, we applied a genome-wide analysis for DNA copy number alterations in the 12 affinity-purified ovarian CCCs using 250K SNP arrays and performed quantitative real-time PCR to determine the DNA copy number in the *PIK3CA* locus in 10 cell lines. We did not observe any DNA copy number change in any of the tumors and cell lines (supplementary Fig. 1). Thus, it is likely that *PIK3CA* mutation is the main molecular genetic change that constitutively activates the PI3K/AKT pathway in ovarian CCC.

Finally, to determine the clinical significance of *PIK3CA* mutation in ovarian CCCs, we correlated its mutation status with various clinicopathological parameters. There was no significant correlation between the *PIK3CA* mutation status and histologic features, clinical stage, patient age, disease-free interval and overall survival ($p > 0.05$ for all clinical parameters examined).

The findings from this study have important biological and clinical ramifications for ovarian cancer. First, although previous reports have detected *PIK3CA* mutations in ovarian CCC, those studies analyzed a small number of cases and therefore the investigators could not draw firm conclusions about the frequency of *PIK3CA* mutations and the generalizability of their findings [13-15]. In the present study, we analyzed a total of 97 ovarian CCCs and demonstrated that more than a third had *PIK3CA* mutations. This observation is important because of the well-established role of PI3K in oncogenesis in several types of human cancer [16-19]. It is particularly interesting that among all the cancer types reported so far, ovarian CCC has the highest frequency of *PIK3CA* mutations.

Our results also provide additional support to the view that ovarian cancer is a heterogeneous group of neoplastic diseases which are characterized by their signature molecular genetic aberrations [20]. Specifically, high-grade serous carcinoma is characterized by frequent mutations of *TP53* and high levels of chromosomal instability [20,21]. In contrast, low-grade serous carcinoma frequently harbors mutations in *KRAS/BRAF/ERBB2*, endometrioid carcinoma has *PTEN* and *CTNNB1* mutations in most of cases, and mucinous carcinoma has *KRAS* mutations in more than half of the cases [1,20] (Fig. 1). The high frequency of *PIK3CA* mutation and the low rate of mutations in *KRAS*, *BRAF*, *TP53*, *PTEN* and *CTNNB*1 indicate that CCCs have a different molecular signature from other surface epithelial tumors. Both ovarian endometrioid carcinoma and CCC are thought to develop from endometriosis [22], but

endometrioid carcinoma has a high frequency of *PTEN* and *CTNNB1* mutations while CCC has a low frequency of mutations in these genes. Thus, our data provide evidence that the underlying genetic events in CCC and endometrioid carcinoma are inherently different despite the fact that the precursor lesion, endometriosis, is the same for both tumors.

From a therapeutic perspective, our results underscore the importance of carefully separating these different types of ovarian tumors in clinical trials evaluating different types of treatments. The relatively high frequency of *PIK3CA* mutations holds promise for new therapeutic approaches using small molecule inhibitors targeting PI3K. New PI3K targeting drugs, including GDC-0941 [23], NVP-BEZ235 [24,25], PI-103 [26], and SF1126, a LY294002 prodrug [27], have recently been developed and are being evaluated in clinical trials [23,25,28]. In the future, it will be important to design clinical trials to evaluate the efficacy of such inhibitors by correlating clinical response with *PIK3CA* mutational status or pathway activation. If such studies show promising results, this would be an important step in the development of customized treatment for a highly malignant type of ovarian cancer.

Table 1. Sequence mutation rates in ovarian clear cell carcinomas.

Sample (n)	KRAS	BRAF	TP53	PIK3CA	CTNNB1	PTEN
JH (10)	20%	0%	10%	50%	0%	0%
TW (8)	0%	0%	ND	50%	0%	ND
Cell line (10)	10%	10%	20%	40%	0%	10%
TW-paraffin (44)	9%	0%	ND	25%	2%	ND
JP-paraffin (25)	0%	0%	ND	32%	8%	ND
Overall: non-paraffin (JH+TW+Cell line)	11%	3%	15%	46%	0%	5%
Overall (97)	7%	1%	15%	33%	1%	5%

JH: freshly purified tumor cells from tumor tissues at the Johns Hopkins University

TW: freshly purified tumor cells from tumor tissues at the National Taiwan University Hospital

TW-paraffin: paraffin-embedded tumors from National Taiwan University Hospital, Taiwan

JP-paraffin: paraffin-embedded tumors from the Seirei Mikatahara Hospital, Japan

ND: not determined

Figure Legend

Figure 1. The mutation profile of *TP53*, *KRAS*, *BRAF*, *PIK3CA*, *PTEN*, and *CTNNB1* in different histological types of ovarian epithelial neoplasms. The frequency of individual mutations is shown in the bar chart in various types of ovarian carcinoma including high-grade (HG) serous carcinoma, low-grade (LG) serous carcinoma, clear cell carcinoma, endometrioid carcinoma (EMCA), and mucinous carcinoma. The mutation frequency is estimated from several studies based on a sizable sample size [1,9,10,14,15,29-37]. The frequency of *PIK3CA* mutation in clear cell carcinoma is based on the current study showing 46% in purified tumors and cell lines. The mutation frequency of *PTEN* and *CTNNB1* has not been determined in low-grade serous carcinomas (ND).

Supplementary Figure 1. DNA copy number changes in the *PIK3CA* locus based on SNP array analysis. The DNA copy number in the chromosome 3 (both p arm and q arm) from 12 affinity-purified ovarian clear cell carcinomas is shown as the inferred log2 ratio. The relative DNA copy number in the heat map is represented as a pseudo-color gradient from high (red boxes) to low (blue boxes). The ideogram is shown on the right.

References

1. Cho KR, Shih IM: Ovarian cancer. Annu Rev Pathol Mech Dis 2009, 4:287-313
2. Takano M, Kikuchi Y, Yaegashi N, Kuzuya K, Ueki M, Tsuda H, Suzuki M, Kigawa J, Takeuchi S, Tsuda H, Moriya T, Sugiyama T: Clear cell carcinoma of the ovary: a retrospective multicentre experience of 254 patients with complete surgical staging. Br J Cancer 2006, 94:1369-1374
3. Chan JK, Teoh D, Hu JM, Shin JY, Osann K, Kapp DS: Do clear cell ovarian carcinomas have poorer prognosis compared to other epithelial cell types? A study of 1411 clear cell ovarian cancers. Gynecol Oncol 2008, 109:370-376
4. Pectasides D, Fountzilas G, Aravantinos G, Kalofonos C, Efstathiou H, Farmakis D, Skarlos D, Pavlidis N, Economopoulos T, Dimopoulos MA: Advanced stage clear-cell epithelial ovarian cancer: the Hellenic Cooperative Oncology Group experience. Gynecol Oncol 2006, 102:285-291
5. Goff BA, Sainz de la Cuesta R, Muntz HG, Fleischhacker D, Ek M, Rice LW, Nikrui N, Tamimi HK, Cain JM, Greer BE, Fuller AF, Jr.: Clear cell carcinoma of the ovary: a distinct histologic type with poor prognosis and resistance to platinum-based chemotherapy in stage III disease. Gynecol Oncol 1996, 60:412-417
6. Sugiyama T, Kamura T, Kigawa J, Terakawa N, Kikuchi Y, Kita T, Suzuki M, Sato I, Taguchi K: Clinical characteristics of clear cell carcinoma of the ovary: a distinct histologic type with poor prognosis and resistance to platinum-based chemotherapy. Cancer 2000, 88:2584-2589
7. Crotzer DR, Sun CC, Coleman RL, Wolf JK, Levenback CF, Gershenson DM: Lack of effective systemic therapy for recurrent clear cell carcinoma of the ovary. Gynecol Oncol 2007, 105:404-408
8. Takano M, Sugiyama T, Yaegashi N, Sakuma M, Suzuki M, Saga Y, Kuzuya K,

Kigawa J, Shimada M, Tsuda H, Moriya T, Yoshizaki A, Kita T, Kikuchi Y: Low response rate of second-line chemotherapy for recurrent or refractory clear cell carcinoma of the ovary: a retrospective Japan Clear Cell Carcinoma Study. Int J Gynecol Cancer 2008, 18:937-942

9. Nakayama K, Nakayama N, Kurman RJ, Cope L, Pohl G, Samuels Y, Velculescu VE, Wang TL, Shih Ie M: Sequence mutations and amplification of PIK3CA and AKT2 genes in purified ovarian serous neoplasms. Cancer Biol Ther 2006, 5:779-785

10. Salani R, Kurman RJ, Giuntoli R, 2nd, Gardner G, Bristow R, Wang TL, Shih IM: Assessment of TP53 mutation using purified tissue samples of ovarian serous carcinomas reveals a higher mutation rate than previously reported and does not correlate with drug resistance. Int J Gynecol Cancer 2008, 18:487-491

11. Slamon DJ GW, Jones LA, Holt JA, Wong SG, Keith DE, Levin WJ, Stuart SG, Udove J, Ullrich A, et al: Studies of the HER-2/neu proto-oncogene in human breast and ovarian cancer. Science 1989, 244:707-712

12. Cheng JQ, Godwin AK, Bellacosa A, Taguchi T, Franke TF, Hamilton TC, Tsichlis PN, Testa JR: AKT2, a putative oncogene encoding a member of a subfamily of protein- serine/threonine kinases, is amplified in human ovarian carcinomas. Proc Natl Acad Sci U S A 1992, 89:9267-9271.

13. Wang Y, Helland A, Holm R, Kristensen GB, Borresen-Dale AL: PIK3CA mutations in advanced ovarian carcinomas. Hum Mutat 2005, 25:322

14. Willner J, Wurz K, Allison KH, Galic V, Garcia RL, Goff BA, Swisher EM: Alternate molecular genetic pathways in ovarian carcinomas of common histological types. Hum Pathol 2007, 38:607-613

15. Campbell IG, Russell SE, Choong DY, Montgomery KG, Ciavarella ML, Hooi CS, Cristiano BE, Pearson RB, Phillips WA: Mutation of the PIK3CA gene in

ovarian and breast cancer. Cancer Res 2004, 64:7678-7681

16. Samuels Y, Diaz LA, Jr., Schmidt-Kittler O, Cummins JM, Delong L, Cheong I, Rago C, Huso DL, Lengauer C, Kinzler KW, Vogelstein B, Velculescu VE: Mutant PIK3CA promotes cell growth and invasion of human cancer cells. Cancer Cell 2005, 7:561-573

17. Samuels Y, Velculescu VE: Oncogenic mutations of PIK3CA in human cancers. Cell Cycle 2004, 3:1221-1224

18. Samuels Y, Wang Z, Bardelli A, Silliman N, Ptak J, Szabo S, Yan H, Gazdar A, Powell SM, Riggins GJ, Willson JK, Markowitz S, Kinzler KW, Vogelstein B, Velculescu VE: High frequency of mutations of the PIK3CA gene in human cancers. Science 2004, 304:554

19. Guerreiro AS, Fattet S, Fischer B, Shalaby T, Jackson SP, Schoenwaelder SM, Grotzer MA, Delattre O, Arcaro A: Targeting the PI3K p110a isoform inhibits medulloblastoma proliferation, chemoresistance, and migration. Clin Cancer Res 2008, 14:6761-6769

20. Shih I-M, Kurman RJ: Ovarian tumorigenesis- a proposed model based on morphological and molecular genetic analysis. Am J Pathol 2004, 164:1511-1518

21. Corney DC, Flesken-Nikitin A, Choi J, Nikitin AY: Role of p53 and Rb in ovarian cancer. Adv Exp Med Biol 2008, 622:99-117

22. Tan DS, Kaye S: Ovarian clear cell adenocarcinoma: a continuing enigma. J Clin Pathol 2007, 60:355-360

23. Folkes AJ, Ahmadi K, Alderton WK, Alix S, Baker SJ, Box G, Chuckowree IS, Clarke PA, Depledge P, Eccles SA, Friedman LS, Hayes A, Hancox TC, Kugendradas A, Lensun L, Moore P, Olivero AG, Pang J, Patel S, Pergl-Wilson GH, Raynaud FI, Robson A, Saghir N, Salphati L, Sohal S, Ultsch MH, Valenti

M, Wallweber HJ, Wan NC, Wiesmann C, Workman P, Zhyvoloup A, Zvelebil MJ, Shuttleworth SJ: The identification of 2-(1H-indazol-4-yl)-6-(4-methanesulfonyl-piperazin-1-ylmethyl)-4-morpholin -4-yl-thieno[3,2-d]pyrimidine (GDC-0941) as a potent, selective, orally bioavailable inhibitor of class I PI3 kinase for the treatment of cancer. J Med Chem 2008, 51:5522-5532

24. Schnell CR, Stauffer F, Allegrini PR, O'Reilly T, McSheehy PM, Dartois C, Stumm M, Cozens R, Littlewood-Evans A, Garcia-Echeverria C, Maira SM: Effects of the dual phosphatidylinositol 3-kinase/mammalian target of rapamycin inhibitor NVP-BEZ235 on the tumor vasculature: implications for clinical imaging. Cancer Res 2008, 68:6598-6607

25. Maira SM, Stauffer F, Brueggen J, Furet P, Schnell C, Fritsch C, Brachmann S, Chene P, De Pover A, Schoemaker K, Fabbro D, Gabriel D, Simonen M, Murphy L, Finan P, Sellers W, Garcia-Echeverria C: Identification and characterization of NVP-BEZ235, a new orally available dual phosphatidylinositol 3-kinase/mammalian target of rapamycin inhibitor with potent in vivo antitumor activity. Mol Cancer Ther 2008, 7:1851-1863

26. Prevo R, Deutsch E, Sampson O, Diplexcito J, Cengel K, Harper J, O'Neill P, McKenna WG, Patel S, Bernhard EJ: Class I PI3 kinase inhibition by the pyridinylfuranopyrimidine inhibitor PI-103 enhances tumor radiosensitivity. Cancer Res 2008, 68:5915-5923

27. Garlich JR, De P, Dey N, Su JD, Peng X, Miller A, Murali R, Lu Y, Mills GB, Kundra V, Shu HK, Peng Q, Durden DL: A vascular targeted pan phosphoinositide 3-kinase inhibitor prodrug, SF1126, with antitumor and antiangiogenic activity. Cancer Res 2008, 68:206-215

28. Marone R, Cmiljanovic V, Giese B, Wymann MP: Targeting phosphoinositide

3-kinase: moving towards therapy. Biochim Biophys Acta 2008, 1784:159-185

29. Gemignani ML, Schlaerth AC, Bogomolniy F, Barakat R, Lin O, Soslow R, Venkatraman E, Boyd J: Role of KRAS and BRAF gene mutations in mucinous ovarian carcinoma. Gyncol Oncol 2003, 90:378-381

30. Ho ES, Lai CR, Hsieh YT, Chen JT, Lin AJ, Hung MH, Liu FS: p53 mutation is infrequent in clear cell carcinoma of the ovary. Gynecol Oncol 2001, 80:189-193

31. Singer G, Oldt R, 3rd, Cohen Y, Wang BG, Sidransky D, Kurman RJ, Shih Ie M: Mutations in BRAF and KRAS characterize the development of low-grade ovarian serous carcinoma. J Natl Cancer Inst 2003, 95:484-486.

32. Milner BJ, Allan LA, Eccles DM, Kitchener HC, Leonard RC, Kelly KF, Parkin DE, Haites NE: p53 mutation is a common genetic event in ovarian carcinoma. Cancer Res 1993, 53:2128-2132.

33. Sieben NL, Macropoulos P, Roemen GM, Kolkman-Uljee SM, Jan Fleuren G, Houmadi R, Diss T, Warren B, Al Adnani M, De Goeij AP, Krausz T, Flanagan AM: In ovarian neoplasms, BRAF, but not KRAS, mutations are restricted to low-grade serous tumours. J Pathol 2004, 202:336-340

34. Obata K, Hoshiai H: Common genetic changes between endometriosis and ovarian cancer. Gynecol Obstet Invest 2000, 50:39-43

35. Bell DA: Origins and molecular pathology of ovarian cancer. Mod Pathol 2005, 18 Suppl 2:S19-32

36. Kurman RJ, Shih Ie M: Pathogenesis of ovarian cancer: lessons from morphology and molecular biology and their clinical implications. Int J Gynecol Pathol 2008, 27:151-160

37. Enomoto T, Weghorst CM, Inoue M, Tanizawa O, Rice JM: K-ras activation occurs frequently in mucinous adenocarcinomas and rarely in other common

epithelial tumors of the human ovary. Am J Pathol 1991, 139:777-785.

Fig. 1 Kuo et al

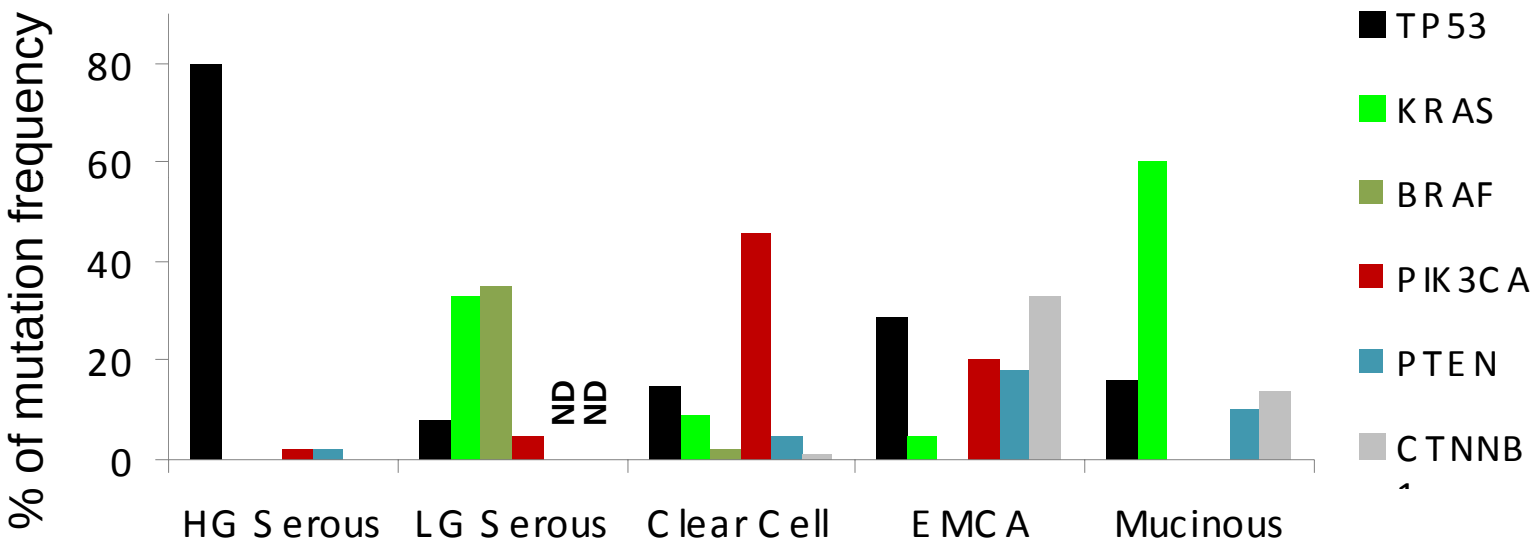

Supplementary Fig. 1 Kuo et al

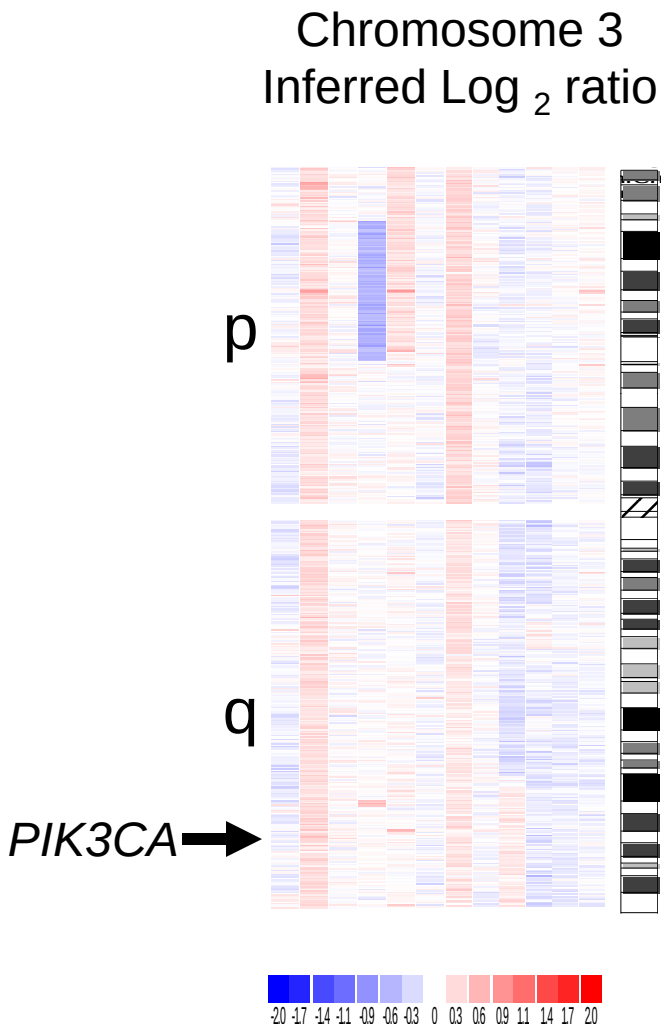

Supplementary Table 1. PCR and Sequencing Primers

Gene	Exon	Primer 1 sequence	Primer 2 sequence
KRAS	1	GTAAAACGACGGCCAGTTTGAAACCCAAGGTACATTTCAG	TCTTAAGCGTCGATGGAGGAG
KRAS	2	GTAAAACGACGGCCAGTATGCATGGCATTAGCAAAGAC	CGTCATCTTTGGAGCAGGAAC
BRAF	15	GTAAAACGACGGCCAGTTTTGTGAATACTGGGAACTATGAAA	TCATCCTAACACATTTCAAGCC
TP53	3	GTAAAACGACGGCCAGTGAGGAATCCCAAAGTTCCAAAC	ACGTTCTGGTAAGGACAAGGG
TP53	4	GTAAAACGACGGCCAGTGGGCCAGACCTAAGAGCAATC	AAGCTCCTGAGGTGTAGACGC
TP53	5	AGGCCCTTAGCCTCTGTAAGC	GTAAAACGACGGCCAGTCTGCTCAGATAGCGATGGTG
TP53	6	GTAAAACGACGGCCAGTAGAAATCGGTAAGAGGTGGGC	CATCCTGGCTAACGGTGAAAC
TP53	7	GTAAAACGACGGCCAGTTTGGGCAGTGCTAGGAAAGAG	GTTGGGAGTAGATGGAGCCTG
PIK3CA	1	TGCTTTGGGACAACCATACATC	CTTGCTTCTTTAAATAGTTCATGCTTT
PIK3CA	1	CCCCTCCATCAACTTCTTCAA	ATTGTATCATACCAATTTCTCGATTG
PIK3CA	9	TCAGCAGTTACTATTCTGTGACTGG	GTAAAACGACGGCCAGTTGCTGAGATCAGCCAAATTCA
PIK3CA	20	GTAAAACGACGGCCAGTGACATTTGAGCAAAGACCTGAAG	TGGATTGTGCAATTCCTATGC
PTEN	1	TTTCCATCCTGCAGAAGAAGC	GTAAAACGACGGCCAGTTCCGTCTAGCCAAACACACC
PTEN	2	GTAAAACGACGGCCAGTTCTGTGATGTATAAACCGTGAGTTTC	CCCTGAAGTCCATTAGGTACGG
PTEN	3	GTAAAACGACGGCCAGTCATGATTACTACTCTAAACCCATAGAAGG	TCAAATATGGGCTAGATGCCA
PTEN	4	ATAAAGATTCAGGCAATGTTTGTTAG	GTAAAACGACGGCCAGTGACCAACTGCCTCAAATAGTAGG
PTEN	5	TGCAACATTTCTAAAGTTACCTACTTG	GTAAAACGACGGCCAGTTTTACTTGTCAATTACACCTCAATAAA
PTEN	6	AATGGCTACGACCCAGTTACC	GTAAAACGACGGCCAGTTTTGGCTTCTTTAGCCCAATG
PTEN	7	GTAAAACGACGGCCAGTTGCAGATACAGAATCCATATTTCG	AATGTCTCACCAATGCCAGAG
PTEN	8	TGCAACAGATAACTCAGATTGCC	GTAAAACGACGGCCAGTTGTCAAGCAAGTTCTTCATCAGC
PTEN	9	GTAAAACGACGGCCAGTAAAGATCATGTTTGTTACAGTGCTTAAA	TGACACAATGTCCTATTGCCA
CTNNB1	2	AAATATTTCAATGGGTCATATCACAG	GTAAAACGACGGCCAGTTCCACAGTTCAGCATTTACCTAAG

Supplemental Table 2. Mutations identified in ovarian clear cell carcinomas

Sample		Gene					
		K-RAS	***BRAF***	***TP53***	***PIK3CA***	***CTNNB1***	***PTEN***
JH1	purified cells	No mut	No mut	No mut	546 Q>K (1636 C>A)	No mut	No mut
JH2	purified cells	No mut	No mut	No mut	No mut	No mut	No mut
JH3	purified cells	No mut	No mut	No mut	542 E>K (1624 G>A)	No mut	No mut
JH4	purified cells	No mut	No mut	No mut	No mut	No mut	No mut
JH5	purified cells	No mut	No mut	No mut	1047 H>R (3140 A>G)	No mut	No mut
JH6	purified cells	No mut	No mut	No mut	No mut	No mut	No mut
JH7	purified cells	12 G>D (35 G>A)	No mut	199 G>V (596 G>T)	No mut	No mut	No mut
JH8	purified cells	12 G>D (35 G>A)	No mut	No mut	No mut	No mut	No mut
JH9	purified cells	No mut	No mut	No mut	1047 H>R (3140 A>G)	No mut	No mut
JH10	purified cells	No mut	No mut	No mut	545 E>A (1634 A>C)	No mut	No mut
TW1	purified cells	No mut	No mut	N.D.	1047 H>R (3140 A>G)	No mut	No mut
TW2	purified cells	No mut	No mut	N.D.	No mut	No mut	No mut
TW3	purified cells	No mut	No mut	N.D.	1047 H>R (3140 A>G)	No mut	No mut
TW4	purified cells	No mut	No mut	N.D.	No mut	No mut	No mut
TW5	purified cells	No mut	No mut	N.D.	1047 H>R (3140 A>G)	No mut	No mut
TW6	purified cells	No mut	No mut	N.D.	No mut	No mut	No mut
TW7	purified cells	No mut	No mut	N.D.	1047 H>L (3140 A>T)	No mut	No mut
TW8	purified cells	No mut	No mut	N.D.	No mut	No mut	No mut
TW-para 1	paraffin tissue	No mut	No mut	N.D.	No mut	No mut	N.D.
TW-para 2	paraffin tissue	No mut	No mut	N.D.	No mut	No mut	N.D.
TW-para 3	paraffin tissue	No mut	No mut	N.D.	No mut	No mut	N.D.
TW-para 4	paraffin tissue	No mut	No mut	N.D.	No mut	No mut	N.D.
TW-para 5	paraffin tissue	No mut	No mut	N.D.	No mut	No mut	N.D.
TW-para 6	paraffin tissue	12 G>D (35 G>A); 13 G>D (38 G>A)	No mut	N.D.	No mut	No mut	N.D.
TW-para 7	paraffin tissue	No mut	No mut	N.D.	No mut	No mut	N.D.
TW-para 8	paraffin tissue	No mut	No mut	N.D.	No mut	No mut	N.D.
TW-para 9	paraffin tissue	No mut	No mut	N.D.	No mut	No mut	N.D.
TW-para 10	paraffin tissue	No mut	No mut	N.D.	No mut	No mut	N.D.
TW-para 11	paraffin tissue	15 G>S (43 G>A)	No mut	N.D.	1024 K>R (3071 A>G)	No mut	N.D.
TW-para 12	paraffin tissue	No mut	No mut	N.D.	No mut	No mut	N.D.
TW-para 13	paraffin tissue	7 G>M (19 G>A)	No mut	N.D.	No mut	No mut	N.D.
TW-para 14	paraffin tissue	No mut	No mut	N.D.	1047 H>R (3140 A>G)	42 T>S (124 A>T)	N.D.

TW-para 15	paraffin tissue	No mut	No mut	N.D.	No mut	No mut	N.D.
TW-para 16	paraffin tissue	No mut	No mut	N.D.	No mut	No mut	N.D.
TW-para 17	paraffin tissue	No mut	No mut	N.D.	545 E>A (1634 A>C)	No mut	N.D.
TW-para 18	paraffin tissue	No mut	No mut	N.D.	No mut	No mut	N.D.
TW-para 19	paraffin tissue	No mut	No mut	N.D.	No mut	No mut	N.D.
TW-para 20	paraffin tissue	No mut	No mut	N.D.	No mut	No mut	N.D.
TW-para 21	paraffin tissue	No mut	No mut	N.D.	No mut	No mut	N.D.
TW-para 22	paraffin tissue	No mut	No mut	N.D.	No mut	No mut	N.D.
TW-para 23	paraffin tissue	No mut	No mut	N.D.	No mut	No mut	N.D.
TW-para 24	paraffin tissue	No mut	No mut	N.D.	No mut	No mut	N.D.
TW-para 25	paraffin tissue	No mut	No mut	N.D.	No mut	No mut	N.D.
TW-para 26	paraffin tissue	No mut	No mut	N.D.	1021 Y>C (3062 A>G)	No mut	N.D.
TW-para 27	paraffin tissue	No mut	No mut	N.D.	No mut	No mut	N.D.
TW-para 28	paraffin tissue	No mut	No mut	N.D.	No mut	No mut	N.D.
TW-para 29	paraffin tissue	12 G>V (35 G>T)	No mut	N.D.	1049 G>R (3145 G>C)	No mut	N.D.
TW-para 30	paraffin tissue	No mut	No mut	N.D.	No mut	No mut	N.D.
TW-para 31	paraffin tissue	No mut	No mut	N.D.	No mut	No mut	N.D.
TW-para 32	paraffin tissue	No mut	No mut	N.D.	No mut	No mut	N.D.
TW-para 33	paraffin tissue	No mut	No mut	N.D.	1047 H>R (3140 A>G)	No mut	N.D.
TW-para 34	paraffin tissue	No mut	No mut	N.D.	545 E>K (1633 G>A)	No mut	N.D.
TW-para 35	paraffin tissue	No mut	No mut	N.D.	No mut	No mut	N.D.
TW-para 36	paraffin tissue	No mut	No mut	N.D.	No mut	No mut	N.D.
TW-para 37	paraffin tissue	No mut	No mut	N.D.	39 E>K (115 G>A); 545 E>A (1634 A>C)	No mut	N.D.
TW-para 38	paraffin tissue	No mut	No mut	N.D.	No mut	No mut	N.D.
TW-para 39	paraffin tissue	No mut	No mut	N.D.	No mut	No mut	N.D.
TW-para 40	paraffin tissue	No mut	No mut	N.D.	No mut	No mut	N.D.
TW-para 41	paraffin tissue	No mut	No mut	N.D.	542 E>K (1624 G>A)	No mut	N.D.
TW-para 42	paraffin tissue	No mut	No mut	N.D.	No mut	No mut	N.D.
TW-para 43	paraffin tissue	No mut	No mut	N.D.	1043 M>I (3129 G>A)	No mut	N.D.
TW-para 44	paraffin tissue	No mut	No mut	N.D.	111 K>E (331 A>G)	No mut	N.D.
JP-para 1	paraffin tissue	No mut	No mut	N.D.	No mut	No mut	N.D.
JP-para 2	paraffin tissue	No mut	No mut	N.D.	546 Q>P (1637 A>C)	No mut	N.D.
JP-para 3	paraffin tissue	No mut	No mut	N.D.	545 E>K (1633 G>A)	No mut	N.D.
JP-para 4	paraffin tissue	No mut	No mut	N.D.	No mut	No mut	N.D.
JP-para 5	paraffin tissue	No mut	No mut	N.D.	1047 H>R (3140 A>G)	29 S>F (86 C>T)	N.D.
JP-para 6	paraffin tissue	No mut	No mut	N.D.	1051 W>X (3153 G>A)	8 M>I (24 G>A)	N.D.

JP-para 7	paraffin tissue	No mut	No mut	N.D.	1037 E>K (3109 G>A)	No mut	N.D.
JP-para 8	paraffin tissue	No mut	No mut	N.D.	No mut	No mut	N.D.
JP-para 9	paraffin tissue	No mut	No mut	N.D.	No mut	No mut	N.D.
JP-para 10	paraffin tissue	No mut	No mut	N.D.	No mut	No mut	N.D.
JP-para 11	paraffin tissue	No mut	No mut	N.D.	1047 H>R (3140 A>G)	No mut	N.D.
JP-para 12	paraffin tissue	No mut	No mut	N.D.	No mut	No mut	N.D.
JP-para 13	paraffin tissue	No mut	No mut	N.D.	1047 H>R (3140 A>G)	No mut	N.D.
JP-para 14	paraffin tissue	No mut	No mut	N.D.	No mut	No mut	N.D.
JP-para 15	paraffin tissue	No mut	No mut	N.D.	No mut	No mut	N.D.
JP-para 16	paraffin tissue	No mut	No mut	N.D.	No mut	No mut	N.D.
JP-para 17	paraffin tissue	No mut	No mut	N.D.	No mut	No mut	N.D.
JP-para 18	paraffin tissue	No mut	No mut	N.D.	1047 H>L (3140 A>T)	No mut	N.D.
JP-para 19	paraffin tissue	No mut	No mut	N.D.	No mut	No mut	N.D.
JP-para 20	paraffin tissue	No mut	No mut	N.D.	No mut	No mut	N.D.
JP-para 21	paraffin tissue	No mut	No mut	N.D.	No mut	No mut	N.D.
JP-para 22	paraffin tissue	No mut	No mut	N.D.	No mut	No mut	N.D.
JP-para 23	paraffin tissue	No mut	No mut	N.D.	No mut	No mut	N.D.
JP-para 24	paraffin tissue	No mut	No mut	N.D.	No mut	No mut	N.D.
JP-para 25	paraffin tissue	No mut	No mut	N.D.	No mut	No mut	N.D.
ES-2	cell line	No mut	600 V>E (1799 T>A)	241 S>F (722 C>T)	No mut	No mut	No mut
KK	cell line	No mut	No mut	No mut	545 E>A (1634 A>C)	No mut	No mut
OV207	cell line	No mut	No mut	273 R>H (818 G>A)	No mut	No mut	No mut
OVCA429	cell line	No mut	No mut	No mut	545 E>K (1633 G>A)	No mut	No mut
OVISE	cell line	No mut	No mut	No mut	No mut	No mut	No mut
OVMANA	cell line	No mut	No mut	No mut	545 E>V (1634 A>T)	No mut	No mut
OVTOKO	cell line	No mut	No mut	No mut	No mut	No mut	No mut
RMG-1	cell line	No mut	No mut	No mut	No mut	No mut	No mut
TOV 21G	cell line	13 G>C (37 G>T)	No mut	No mut	1047 H>Y (3139 C>T)	No mut	89682921 delG (425 delG; 89707755 delA (795 delA)[#]
JHOC5	cell line	No mut	No mut	No mut	No mut	No mut	No mut

* N.D., Not determined; No mut, no mutations identified. For the genes analyzed, we evaluated exon 1 and 2 of KRAS, exon 15 of BRAF, exons 3-7 of TP53, exons 1, 9 and 20 of PIK3CA, exon 2 of CTNNB1, and exons 1-9 of PTEN.

[#]Indicates genomic positions for two deletions in coding sequence of PTEN.